Final Technical Report on the

EFFECTS OF ASYMMETRY ON THE DYNAMIC STABILITY OF AIRCRAFT

by

R. E. Fantino

E. K. Parsons

J. D. Powell

R. S. Shevell

Submitted to

NASA Ames Research Center

Moffett Field, Ca.

by

Department of Aeronautics and Astronautics

Stanford, University

J. David Powell, Principal Investigator

Grant No. NGR -05-020-663

June 1975

ABSTRACT

The oblique wing concept for transonic aircraft has been proposed to reduce drag. This work investigates the dynamic stability of the aircraft by analytically determining the stability derivatives at angles of skew ranging from 0^{o} and 45^{o} and using these stability derivatives in a linear analysis of the coupled aircraft behavior. The stability derivatives were obtained using a lifting line aerodynamic theory and found to give reasonable agreement with derivatives developed in a Boeing study for the same aircraft.

In the dynamic analysis, no instability or large changes occurred in the root locations for skew angles varying from 0^{o} to 45^{o} with the exception of roll convergence. The damping in roll, however, decreased by an order of magnitude. Furthermore, rolling was a prominent feature of all the oscillatory mode shapes at high skew angles.

TABLE OF CONTENTS

LIST OF SYMBOLS

a_0	2-D Section Lift Slope
AR	Aspect Ratio
b	Actual Wing Span
b_0	Unyawed Wing Span
c or C	Local Wing Chord
c_p	Pivot - C.G. distance (Fig. 3.5)
$\bar{c}$	Mean Aerodynamic Chord for Unyawed Wing
c_{R_0}	Root Chord for Unyawed Wing
C_{ℓ_p}	Rolling Moment Stability Derivative due to Roll Rate
C_{ℓ_q}	Rolling Moment Stability Derivative due to Pitch Rate
C_{ℓ_r}	Rolling Moment Stability Derivative due to Yaw Rate
C_{ℓ_α}	Rolling Moment Stability Derivative due to Angle of Attack
C_{ℓ_β}	Rolling Moment Stability Derivative due to Sideslip
C_m	Pitching Moment Coefficient
C_{m_p}	Pitching Moment Stability Derivative due to Roll Rate
C_{m_q}	Pitching Moment Stability Derivative due to Pitch Rate
C_{m_r}	Pitching Moment Stability Derivative due to Yaw Rate
C_{m_α}	Pitching Moment Stability Derivative due to Angle of Attack
$C_{m_{\dot{\alpha}}}$	Pitching Moment Stability Derivative due to Angle of Attack Rate
C_{m_β}	Pitching Moment Stability Derivative due to Sideslip

C_{n_p}	Yawing Moment Stability Derivative due to Roll Rate
C_{n_q}	Yawing Moment Stability Derivative due to Pitch Rate
C_{n_r}	Yawing Moment Stability Derivative due to Yaw Rate
C_{n_α}	Yawing Moment Stability Derivative due to Angle of Attack
C_{n_β}	Yawing Moment Stability Derivative due to Sideslip
C_x	Horizontal Force Coefficient
C_{y_α}	Side Force Stability Derivative due to Angle of Attack
C_{y_p}	Side Force Stability Derivative due to Roll Rate
C_{y_r}	Side Force Stability Derivative due to yaw rate
C_{y_β}	Side Force Stability Derivative due to Sideslip
C_{z_p}	Vertical Force Stability Derivative due to Roll Rate
C_{z_q}	Vertical Force Stability Derivative due to Pitch Rate
C_{z_α}	Vertical Force Stability Derivative due to Angle of Attack
$C_{z_{\dot{\alpha}}}$	Vertical Force Stability Derivative due to Angle of Attack Rate
C_{z_β}	Vertical Force Stability Derivative due to Sideslip
C_L	Lift Coefficient
$[C_L(y)]_B$	Section Basic-Lift Coefficient
$[C_L(y)]_F$	Flat Wing Section Lift Coefficient
$C_{L_\alpha}(y)$	Section Lift Slope
$[C_L(y)]_{Tot}$	Section Total Lift Coefficient [Ref. Eq. 2.5]
C_{D_i}	Induced Drag Coefficient

$C_{D_i}(y)$	Section Induced Drag Coefficient
$(C_{D_i}(y)]_B$	Section Induced Drag due to Basic Lift
D	Drag Force
D_i	Section Induced Drag Force
$(D_i)_y$	Side Component of the Section Induced Drag Force
$\bar{d}$	Section Drag
d_i	Section Induced Drag
FWLD	Flat Wing Lift Distribution
$\bar{F}$	External Forces
F_x	x-Component of the Aerodynamic Force
F_y	y-Component of the Aerodynamic Force
F_z	z-Component of the Aerodynamic Force
$(F_y)_w$	Side Force due to Induced Drag
$(F_y)_L$	Side Force due to Wing Lift
$\tilde{I}$	Inertia Matrix
I_{xx}	Roll Moment of Inertia in Body Axes
I'_{xx}	Roll Moment of Inertia in Stability Axes
I_{yy}	Pitch Moment of Inertia in Body Axes
I'_{yy}	Pitch Moment of Inertia in Stability Axes
I_{zz}	Yaw Moment of Inertia in Body Axes
I'_{zz}	Yaw Moment of Inertia in Stability Axes
I_{xy}	Roll-Pitch Product of Inertia in Body Axes
I'_{xy}	Roll-Pitch Product of Inertia in Stability Axes
I_{xz}	Roll-Yaw Product of Inertia in Body Axes
I'_{xz}	Roll-Yaw Product of Inertia in Stability Axes

I_b	Inertia Matrix in Body Axes
I_s	Inertia Matrix in Stability Axes
K_{ij}	Component of $[S_1]$ Matrix
L	Wing Lift (Force)
$\mathfrak{L}$	Rolling Moment (Stability Axes)
$\mathfrak{L}_S$	Section Rolling Moment (Stability Axes)
ℓ	Section Lift Force
M	Pitching Moment (Stability Axes)
M.A.C.	Mean Aerodynamic Chord
M_S	Section Pitching Moment (Stability Axes)
m_0	Section Lift Slope
N	Yawing Moment (Stability Axes)
N_S	Section Yawing Moment (Stability Axes)
p	Roll Rate
q	Pitch Rate, Dynamic Pressure
r	Rate of Yaw
$[S_1]$	Aerodynamic Influence Matrix
$[S_2]$	Structural Deflection Matrix
$\overline{T}$	External Moments
u	x-Axis Velocity Component (Stability Axes)
V	Flight Air Speed
V_0 , V_{TO}	Cruise Airspeed
W	Downwash Velocity
$\left(\frac{W}{V}\right)_{3/4C}$	Downwash Angle at Three-Quarter Chord Point
w	z-Axis Velocity Component (Stability Axes)
X	Section Horizontal Force (Stability Axes)

$\bar{x}$	Moment Arm about Longitudinal Stability Axis
Y	Section Side Force (Stability Axes)
$\bar{y}$	Moment Arm about Lateral Stability Axis
y_{MAC}	Moment Arm about Quarter-Chord Line at $\Lambda = 0$
Z	Section Vertical Force (Stability Axes)
α	Perturbation Angle of Attack
α_0	Cruise Angle of Attack
α_f	Section Total Angle of Attack
β	Sideslip Angle
γ_0	(Figure 3.4)
Γ	Strength of Line Vortex
Δ	Increment (except when $\Delta\varepsilon(y)$)
Λ_0	Cruise Yaw Angle of Wing
$\varepsilon_0(y)$	Flat Wing Section Downwash Angle [rad]
$\Delta\varepsilon(y)$	Section Downwash Angle due to Twist [rad]
θ	Pitch Attitude Angle
$\theta(y)$	Section Twist
$\varphi(y)$	Wing Built-in Dihedral (unyawed wing)
ρ	Air Density
ω_n	Natural Frequency of Airplane Response Mode

LIST OF FIGURES

LIST OF TABLES

I - INTRODUCTION

1.1 Background.

The oblique wing solution for a transonic transport has been studied increasingly in the past few years. This is not a new idea; it was first proposed more than 25 years ago and, in addition to work in this country, it appears that German aerodynamicists made classified studies of this configuration during World War II, although the project never reached the stage of flight tests [Ref. 1].

In 1947, a first attempt to investigate the stability of an oblique wing was made in the NACA Free Flight Tunnel. The results of the investigation indicated that is was possible to skew the wing as a unit to angles as great as 40^{o} without encountering serious stability and control difficulties. At an angle of skew of 60^{o}, however, the aileron control became unsatisfactorily weak [Ref. 2].

For supersonic speeds, in addition to the friction and vortex drag, the wing experiences a wave drag associated with the thickness or volume of the wing, as well as with the lift distribution. The vortex drag is independent of the distribution of lift in the flight direction, whereas the wave drag does depend on the distribution in the direction of flight. However, it diminishes as the length of the wing in the flight direction increases. In fact, linear theory shows that the wave drag due to lift diminishes approximately as the inverse square of the length, while wave drag due to volume diminishes as the inverse of the fourth power; furthermore, spreading the lift over a greater length diminishes the sonic boom intensity [Ref. 3].

Structurally, an oblique wing presents the advantage of having a structure continuous across the pivot and makes tension the primary load on the pivot. It is well known that swept-forward wings show a tendency for aeroelastic divergence and this remains an area of concern for the oblique wing also. In any case, recent Boeing studies show that for the unrestrained airplane it is possible to reach a static stability without a severe penalty in weight. Oscillatory aeroelastic instability occurs at speeds higher than those at which the clamped fuselage static instability occurs (the clamped fuselage being a more conservative approach) [Ref. 4].

The object of this study is to analyze the aerodynamics and dynamics of oblique wing aircraft.

So far, with the exception of limited work based on extensions of symmetric aircraft theory to the yawed wing aircraft concept, only Boeing Commercial Airplane Company and NASA-Ames Research Center have done systematic studies on the dynamics of oblique wing aircraft. The study by Boeing [Ref. 25], a NASA sponsored one, was aimed toward a design investigation for flight in high transonic speed regime. The yawed wing aircraft was chosen as the most promising configuration for that regime. During this work, we shall use the design solution for a yawed wing aircraft chosen by Boeing and compare portions of our results with theirs.

The work done at NASA-Ames Research Center in the last few years has been characterized by several wind tunnel tests to investigate wing aerodynamic coefficients at different skew angles. Future programs are

very interesting. A remote-pilot vehicle (RPV) with an oblique wing, having 26' (unyawed) span, has already been built. The flight tests, investigating low subsonic speed, are expected to start before the end of the year. A pressure model, based on Boeing design 5-3 [Ref. 25] should be completed within two years.

A supersonic drone, the Firebee II, a Flight Research Center (FRC) project capable of Mach 1.4, should be completed in three years. The data gathered from this project will be used for the one which involves the modification of a NASA fighter, the F-8, with an oblique wing. This last project, another FRC program, should be completed within three years.

Very recently, Boeing has considered an oblique wing design for a commercial transport cruising at Mach .95.

1.2 Synopsis and Contributions.

As an aid to the reader, the remaining chapters of this report are briefly summarized below.

Chapter II deals with the wing aerodynamics. Spanwise distribution of lift and induced drag are computed according to the strip theory and lifting line theory methods. An empirical correction to Schrenk's method for evaluating spanwise lift distribution [Ref. 6] is then proposed for the oblique wing.

In Chapter III, the basic features of an oblique wing aircraft are first analyzed. A lift contribution to the side force due to wing

rotation has been found and its derivation is described; the induced drag also introduces a side component and its magnitude is computed. The new derivatives due to the oblique wing and the general methodology for evaluating stability derivatives are also described in this Chapter.

Chapter IV deals with the derivation of the equation of motion.

The numerical results are given in Chapter V. First, the spanwise distribution of lift, downwash, and induced drag, as computed by strip and lifting line theory, are reported and compared. Then, the results for rigid and flexible wing, as computed by lifting line theory, are described. Special emphasis is given to the spanwise distribution of the increments of the aerodynamic forces during simulated perturbed conditions, and the resulting stability derivatives. Root loci vs. skew angle along with the mode shapes are shown for all the natural modes.

Chapter VI contains the final conclusions and remarks.

II AERODYNAMICS

2.1 Generalities

The lift generated by a wing can be divided into two contributions: lift due to twist and camber, and lift due to the flat wing at angle of attack.

According to linear theory these two contributions are independent of each other and the lift is simply equal to their superposition. In addition, the twist contribution does not depend on the angle of attack and therefore on its variations, but it does depend on sweep and speed changes (or, more exactly, on dynamic pressure variations). In a stability analysis we must know the spanwise distribution of the aerodynamic force and how such distribution varies when the wing undergoes perturbations. Let us now limit ourselves to the lift component of the aerodynamic force since drag and side forces can be derived from the knowledge of the lift.

For a symmetric aircraft it is possible to obtain the lift distribution for the perturbed condition by applying strip theory to the cruise spanwise lift distribution [Ref. 7]. Though an approximate one, this method produces satisfactory results in the linear range.

The perturbations considered in a stability analysis can be divided into two groups:

1) perturbations which affect the total lift distribution (flat wing plus twist contribution)
2) perturbations which affect only the flat wing.

To the first group belong the u , r , and β perturbations; to

the second group the perturbations involving change in the local angle of attack (α , p , and q).

For a symmetric aircraft the flat wing spanwise lift distribution for the cruise condition is symmetric.

Let us now consider the flat wing lift distribution (FWLD) of a skewed wing. For such a wing at no sweep, the lift distribution is symmetric and elliptic (because of the chord distribution). When the wing is swept, the new spanwise lift distribution will now show an increase in lift on the aft part of the wing and a decrease on the forward one, because of an upwash generation in the first case and a downwash increase in the second one. The need for twist in this wing will be based now not on a 'tip stall last' requirement, but primarily on the need to obtain a symmetric lift distribution from the asymmetric flat wing lift. Fig. 2.1 shows the asymmetric lift, lift due to twist, and total lift versus span. The accurate evaluation of the change in aerodynamic loading will lead to good precision in computing the wing contribution to stability derivatives. We shall now follow two approaches in determining the spanwise lift distribution during the perturbed motion. The first, based on strip theory, can be used for all perturbations, but in the case of sideslip it fails to give any acceptable result. In order to improve this situation an empirical method, based on a modification of the Pope-Schrenk method [Ref. 6] which can compute the spanwise lift distribution for a flat oblique wing was obtained and will be briefly discussed in section 2.5 .

The second approach is based on the evaluation of the spanwise lift

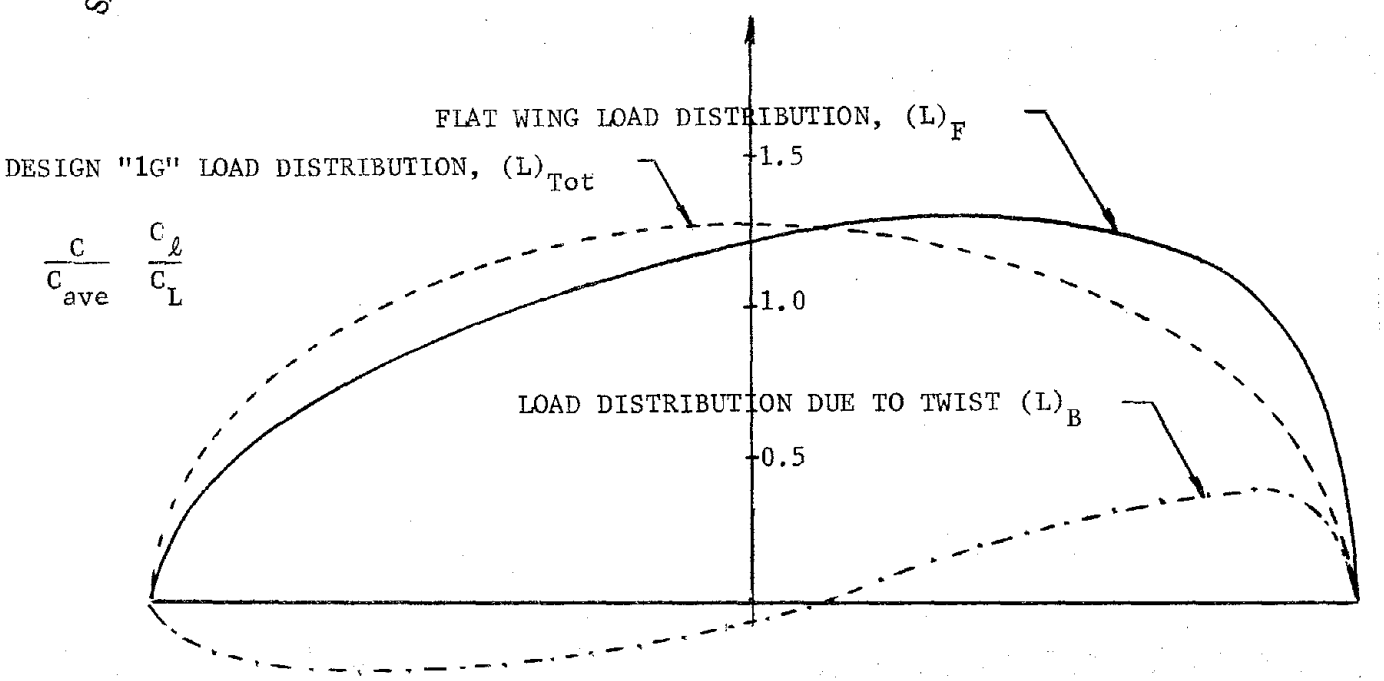

FIGURE 2.1 - Total Lift and its Components

distribution of an oblique wing by means of linear aerodynamic theory. In this case, the spanwise lift distribution is computed for both cruise and perturbed conditions. This second method also allows the static effects of a flexible wing to be included. The load distributions obtained by means of these two methods will then be used in determining the stability derivatives and the results compared. Once we have computed the stability derivatives we shall use these values in the equations of motion and determine the natural behavior and the time response to control disturbances.

2.2 Reference Axes

To discuss the problem of stability, it is necessary to set up a system of reference axes which form the basis of a system of notation used to describe the motions of an airplane. Two basic body fixed axes systems, each consisting of three mutually perpendicular axes passing through the center of gravity of the airplane, adequately cover most of the aerodynamic problems in stability considerations. These are the "body axes" and the "wind axes", which will be referred to as "stability axes".

2.2.1 Body Axes (x_b , y_b , z_b).

The body axes system is rigidly fixed in the airplane and is the system of mutually perpendicular axes passing through the airplane's center of gravity and whose X-axis is parallel to the thrust axis, the wing mean aerodynamic chord, or some other longitudinal reference and is positive in the direction of the nose of the airplane. Herein it is

taken along the body centerline reference. Figure 2.2 shows this system together with all forces, moments, displacements, and velocities. The XZ plane is the plane of symmetry for the airplane.

2.2.2 Stability Axes (x_s , y_s , z_s).

The stability axes system differs from the body axes system in that the X-axis is parallel to the relative wind, positive forward. The Z-axis is positive down (Fig. 2.3). The Y-axis is positive to the right. The moment, angle, and angular velocity conventions are given by the right hand rule.

The stability axes system is the one used for basic aerodynamic performance work, and it will be used in our analysis. In our study we shall also assume that for zero angle of attack stability and body axes will coincide.

2.3 Strip Theory

The strip hypothesis asserts that we may calculate the aerodynamic force on each strip as if it were an isolated airfoil moving with the resultant velocity which it has because of its local position on the aircraft [Ref. 7].

The strip hypothesis is a first approximation to the actual case where the trailing vortices from each strip possibly interfere with the others, but this first approximation is confirmed by experiments to give results which are in excellent agreement with the facts as observed, even at incidences above the stall, for a symmetric aircraft. Unfortu-

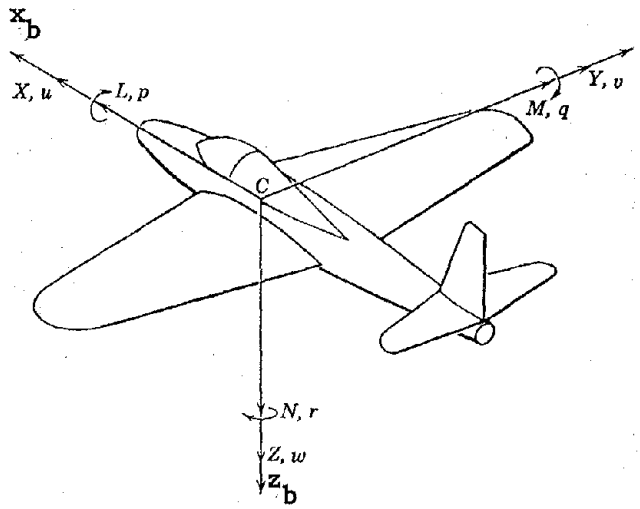

Notation for body axes.

L = rolling moment p = rate of roll
M = pitching moment q = rate of pitch
N = yawing moment r = rate of yaw
$[X, Y, Z]$ = components of resultant aerodynamic force
$[u, v, w]$ = components of velocity of C relative to atmosphere

Figure 2.2 - Body Axes [Ref. 21]

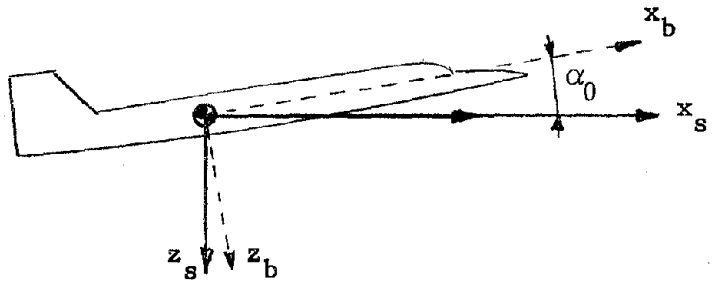

Figure 2.3 - Stability Axes

nately, when dealing with motions involving rate of pitch or rate of roll, the strip theory fails to give a good approximation for the case of an oblique wing, since it predicts no lift change at the wing root chord for the case of a roll, or at the wing station whose quarter chord is crossing the y_s axis, for the case of pitch.

The advantage of this approach is that it allows us to evaluate the stability derivatives using different sources of data, such as wind tunnel or flight tests, and computer results.

2.3.1 Variations in Aerodynamic Forces due to a Perturbation α .

Since the twist (or dihedral) contributions are independent of changes in angle of attack, only the flat wing lift distribution (FWLD) needs to be considered. (Subscript F will indicate flat wing quantity).

We can now introduce the following approximations.

2.3.1.1 Section Lift Slope.

Assuming the FWLD is given, the local lift slope can be computed as

$$C_{L_\alpha}(y) = \frac{[C_L(y)]_F}{\alpha_0} \qquad (2.1)$$

where

$C_{L_\alpha}(y)$ = local lift slope at station y (1/rad)

$[C_L(y)]_F$ = local lift coefficient of the flat wing at station y

α_0 = angle of attack for cruising condition (rad).

2.3.1.2 Section Downwash.

The downwash is a consequence of the wing not having an infinite span. For a 2-D wing, the section lift coefficient is given by

$$[C_L(y)_{2\text{-}D}]_{Tot} = m_0[\alpha_0 + \theta(y)] = m_0\alpha_0 + m_0\theta(y) \qquad (2.2)$$

where

m_0 = 2-D section lift slope

$\theta(y)$ = section twist.

The presence of trailing vortices in a finite wing introduces local downwash velocities whose effect is to reduce the local angle of attack and, therefore, the lift produced by the wing. The two terms of (Eq. 2.2) will become, for a 3-D wing

$$\begin{aligned} a_0\alpha_0 &= m_0[\alpha_0 - \epsilon_0(y)] \\ a_0\theta(y) &= m_0[\theta(y) - \Delta\epsilon(y)] \end{aligned} \qquad (2.3)$$

where

$\epsilon_0(y)$ = flat wing downwash angle

$\Delta\epsilon(y)$ = downwash angle due to twist.

Therefore, the section total lift coefficient for a 3-D wing is

$$[C_L(y)]_{Tot} = m_0\left\{[\alpha_0 - \epsilon_0(y)] + [\theta(y) - \Delta\epsilon(y)]\right\} \qquad (2.4)$$

The previous expression applies to a straight as well as to a skewed or swept back wing; the only change, assuming all quantities are measured

in the flight direction, would occur in the value of a_0, the 2-D section lift slope. We refer to R.T. Jones [Ref. 7] for a detailed discussion of the derivation of a_0.

We shall now evaluate the downwash angles by computing the difference in the local lift distribution from the 2-D case. This is a "crude" approximation, but in a strip theory analysis it is the only way to evaluate the downwash velocity and, therefore, the spanwise induced drag distribution.

In section 5.2.1 we shall compare the downwash results obtained with this method against the corresponding results obtained applying the method based on linear theory described in the next section.

Let us define

$$[C_L(y)]_{Tot} = [C_L(y)]_F + [C_L(y)]_B \tag{2.5}$$

where

$[C_L(y)]_F$ = flat wing section lift coefficient

$[C_L(y)]_B$ = section basic-lift coefficient. It represents the α-independent contribution to lift due to twist.

$$[C_L(y)]_F = a_0[\alpha_0 - \epsilon_0(y)] \tag{2.6}$$

$$[C_L(y)]_B = a_0[\theta(y) - \Delta\epsilon(y)] \tag{2.7}$$

We can now assume, according to linear theory, that the two downwashes are independent from each other, and furthermore, that the downwash due to twist does not depend on the angle of attack. With these

assumptions we have

$$[C_L(y)]_F = a_0[\alpha_0 - \epsilon_0(y)] = a_0 \left\{1 - \frac{\partial \epsilon_0(y)}{\alpha}\right\}\alpha_0 \tag{2.8}$$

$$\frac{\partial \epsilon_0(y)}{\partial \alpha} = 1 - \frac{[C_L(y)]_F}{a_0 \alpha_0} = 1 - \frac{[C_{L_\alpha}(y)]}{a_0} \tag{2.9}$$

$$\epsilon_0(y) = \frac{\partial \epsilon_0(y)}{\partial \alpha}\ \alpha_0 \tag{2.10}$$

The total downwash is therefore given by

$$[\epsilon(y)]_{Tot} = \epsilon_0(y) + \Delta\epsilon(y) \tag{2.11}$$

$$\frac{\partial[\epsilon(y)]_{Tot}}{\partial \alpha} = \frac{\partial \epsilon_0(y)}{\partial \alpha} + \frac{\Delta\epsilon(y)}{\partial \alpha} = 1 - \frac{C_{L_\alpha}(y)}{a_0} \tag{2.12}$$

2.3.1.3 Section Induced Drag.

The aerodynamic drag in a finite wing has two components: the first is due to skin friction and pressure distributions on the boundary, the second is the one induced by the lift because of the presence of trailing vortices.

Both components are normally of the same order, and dependent on the aircraft speed [Ref.15]. The analytic spanwise evaluation of these two components is a difficult task.

According to Multhopp [Ref. 9] we may write the induced drag coefficient for the wing as

$$C_{D_i} = \frac{1}{2S} \int_{-b/2}^{b/2} C\, C_L(y)\, \alpha_i \, dy \tag{2.13}$$

where the so-called induced incidence is

$$\alpha_i = \frac{1}{8\pi} \int_{-b/2}^{b/2} \frac{1}{y - \eta} \frac{d}{d\eta} \left[C\, C_L(y) \right] d\eta \tag{2.14}$$

and the section induced drag coefficient is given by

$$C_{D_i}(y) = C_L(y)\alpha_i \tag{2.15}$$

Garner, [Ref. 10] who has discussed induced drag and its spanwise distribution in incompressible flow, has shown that, for swept back wings, the quantity $C\, C_L(y)\, \alpha_i$ does not give an acceptable spanwise distribution of induced drag as suggested by Robinson and Laurmann [Ref. 11]. This conclusion can be expected since the induced incidence α_i, as computed in Eqn. (2.14) implies that all the bound vortices of the horseshoe vortex system, used as a model for the wing, lie on a straight line perpendicular to the velocity. Therefore, the downwash angles correspond to the ones of a straight wing and the induced drag obtained is the product of the lift distribution of a swept wing times the downwash angle of a straight wing having the same wing span and the same spanwise lift distribution.

We shall return to this subject when we evaluate the induced drag distributions by means of linear theory. For the sake of clarity we shall recall that the downwash angle is the ratio $\frac{w}{V}$ where

w = downwash velocity measured at the lifting line

V = free stream velocity.

In our strip analysis the downwash angles are obtained directly from the actual spanwise lift distribution; we assume that the downwash angle is the cause of the difference in lift coefficient from the corresponding 2-D one, and no assumptions are made on the wing geometry. We may therefore expect a better accuracy in the estimate of the spanwise drag distribution.

Let us now see how to relate the previous discussion to the evaluation of stability derivatives by means of strip theory.

For the lift case we have one term, the basic lift, which is "α independent" and the other, the flat wing, which does depend on α ; the same considerations can be applied to the drag. In the "α independent" drag contribution we can group skin friction, pressure distorsions, and, if we extend to the drag the same assumptions made for the lift, also the induced drag due to basic lift. This approximation is quite accurate for skin friction and pressure distortion, but it becomes less accurate when considering the induced drag of the basic lift, as is shown next.

The total section induced drag is obtained by substituting into Eqn.(2.15) the total values derived in the previous sections

$$[C_{D_i}(y)]_{Tot} = [C_L(y)]_{Tot}[\epsilon_0(y)]_{Tot}$$

$$= \left\{[C_L(y)]_F + [C_L(y)]_B\right\} [\epsilon_0(y) + \Delta\epsilon(y)]$$

$$= [C_L(y)]_F [\epsilon_0(y) + \Delta\epsilon(y)] + [C_L(y)]_B [\epsilon_0(y) + \Delta\epsilon(y)] \tag{2.16}$$

We can see that the induced drag produced by the basic lift distribution

$$[C_{D_i}(y)]_B = [C_L(y)]_B [\epsilon_0(y) + \Delta\epsilon(y)] \tag{2.17}$$

has the term $[C_L(y)]_B \epsilon_0(y)$ that is α dependent since $\epsilon_0(y)$, as discussed in the previous section, is α dependent.

Therefore, only the quantity $[C_L(y)]_B \Delta\epsilon(y)$ can be assumed, within the range of linear theory, as α independent, whereas

$$[C_L(y)]_B \epsilon_0(y) + [C_L(y)]_F [\epsilon_0(y) + \Delta\epsilon(y)] \tag{2.18}$$

is the α dependent component of the drag. The change in the section drag for perturbations introducing a local change in the angle of attack can now be computed as the rate of change of Eqn. (2.18) with α

$$\frac{\partial C_{D_i}(y)}{\partial\alpha} = \frac{\partial}{\partial\alpha} [C_L(y)]_B \epsilon_0(y) + [C_L(y)]_F [\epsilon_0(y) + \Delta\epsilon(y)]$$

$$= [C_L(y)]_B \frac{\partial\epsilon_0(y)}{\partial\alpha} + C_{L_\alpha}(y) [\epsilon_0(y) + \Delta\epsilon(y)] + C_L(y)]_F \tag{2.19}$$

and by substituting Eqns. (2.5), (2.11) and (2.12) into (2.19) we obtain

$$\frac{\partial C_{D_i}(y)}{\partial\alpha} = [C_L(y)]_{Tot} \left[1 - \frac{C_{L_\alpha}(y)}{\alpha_0}\right] + C_{L_\alpha}(y) [\epsilon_0(y)]_{Tot} \tag{2.20}$$

2.3.2 Evaluation of Stability Derivatives by Means of Strip Theory.

Assuming the spanwise lift distribution is given for the flat wing as well as for the wing with the nominal twist and dihedral, it is possible to evaluate the stability derivatives by using the approximations used in section 2.3.1 and the expressions given in sections 3.3.2 and 3.3.4 .

For the stability derivatives due to side-slip it is necessary to know the spanwise lift distribution corresponding to the new sweep angle differing from the nominal one by $\Lambda = -\beta$. Because of the peculiarity of the shape of the FWLD and its dependence on the sweep angle, an approximation assuming

$$\left([C\,C_L(y)]_{Tot}\right)_{\Lambda} = \left([C\,C_L(y)]_{Tot}\right)_{\Lambda_0} \frac{\cos^2\Lambda}{\cos^2\Lambda_0} \qquad (2.21)$$

where

$$\Lambda = \Lambda_0 - \beta$$

would fail to give an acceptable result. The knowledge of the spanwise lift distribution for the new sweep angle would therefore be required.

For the case when such lift would not be available, an empirical correction to the Pope-Schrenk's method [Ref. 6,12] was derived and it is described in section 2.5 .

2.4 Lifting Line Theory

2.4.1 Introduction

A more accurate way of evaluating the stability derivatives, specially roll and pitch derivatives, is to use linear aerodynamic theory. The literature offers a wide variety of methods which can be used; many of these are very complex and allow the user to evaluate both the spanwise and chord-wise load distribution. The simplest three-dimensional wing theory is that based on the concept of the lifting line. In this theory the wing is replaced by a straight line [Ref. 13]. The circulation about the wing associated with the lift is replaced by a vortex filament. This vortex filament lies along the straight line; and at each spanwise station, the strength of the vortex is proportional to the local intensity of the lift. According to Helmholtz's theorem, a vortex filament cannot terminate in the fluid. The variation of vortex strength along the straight line is therefore assumed to result from superposition of a number of horseshoe-shaped vortices, as shown in Figure 2.4 . The portions of the vortices lying along the span are called the "bound vortices". The portions of the vortices extending downstream indefinitely are called the "trailing vortices".

The effect of trailing vortices corresponding to a positive lift is to induce a downward component of velocity at and behind the wing. This downward component is called the "downwash". The magnitude of the downwash at any section along the span is equal to the sum of the effects of all the trailing vortices along the entire span. The effect of the downwash is to change the relative direction of the air stream over the

section.

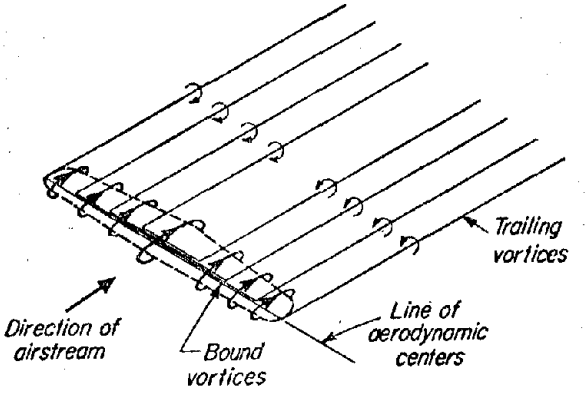

Figure 2.4 - Vortex Pattern Representing a Lifting Wing
[Ref. 13]

The section is assumed to have the same aerodynamic characteristics with respect to the rotated air stream as it has in normal two-dimensional flow. The rotation of the flow effectively reduces the angle of attack. Inasmuch as the downwash is proportional to the lift coefficient, the effect of the trailing vortices is to reduce the slope of the lift curve. The rotation of the flow also causes a corresponding rotation of the lift vector to produce a drag component in the direction of motion.

The methods using discrete vortices to represent the continuous distribution of circulation of the vortex sheet are attempts to simplify the computations. In the methods employing discrete vortices, two-dimensional theory is used to determine the most representative locations of the vortices as well as of the control points. If only one vortex line is used, it is placed along the center-of-pressure line in two-dimensional flows, which for a flat plate at an angle of attack and at subsonic speeds

is the quarter chord line.

For subsonic speeds, the downwash varies inversely with the distance behind the quarter chord line; at the position of the three-quarter chord line it just equals in magnitude the vertical component of the flow tangential to the flat plate having the same circulation. Conversely, if the condition of tangential flow is satisfied at the three-quarter chord line, the strength of the concentrated vortex will indicate the lift on one wing due to angle of attack. Of course, these methods of obtaining correspondence between the lifting lines and the vortex sheets loose their validity near the corners of the wing, where the flow differs sharply from the two-dimensional.

In a stability analysis it is not required to have great accuracy in the chordwise load distribution. Therefore, it is sufficient to use only one vortex line placed, for subsonic cruise condition, at the quarter-chord point. In doing so, little is lost in accuracy and a lot is gained in simplicity.

The supersonic case has to be approached in a different way according to the properties of the supersonic flow. The method outlined in this chapter applies to subsonic speeds only, but it can be extended to the supersonic case. It can be shown that the horseshoe-vortex system of Figure 2.4 is equivalent to the one where each horseshoe vortex has a constant strength equal to the sum of the strength of the bound vortices contained at the corresponding section of Figure 2.5 .

When the wing is skewed, two models can be used. Figure 2.6 shows the first one where the bound vortices are aligned with the wing span ,

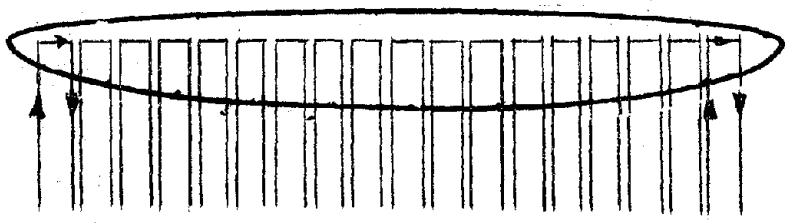

Figure 2.5 - Horseshoe Vortex Pattern (unyawed wing)

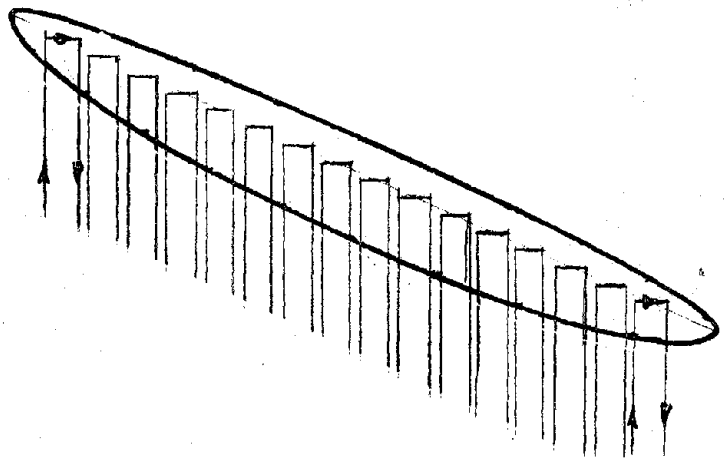

Figure 2.6 - Bound Vortex Normal to Flight Stream

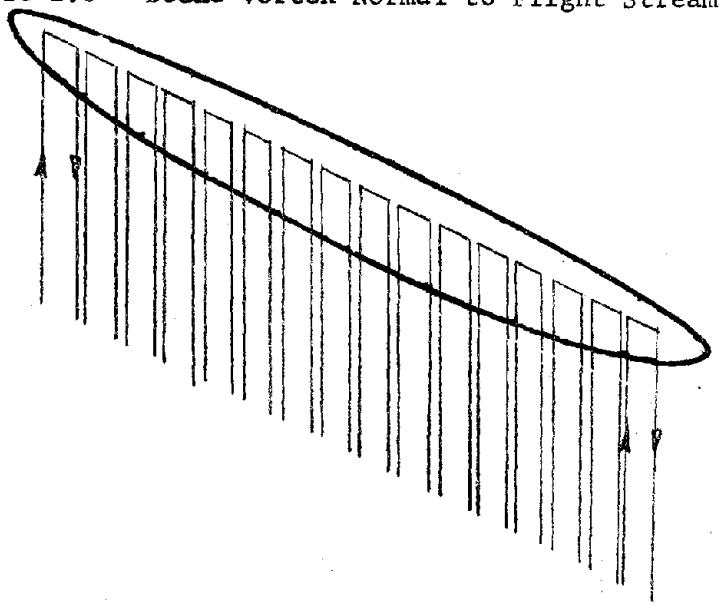

Figure 2.7 - Bound Vortex Parallel to Wing Span

and are at a skew angle with respect to the free stream velocity.

The second model, shown in Figure 2.7, assumes that the bound vortices are perpendicular to the flight direction. This model corresponds to the case where the wing at a skew angle is actually replaced by a finite number of straight wings, and will be used in this study.

The first model is expected to give a better accuracy when the number of horseshoe vortices is small, but the two models coincide when the number of horseshoe vortices goes to infinity.

The method used in this study is based on a modification of the Weissinger-L-Method and applies at subcritical Mach Number. This method is derived from excellent work done by Gray and Schenk in 1953 [Ref. 14] and has been modified for the oblique wing case. Among the advantages of such an approach to the evaluation of the spanwise distribution of the loading, is the possibility of evaluating the loading increments due to aileron or flap deflection, effects of wing flexibility, and accelerations on the wing. These features are fully described in Appendix D.

2.4.2 Steady State Loading on an Airplane with an Oblique Wing.

The fundamental problem involved is the development of a series of equations which relate the spanwise lift distribution for an arbitrary wing plan form in a given flight condition to the properties and attitudes of the individual sections that form the wing.

For a 2-D wing, the following relationships can be found in any

standard textbook on aerodynamics [Ref.7,15,17]:

$$\ell = \rho V \Gamma = q\, m_0\, C\, \alpha_f \tag{2.22}$$

$$W_r = \frac{\Gamma}{2\pi r} \tag{2.23}$$

where

m_0 = local lift slope

C = local chord length

ℓ = section lift

α_f = total angle of attack (see Fig. 2.8)

$q = \frac{1}{2} \rho V^2$ = dynamic pressure

Γ = circulation

At a specific distance r behind the lifting line, the resultant of the downwash velocity W_r and the flight velocity V is parallel to the section zero lift line. Then,

$$W_r = \alpha_f V \tag{2.24}$$

from Eqn. (2.22) we obtain

$$\Gamma = \frac{m_0\, q\, C\, \alpha_f}{\rho V} = m_0 \frac{V}{2} C \alpha_f \tag{2.25}$$

Substituting (2.25) into (2.23) results in

$$W_r = \frac{m_0}{2\pi} \frac{C/2}{r} \alpha_f V \tag{2.26}$$

Equating (2.26) and (2.24)

$$\alpha_f V = \frac{m_0}{2\pi} \frac{C/2}{r} \alpha_f V$$

or

$$\frac{m_0}{2\pi} \frac{C/2}{r} = 1 \tag{2.27}$$

Since the theoretical section 2-D lift curve slope is 2π , r must equal C/2 , which is the distance between the lifting line and the three-quarter-chord point.

Therefore, for the 2-D (unswept wing) case

$$\left(\frac{W}{V}\right)_{3C/4} = \alpha_f \tag{2.28}$$

corresponds to the control point where no flow exists normal to the zero lift line. Whenever the local lift slope differs from 2π , expression (2.28) becomes

$$\left(\frac{W}{V}\right)_{3C/4} = \frac{m_0}{2\pi}\,\alpha_f \tag{2.29}$$

The essential difference between a 2-D wing and a wing of finite aspect ratio arises from non uniform spanwise loading which produces the trailing vortices. The equations presented so far are considered to apply to a finite wing when the effects of all the vortices, both bound and trailing, have been taken into account.

Equation (2.29) can be written in matrix form

$$\left\{\frac{W}{V}\right\}_{3C/4} = \left[\frac{m_0}{2\pi}\right] \left\{\alpha_f\right\} \tag{2.30}$$

This matrix relation represents a series of equations, each applicable to a particular station on the span of the wing.

The elements of $\left\{\frac{W}{V}\right\}_{3/4C}$, every one of which is affected by the bound and trailing vortices of the wing stations can be evaluated from

$$\left\{\frac{W}{V}\right\}_{3/4\ C} = \frac{1}{4\pi V}\,[S1]\,\{\Gamma\} \tag{2.31}$$

and by expressing $\{\Gamma\}$ in terms of $\{\ell\}$.

The [S1] matrix is the downwash matrix and is derived in Appendix D.

Combining equations (2.30) we obtain

$$\frac{1}{8\pi q}\,[S1]\,\{\ell\} = \left[\frac{m_0}{2\pi}\right]\,\{\alpha_f\} \tag{2.32}$$

or

$$\left[\frac{1}{4qm_0}\right][S1]\,\{\ell\} = \{\alpha_f\} \tag{2.33}$$

2.4.3 Section Final Angle of Attack $\{\alpha_f\}$.

The final angle of attack across the span $\{\alpha_f\}$ can be considered to be composed of three essential parts (see Fig. 2.8).

$$\{\alpha_f\} = \{\alpha_r\} + \{\alpha_g\} + \{\alpha_s\} \tag{2.34}$$

where

$\{\alpha_s\}$ = angle of attack caused by structural deflection of a flexible wing

$\{\alpha_g\}$ = angle of attack caused by built-in twist, apparent or aerodynamic twists, control deflection, angular velocities.

$\{\alpha_r\}$ = flat (and rigid) wing angle of attack (measured w.r.t. root-section zero-lift line).

The angle of attack $\{\alpha_s\}$, caused by structural deflection of a flexible wing due to the section lift at the section aerodynamic centers is linearly related to the matrix $\{\ell\}$ as

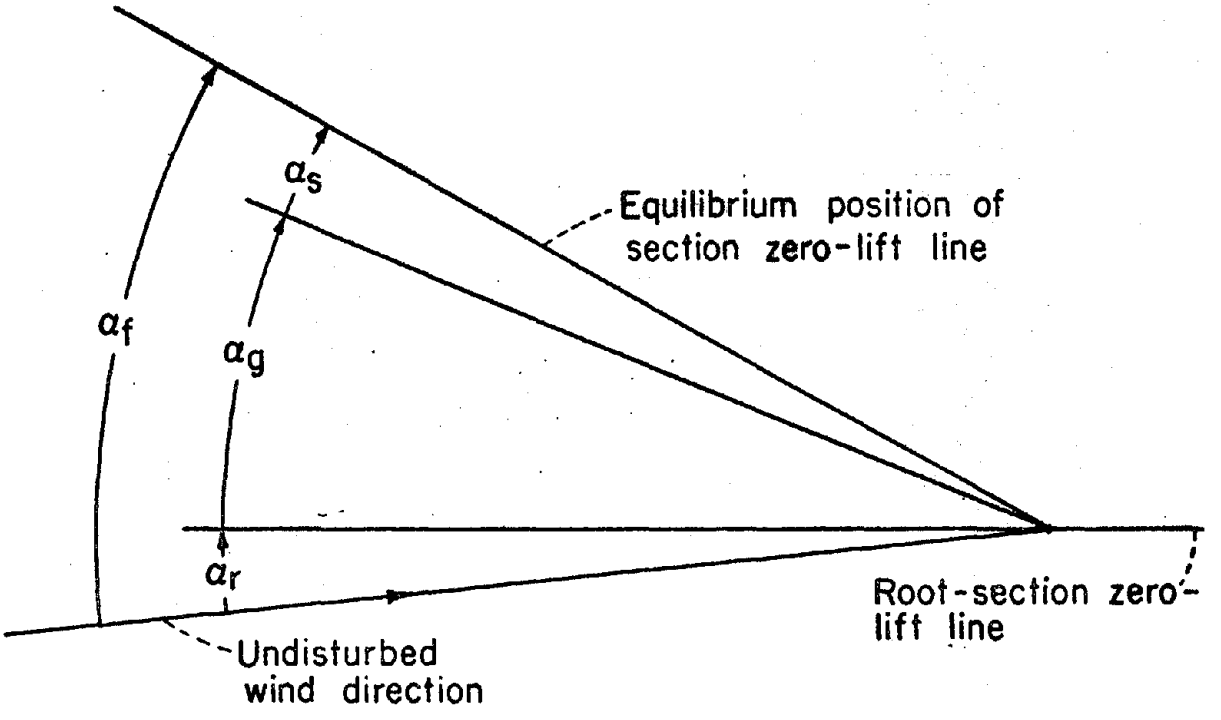

Figure 2.8 - Final Angle of Attack

$$\{\alpha_s\} = [S_2]\ \{\ell\} \tag{2.35}$$

where $[S_2]$ = structural deflection matrix (described in Appendix D).

The contributions to the angle of attack α_g are described in Appendix D.

2.4.4 Section Induced Drag.

As discussed in section 2.3.1, only the induced drag varies with α. The induced drag arises from the rotation of the aerodynamic forces due to the downwash velocities induced by the trailing vortices.

In our model, where the wing has been replaced by a lifting line placed, for the subsonic analysis, at the quarter-chord line, the section induced drag can be evaluated by computing the downwash angle $(\alpha_i)_i$ at the station bound vortex. This is similar to what is done for $\left(\frac{W}{V}\right)_{3/4\ C}$, except that downwash induced by a bound vortex on itself is zero.

Therefore

$$(\alpha_i)_i = \left(\frac{W_i}{V}\right)_{C/4} = \frac{1}{V_{T0}} \sum_j (K_{ij})_{C/4}\ \Gamma_j = \frac{1}{\rho V_{T0}^2} \sum_j (K_{ij})_{C/4}\ \ell_j \tag{2.36}$$

where $(Kij)_{C/4}$ is the same as computed in Appendix D with the following two exceptions:

1) the term $\frac{C_i}{2}$, distance of the control point from the lifting line, must be dropped since the downwash is now evaluated at the lifting line;

2) the contribution to the downwash sould be disregarded for the case when the control point is within the horseshoe vortex, as discussed in Appendix D.

A more accurate result would be obtained using the vortex lattice method. The results obtained in this analysis are discussed in Reference 16.

2.5 An Empirical Correction to Schrenk's Method

Another approach to the problem of spanwise load distribution having much less theoretical foundation is presented by Flatt [Ref. 18]. It follows a method first presented by Schrenk [Ref. 19].

Schrenk's method makes allowance for the effect of the varying downwash along the span of a nonelliptic wing by assuming that the final span load distribution for an untwisted wing is halfway between the actual planform shape and a semi-ellipse of the same area. However, Schrenk and Flatt did not consider a swept back wing; Alan Pope and William R. Haney, assuming that the effect of sweepback on the non-dimensional span loading is linear, proposed an empirical correction [Ref. 6, 12] to take care of the effect of sweep back. It has been successfully employed in preliminary design of subsonic aircraft.

The following empirical formula which was obtained during our study of the oblique wing, can be applied to Schrenk's method.

$$\left(\frac{c\,C_\ell}{c_R C_L}\right)_\Lambda = \left(\frac{c\,C_\ell}{c_R C_L}\right)_{\Lambda=0} - \left\{1 - \left[1 + \frac{\left(y+\frac{b}{2}\right)}{b}\right]\left(\frac{y}{b\tan\Lambda}\right)\right\}(1-\cos\Lambda)\sqrt{1-\frac{2y}{b}^2} \qquad (2.37)$$

where

Λ = skew angle

$c_R = c_{R_0}/\cos\Lambda$: root chord measured in the flight direction

$b = b_0 \cos\Lambda$: actual wing span

b_0 = wing span for the unskewed wing.

Since the goal of this method is to provide, in a fast way, the shape of the spanwise lift distribution, the wing lift coefficient is assumed to be known. In addition, the new spanwise lift distribution obtained with this correction must be normalized by multiplying it times the ratio of the wing lift coefficient to the lift coefficient obtained by integration of the new lift distribution.

The results of this correction, for the case of a flat wing, were checked against the lift distribution as computed by the numerical program of Reference 20.

Figures 2.9a, b, and c show the comparison between the two methods for three different cases.

To date, no check has been done for the case of a wing having twist. The major difficulty for this case is to estimate the downwash velocities produced by the lift due to twist and, therefore, to determine the effective twist.

Though for symmetric wings experience suggests that an effectiveness of 50% is an acceptable assumption, we do not expect that the same can be applied to a skewed wing.

As pointed out before, the effect of a positive sideslip corresponds,

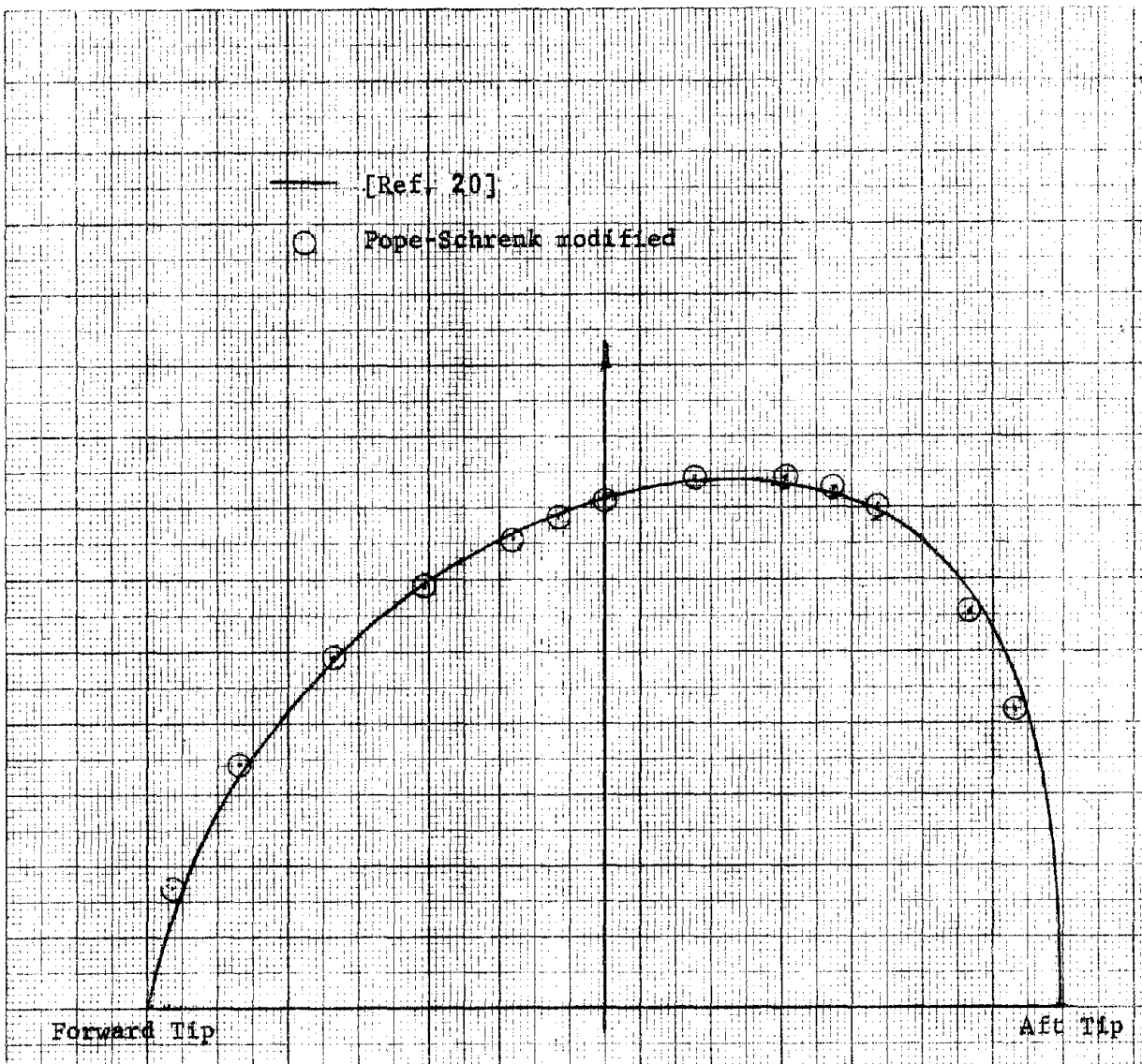

Mach Number $M = 1.0$

Sweep Angle $\Lambda = 45^{\circ}$

Figure 2.9a - Spanwise Lift Distribution

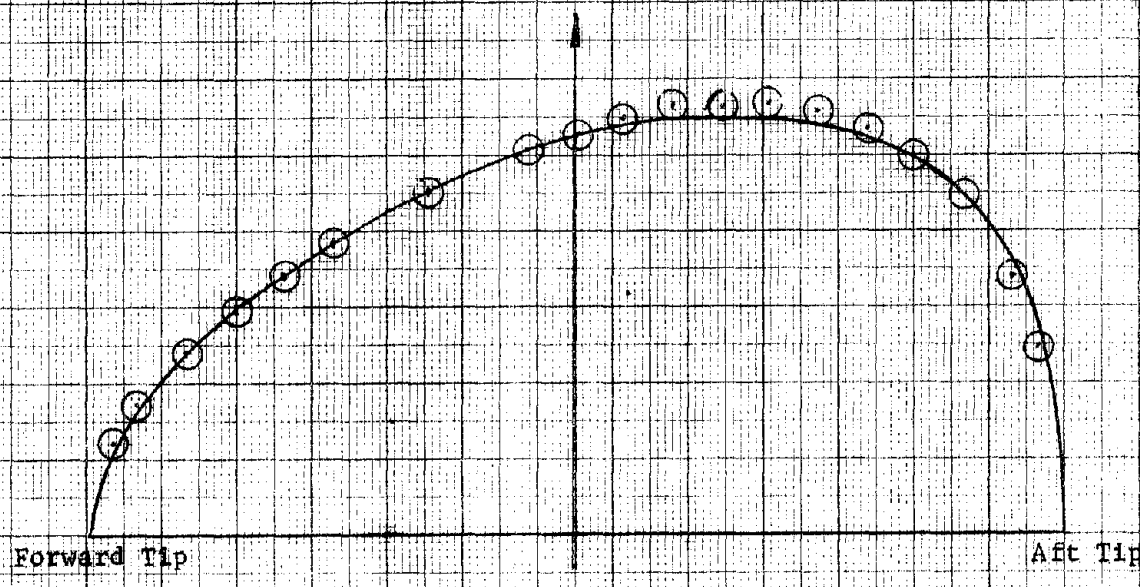

Mach Number $M = 1.2$

Sweep Angle $\Lambda = 55^{o}$

Figure 2.9b - Spanwise Lift Distribution

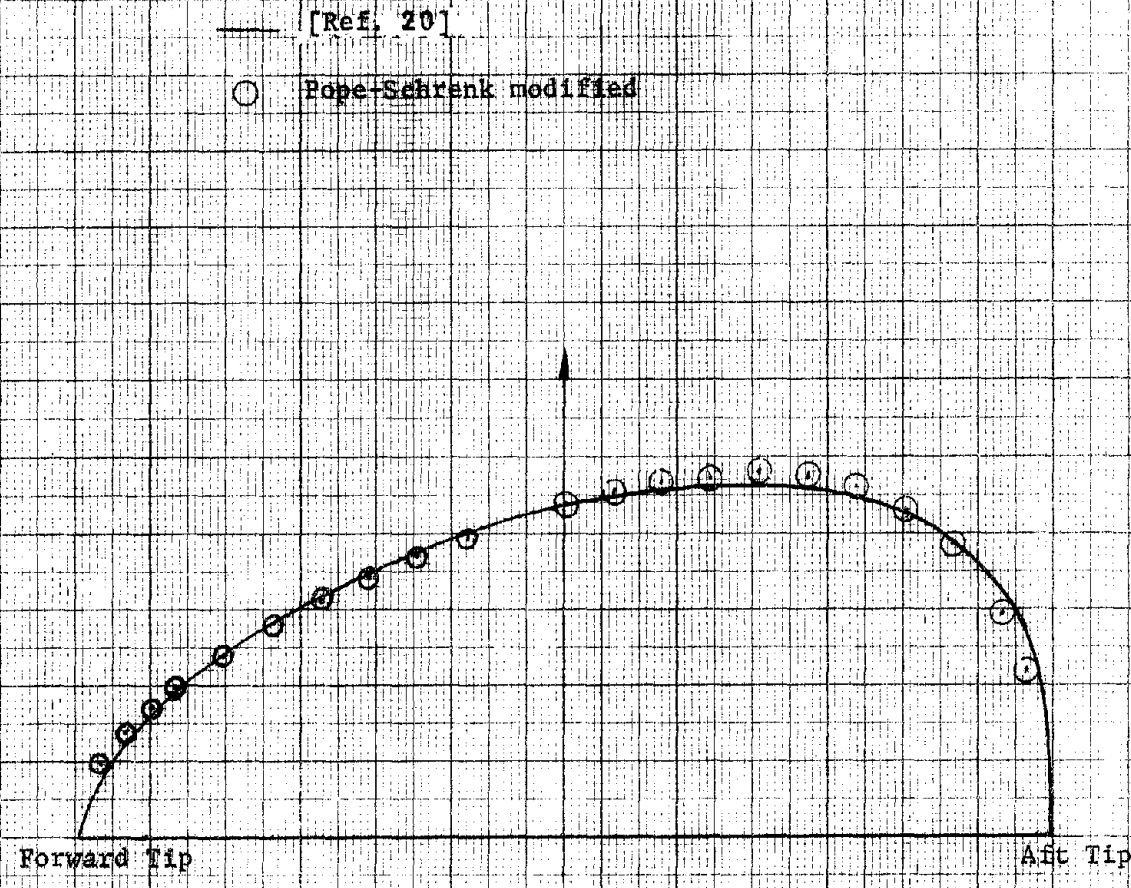

Mach Number M = 1.4

Sweep Angle $\Lambda = 55^{\circ}$

Figure 2.9c - Spanwise Lift Distribution

for an oblique wing, to a negative change in sweep and the perturbation will therefore affect both the FWLD and the basic lift distribution.

To a first order approximation it is possible to assume that the change in the shape of the lift distribution for the total lift will be proportional to the change with sweep of the FWLD.

Therefore, the simulation of a sideslip can be done by

1) determining , with the Pope-Schrenk's method corrected for the skewed case, the FWLD for both the cruise sweep Λ_0 , and the sideslip condition $\Lambda = \Lambda_0 - \beta$;

2) multiplying the spanwise distribution of the ratio of the FWLD at $\Lambda = \Lambda_0$ to the FWLD at $\Lambda = \Lambda_0 - \beta$ times the total lift distribution for the cruise condition in order to obtain the corresponding distribution for the sideslip condition.

2.6 Summary.

The reference axes system used in this work, the stability axes, has first been defined. The method for evaluating variations in the aerodynamic forces due to perturbations was then outlined. A simplified method, based on strip theory, for computing spanwise distribution of the induced drag was also proposed.

A second and more systematic way of computing spanwise lift distribution based on lifting line and including effects of wing flexibility was the described. The spanwise induced drag distribution was then evaluated by using lifting line theory.

In the last section of this Chapter, an empirical correction to Schrenk' method for the oblique wing case was proposed.

III STABILITY DERIVATIVES

3.1 Basic Features

3.1.1 Flat Wing Lift Distribution (FWLD).

In section 2.1 we have described how the FWLD behaves when the wing is skewed. This behavior is undoubtedly one of the most important elements of difference from the symmetric case. The upward field generated by the forward wing, causes the aft wing to "feel" a higher angle of attack. This, as we mentioned before, is the cause of the loss of symmetry in FWLD, but, because of the higher angle of attack actually experienced by the aft wing, the stall condition will be reached in this region first. This is similar to the case of a tip stall for a symmetric wing, except that now only one tip would stall and the loss in balance would produce not only rolling but also pitching moments. The recovery from such a stall is very difficult.

This can be explained if we analyze in detail the motion of the aircraft following the stall of the aft wing.

As we mentioned before, the loss in the lift symmetry introduces, in the case of the left wing forward, positive pitching and rolling moments. The nose-up motion deriving from the pitching moment introduces an increase in the angle of attack of the whole wing as well as an angular velocity; whereas the rolling moment produces only an angular velocity.

The effect of these two angular velocities results in a linear

variation of the local angle of attack for the wing, increasing it on the aft part and decreasing it on the forward one.

Therefore, the aft wing will experience a further increase in the angle of attack which will worsen the stall condition and extend it inboard.

On the forward wing, instead, the increase in angle of attack of the whole wing is counteracted by the decrease deriving from the angular velocities and the final trend is consequently toward a delay in the forward wing stall, which makes the nose-down attitude, required for a recovery, difficult to achieve.

The center of pressure of the flat wing lift distribution (FWLD) lies on the aft portion of the wing and produces both pitching and rolling moments as the angle of attack varies, introducing new important derivatives. In fact, any change in the angle of attack affects the FWLD only and destroys the symmetry in the total lift distribution obtained by twisting the wing. The consequence of this is a loss in the moments' balance. Figure 3.1 shows the variation in spanwise lift distribution, as given by linear theory, for a case where, for the sake of clarity, the "perturbation" α is assumed to be equal to 50% of α_0. It will be seen that a positive change in α produces an increase in the lift whose aerodynamic center is displaced toward a point in the aft part of the wing, thus producing a rolling moment as well as a pitching moment. By considering the corresponding change in induced drag, it is possible to evaluate the yawing moment.

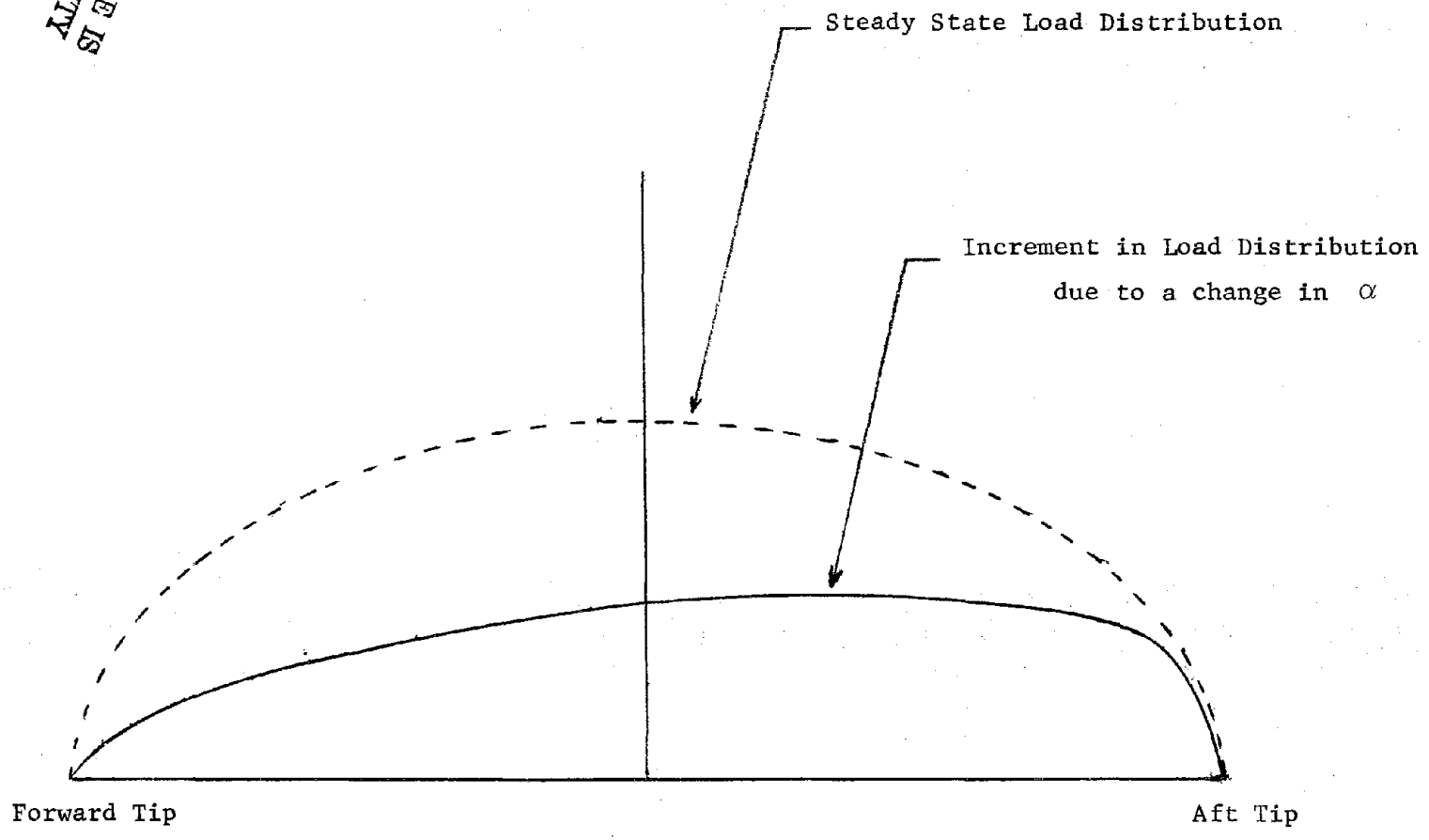

Figure 3.1 - Increment in Load Distribution due to a Change in α .

3.1.2 Side Force

A wing at a skewed angle experiences a side force deriving from the induced drag component in the y direction. Let us now derive its magnitude.

Figure 3.2 shows a section of a wing at a skew angle Λ.

The principle of independence [Ref. 8] assumes that, in a frictionless flow, all the results of the two-dimensional flow theory can be applied immediately to an infinite oblique wing simply by subtracting the axial component of velocity.

No matter whether we consider the free stream direction or the direction normal to the leading edge, the lift generated by the wing section is obviously the same. Therefore, the lift force is given by

$$\ell = \frac{1}{2} \rho V_0^2 C_{L_0} [C_0 \cdot 1] = \frac{1}{2} \rho V^2 C_L \frac{C \cdot 1}{\cos\Lambda} \tag{3.1}$$

where the subscript 0 defines the quantity in the flight direction.

Since

$$V = V_0 \cos\Lambda \tag{3.2}$$

and

$$C = C_0 \cos\Lambda \tag{3.3}$$

from 3.1 it is possible to derive the well known relationship

$$C_{L_0} = C_L \cos^2\Lambda \tag{3.4}$$

Figure 3.2a shows the decomposition of the velocity vector into two components; one normal and one parallel to the leading edge. The two elementary strips have the same area.

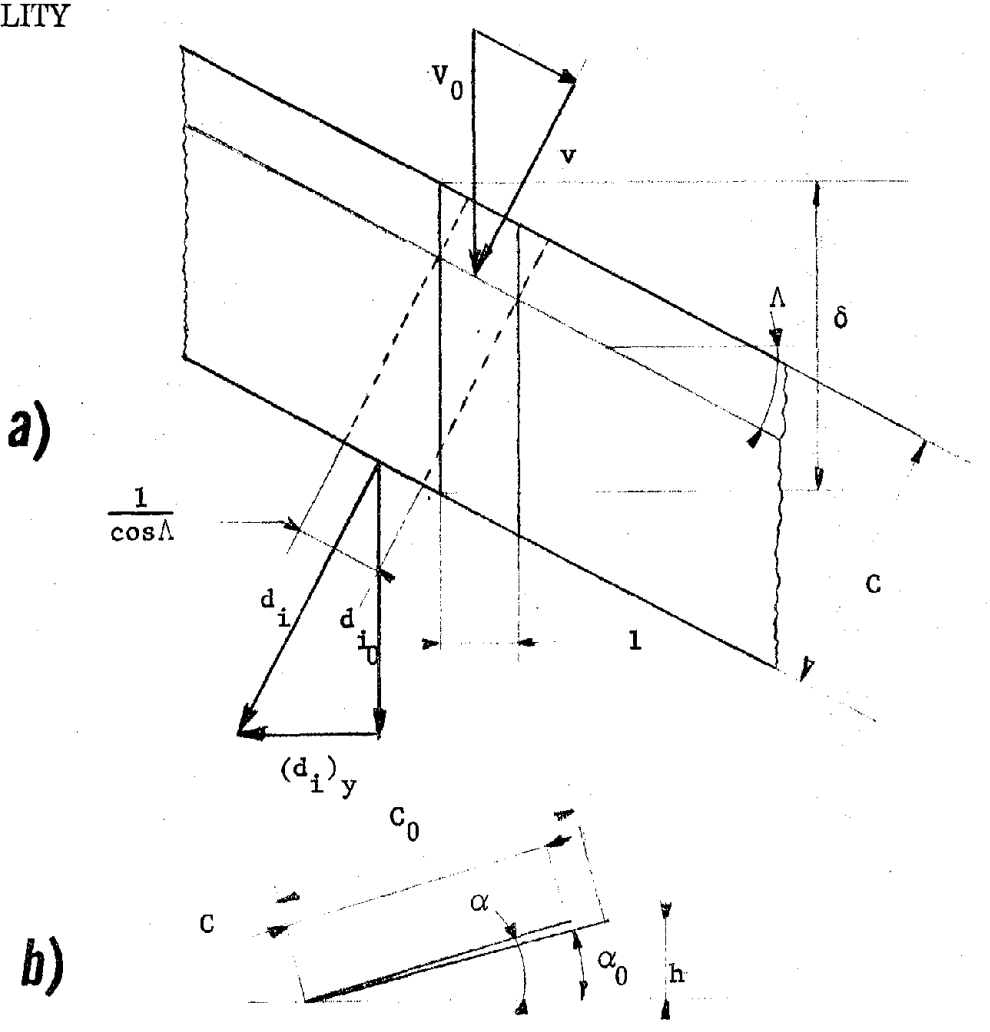

Figure 3.2 - Side Force due to Induced Drag.

If we now introduce a plane defined by the velocity vector $\bar{V}_0$ and by the trailing edge segment where the two strips coincide, we can derive the relationship between the angles of attack measured in the two directions. This relationship is useful when evaluating the angle of attack during sideslip. This can be done by simply noticing that the

height from the leading edge to the previously defined plane is the same at the point k_0 as well as at k. This, of course, implies that the leading edge is a straight line. The effects of twist or dihedral would then be superimposed.

The distance h being a constant, by pure trigonometric considerations applied to Figure 3.2b we obtain

$$\begin{aligned} C_0 \sin\alpha_0 &= h \\ C \sin\alpha &= h \end{aligned} \tag{3.5}$$

and from (3.3) we obtain

$$\sin\alpha_0 = \sin\alpha \cos\Lambda \tag{3.6}$$

Therefore

$$\alpha = \sin^{-1}\left(\frac{\sin\alpha_0}{\cos\Lambda}\right) \tag{3.7}$$

and for small angle of attack

$$\alpha = \frac{\alpha_0}{\cos\Lambda} \tag{3.8}$$

The induced drag measured in the flight direction and the corresponding one measured in the direction normal to the leading edge are not the same.

The lift is the same in both cases, but the downwash angles are not.

The downwash velocity at the lifting line [see 2.3.1 and 2.4.4] must be computed with respect to the flight direction, since it is the wing span measured with respect to such direction that will determine the downwash velocity.

An easy mistake would be to extend the use of the well known expression for the downwash angle (for an elliptic lift distribution)

$$\frac{W_0}{V_0} = \frac{C_{L_0}}{\pi AR_0} \tag{3.9}$$

to the case normal to the leading edge

$$\frac{W}{V} = \frac{C_L}{\pi AR}$$

In fact, using equation 3.4 and since $AR = AR_0 / \cos^2\Lambda$, we find that

$$\frac{C_{L_0}}{\pi AR_0} = \frac{C_L}{\pi AR_0} \tag{3.10}$$

This implies that the induced drag measured in the two directions is identical, since

$$d_{i_0} = \ell \frac{C_{L_0}}{\pi AR_0}$$

and

$$d_i = \ell \frac{C_L}{\pi AR} = \ell \frac{C_{L_0}}{\pi AR_0}$$

where

d_{i_0} = section induced drag, flight direction

d_i = section induced drag, direction normal to the leading edge.

The downwash velocity at the lifting line is induced by trailing vortices aligned with the flight direction.

We shall call the downwash measured this way W_i.

The downwash angles in the desired direction can bow be computed by dividing W_i by the corresponding velocity. Thus, the section induced drag measured in the flight direction is given by

$$d_{i_0} = \ell \frac{W_i}{V_0}$$

and, in a direction normal to the leading edge

$$d_i = \ell \frac{W_i}{V} = \ell \frac{W_i}{V_0 \cos\Lambda} \tag{3.11}$$

or

$$d_i = \frac{d_{i_0}}{\cos\Lambda} \tag{3.12}$$

Equation 3.12 shows that the induced drag measured normally to the leading edge is greater than the component in the flight direction.

In a symmetric swept back (or swept forward) wing, the two side-components would cancel each other so that the total induced drag actually experienced by the wing coincides with the component in the flight direction. For the oblique wing, the lack of symmetry introduces a side component of the induced drag whose section magnitude is given by

$$(d_i)_y = d_i \sin\Lambda = d_{i_0} \tan\Lambda \tag{3.13}$$

Therefore, for the case of the left wing forward, the side force contribution due to the induced drag of the wing is

$$(F_y) = - (D_i)_0 \tan\Lambda \tag{3.14}$$

In addition to the side force $(F_y)_D$ due to the drag component in the y direction, a second term must be introduced when the wing is swept and at an angle of attack. The wing rotates perpendicularly to x_b and, therefore, parallel to z_b (Fig. 3.3).

Let us now consider the wing position w.r.t. the stability axes for the case $\alpha_0 \neq 0$ and $\Lambda \neq 0$ (Fig. 3.3). This position can be better visualized by considering these two steps: 1) a rotation of the aircraft about its $y_s \equiv y_b$ axis by an angle α_0 ; 2) a rotation of the wing

about z_b by an angle Λ. The final position of the wing is no longer parallel to the y_s axis, the left (forward) tip being higher than the aft one. By idealizing the wing with a straight line and considering its projection y_3 onto the z_s, y_s plane, we define the angle γ_0 (Fig. 3.3b). The lift vector being by definition perpendicular to the wing axis and to the velocity (parallel to x_s), will therefore be banked by an angle producing a contribution (positive in this case) to the side force. This feature would not be present in a flying wing since, by banking the wing by γ_0, it would be possible to realign lift and gravity, whereas in a conventional configuration the lift produced by the tail and the different inertia properties produce a somewhat more complex picture.

We can now quantify this side force for the case of a straight rigid wing, by introducing some geometric considerations.

Let us consider the wing for $\alpha_0 = \Lambda = 0$ and assume for simplicity that our stability axes have their origin at the wing pivot; in this case the y_s axes would be aligned with the wing span.

Let us now rotate α_0 about y_s; we obtain the set of axes x_b, y_b, z_b, where $y_b = y_s$ is still aligned with the wing span.

The rotation matrix for such transformation is

$$\begin{bmatrix} x_b \\ y_b \\ z_b \end{bmatrix} = \begin{bmatrix} \cos\alpha_0 & 0 & -\sin\alpha_0 \\ 0 & 1 & 0 \\ \sin\alpha_0 & 0 & \cos\alpha_0 \end{bmatrix} \begin{bmatrix} x_s \\ y_s \\ z_s \end{bmatrix}$$

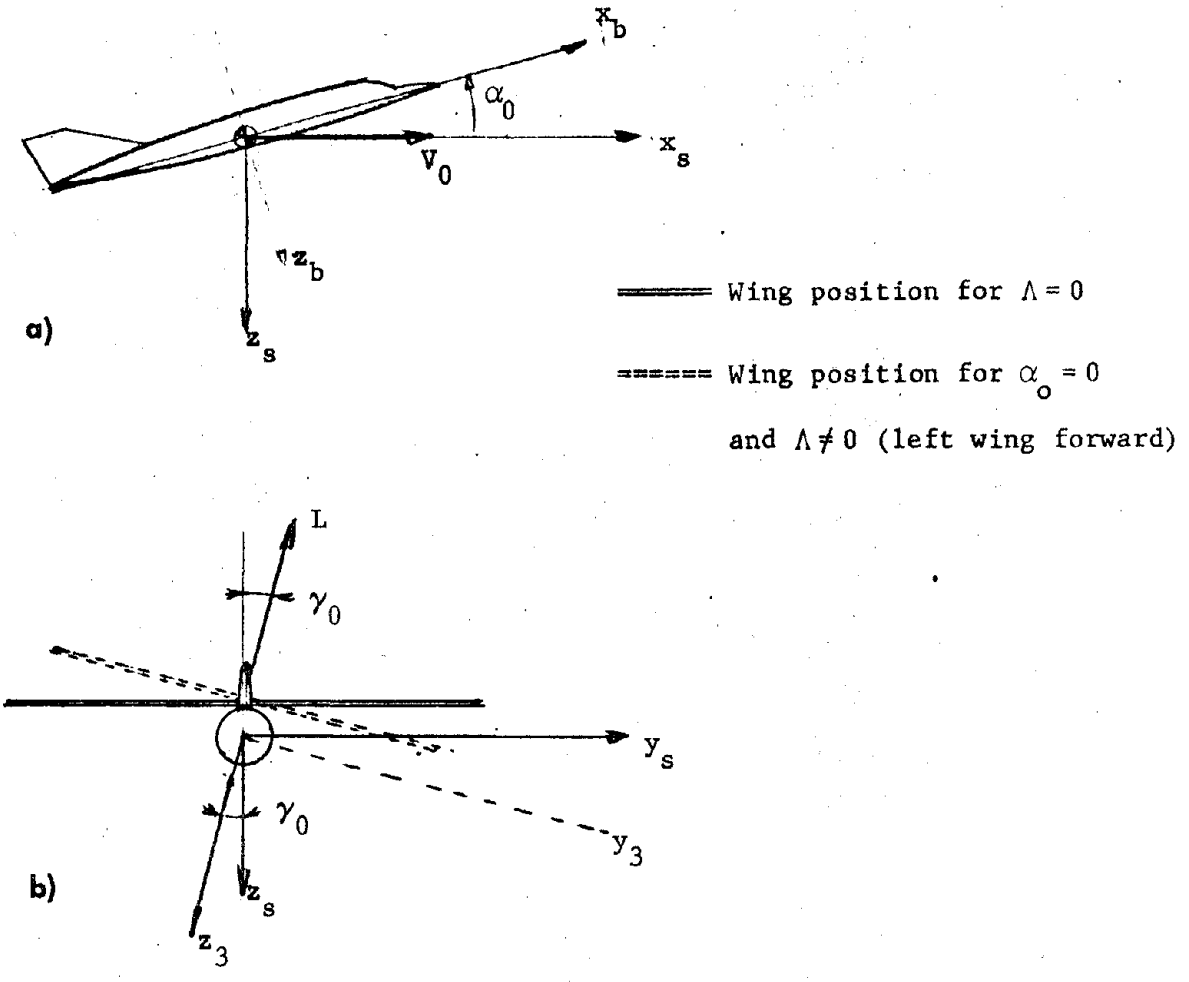

Figure 3.3 - Side Force due to Wing Rotation

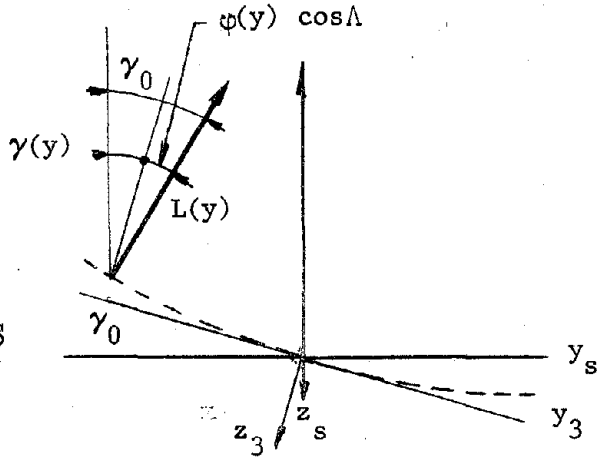

Figure 3.4 - Effects of Wing Bending on Side Force

If we now rotate the wing by Λ about its pivot, the wing axes will be defined by the following matrix transformation

$$\begin{bmatrix} x_w \\ y_w \\ z_w \end{bmatrix} = \begin{bmatrix} \cos\Lambda & \sin\Lambda & 0 \\ -\sin\Lambda & \cos\Lambda & 0 \\ 0 & 0 & 1 \end{bmatrix} \begin{bmatrix} x_b \\ y_b \\ z_b \end{bmatrix} = \begin{bmatrix} \cos\alpha_0 \cos\Lambda & \sin\Lambda & -\sin\alpha_0 \cos\Lambda \\ -\sin\Lambda \cos\alpha_0 & \cos\Lambda & \sin\Lambda \sin\alpha_0 \\ \sin\alpha_0 & 0 & \cos\alpha_0 \end{bmatrix} \begin{bmatrix} x_s \\ y_s \\ z_s \end{bmatrix}$$

$$\begin{bmatrix} x_w \\ y_w \\ z_w \end{bmatrix} = [R] \begin{bmatrix} x_s \\ y_s \\ z_s \end{bmatrix}$$

The lift vector is perpendicular to the plane defined by U_0 and y_w and in terms of the stability axes

$$\bar{U}_0 = U_0 \hat{x}_s \qquad (\wedge \triangleq \text{unit vector})$$

$$\hat{y}_w \text{ (in stability axes)} = [R]^{-1} \begin{bmatrix} 0 \\ 1 \\ 0 \end{bmatrix} = [R]^T \begin{bmatrix} 0 \\ 1 \\ 0 \end{bmatrix} = \begin{pmatrix} -\sin\Lambda \cos\alpha_0 \\ \cos\Lambda \\ \sin\Lambda \sin\alpha_0 \end{pmatrix}$$

Let us define

$$\bar{L} = -L \hat{z}_3$$

where $\hat{z}_3$ is a unit vector $\perp$ to $\hat{x}_s$ and $\hat{y}_w$

or $\hat{z}_3 \cdot \hat{x}_s = 0$

$\hat{z}_3 \cdot \hat{y}_w = 0$

since $\hat{x}_s$ (in stability axes) $= \begin{pmatrix} 1 \\ 0 \\ 0 \end{pmatrix}$ and $\hat{z}_3 = \begin{pmatrix} z_{e_x} \\ z_{3_y} \\ z_{3_z} \end{pmatrix}$ we have

$$z_{3_x} = 0$$

$$\cos\Lambda \, z_{3_y} + z_{3_z} \sin\Lambda \sin\alpha_0 = 0$$

therefore

$$\hat{z}_3 = \begin{pmatrix} 0 \\ -\tan\Lambda \sin\alpha_0 \\ 1 \end{pmatrix} \frac{1}{\sqrt{1+\tan^2\Lambda \sin^2\alpha_0}}$$

We can now define $\hat{y}_3$ to $\hat{x}_s$ and $\hat{z}_3$

$$\hat{y}_3 \cdot \hat{x}_s = 0 \quad = \quad y_{3_x} = 0$$

$$\hat{y}_3 \cdot \hat{z}_3 = 0 \quad \rightarrow \quad - y_{3_y} \tan\Lambda \sin\alpha_0 + y_{3_z} = 0$$

$$\hat{y}_3 = \begin{pmatrix} 0 \\ 1 \\ \tan\Lambda \sin\alpha_0 \end{pmatrix} \frac{1}{\sqrt{1 + \tan^2\Lambda \sin^2\alpha_0}}$$

$$\hat{x}_3 \equiv \hat{x}_s = \begin{pmatrix} 1 \\ 0 \\ 0 \end{pmatrix}$$

The aerodynamic force in the x_3 , y_3 , z_3 reference axes has the following components

$$\overline{F} = \begin{pmatrix} - D \\ (F_y)_D \\ - L_0 \end{pmatrix}$$

We can now express these in terms of our stability axes

$$\begin{bmatrix} F_x \\ F_y \\ F_z \end{bmatrix} = \begin{bmatrix} 1 & 0 & 0 \\ 0 & \dfrac{1}{1+\tan^2\Lambda \sin^2\alpha_0} & \dfrac{-\tan\Lambda \sin\alpha_0}{1+\tan^2\Lambda \sin^2\alpha_0} \\ 0 & \dfrac{\tan\Lambda \sin\alpha_0}{1+\tan^2\Lambda \sin^2\alpha_0} & \dfrac{1}{1+\tan^2\Lambda \sin^2\alpha_0} \end{bmatrix} \begin{bmatrix} - D \\ (F_y)_D \\ - L \end{bmatrix}$$

The value of γ_0 w.r.t. the stability axes x_s , y_s , z_s is found to be

$$\sin \gamma_0 = \frac{\tan\Lambda \sin\alpha_0}{(1 + \tan^2\Lambda \sin^2\alpha_0)} \tag{3.15}$$

and for small angles

$$\gamma_0 = \alpha_0 \tan\Lambda \tag{3.16}$$

The corresponding lift contribution to the side force is

$$(F_y)_L = (L)_{Tot} \sin \gamma_0 \simeq (L)_{Tot} \alpha_0 \tan\Lambda \tag{3.17}$$

All the previous analyses can be extended to the case of a flexible wing having a built-in dihedral (and neglecting the twist contribution) by superposing a correction to the angle (Fig. 3.4)

$$\gamma(y) = \gamma_0 + \varphi(y) \cos\Lambda \text{ (+ bending modes)} \tag{3.18}$$

where

$$\varphi(y) = \text{geometric dihedral at } \Lambda = 0$$

In this case the side force has to be evaluated by means of an integration along y_s. The equilibrium condition may be reached by banking the aircraft by an angle Φ_0 which, in terms of stability axes, corresponds to introducing a gravity component in the y_s direction. For a straight rigid wing with no twist, considering total side force (contribution of the oblique wing itself and contribution of the geometry of the wing rotation) and gravity, the equilibrium equation is

$$Y = (F_y)_D + (F_y)_L + mg \sin \Phi_0 \simeq (L)_{Tot}\ \alpha_0 \tan\Lambda + (F_y)_D + mg \sin \Phi_0$$

$$\Phi_0 \simeq - \frac{1}{mg} \left[(L)_{Tot}\ \alpha_0 \tan\Lambda + (F_y)_D \right]$$

Since for the trimmed condition $(L)_{Tot} = mg$

$$\Phi_0 = - \left[\alpha_0 \tan\Lambda + (F_y)_D \right]$$

3.1.3 Wing Rotation.

Figure 3.5 shows the geometry of the wing rotation about the pivot and the moment arms of the aerodynamic forces with respect to the center of mass (C.G.) of the aircraft.

The aerodynamic force, as assumed in this study, is applied at the quarter chord. Since the wing is straight we can also assume that the line joining all quarter-chord points is straight. Such line is represented by line "m" in the unswept condition, and by line "n" in the

swept one. The moment arm $\bar{x}$ about x_s is used when computing yawing and rolling moments as well as when computing the section perturbation velocity due to rate of pitch and/or rate of yaw.

The moment arm $\bar{y}$, about the y_s axis, is used when computing angular velocities due to rate of pitch and the pitching moments.

In determining the pitch stiffness C_{m_α} [Ref. 21] it is convenient to refer to the quarter-chord line for the unswept case, the moment arm about such line is indicated by y_{MAC}.

Since the wing rotation affects the magnitude of the above moment arms, it will also modify the magnitude of all aerodynamic moments.

The wing rotation also affects the position of the ailerons with respect to the aircraft centerline. Figure 3.6 shows the ailerons and section of wing which is affected by their deflection. Figure 3.6a shows the case for zero sweep. The shadowed area is defined by two straight lines aligned with the free stream velocity V_{T0} passing through the aileron's outer and inner stations. When the wing is swept, (Fig. 3.6b) we can notice that the two straight lines defining the area affected by the aileron are now passing to the left of the corresponding point on the quarter chord line for the unswept case.

The result of this is an increase in the moment arm about the longitudinal axis for the left aileron, and a decrease in the moment arm for the right wing. The position of the pivot behind the quarter chord line will reduce and eventually eliminate such an effect.

By simple geometric considerations, we can compute the quantities

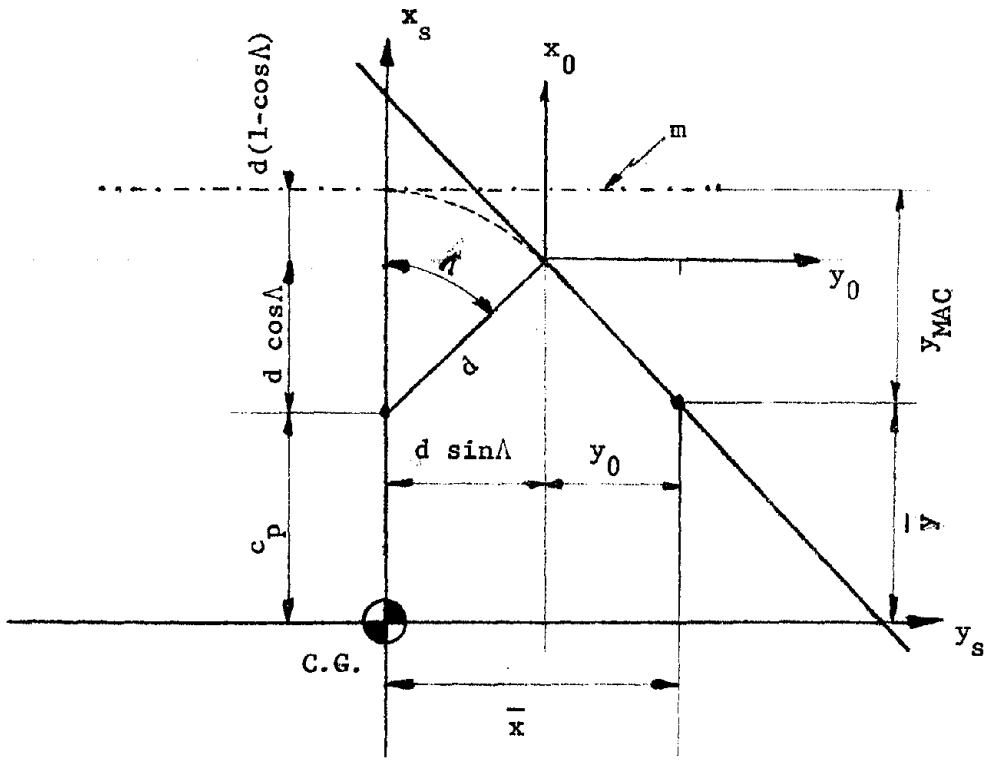

x_s , y_s = stability axes

x_0 , y_0 = axes parallel to stability axes centered at wing root quarter-chord.

c_p = pivot-C.G. distance

d = pivot quarter-chord distance

$\bar{x}$ = moment arm about x_s

$\bar{y}$ = moment arm about y_s

y_{MAC} = moment arm about m (quarter-chord line for $\Lambda = 0$)

Geometric expressions for the moment arms:

$$\bar{x} = y_0 \tan\Lambda + d \sin\Lambda$$

$$\bar{y} = c_p + d\cos\Lambda - y_0 \tan\Lambda$$

$$y_{MAC} = c_p + d(\cos\Lambda - 1) - y_0 \tan\Lambda$$

Figure 3.5 - Geometry of Wing Rotation and Moment Arms

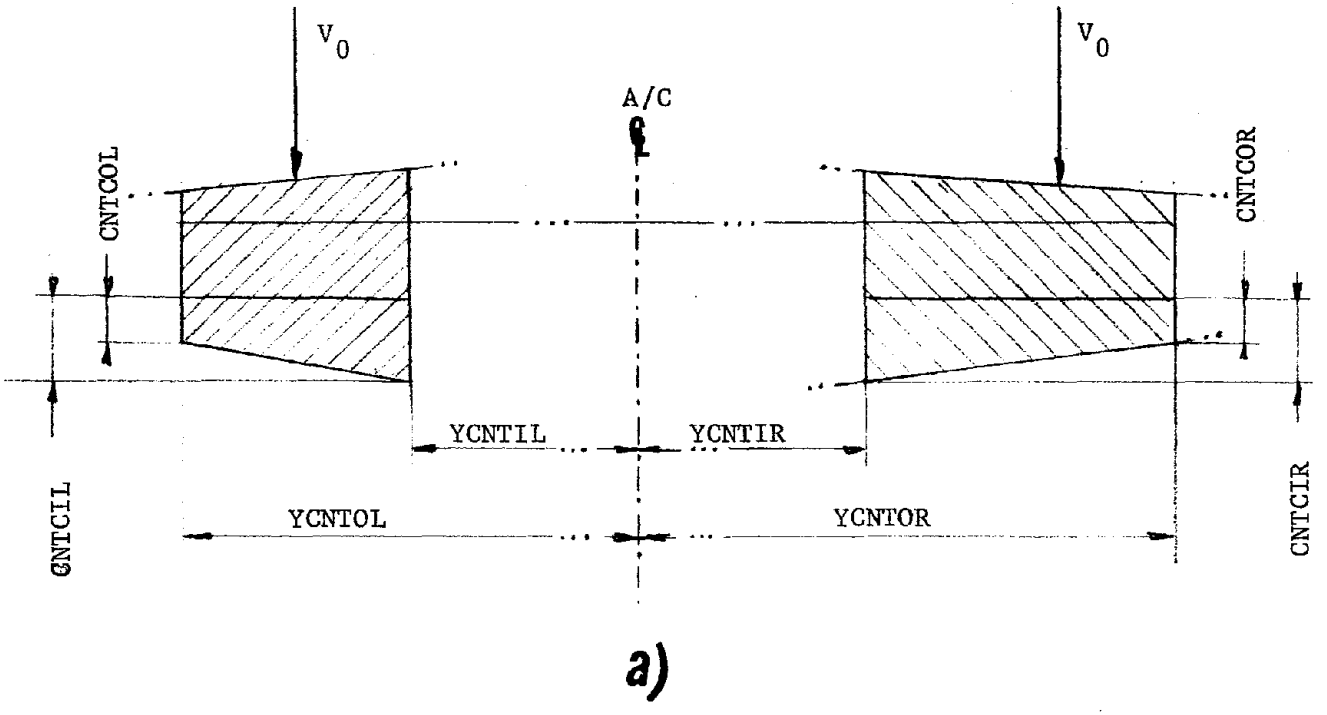

Figure 3.6 - Influence of Wing Rotation on Ailerons Geometry

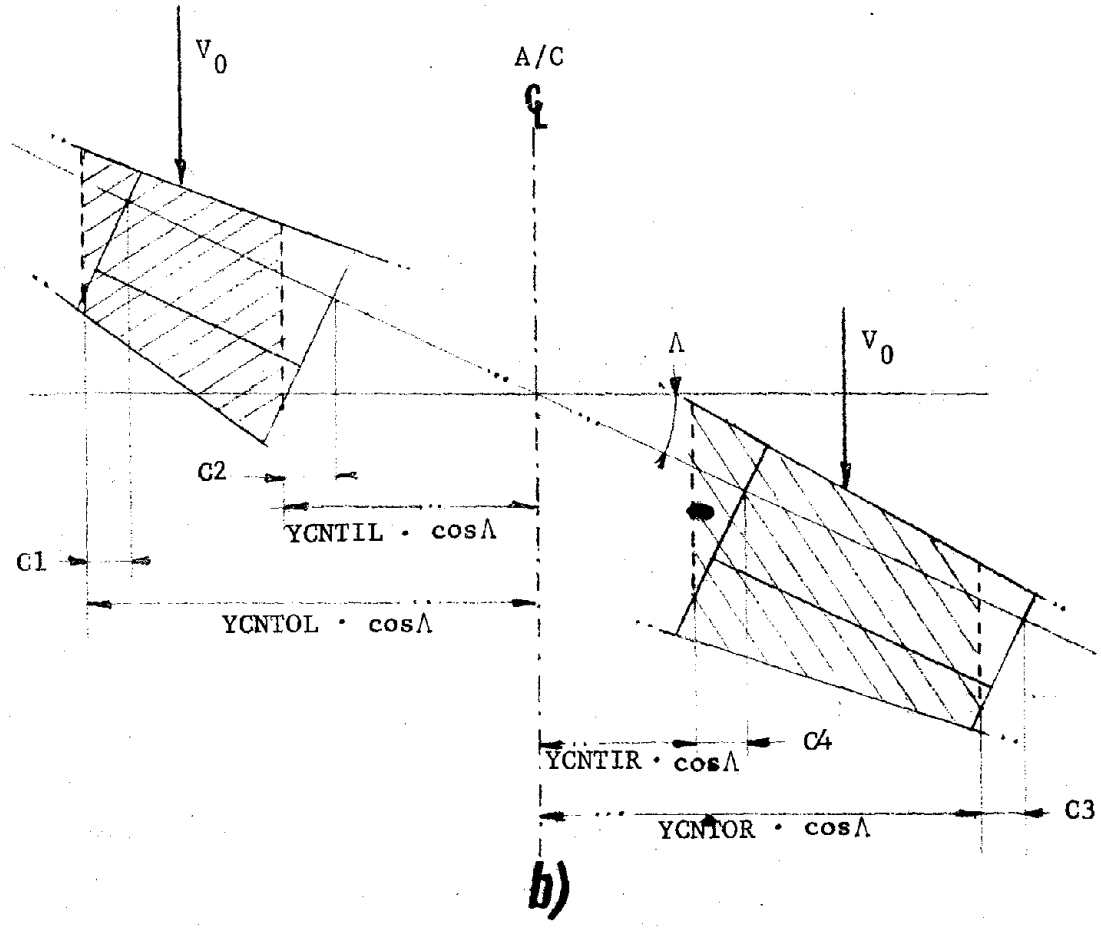

Figure 3.6 Influence of Wing Rotation on Ailerons Geometry

C_1 and C_2, C_3 and C_4 (C_3 and C_4 being the same as C_1 and C_2 for the case when the ailerons are symmetric with respect to the wing centerline).

3.2 Derivatives

3.2.1 General Methodology.

The perturbation quantities considered in a stability analysis are:

- velocity in the x direction: u
- velocity (sideslip) in the y direction: v
- velocity in the z direction: w
- rate of roll (or angular velocity about the x axis): p
- rate of pitch (or angular velocity about the y axis): q
- rate of yaw (or angular velocity about the z axis): r .

Of these quantities, the second and third are generally normalized with respect to the free stream velocity V_{T0}. In doing so the new perturbation quantities are

$$\alpha \triangleq \frac{u}{V_{T0}} \qquad \beta \triangleq \frac{v}{V_{T0}} \tag{3.20}$$

which correspond respectively to a change in the angle of attack and a change in the sideslip angle as can be seen in Figure 3.7.

While the effects of a perturbation u, β, or r must be considered separately, the perturbations p and q can be dealt with in the same fashion as for α, since in fact they all affect the local angle of attack, as will be shown in the next section.

We shall now describe the general methodology for evaluating the

$$\alpha \simeq \tan\alpha = \frac{w}{V_{TO}}$$

$$V = \sqrt{V_{TO}^2 + w^2} \simeq V_{TO}$$

$$\beta \simeq \tan\beta = \frac{v}{V_{TO}}$$

$$V' = \sqrt{V_{TO}^2 + v^2} \simeq V_{TO}$$

Figure 3.7 - Perturbation Angles

stability derivatives in a systematic way according to the previous subdivision; a much more complete discussion can be found in References 15, 21, and 22. Such methodology applies to dimensional stability derivatives.

We refer to Appendix A for the relationship between non-dimensional and dimensional derivatives, and to Appendix B for detailed calculations of the non-dimensional stability derivatives.

3.2.2 α , p , q Derivatives.

Let us now concentrate on a section of our wing. Whenever we consider a positive perturbation α in the local angle of attack, the wing actually experiences a new perturbation velocity w . The result of this velocity w is that the free stream velocity becomes V having a new direction which differs by an angle α from the previous one. Consequently, the lift and drag components of the aerodynamic force must now be referred to this new direction. This result is shown in Figure 3.8.

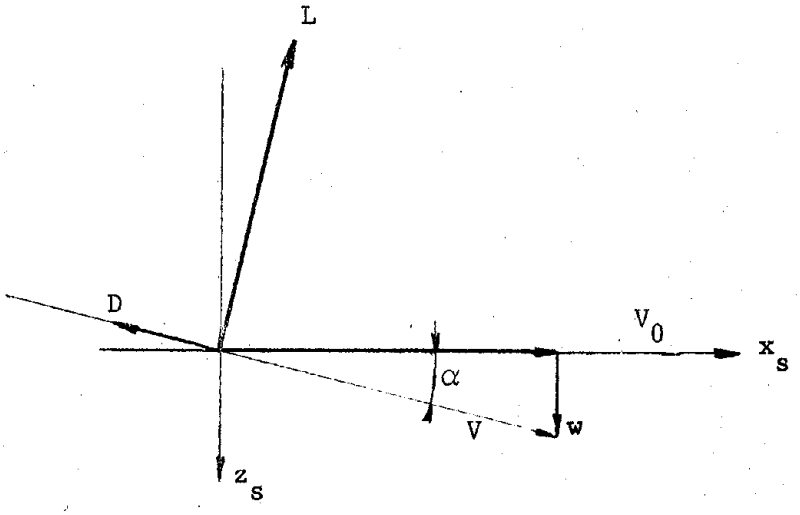

Figure 3.8 Section lift and drag force for an α perturbation.

Let us now evaluate the forces with respect to the stability axes system for this perturbed case.

$$
\begin{aligned}
X &= \ell \sin\alpha - \bar{d} \cos\alpha \simeq \ell\, \alpha - \bar{d} \\
Y &= \ell\, \gamma - \bar{d} \tan\Lambda \\
Z &= - \ell \cos\alpha - \bar{d} \sin\alpha \simeq [\ell + \bar{d}\, \alpha]
\end{aligned}
\tag{3.21a}
$$

and the corresponding moments are:

$$
\begin{aligned}
\mathcal{L}_S &= Z \bar{x} \\
M_S &= -Z \bar{y}_{MAC} \\
N_S &= -X \bar{x} + Y\bar{y}
\end{aligned}
\tag{3.21b}
$$

For the equilibrium case, the equations are

$$
\begin{aligned}
X_0 &= - \bar{d}_0 \\
Y_0 &= \ell_0\gamma_0 - \bar{d}_0 \tan(\Lambda) \\
Z_0 &= - \ell_0 \\
\mathcal{L}_S &= Z_0 \bar{x} \\
M_{0_S} &= -Z_0 \bar{y}_{MAC} \\
N_{0_S} &= -X_0 \bar{x} + Y_0\bar{y}
\end{aligned}
\tag{3.22}
$$

The changes due to the perturbation α are therefore given by

$$
\begin{aligned}
\Delta X &= X - X_0 = \ell\, \alpha - \Delta\bar{d} \\
\Delta Y &= \ell\gamma - \ell_0\gamma_0 - \Delta\bar{d} \tan\Lambda \\
\Delta Z &= \Delta\ell + \bar{d}\alpha \\
\Delta\mathcal{L}_S &= \Delta Z\bar{x} \\
\Delta M_S &= - \Delta Z\bar{y}_{MAC} \\
\Delta N_S &= - \Delta X\bar{x} + \Delta Y\bar{y}
\end{aligned}
\tag{3.23}
$$

Because of the small perturbation assumption these equations can be linearized by expanding them in a Taylor series about the equilibrium condition (or $\alpha = 0$) and retaining only the first-order terms. For the first equation, this approach leads to

$$\Delta X = \frac{\partial}{\partial \alpha}\left[\ell\alpha - \Delta \bar{d}\right]_{\alpha=0} \alpha \tag{3.24}$$

and the same can be done for the other equations.

This is the classical assumption of linear aerodynamic theory which is to accept the following approximation for stability derivatives:

$$A_b = \left(\frac{\partial A}{\partial b}\right)_{b=0} \tag{3.25}$$

where

A = any aerodynamic force (or moment)

b = any perturbation quantity.

Consequently, the stability derivatives at our section for a perturbation α are given by

$$X_\alpha = \left(\frac{\partial X}{\partial \alpha}\right)_{\alpha=0} \quad ; \quad Y_\alpha = \left(\frac{\partial Y}{\partial \alpha}\right)_{\alpha=0} \quad ; \quad Z_\alpha = \left(\frac{\partial Z}{\partial \alpha}\right)_{\alpha=0}$$

$$\mathcal{L}_{S_\alpha} = Z_\alpha \bar{x} \quad ; \quad M_{S_\alpha} = Z_\alpha \bar{y}_{MAC} \quad ; \quad N_{S_\alpha} = X_\alpha \bar{x} + Y_\alpha \bar{y} \tag{3.26}$$

where

$$X_\alpha = \left[\frac{\partial}{\partial \alpha}\left(\ell\,\alpha - \Delta\bar{d}\right)\right]_{\alpha=0} = \left[\ell + \frac{\partial \ell}{\partial \alpha}\,\alpha - \frac{\partial \bar{d}}{\partial \alpha}\right]_{\alpha=0} = \ell_0 - \left(\frac{\partial \bar{d}}{\partial \alpha}\right)_{\alpha=0} \tag{3.27}$$

$$Y_\alpha = \left[\frac{\partial}{\partial\alpha}\left(\ell\gamma - \ell_0\gamma_0 - \Delta\bar{d}\,\tan\Lambda\right)\right]_{\alpha=0}$$

$$= \left[\frac{\partial\ell}{\partial\alpha}\gamma + \ell\frac{\partial\gamma}{\partial\alpha} - \frac{\partial\bar{d}}{\partial\alpha}\tan\Lambda\right]_{\alpha=0} = \ell_\alpha\gamma_0 + \ell_0\frac{\partial\gamma}{\partial\alpha} - \frac{\partial\bar{d}}{\partial\alpha}\tan\Lambda \tag{3.28}$$

$$Z_\alpha = \left[\frac{\partial}{\partial\alpha}\left(\ell + \bar{d}\alpha\right)\right]_{\alpha=0} + \left[\frac{\partial\ell}{\partial\alpha} + \frac{\partial\bar{d}}{\partial\alpha}\alpha + \bar{d}\right]_{\alpha=0} = \ell_\alpha + \bar{d}_0 \tag{3.29}$$

$$\frac{\partial\gamma}{\partial\alpha} = \frac{\partial}{\partial\alpha}\left[\alpha\tan\Lambda + \text{const terms}\right]_{\alpha=0} = \tan\Lambda \tag{3.30}$$

The same approach can be used when studying α_p and α_q perturbations. In both cases the perturbation will produce a change in the angle of attack. Such change will no longer be constant along the span, but will be

$$\alpha_q = \frac{q}{V_{T0}}\bar{y} \tag{3.31}$$

for the pitch, and

$$\alpha_p = \frac{p}{V_{T0}}\bar{x} \tag{3.32}$$

for roll.

Although the distribution in the angle of attack is antisymmetric, the corresponding increment in lift, and consequently drag, because of the shape of the FWLD will not be asymmetric. The asymmetry in lift, case of a symmetric wing in roll, does not produce any variation to the lift vector. Loss of asymmetry introduces a change in the total vertical force Z as well as in X.

The same approach used for the α derivatives can be applied to the evaluation of roll and pitch derivatives.

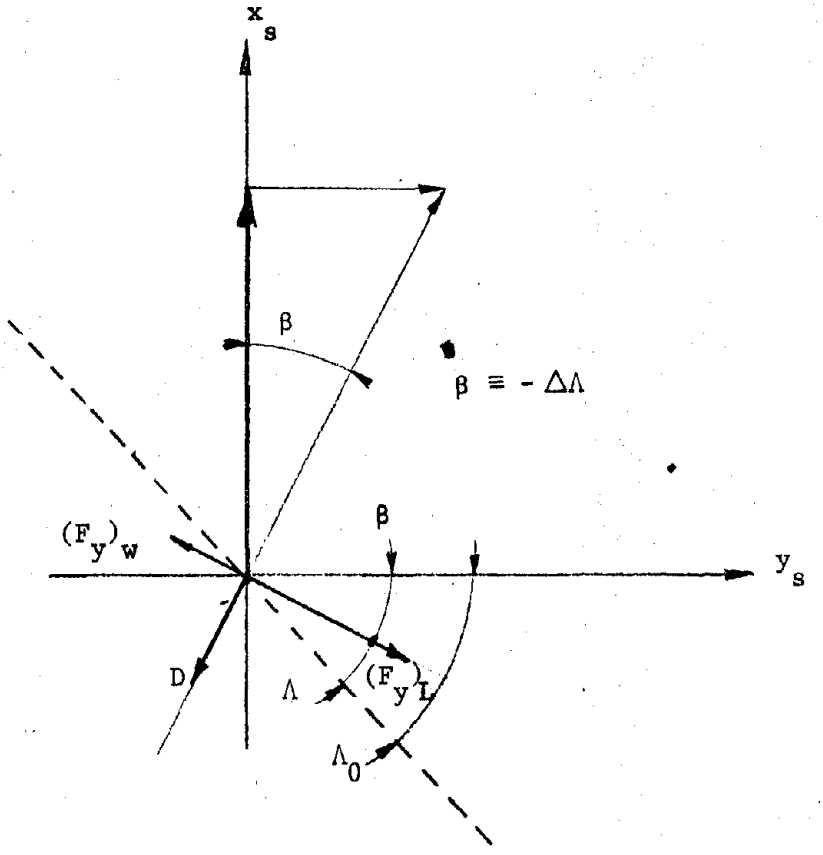

Figure 3.9 - Sideslip

The only differences are:

a) the section perturbation angle of attack which is no longer a constant as in the previous case, but varies according to Eqns. (3.31) and (3.32);

b) the linear operator $\frac{\partial}{\partial \alpha}$ must be replaced, for the pitch by

$$\frac{\partial}{\partial q} = \frac{\partial}{\partial \alpha}\frac{\partial \alpha}{\partial q} = \frac{\bar{y}}{V_{T0}}\frac{\partial}{\partial \alpha} \tag{3.33}$$

and for the roll by

$$\frac{\partial}{\partial p} = \frac{\partial}{\partial \alpha}\frac{\partial \alpha}{\partial p} = \frac{\bar{x}}{V_{T0}}\frac{\partial}{\partial \alpha} \tag{3.34}$$

The angle γ remains unchanged.

The wing aerodynamic derivatives with respect to the stability axes can be obtained by integrating the section values over the span.

3.2.3 β Derivatives.

The effect of introducing a sideslip angle β corresponds to a negative $\Delta\Lambda$ for the wing (Fig. 3.9). Consequently, for the wing

$$\frac{\partial}{\partial \beta} = -\frac{\partial}{\partial \Lambda} \tag{3.35}$$

The evaluation of the β derivatives is not trivial when considering the aerodynamic moments. In this case, because both FWLD as well as the distribution of lift due to twist will be affected, it is not as simple to derive analytic expressions as for the previous cases. A numerical calculation would be possible by considering results at two

different wing sweeps and then comparing them. For the cases where no moments are involved, the total aerodynamic forces considered are

$$F_x = - D \cos\beta - \left[\left(F_y\right)_L + \left(F_y\right)_w\right] \sin\beta \simeq - D - \left|\left(F_y\right)_L + \left(F_y\right)_w\right| \beta$$

$$F_y = - D \sin\beta + \left[\left(F_y\right)_L + \left(F_y\right)_w\right] \cos\beta \simeq - D\beta + \left[\left(F_y\right)_L + \left(F_y\right)_w\right] \tag{3.36}$$

$$F_z = - \left(L\right)_{Tot}$$

In addition, the following approximation can be made.

$$\left(L\right)_{Tot} = \left[\left(L\right)_{Tot}\right]_{\Lambda = 0} \cos^2\Lambda \tag{3.37}$$

$$\left(D\right)_{Tot} = D_0 + \frac{\left(L\right)_{Tot} \left(C_L\right)_{Tot}}{\pi \mathcal{AR}} = D_0 + \left|\left(L\right)_{Tot} \left(C_L\right)_{Tot}\right| \frac{\cos^4\Lambda}{\pi \mathcal{AR}} \tag{3.38}$$

and, since $\mathcal{AR} = \left(\mathcal{AR}\right)_{\Lambda = 0} \cos^2\Lambda$, it is possible to evaluate the β derivatives of these forces.

3.2.4 r Derivatives.

The new yawing derivatives introduced by the oblique wing are due to two factors: a) side force and b) aerodynamic coupling between rolling and pitching moment. A rate of yaw increases the local stream velocity according to the relation

$$\Delta U = - \bar{x} \cdot r \tag{3.39}$$

Therefore, for the dynamic pressure the variation is

$$q(y) = \frac{1}{2}\rho U^2 = \frac{1}{2}\rho(U_0 + \Delta U)^2 = \frac{1}{2}\rho\left(U_0^2 + 2U_0\Delta U + \cancel{\Delta U^2}\right)^{\text{H.O.T.}}$$

$$q(y) = \frac{1}{2}\rho\left(U_0^2 + 2U_0\Delta U\right) \qquad (3.40)$$

Substituting (3.39) into (3.40), we obtain

$$q(y) = q\left(1 - 2\frac{\bar{x}}{U_0}r\right) \qquad (3.41)$$

The linear antisymmetric change in $q(y)$ due to the perturbation r will now affect the aerodynamic forces due to both the flat wing and twist (including effects of dihedral and camber) contributions. Since the antisymmetric variation in $q(y)$ is applied to a symmetric (cruise condition) distribution, the variation in the loading distribution will also be antisymmetric, like for the case of a symmetric aircraft. Therefore, when first order variations only are considered, no changes will occur in the wing total aerodynamic forces, but all three aerodynamic moments will be affected.

Since $q(y)$ is the only term which changes in the expressions for X, Y, and Z, the evaluation of the yaw derivatives is reduced to computing

$$\frac{\partial X}{\partial r} = \frac{X_0}{q}\frac{\partial}{\partial r}\left[q\left(1 - 2\frac{\bar{x}}{U_0}r\right)\right] = -X_0 \cdot 2\frac{\bar{x}}{U_0} \qquad (3.42)$$

and similarly for y, and Z,

$$\frac{\partial Y}{\partial r} = -Y_0\, 2\frac{\bar{x}}{U_0} \qquad (3.43)$$

$$\frac{\partial Z}{\partial r} = - Z_0 \, 2 \, \frac{\bar{x}}{U_0} \tag{3.44}$$

A simple integration over the span of the last three expressions will determine the yaw derivatives of the aerodynamic forces. For the $\mathscr{L}_S$, M_S and N_S moments, the expressions to be integrated are

$$\mathscr{L}_S = - Z_0 \, 2 \, \frac{\bar{x}}{U_0} \, \bar{x}$$

$$M_S = + Z_0 \, 2 \, \frac{\bar{x}}{U_0} \, \bar{y} \tag{3.45}$$

$$N_S = + X_0 \, 2 \, \frac{\bar{x}}{U_0} \, \bar{x} - y_0 \, 2 \, \frac{\bar{x}}{U_0} \, \bar{y}$$

3.3 Summary.

In this Chapter we have introduced and evaluated the two side force contributions, one due to induced drag and one due to wing rotation, that an oblique wing aircraft would experience. The effects of wing rotation were then analyzed. The general methodology for computing stability derivatives was also discussed.

IV EQUATIONS OF MOTION

4.1 Rigid Body

The equations of motion for the aircraft can be derived from Newton's Second Law of Motion, which states that the summation of all external forces acting on a body must be equal to the time rate of change of the momentum of the body, and the summation of the external moments acting on a body must be equal to the time rate of change of the moment of momentum (angular momentum). The time rates of change are all taken with respect to inertial space. These laws can be expressed by two vector equations.

$$\frac{I}{V} = \frac{1}{m}\sum \bar{F} \tag{4.1}$$

$$\frac{I}{H} = \sum \bar{T} \tag{4.2}$$

where I indicates the time rate of change with respect to inertial space.

Now, the external forces and moments consist of equilibrium values plus a perturbation value which stems from a difference from this equilibrium condition. Thus,

$$\begin{aligned} \bar{F} &= \bar{F}_0 + \Delta\bar{F} \\ \bar{T} &= \bar{T}_0 + \Delta\bar{T} \end{aligned} \tag{4.3}$$

In the dynamic analyses to follow, the aircraft is always considered to be in equilibrium before a disturbance is introduced. Thus, $\bar{F}_0$ and $\bar{T}_0$ are identically zero.

The equilibrium forces consist of lift, drag, thrust, and gravity, and the equilibrium moments consist of moments resulting from the lift and drag generated by the various portions of the aircraft and the thrust.

The following observations are made to achieve a linear analysis. First, the aircraft is in an equilibrium condition before perturbation. Second, the mass of the aircraft remains constant during any particular dynamic analysis. Third, it is assumed that the aircraft is a rigid body. Fourth, it is assumed that the earth is an inertial reference and unless otherwise stated, the atmosphere is assumed to be fixed with respect to the earth. The time rate of change of the velocity vector with respect to the earth, in the assumed reference axes, is given by

$$\frac{I}{V} = \frac{S}{V} + \bar{\omega} \times \bar{v} \tag{4.4}$$

where S indicates time rate of change with respect to the assumed reference axes system (non inertial); ω is the angular velocity of the aircraft with respect to the earth; and x signifies the cross product.

Similarly

$$\frac{I}{H} = \frac{S}{H} + \omega \times \bar{H} \tag{4.5}$$

V and w can be written as

$$\begin{aligned} \bar{w} &= \bar{w}_0 + \overline{\Delta w} \\ \bar{V} &= \bar{V}_0 + \overline{\Delta V} \end{aligned} \tag{4.6}$$

where $\overline{w_0}$ and $\overline{V_0}$ represent the steady state conditions and $\overline{\Delta w}$ and $\overline{\Delta V}$ are the perturbation quantities.

Their components in stability axes are:

$$\overline{\omega_0} = \begin{bmatrix} P \\ Q \\ R \end{bmatrix} \qquad \overline{\Delta\omega} = \begin{bmatrix} p \\ q \\ r \end{bmatrix}$$

$$\overline{V_0} = \begin{bmatrix} U_0 \\ V_0 \\ W_0 \end{bmatrix} \qquad \overline{\Delta V} = \begin{bmatrix} u \\ v \\ w \end{bmatrix} \tag{4.7}$$

The angular momentum is given by the dot product of the inertia tensor, I, and the angular velocity vector, ω

$$\overline{H} = \tilde{I} \cdot \overline{\omega} \tag{4.8}$$

and Equation (2.5), $\tilde{I}$ being time invariant because of assumption number four, can be rewritten as

$$\frac{I}{H} = \tilde{I} \cdot \frac{S}{\omega} + \overline{\omega} \times (\tilde{I} \cdot \overline{\omega}) \tag{4.9}$$

The inertia matrix of an oblique wing aircraft differs from the one of a symmetric aircraft because of the non-zero product of inertia I_{xy}. For an oblique wing aircraft, the inertia matrix in body axes is

$$I_b = \begin{bmatrix} I_{xx} & I_{xy} & I_{xz} \\ I_{xy} & I_{yy} & 0 \\ I_{xz} & 0 & I_{zz} \end{bmatrix}$$

Because our stability analysis is based on the stability axes system previously introduced, it is necessary to transform the inertia matrix from body to stability axes. This transformation is carried out in detail in Appendix E.

Because of the transformation the inertia matrix in stability axes

will no longer have a zero I_{yz} . In fact, as shown in Appendix C, it is given by

$$I'_{yz} = - I_{xy} \sin\alpha \tag{4.10}$$

where the prime denotes stability axes.

The equilibrium condition we are going to consider in our analysis is that of straight level flight, therefore

$$P = Q = R = V_0 = W_0 = 0 \tag{4.11}$$

For this condition, after substituting (2.4) into (2.1), and after some algebra, we obtain

$$\frac{1}{m}\bar{F} = \frac{1}{m}\begin{bmatrix} F_x \\ F_y \\ F_z \end{bmatrix} = \underbrace{\begin{bmatrix} \dot{u} \\ \dot{v} + u_0 r \\ \dot{w} - q u_0 \end{bmatrix}}_{\text{linear terms}} + \underbrace{\begin{bmatrix} qw - rv \\ ru - pw \\ vp - qu \end{bmatrix}}_{\text{non linear terms}} \tag{4.12}$$

Similarly, Equation (2.2) becomes

$$\bar{T} = \begin{bmatrix} \bar{\mathcal{L}} \\ \bar{M} \\ \bar{N} \end{bmatrix} = \underbrace{\begin{bmatrix} I'_{xx}\dot{p} + I'_{xy}\dot{q} + I'_{xz}\dot{r} \\ I'_{xy}\dot{p} + I'_{yy}\dot{q} + I'_{yz}\dot{r} \\ I'_{xz}\dot{p} + I'_{yz}\dot{q} + I'_{zz}\dot{r} \end{bmatrix}}_{\text{linear terms}} + \underbrace{\begin{bmatrix} (I'_{xz}q - I'_{xy}r)q + (I'_{zz} - I'_{yy})qr \\ I'_{xz}(r^2 - p^2) + I'_{xy}qr + (I'_{xx} - I'_{zz})pr \\ I'_{xy}(p^2 - q^2) - I'_{xz}qr + (I'_{yy} - I'_{xx})pq \end{bmatrix}}_{\text{non linear terms}} \tag{4.13}$$

It is now necessary to expand the applied forces and moments and to express them in terms of the changes in the forces and moments that cause or result from these perturbations. These latter forces are usually of an aerodynamic and gravitational origin.

If it is assumed that, as the disturbances are small, the partial

derivatives are linear, the differentials can be replaced by the actual increments, and $\bar{F}$ and $\bar{T}$ can be written as

$$\bar{F} = \Delta\bar{F} = \sum_i \left(\frac{\partial \bar{F}}{\partial b_i}\right)_{b_i=0} b_i$$

$$\bar{T} = \overline{\Delta T} = \sum_i \left(\frac{\partial \bar{T}}{\partial b_i}\right)_{b_i=0} b_i \qquad (4.14)$$

where $\left(\frac{\partial \bar{F}}{\partial b_i}\right)_{b_i=0}$ and $\left(\frac{\partial \bar{T}}{\partial b_i}\right)_{b_i=0}$ represent the aerodynamic stability derivatives evaluated at the steady state condition when the perturbation variable b_i is zero.

The linearized set of equations therefore is:

$$\dot{u} = \sum_i \left(\frac{\partial F_x}{\partial b_i}\right)_{b_i=0} b_i$$

$$\dot{v} + u_0 r = \sum_i \left(\frac{\partial F_y}{\partial b_i}\right)_{b_i=0} b_i$$

$$\dot{w} - q u_0 = \sum_i \left(\frac{\partial F_z}{\partial b_i}\right)_{b_i=0} b_i \qquad (4.15)$$

$$I'_{xx}\,\dot{p} + I'_{xy}\,\dot{q} + I'_{xz}\,\dot{r} = \sum_i \left(\frac{\partial \bar{L}}{\partial b_i}\right)_{b_i=0} b_i$$

$$I'_{xy}\,\dot{p} + I'_{yy}\,\dot{q} + I'_{yz}\,\dot{r} = \sum_i \left(\frac{\partial \bar{M}}{\partial b_i}\right)_{b_i=0} b_i$$

$$I'_{xz}\,\dot{p} + I'_{yz}\,\dot{q} + I'_{zz}\,\dot{r} = \sum_i \left(\frac{\partial \bar{N}}{\partial b_i}\right)_{b_i=0} b_i \qquad (4.15)$$

In the set of Equations (4.15) the terms $I'_{xy}\,\dot{q}$ and $I'_{xy}\,\dot{p}$, not present in the case of a symmetric aircraft, introduce the inertia coupling between pitch and roll motions. The terms $I'_{yz}\,\dot{q}$ and $I'_{yz}\,\dot{r}$ have also a coupling effect and seem to make the coupling between longitudinal and lateral dynamics even stronger, but their coupling is only apparent since it depends on our choice of axes system.

In addition to the inertia coupling existing in symmetric wing aircraft between roll and yaw, oblique wing aircraft experience an inertia coupling of pitch and yaw motions. In table 4.1 we report the matrix representation of the set of Equations (4.15) in terms of Laplace transform.

4.2 Effects of Flexibility.

The analysis done so far applies to a rigid aircraft.

Now, it is known that the stability and control characteristics of flight vehicles may be profoundly influenced by the elastic distortions of the structure under aerodynamic load. Many of the important effects of distortion can be accounted for simply by altering the aerodynamic derivatives. The assumption is made that the changes in aerodynamic

$$
\begin{bmatrix}
S - F_{x_u} & -(F_{x_\alpha} + sF_{x_{\dot\alpha}}) & -(F_{x_\beta} + SF_{x_{\dot\beta}}) & -S F_{x_p} & -(F_{x_\theta} + SF_{x_q}) & -F_{x_r} \\
-F_{y_u} & -(F_{y_\alpha} + SF_{y_{\dot\alpha}}) & \left[S(U_0 - F_{y_{\dot\beta}}) - F_{y_\beta}\right] & -\left[S(W_0 + F_{y_p}) + F_{y_\phi}\right] & -SF_{y_q} & U_0 - F_{y_r} + \frac{F_{y_\psi}}{S} \\
-F_{z_u} & \left[S(U_0 - F_{z_{\dot\alpha}}) - F_{z_\alpha}\right] & -(F_{z_\beta} + SF_{z_{\dot\beta}}) & S(V_0 - F_{z_p}) & -S(U_0 + F_{z_q}) & -F_{z_r} \\
-\bar{F}_u & -(\bar{F}_\alpha + s\bar{F}_{\dot\alpha}) & -(\bar{F}_\beta + S\bar{F}_{\dot\beta}) & S(I'_x S - \bar{F}_p) & S(I'_{xy} S - \bar{F}_q) & I'_{xz} S - \bar{F}_r \\
-\bar{M}_u & -(\bar{M}_\alpha + S\bar{M}_{\dot\alpha}) & -(\bar{M}_\beta + S\bar{M}_{\dot\beta}) & S(I'_{yx} S - \bar{M}_p) & S(I'_y S - \bar{M}_q) & I'_{yz} S - \bar{M}_r \\
-\bar{N}_u & -(\bar{N}_\alpha + S\bar{N}_{\dot\alpha}) & -(\bar{N}_\beta + S\bar{N}_{\dot\beta}) & S(I'_{xz} S - \bar{N}_p) & I'_{yz} S^2 - S\bar{N}_q & I'_z S - \bar{N}_r
\end{bmatrix}
\begin{bmatrix} u \\ \alpha \\ \beta \\ p/S \\ \theta \\ r \end{bmatrix}
\triangleq D F_x(s)
$$

TABLE 4.1 Laplace Transform of the Equation of Motion.

loading take place so slowly that the structure is at all times in static equilibrium. This is equivalent to assuming that the natural frequencies of vibration of the structure are much higher than the natural frequencies of the rigid-body motions. Thus, a change in load produces a proportional change in the shape of the vehicle, which in turn influences the load.

When the separation in frequency between the elastic degrees of freedom and the rigid-body motions is not large, then significant inertial coupling can occur between the two. In that case, a dynamic analysis is required, which takes account of the time dependence of the elastic motions.

The elastic motions have no inertial coupling with the rigid-body motions except through $\dot{\tilde{I}}$. However, it has already been assumed, in the previous paragraph, that such time rate is second-order and negligible in the small-perturbation theory.

The only coupling existing between elastic and rigid body motions is due to the aerodynamics.

The aerodynamic derivatives associated with the deformations of the airplane are of two kinds: those that appear in the rigid body equations, and those that appear in the added equations of the elastic degrees of freedom.

In our analysis we shall use a quasi-steady approach neglecting unsteady aerodynamic effects and assuming that only the wing is flexible.

Therefore, we shall also neglect the added equations of the elastic

degrees of freedom and refer to Ashley, Etkin, and Blakelock [15, 21, 22] for the complete study.

In a quasi-steady analysis the effects of flexibility on the wing are basically reduced to static bending and torsion.

Because of this bending, the aerodynamic center shifts forward changing the value of all the aerodynamic moments and their related derivatives. The side force due to lift is also affected. These static effects have been included in our numerical analysis and will be described in that section.

V NUMERICAL ANALYSIS

5.1 Model Description

In the previous chapters we have discussed qualitatively the influence of an oblique wing on the aerodynamics and dynamics of aircraft. In this chapter we shall attempt to quantify these new properties and evaluate their influence on the stability of an oblique wing aircraft.

The aircraft configuration that has been studied is the Boeing single-body yawed wing aircraft model 5.3 (Fig. 5.1), that was studied for NASA [Ref. 24]. Unlike what is shown in Figure 5.1, our analysis, as well as the one done by Boeing, was carried out for the "left wing forward" case. The nominal configuration and flight condition for the simulation were:

Mach number = 0.8

Altitude = 20,000 ft (6096 m)

Gross weight = 400,000 lb (181,440 Kg.)

Wing sweep = 45 degrees

C.G. location = .355 $(\text{M.A.C.})_{\Lambda=0}$ (body station 57.8 m)

The inertia properties being referred to body axes were transformed to the equivalent in stability axes according to the transformation described in Appendix C.

The .355 M.A.C. center of gravity location in the nominal configuration produced a longitudinally unstable vehicle. This condition was selected by Boeing in order to achieve a more satisfactory overall vehicle design; since the design included a longitudinal S.A.S. this was also the case in the Boeing SST design in the subsonic regime.

In the unstable (without SAS) configuration, the normally complex short period roots migrate significantly; one moving to the positive real axis and one combining with the "rolling convergence" root to form a new complex pair in the LHP.

In order to study the effect of the oblique wing under more "normal" conditions, we chose to modify the nominal configuration so as to achieve a stable configuration for the zero sweep ($\Lambda = 0^{o}$) condition. This was accomplished by moving the C.G. forward.

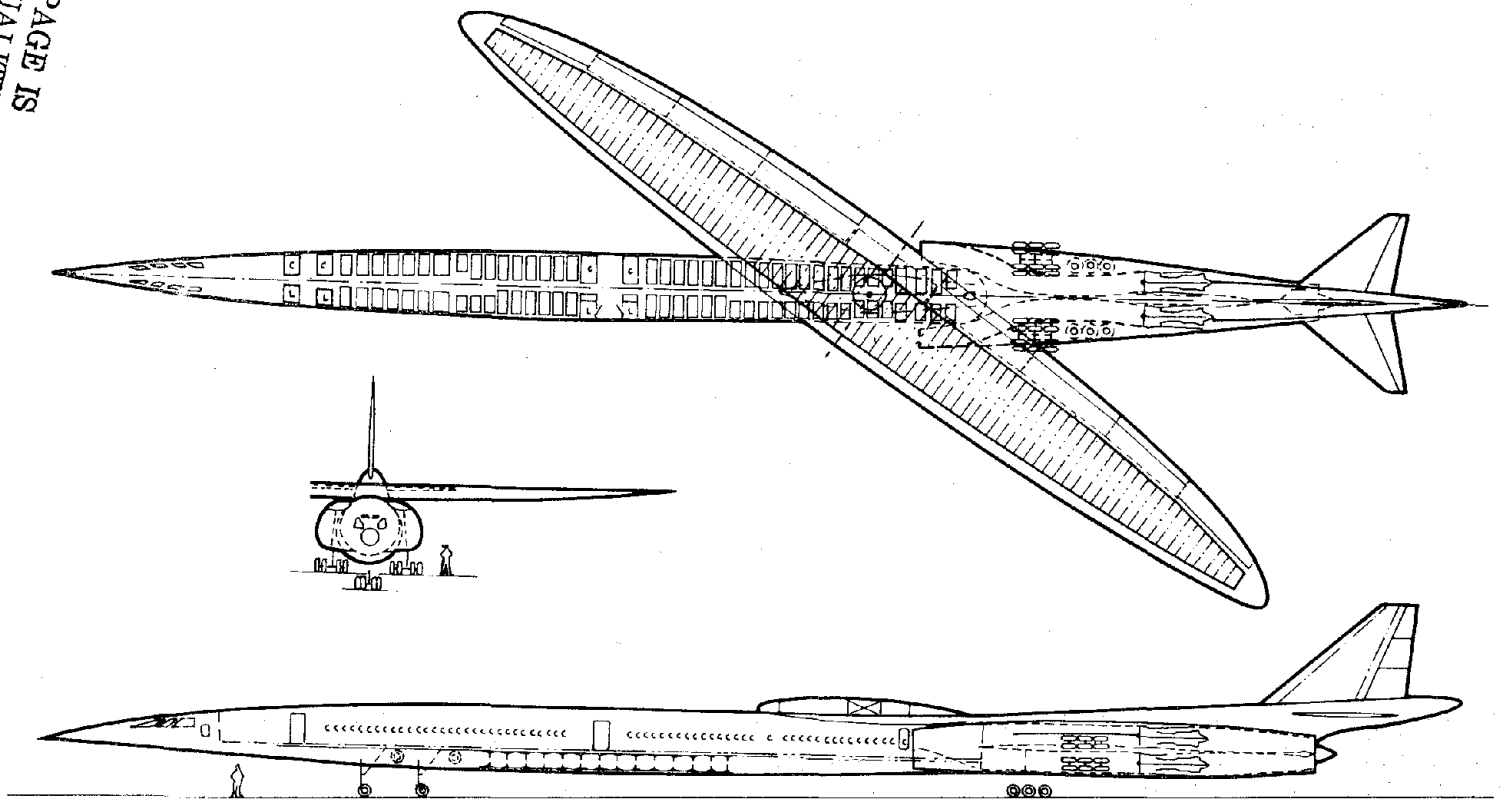

FIGURE 5.1 NASA-BOEING DESIGN FOR OBLIQUE-WINGED TRANSPORT
(Courtesy of NASA)

5.2 Aerodynamic Results

In chapter II we described two different methods for evaluating the spanwise lift distribution for the oblique wing and how to obtain the spanwise induced drag distribution from the knowledge of the lift.

Two numerical programs, based on these two methods, have been written: OWSD/ST computes the stability derivatives for a rigid oblique wing aircraft by means of strip theory; OWSD/LT , instead, applies the linear theory approach and can also include the static effects of a flexible wing.

We shall now report the numerical results obtained with the two methods, for a wing at a skew angle Λ of 45^{o}.

In our strip theory analysis, the wing was assumed to be rigid; therefore, the results obtained with that analysis will be compared against the rigid wing case of linear theory. The, we shall compare the results given by linear theory for the rigid and flexible wing.

5.2.1 Comparison between Strip Theory and Linear Theory (Rigid Case).

Figure 5.2 shows the spanwise lift distribution at $\Lambda = 45^{o}$ as computed by means of the lifting line method, for the flat wing as well as for the case including built-in twist. The twist is linear, and the tip values were chosen so that the resultant lift was acting at the wing centerline. In a real design the airfoil camber distribution would be so that the cruise lift is acting at 50% chord. The assumed twist distribution certainly is not the optimal one, leading to a minimum induced drag, but, at least, it produces no rolling moment

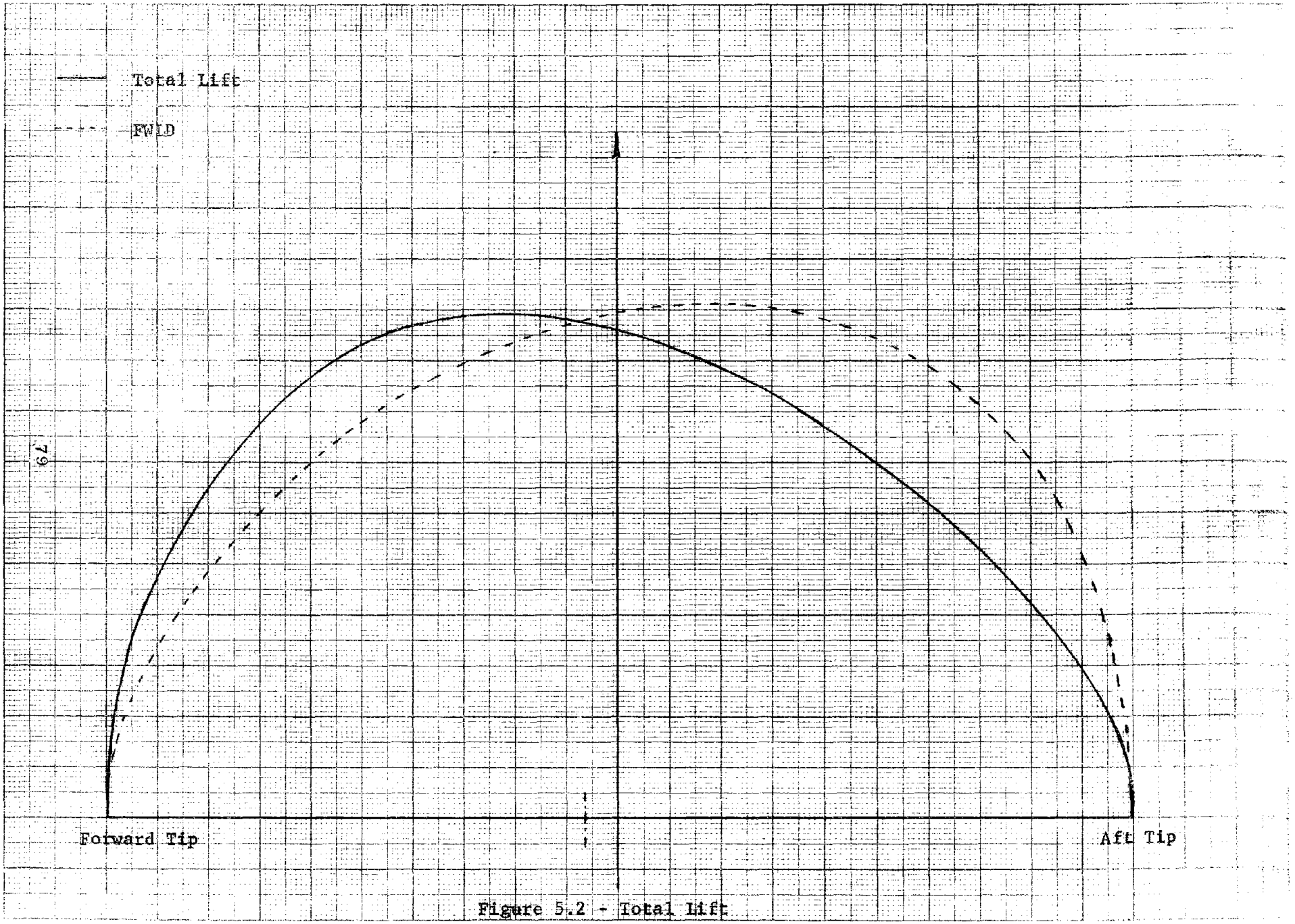

Figure 5.2 - Total Lift

and, for the purposes of our analysis, is a satisfactory cruise condition.

The twist values, for the unswept wing, are

Left tip = + 2.6 degrees

Right tip = - 3.35 degrees

The downwash angles for the flat wing computed by the two methods are shown in Figure 5.3. The lifting line approach (Fig. 5.3a) shows a large variation in the spanwise distribution of the downwash; it also indicates that the right wing, beyond the 60% half span, experiences an upwash which, in terms of horizontal force, results in a thrust.

The induced drag distribution is shown in Figure 5.5 where the negative value corresponds to the thrust mentioned before.

The results obtained by means of strip theory show a slight variation in the downwash angle distribution and the corresponding induced drag distribution appears to be almost symmetric about the wing centerline. The drag distribution, as obtained with the lifting line theory, produces a yawing moment which tends to unskew the wing. This effect is not shown in the results obtained with strip theory.

The tendency to unskew the wing has been experienced also during wind tunnel tests run at NASA-Ames Research Center. Since the model was not a pressure one, it is not possible to tell whether this was due only to a higher drag on the forward wing, or also to a thrust force in the aft one.

The side force distribution (Fig. 5.4) predicted by the two methods differs since the drag terms differ. The side force predicted by the

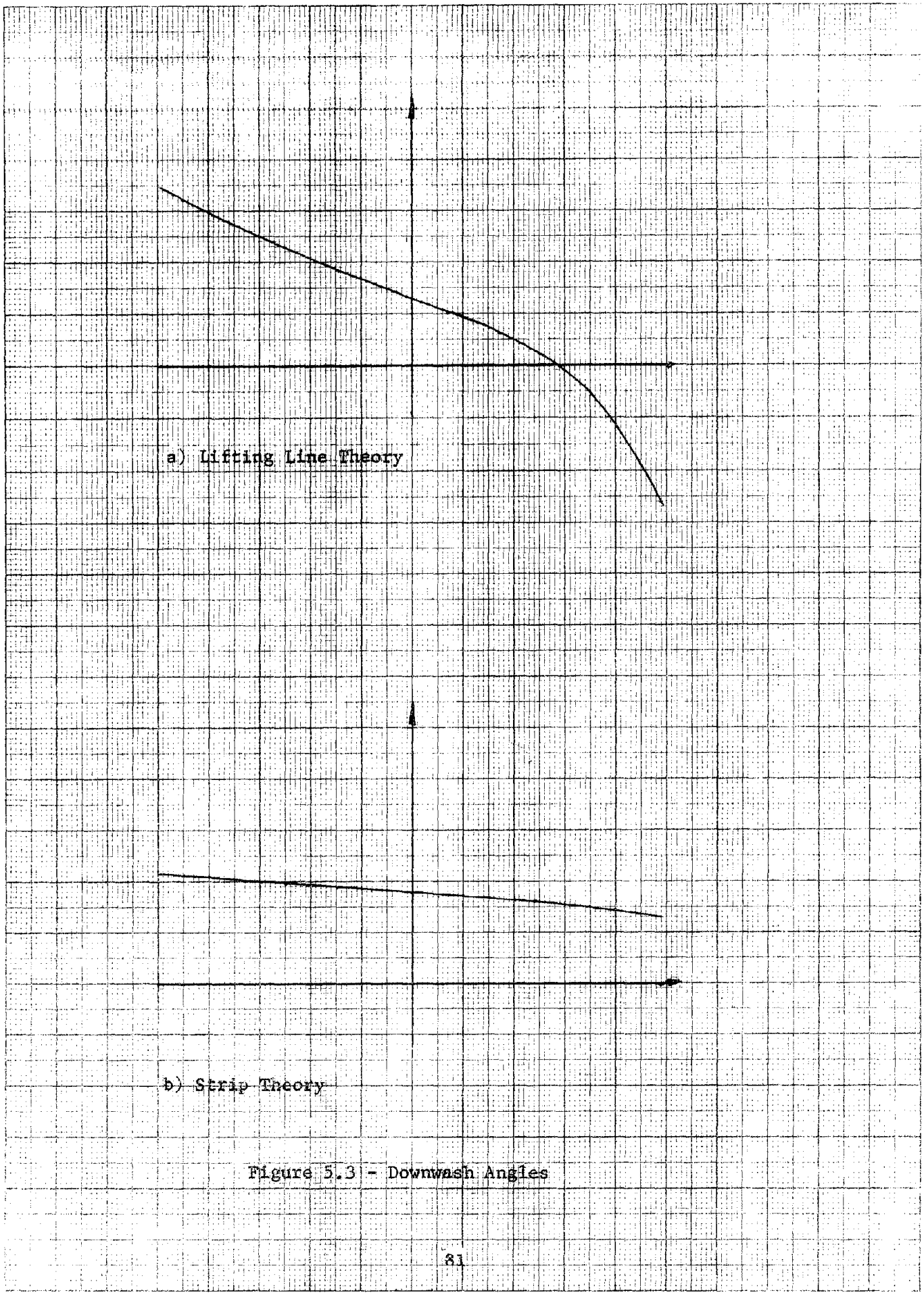

Figure 5.3 - Downwash Angles

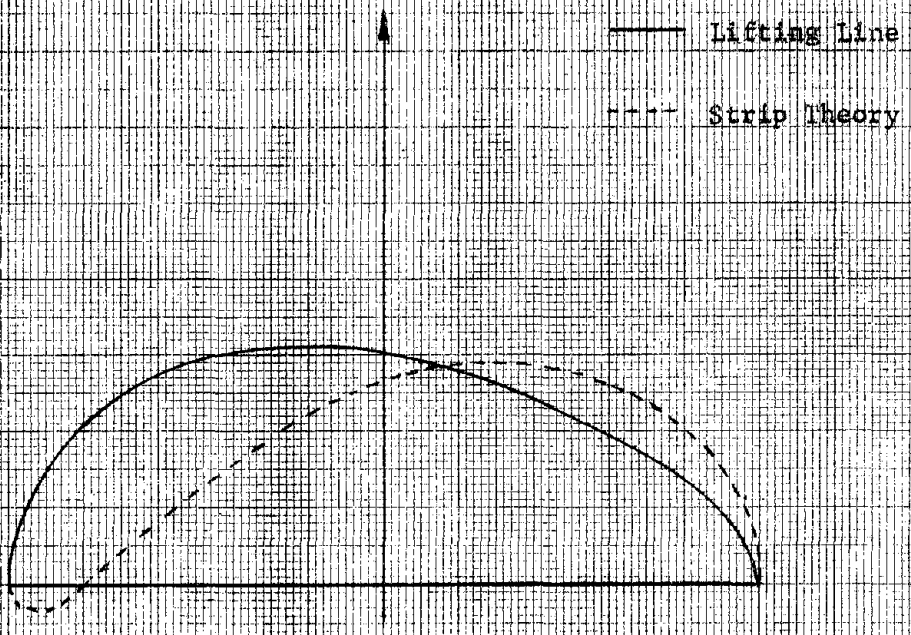

Figure 5.4 - Side Force

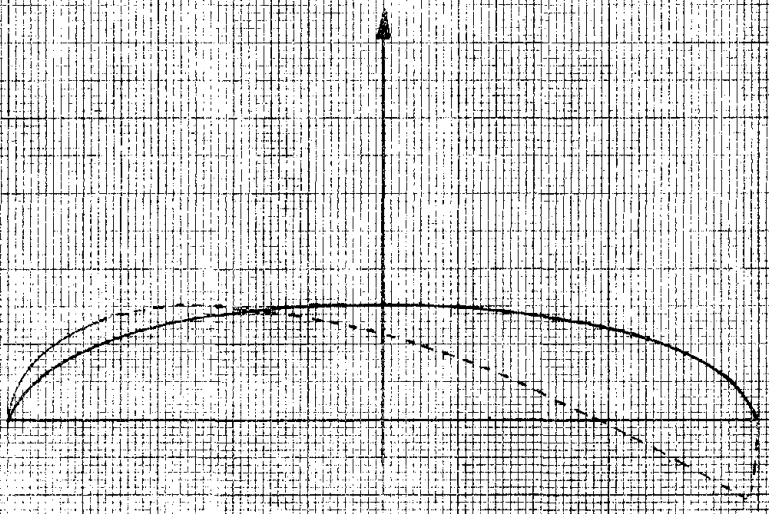

Figure 5.5 - Flat Wing Induced Drag

lifting line theory increases the unyawing moment produced by the drag, instead, the strip theory result shows the opposite effect.

We can therefore conclude that the spanwise induced drag distribution, as computed by means of strip theory, is a poor approximation.

We shall now continue in the comparison between the two methods for the cases when perturbations are considered. Unfortunately, the numerical program computing stability derivatives according to strip theory computes only the nondimensional lift distribution. Thus it is only possible to compare the results obtained with the two methods qualitatively.

The first perturbation quantity considered is α.

Figures 5.6 and 5.7 show respectively the ΔF_x (positive forward) and ΔF_y. For the sake of clarity we recall that, for the perturbed case ΔF_x is given by

$$\Delta F_x \simeq L_0 \alpha - D$$

Figure 5.8 shows the change in lift due to a roll perturbation.

According to strip theory, no change occurs in the lift at the aircraft centerline, whereas the lifting line solution shows, for positive rate of roll, a negative ΔZ at the aircraft centerline.

A greater difference shows up in the change in lift due to a pitch perturbation. This greater difference is also due to the fact that, in the case of strip theory, the vertical velocity introducing the aerodynamic twist is computed at the quarter-chord, whereas, in the lifting line method, it is evaluated at the 3/4-chord point.

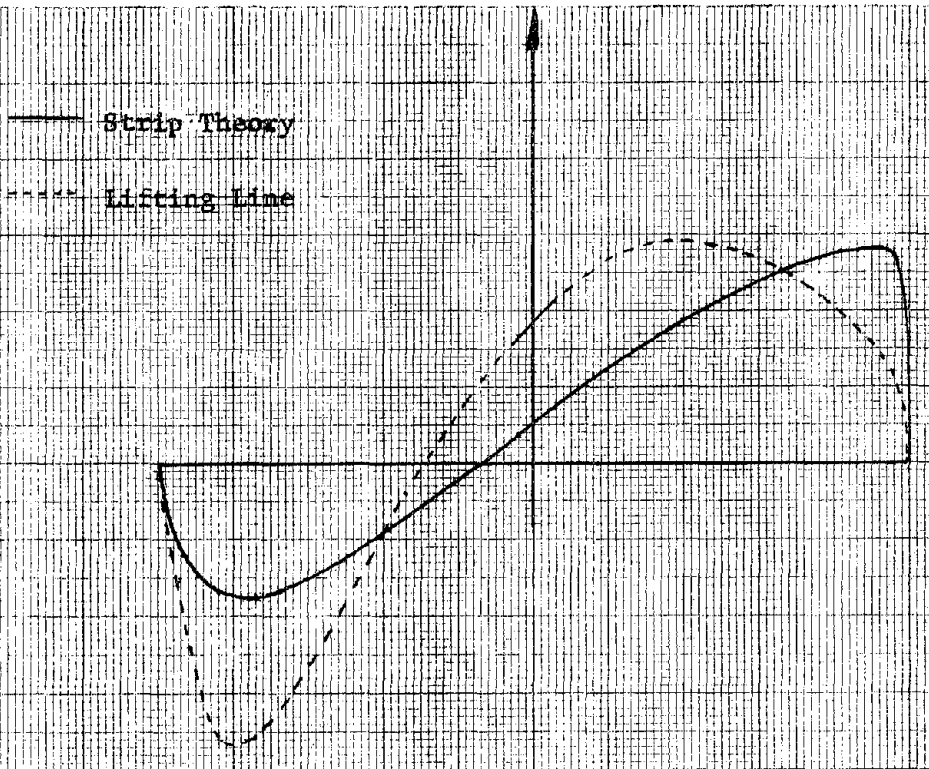

Figure 5.6 - Δx due to α Perturbation.

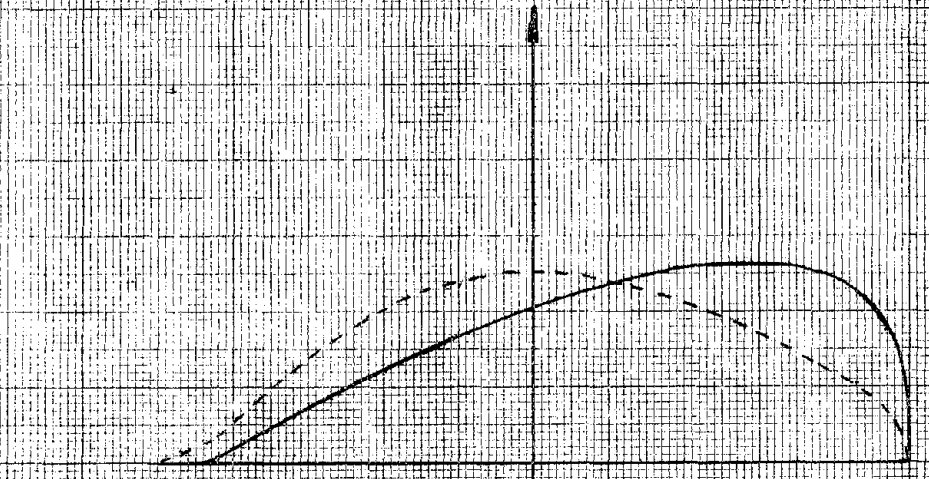

Figure 5.7 - Δy due to α Perturbation.

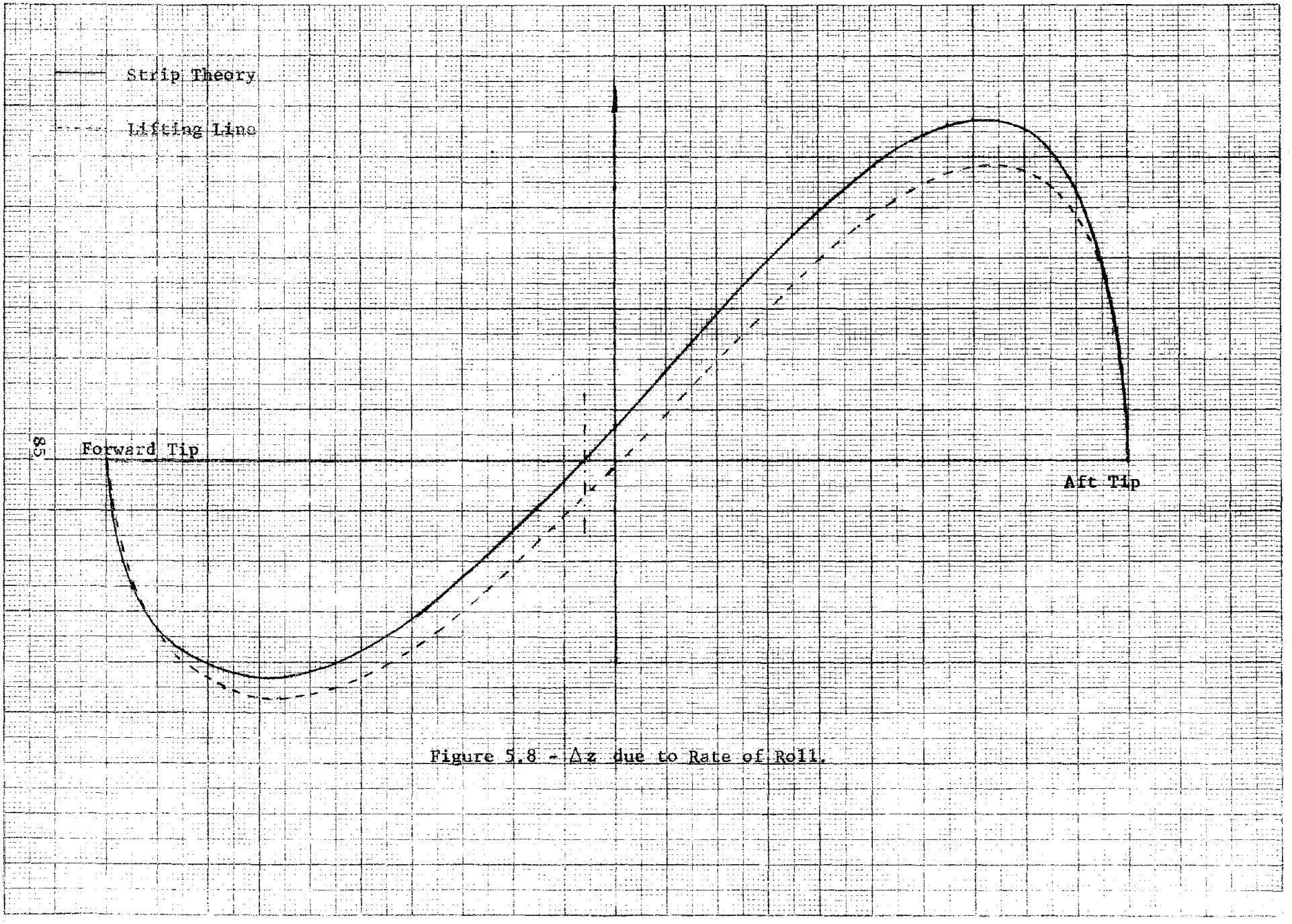

Figure 5.8 - Δz due to Rate of Roll.

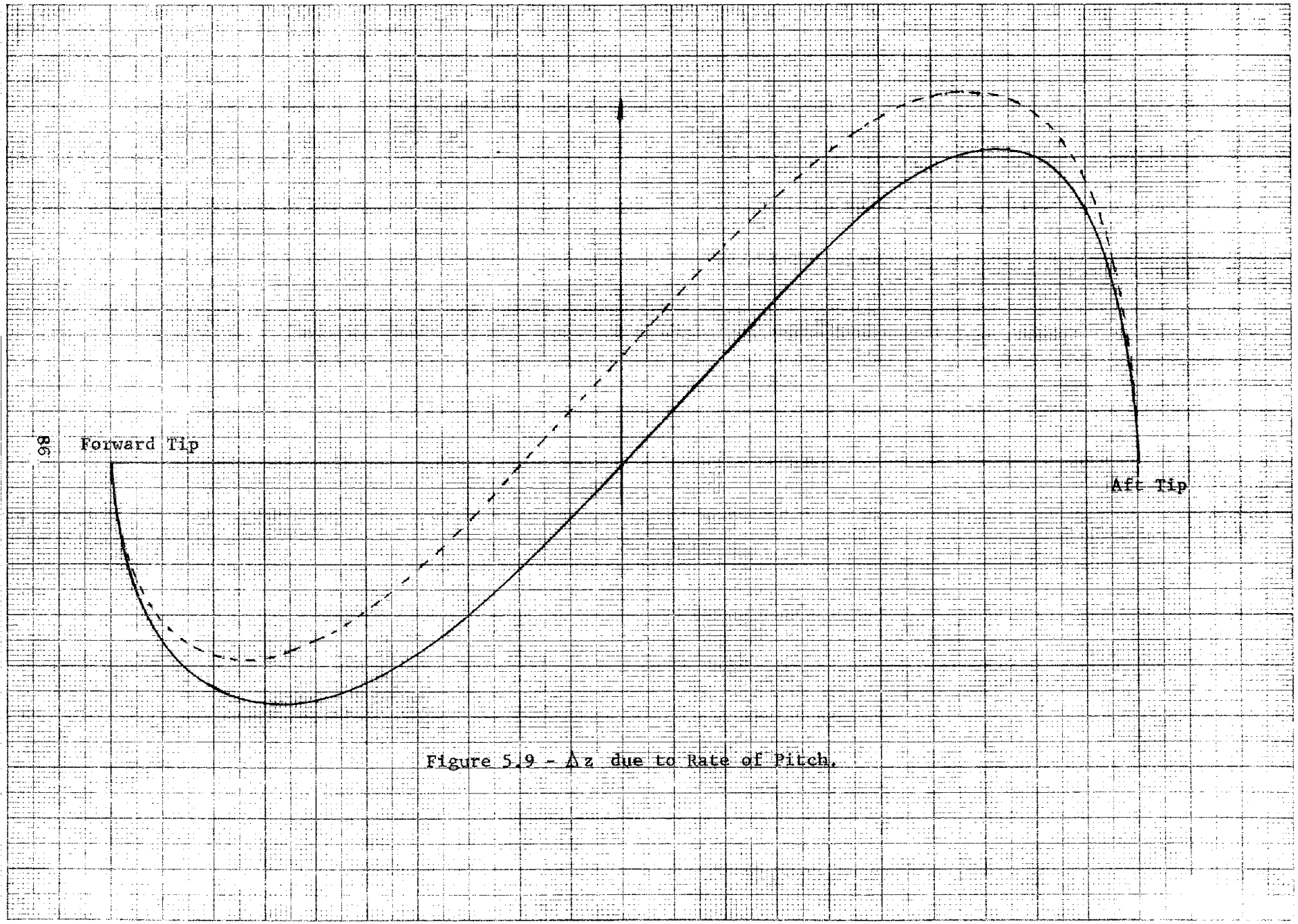

Figure 5.9 - Δz due to Rate of Pitch.

Figure 5.10 - Total Lift for Sideslip (negative).

Figure 5.10 shows the total lift distribution for a negative sideslip of 5 degrees.

We shall return on the sideslip case in the next section, where we discuss in detail the behavior of the oblique wing in sideslip. For the moment, we shall only point out how good the agreement is between the lifting line theory results and those obtained with the empirical method described in section 2.5.

5.2.2 Comparison between Rigid and Elastic Wing (Linear Theory).

The lifting line method described in section 2.4 implies the knowledge of the station 2-D lift slope. For this reason a value for this is considered an input data for the numerical program OWSD/LT. In our analysis the section liftslope has been assumed to be constant along the span. This is not true in most cases and specially for our model, since the thickness to chord ratio varies along the span. The value of the 2-D lift slope has been adjusted so that the wing lift slope coincides with the value computed by Boeing [Ref. 24] in its study. No built-in dihedral was assumed, but only a linear twist was introduced, satisfying (as mentioned in the previous section) the zero rolling moment condition.

In our model, the pivot location (50% root chord) does not coincide with the quarter-chord line (where the lift force is assumed to be acting); therefore, when the wing is skewed, the wing center line does not coincide with the aircraft centerline. For that reason the right wing has a span larger than the left one. Therefore, the lift distribution for the cruise

condition, satisfying the equilibrium condition about the roll axis, can no longer be symmetric in order to balance out this asymmetry in the two semiwings. This asymmetry can be noticed in Figure 5.11 which shows the spanwise lift distribution at $\Lambda = 45^{o}$ (rigid and flexible wing) for this twist distribution and for an angle of attack of 3.75 degrees (.0652 rad.). Since the twist was computed for the rigid wing case, the lift distribution of the elastic wing will produce a strong positive rolling moment. The flat wing case is shown in the next figure (Fig. 5.12) for the same angle of attack.

It is interesting to notice that the flexible wing case produces almost no rolling moment about the aircraft centerline (The resultant lift vector is applied at the quarter-chord station having a distance to the right of the longitudinal axis equal to 0.72 ft).

Such a small difference does not even require a built-in twist, but only a little aileron correction. At this point it should be pointed out that the built-in twist is, for an oblique wing aircraft, a poor design solution. In fact, since the twist measured in the flight direction varies with the cosine of the sweep angle, the twist correction is maximal when the wing is unskewed (and then we do not need any twist correction since the FWLD is symmetric) and decreases when we skew the wing.

A built-in dihedral is, therefore, a far better solution, producing no twist for the unskewed case, and increasing the twist correction when the skew angle increases.

We shall complete the analysis of the cruise condition, as from our

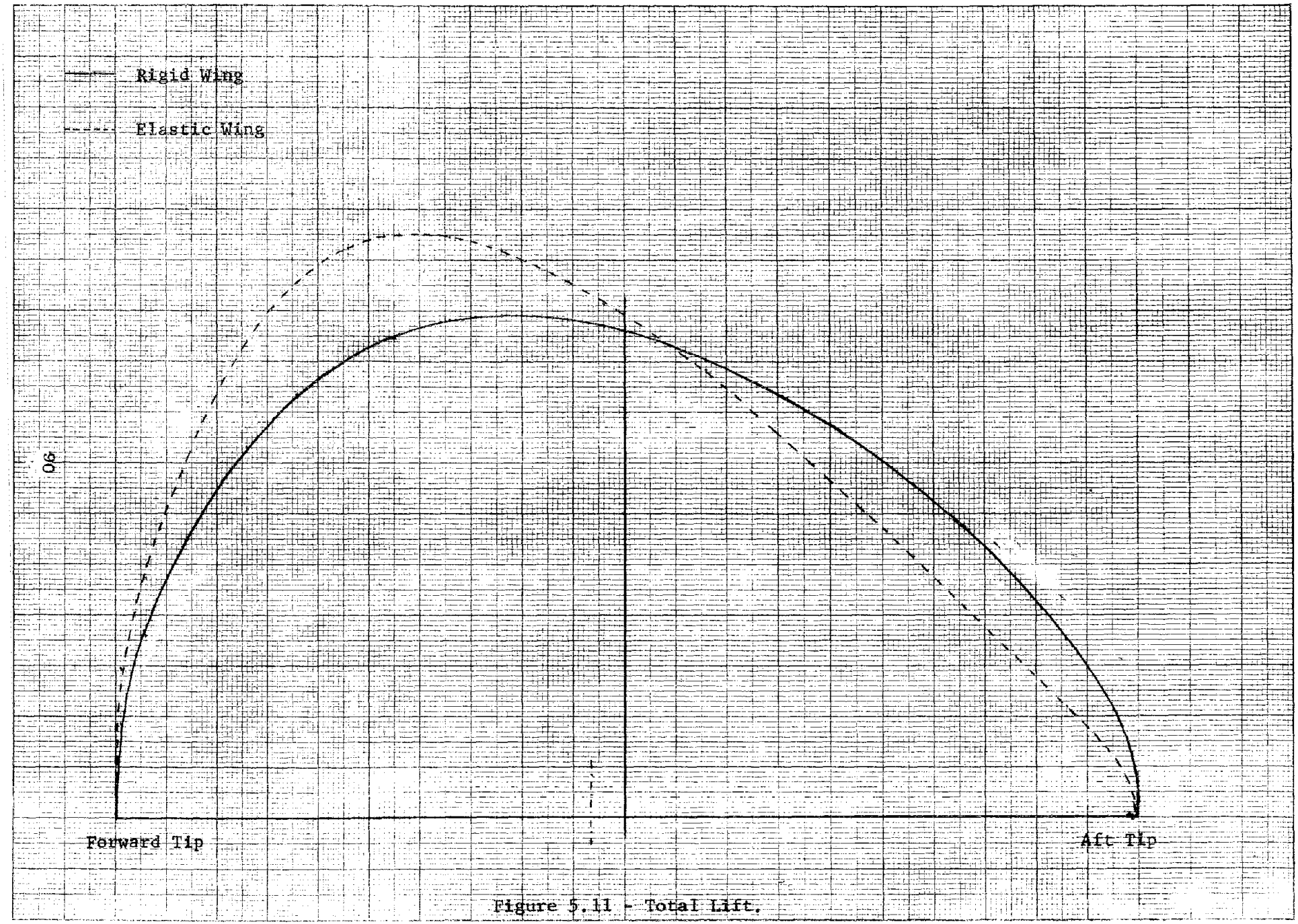

Figure 5.11 - Total Lift.

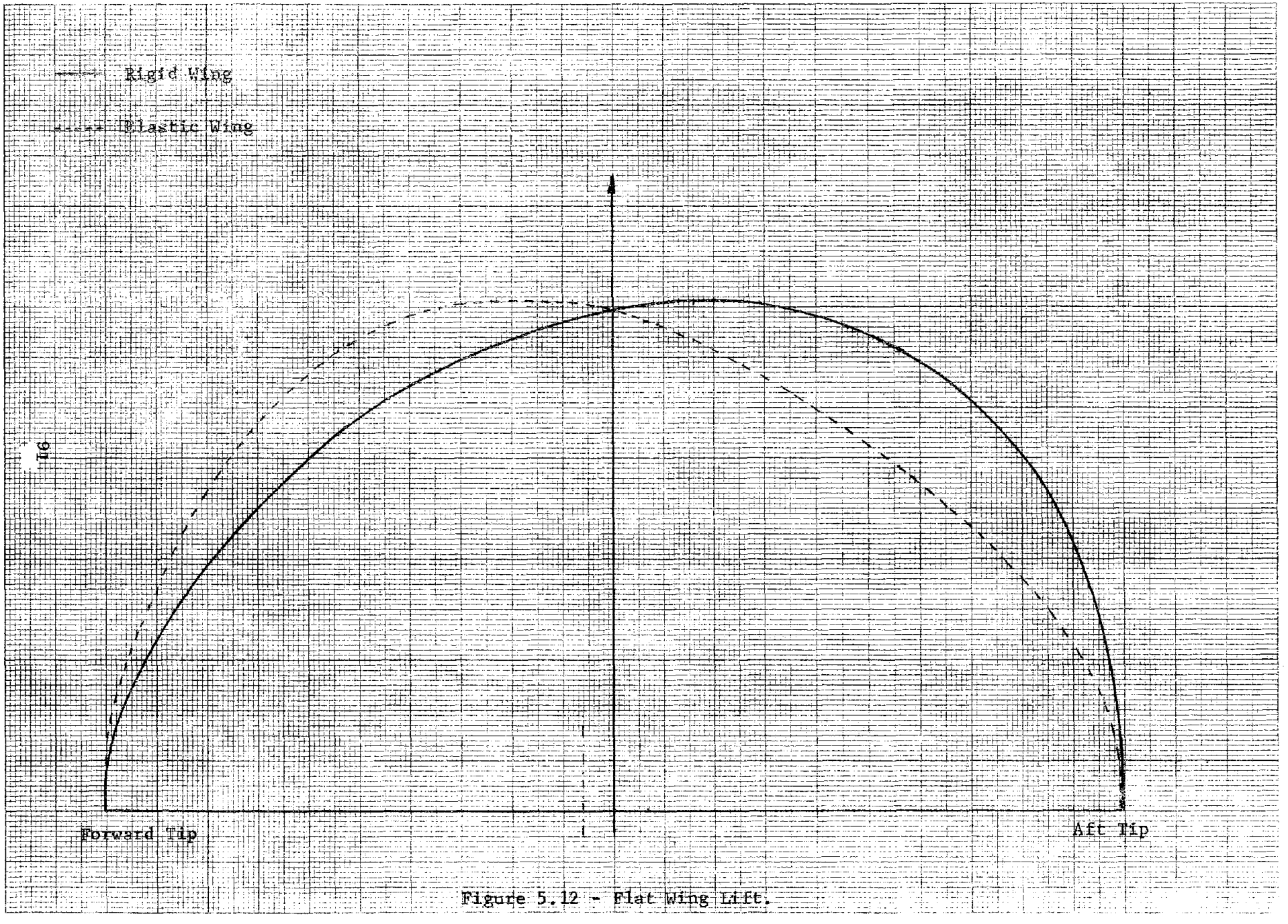

Figure 5.12 - Flat Wing Lift.

numerical model, with Figure 5.13. Figure 5.13a shows the downwash distribution for the flat wing, where the negative values correspond to the upwash. The flat wing drag distribution corresponding to this downwash is shown in Figure 5.13b. The flexible wing shows a much higher drag on the forward (left) wing and a thrust over a larger portion of the aft wing. This is expected; in fact the forward wing, by bending, increases the angle of attack and consequently the lift (this behavior is well known as the divergence problem of a swept forward wing), whereas the opposite happens on the aft one.

The direct consequence of the higher lift of the forward wing is an increase in the upwash velocities induced on the aft one. Instead, for the aft wing, the decrease in lift will result in a decrease in the upwash field induced on the forward one and, consequently, lead toward a further increase in the downwash of the aft wing. These are the reasons why the flexible wing experiences a higher downwash value on the forward wing, and a larger portion of the right one is affected by the upwash velocities.

Then, when we multiply the lift (a positive value) times the corresponding downwash, in order to obtain the spanwise induced drag distribution, we multiply the already greater downwash times a larger value of lift for the left wing. For the right wing, instead, the lift magnitude is smaller and this is the reason why, though affecting a larger portion of the aft wing, the thrust reaches a lower maximum value than the corresponding one for the rigid case.

We shall now continue our comparison analyzing the results for the

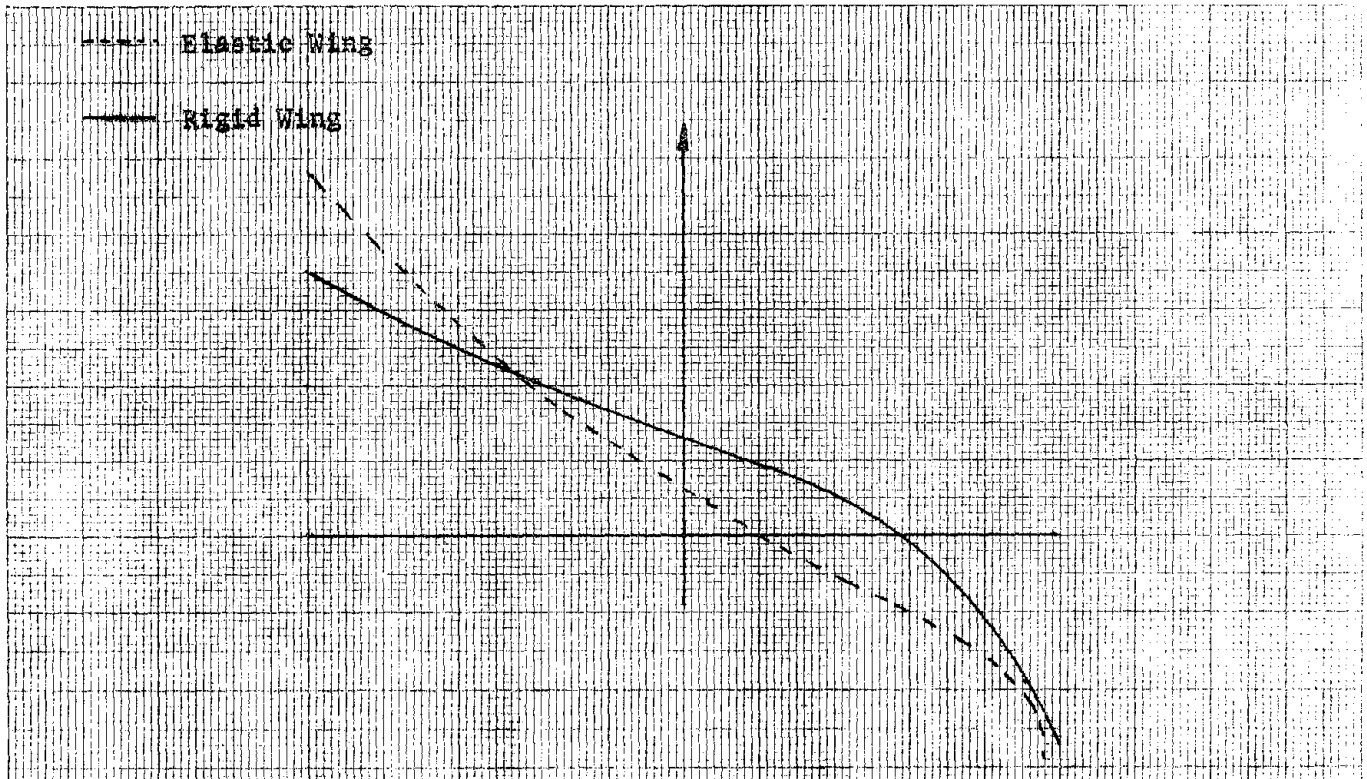

Figure 5.13a - Downwash Angle.

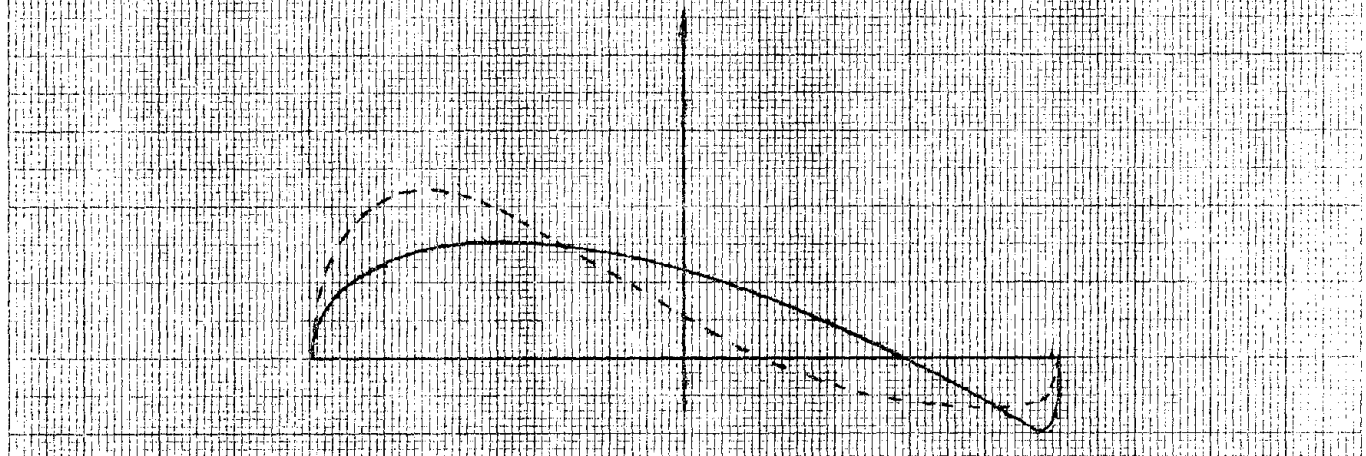

Figure 5.13b - Flat Wing Induced Drag.

cases simulating perturbed states as are assumed in our computation of the stability derivatives.

The numerical program OWSD/LT evaluates the stability derivatives by first computing the distribution of the aerodynamic forces (lift, drag, and side force) for the perturbed condition, then evaluating the increment from the corresponding cruise distribution, and finally integrating these increments as well as their product with the corresponding moment arms in order to obtain the incremental moments over the entire wing span.

The desired values of the stability derivatives are then obtained by dividing the results of the integrations by the perturbation quantity and by the appropriate nondimensionalizing factors [See Appendices A and B]. Then, derivatives are computed with standard expressions [Appendix B and/or Ref. 15, 21] and the yaw derivatives can be evaluated according to strip theory as described in section 3.2.4. Therefore, for both of them it is necessary to simulate the perturbed condition. Consequently, the conditions to be simulated have been reduced to: angle of attack, roll, pitch, and sideslip.

The α-perturbation has been simulated by increasing the cruise angle of attack by 3 degrees (.05236 rad.). The new lift distribution, including twist contribution, is shown in Figure 5.14.

The rigid wing shows a visible increase in the aft wing lift, due to the increase in the flat wing lift. For the elastic one, this effect is much less pronounced. These two behaviors can be predicted by looking at the shape of the FWLD (Fig. 5.12); in fact, a change in α will introduce a

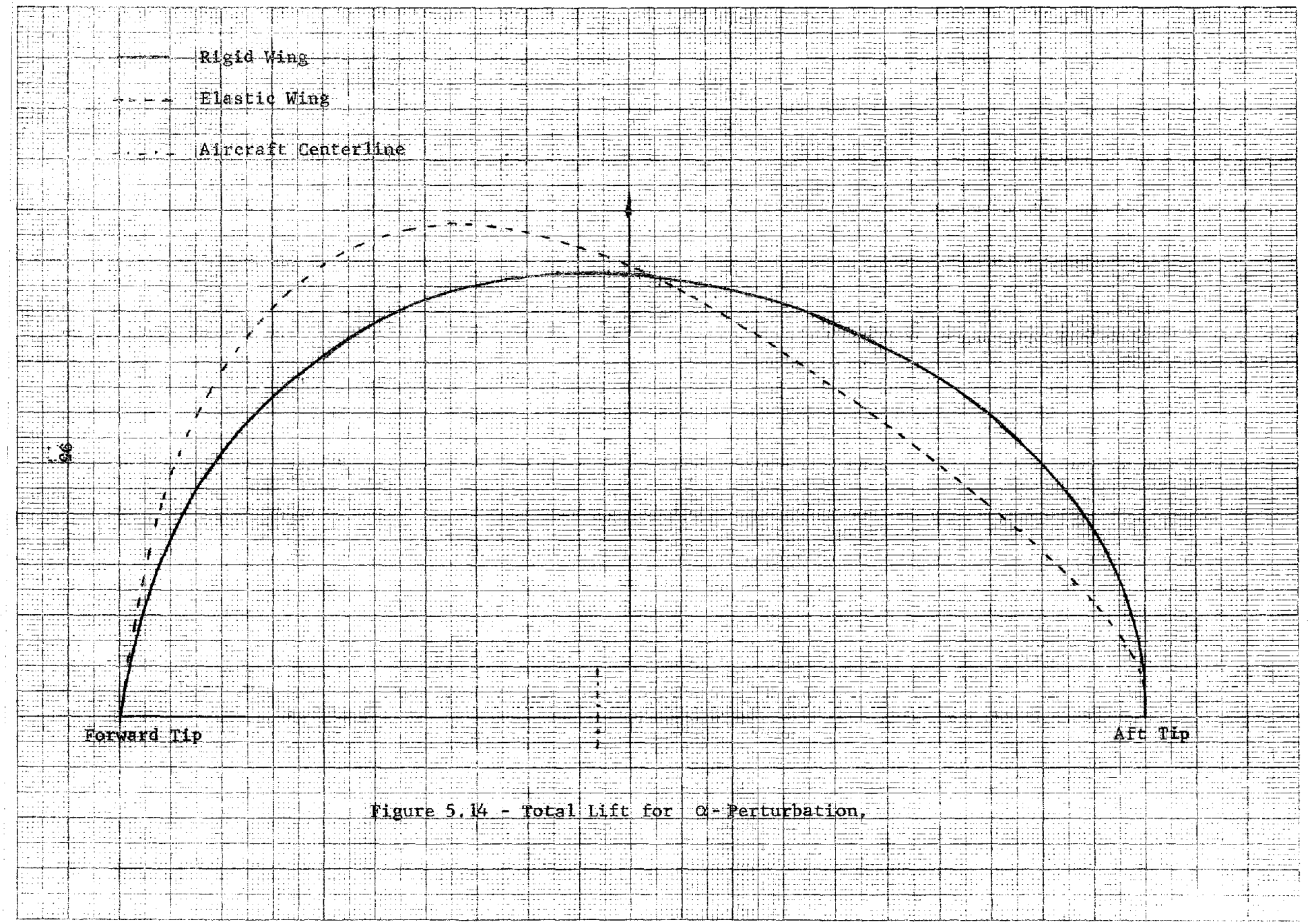

Figure 5.14 - Total Lift for α- Perturbation,

first order variation in the lift, proportional to these shapes. The variation, ΔF_x, in the horizontal force (Fig. 5.15a) is strongly affected by the lift contribution in that direction during the perturbation, as we have discussed in section 3.2.2; in fact

$$\Delta F_x = \ell \ \alpha - (\bar{d} - \bar{d}_0)$$

The increase in lift for the rigid wing is more pronounced in the aft part where it contributes to the thrust already experienced because of the upwash field, but on the forward wing its increase is not sufficient to offset the drag increase.

For the elastic wing, the FWLD has a more symmetric shape than for the rigid one; we would therefore expect the transition point from negative (drag) to positive (thrust) X-force to occur further outboard on the left wing, instead, the two shapes behave similarly, except for the magnitude. This is not the case, according to our results, and the reason is probably because of the downwash distribution: stronger downwash on the forward wing, and consequently a higher induced drag to counteract the higher increase in lift; but also stronger upwash on the aft one with higher resultant thrust where the lift increment is lower than the rigid case. The same reasoning can be applied to the variation in the sideforce (Fig. 5.15b), where the two shapes look similar, although they differ in magnitude.

The perturbations due to roll and pitch are simulated by introducing an aerodynamic twist corresponding to a linear variation in the free stream vertical velocity [See section 3.2.2]. The roll angular velocity is chosen to be such that the twist is equal to -5 degrees at the

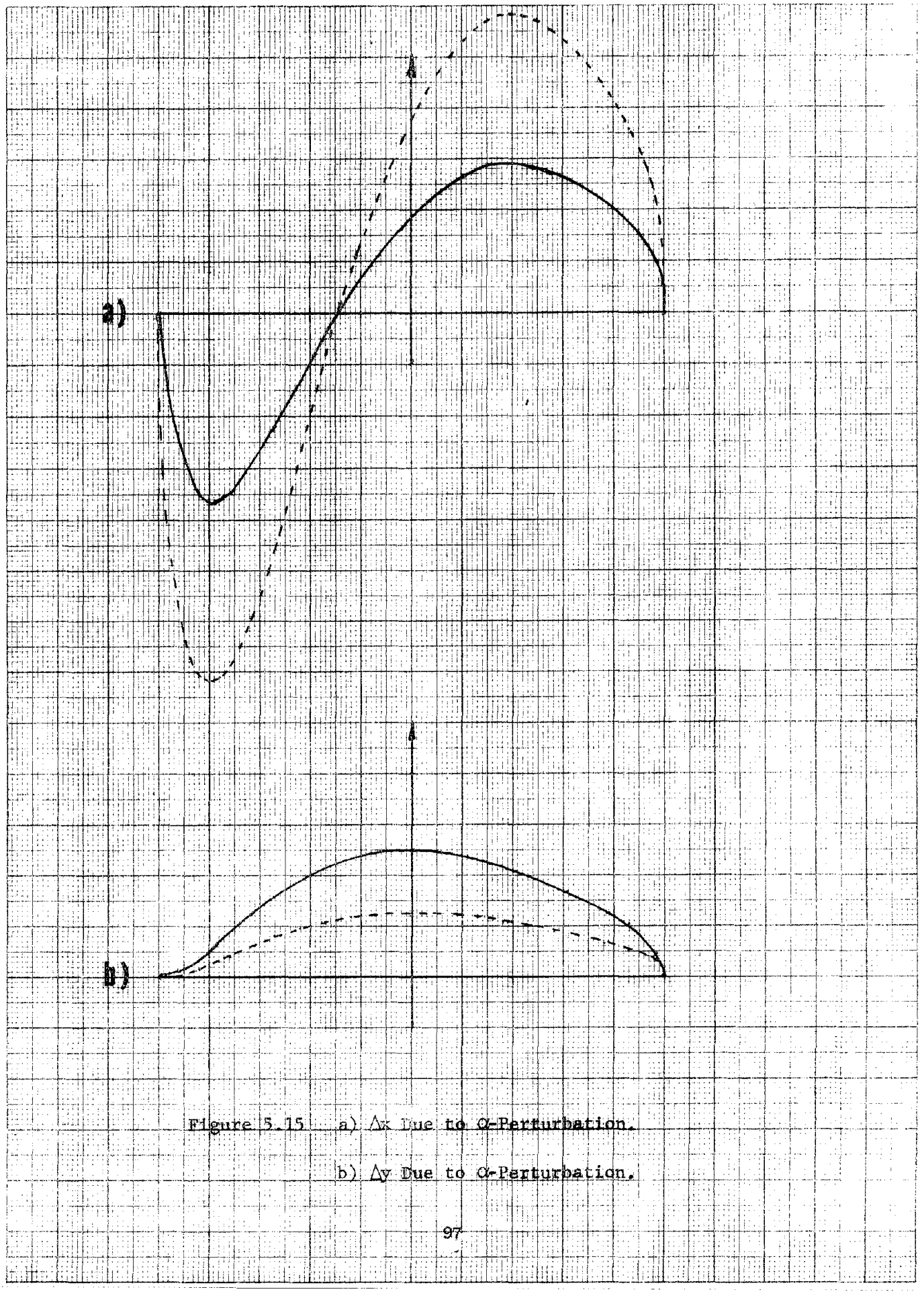

Figure 5.15 a) Δx Due to α-Perturbation.

b) Δy Due to α-Perturbation.

left tip and zero at the aircraft centerline [see Eq. 3.31].

For the pitch velocity, the left tip condition remains - 5 degrees and zero twist now coincides with the wing station corresponding to the intersection of the quarter-chord line with the lateral axis y_s .

The three different twists used in our study are shown in Figure 5.16.

Figure 5.16a shows the built-in twist; the aerodynamic twist corresponding to our roll simulation is shown in Figure 5.16b. The aerodynamic twist due to the pitch simulation (Fig. 5.16c) is not perfectly linear because the downwash velocities have been measured at the 3/4-chord points, which do not lie on a straight line. As we would expect, the aerodynamic twist introduced by a positive rolling motion increases the lift distribution on the aft wing and decreases it on the forward one.

Figure 5.17 shows the spanwise lift distribution corresponding to the cruise angle of attack plus a twist given by the superposition of twists a) and b) of Figure 5.16. The increment in the vertical force is ofgreatest interest. Although such an increment has a contribution due to the drag, according to [see section 3.3.2]

$$\Delta Z = \Delta \ell + \bar{d}\,\alpha$$

where

$$\alpha = \frac{p}{V_{TO}}\,\bar{x}$$

such a contribution is negligible compared to the actual lift changes, therefore the ΔZ shown in Figure 5.18 can be thought of as the actual change in lift without any serious loss in accuracy.

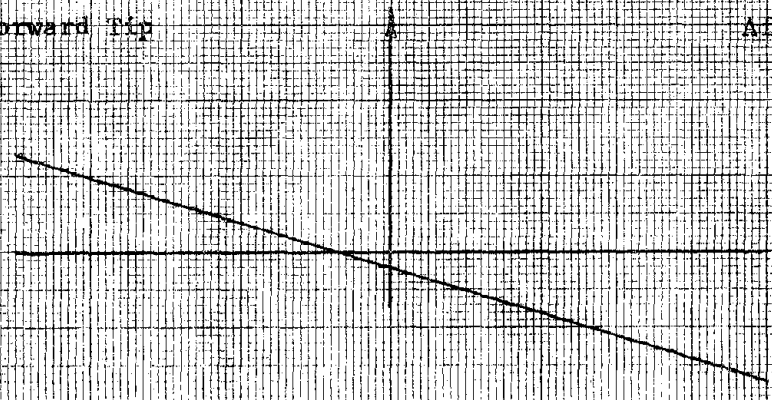

a) Built-in Linear Twist (at $\Lambda = 0^{o}$).

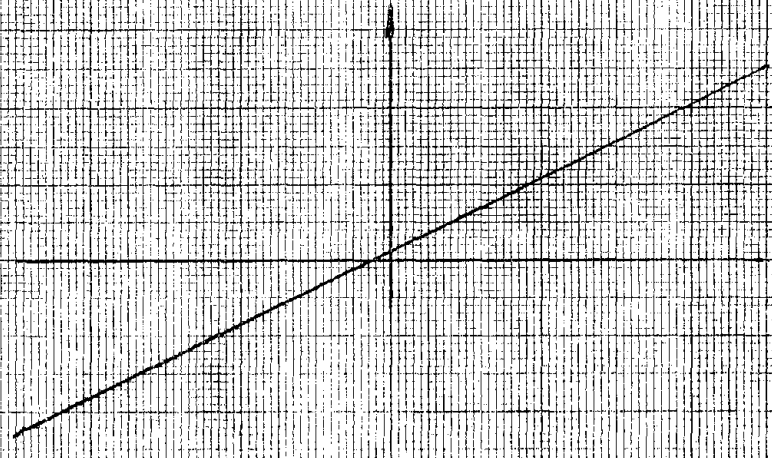

b) Aerodynamic Twist due to Roll Perturbation.

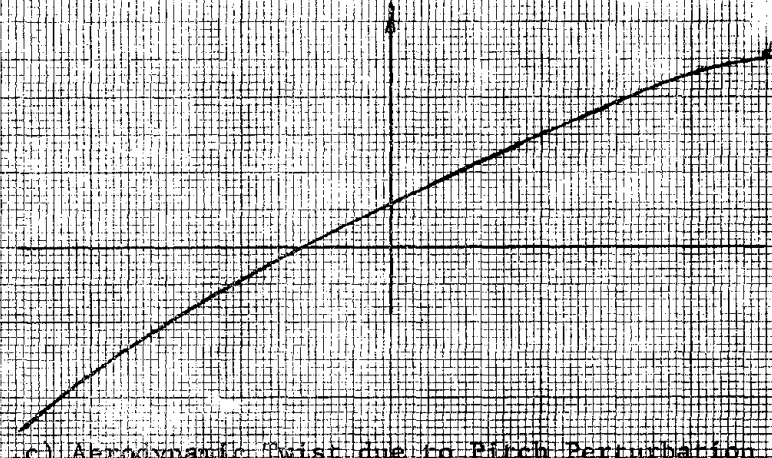

c) Aerodynamic Twist due to Pitch Perturbation.

Figure 5.16 - Twist.

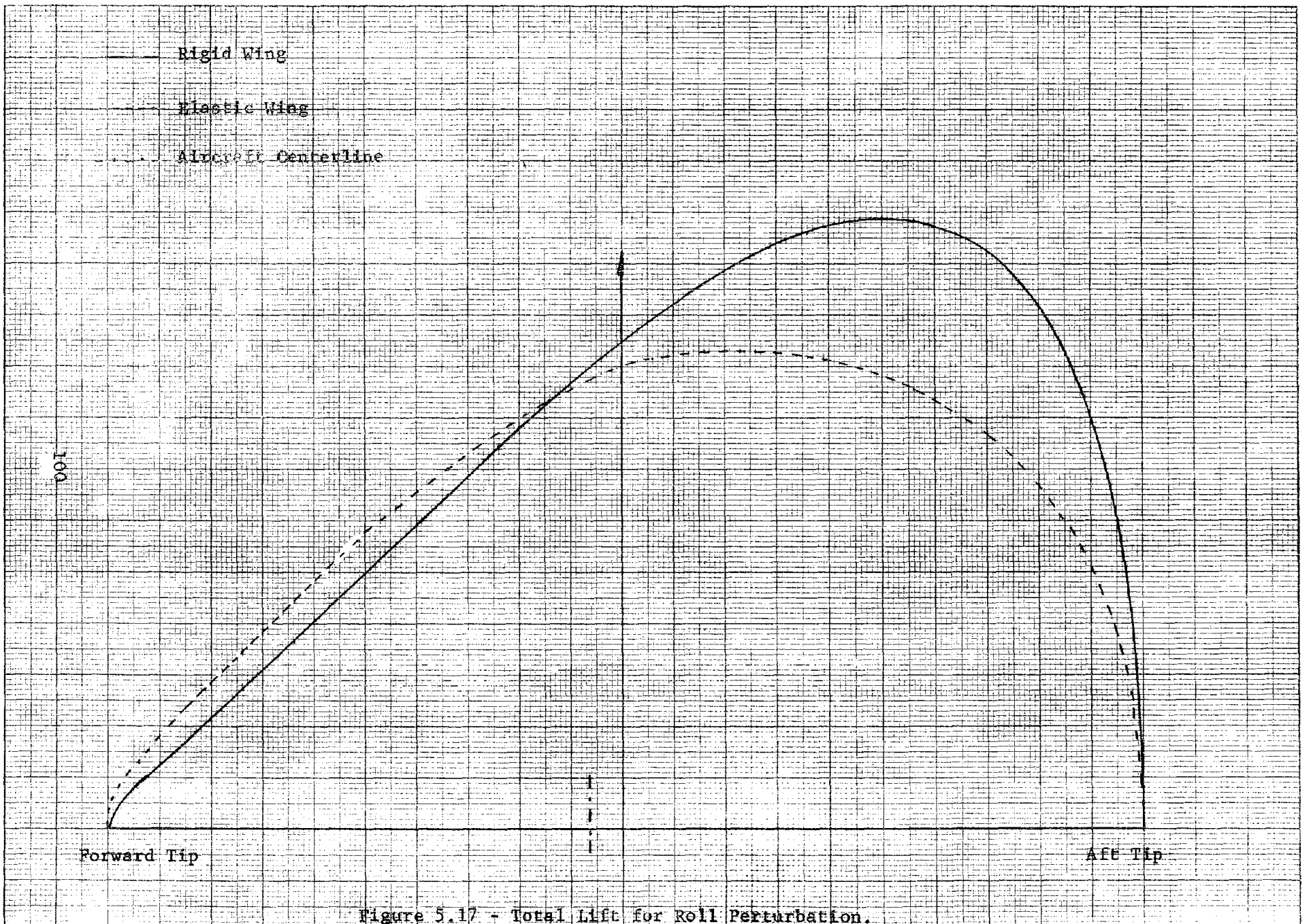

Figure 5.17 - Total Lift for Roll Perturbation.

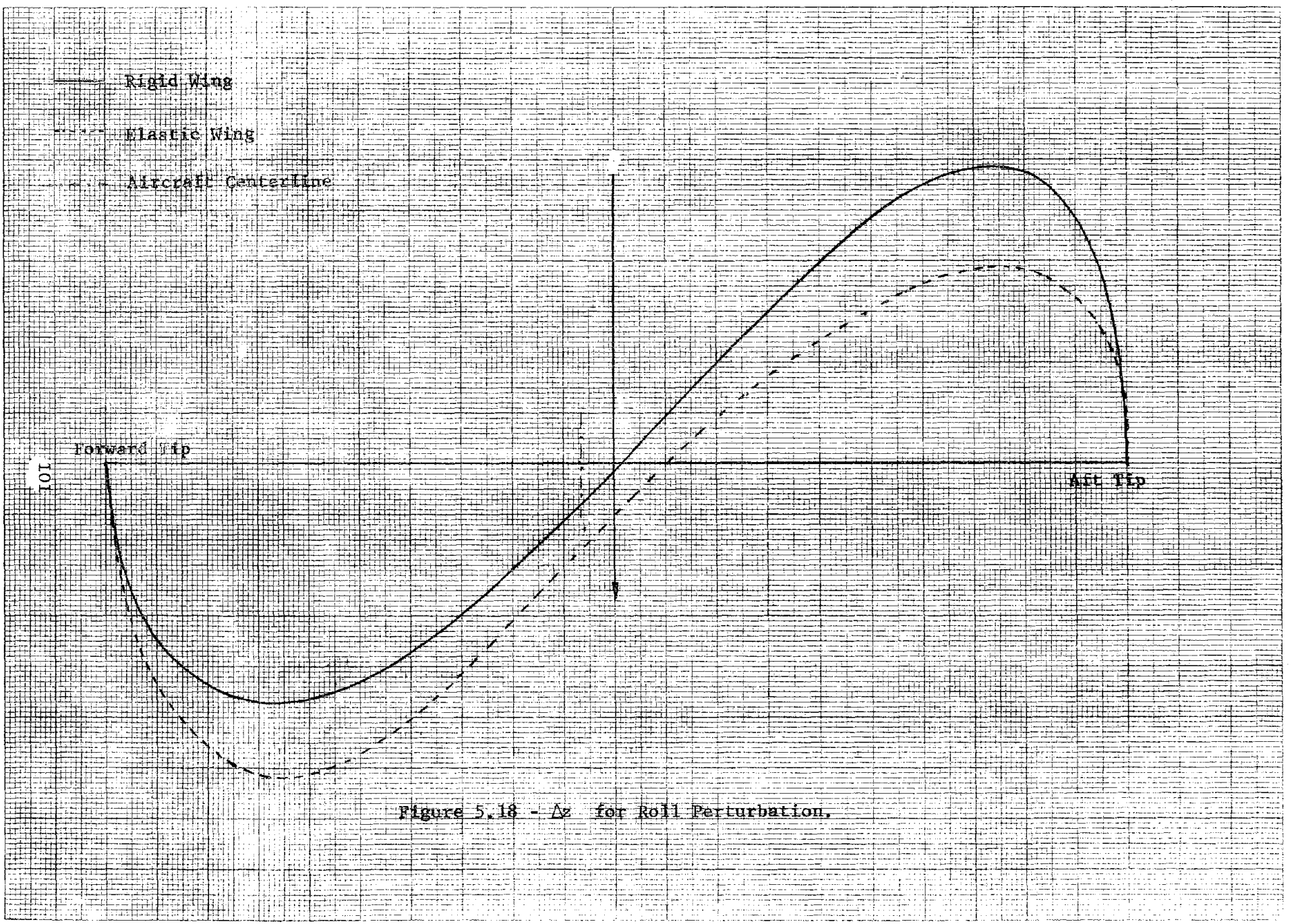

Figure 5.18 - Δz for Roll Perturbation.

From those distributions we notice that the rigid wing shows a positive variation on the aft wing, larger, in magnitude, than the negative one. The opposite is true for the flexible wing. Moreover, if we look at the shape of the corresponding case, as simulated by strip theory, we can observe how erroneous the strip theory approximation is for the flexible wing case.

The variations Δx and Δy look quite complex (Fig. 5.19 a) and b)).

The most important derivative computed from these two distributions is the yawing moment. In a symmetric aircraft the side force is always negligible. This, as we have proposed in section 3.1.2, is not true for an oblique wing aircraft, in fact the side force has a magnitude comparable with the horizontal one even in a perturbed condition. By inspection, we can also notice that the yawing moment produced by the Δx and Δy distributions is, in this case, negative , and the rigid wing shows a larger magnitude.

The same analysis can be extended to the pitch perturbation; there is only one difference: the way the aerodynamic twist is measured in our linear theory model.

Eqn. 3.31 implies a linear variation in the aerodynamic theory; this is a common assumption and was used also in our strip theory analysis. The linear theory, as we mentioned earlier, implies the evaluation of the vertical velocities, induced by the angular velocity q , at 3/4-chord. Figures 5.20 and 5.21 respectively show the spanwise lift distribution corresponding to the cruise angle of attack plus the superposition of

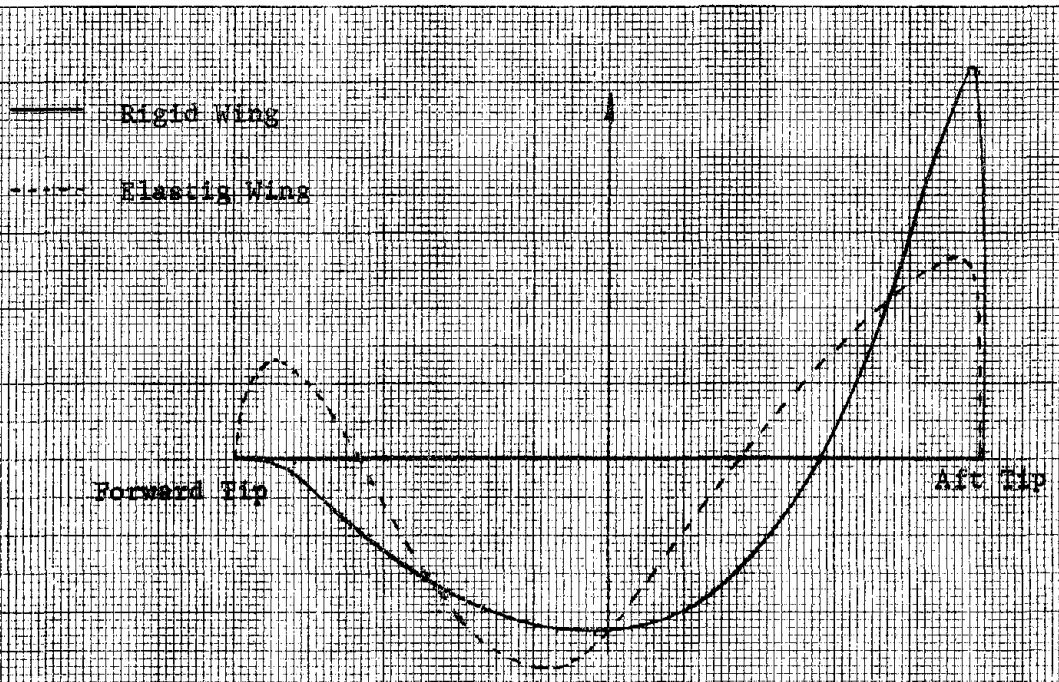

Figure 5.19a - Δx for Roll Perturbation.

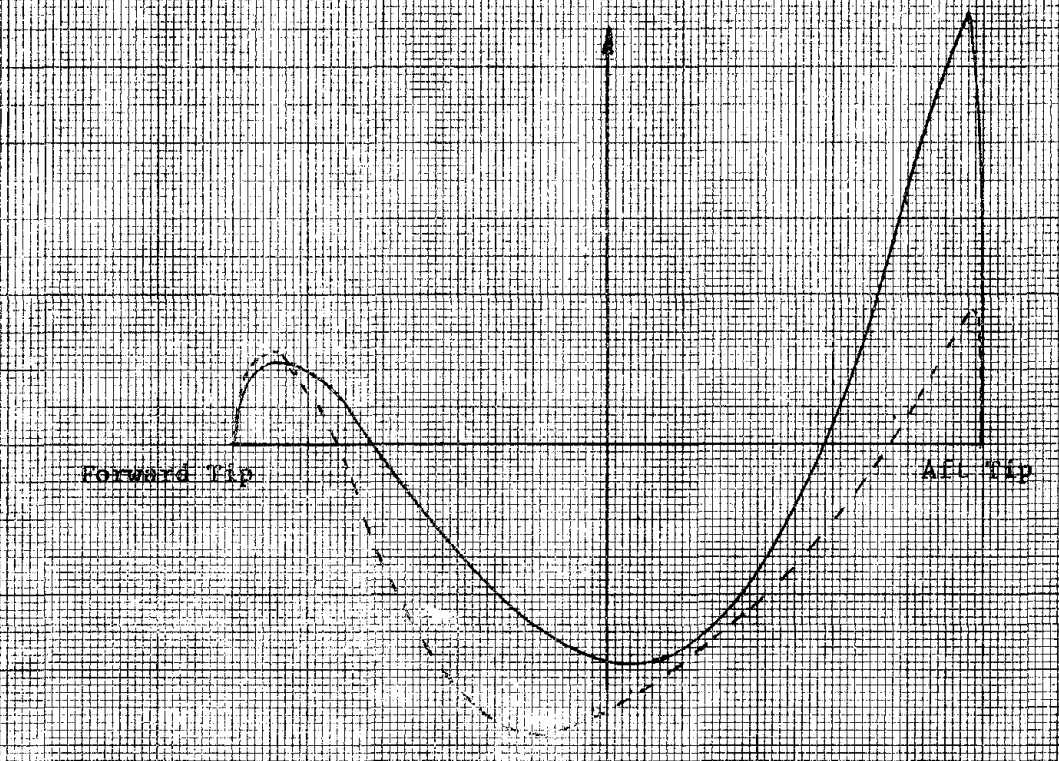

Figure 5.19b - Δy for Roll Perturbation.

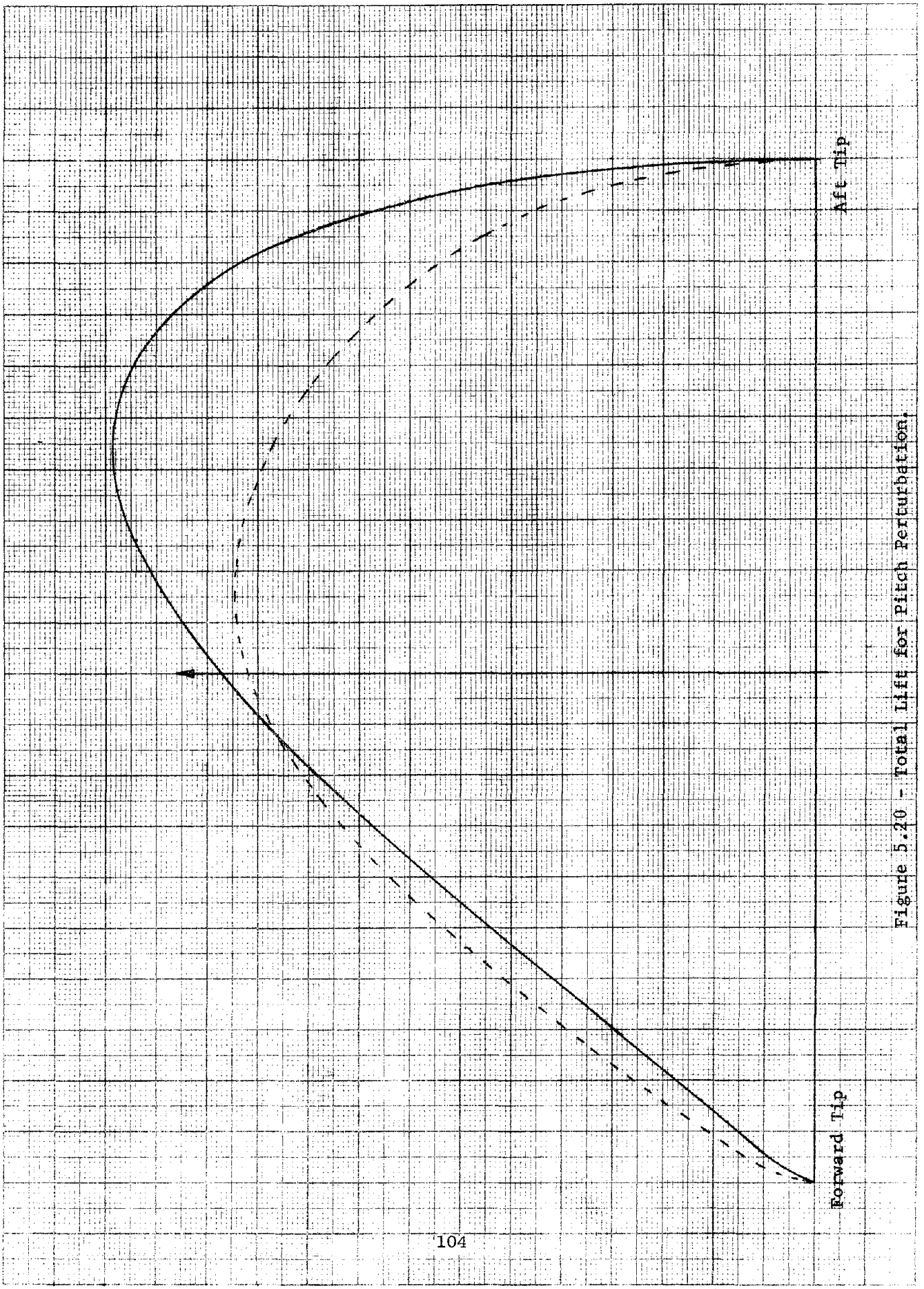

Figure 5.20 - Total Lift for Pitch Perturbation.

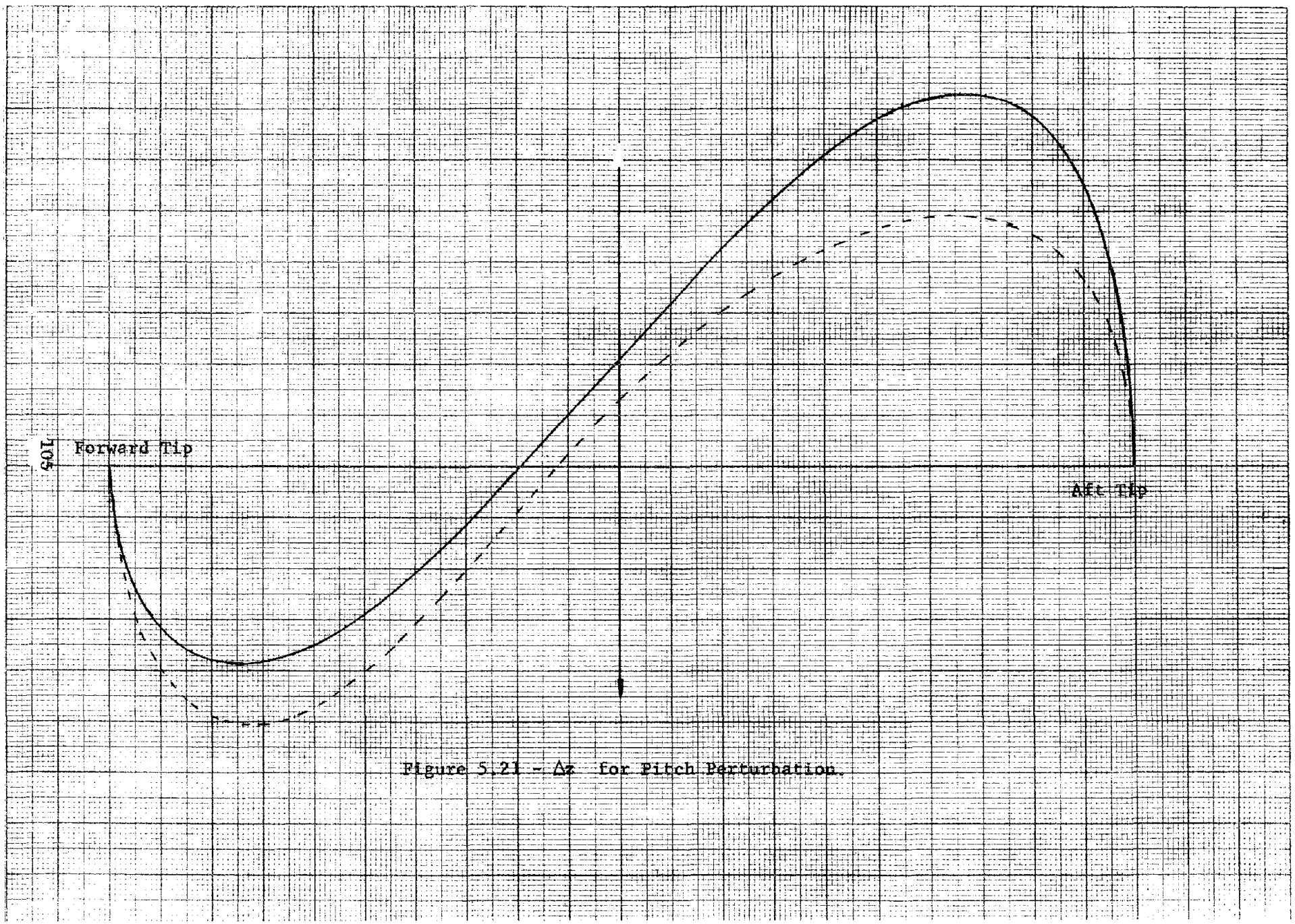

Figure 5.21 - Δz for Pitch Perturbation.

the twists of Figures 5.16a and 5.16c.

Figure 5.22 shows the ΔZ distribution and 5.22b the ΔY distribution.

In our model, the sideslip is simulated by increasing the skew angle by 5 degrees. This, as we have already mentioned, corresponds to a negative sideslip according to the reference axes system chosen. Thus, when looking at the variations in the aerodynamic forces, we must change the sign when considering the sideslip case. Figure 5.23 shows the total lift distribution for the new skew angle.

Increasing the skew angle, the angle of attack measured in the flight direction decreases (Eq. 3.8). In our case, the relationship between perturbed and cruise angle of attack is:

$$\alpha_{50^o} = \alpha_{45^o} \frac{\cos 45^o}{\cos 50^o}$$

The results shown in Figure 5.24 are of great interest.

Increasing the skew angle (which corresponds to a negative slip), the total lift decreases and the spanwise distribution of such variation is asymmetric (Fig. 5.24). This asymmetry will result in negative pitching and rolling moments; therefore, a positive sideslip introduces positive rolling and pitching moments. This is an unstable behavior and can be visualized by considering the trend of the spanwise lift distribution when the wing is skewed.

The upwash field generated by the forward wing introduces the build-up in lift on the aft wing.

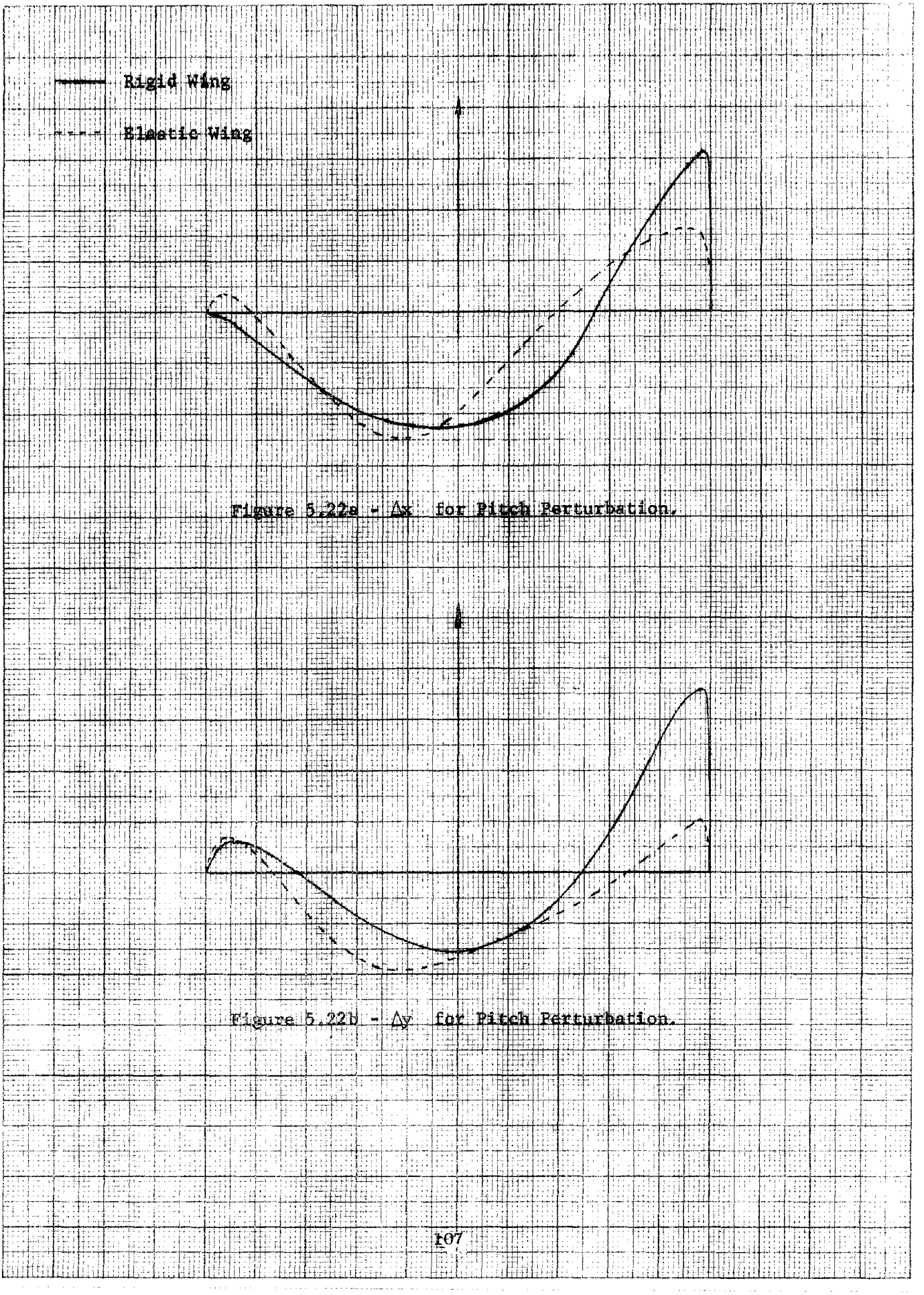

Figure 5.22a - Δx for Pitch Perturbation.

Figure 5.22b - Δy for Pitch Perturbation.

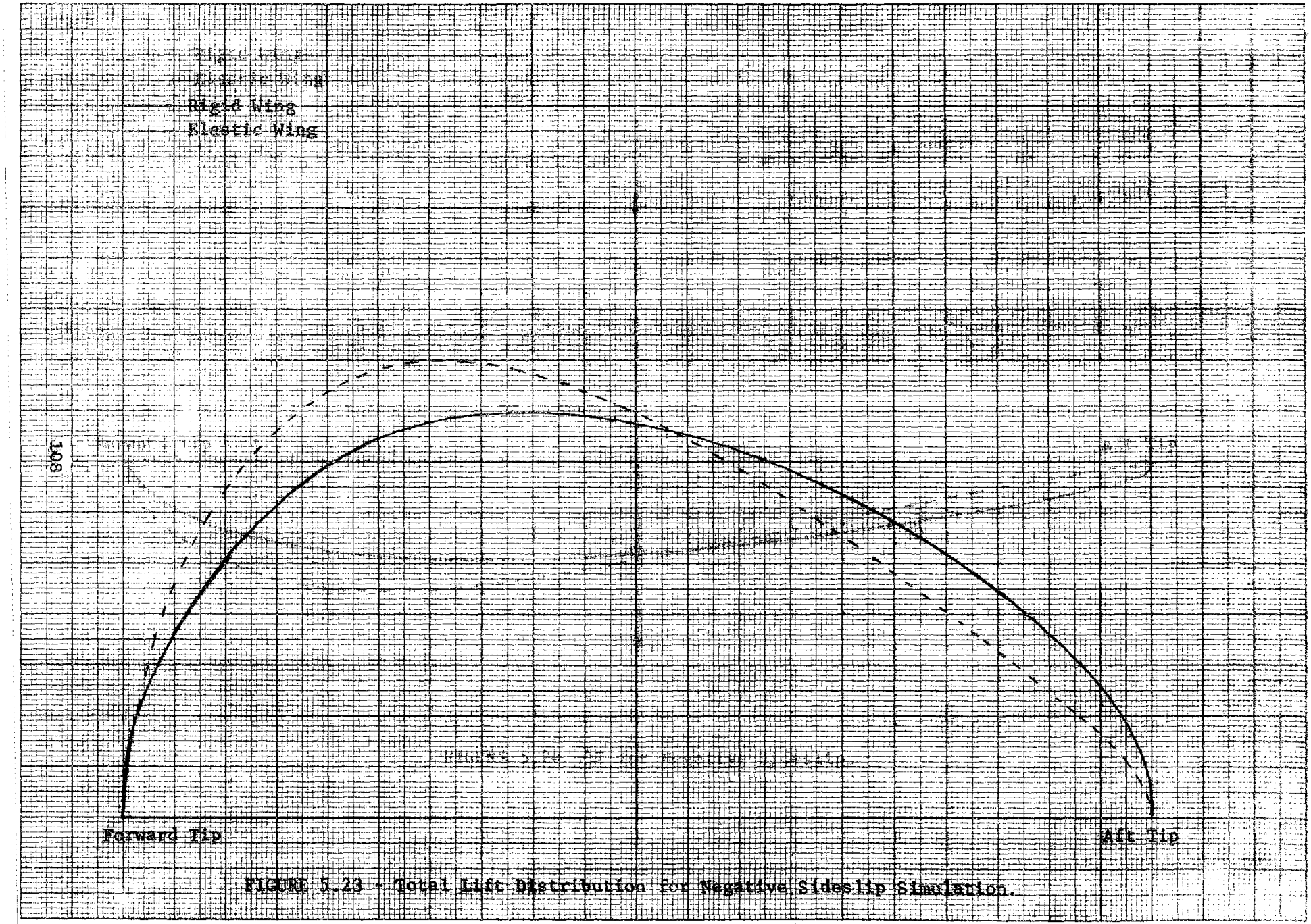

FIGURE 5.23 - Total Lift Distribution for Negative Sideslip Simulation.

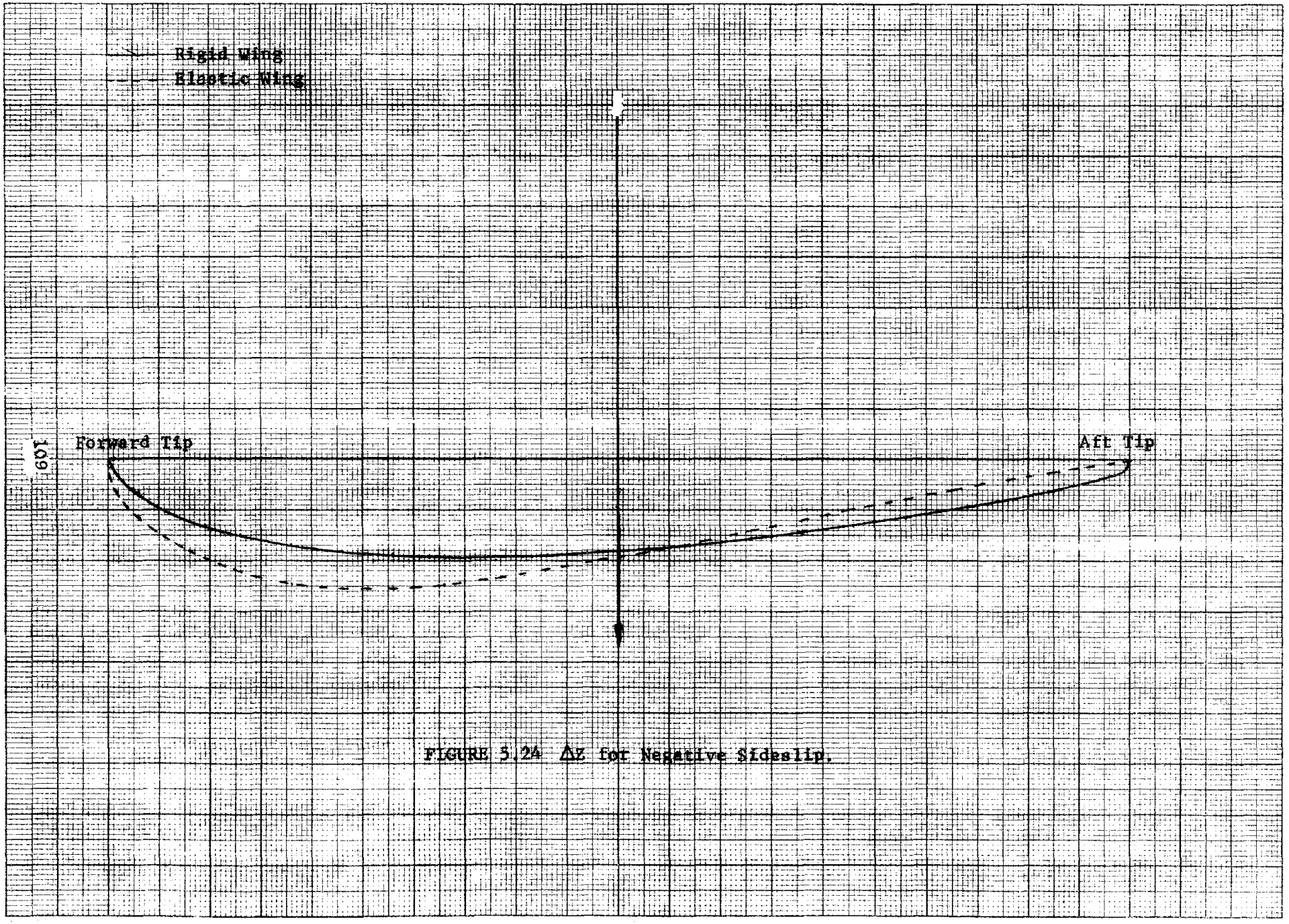

FIGURE 5.24 Δz for Negative Sideslip.

As we increase the skew angle, this build-up will shift more and more towards the aft wing tip. Thus, this shift will introduce negative pitching and rolling moments (left wing forward case). When we unskew the wing, the trend will be the opposite; consequently the lift build-up will shift towards the center decreasing the magnitude of the negative rolling and pitching moments. These are positive increments in the moments and the reduction in skew angle corresponds to the sideslip situation. The effects of flexibility worsen this undesired behavior.

In our model, we have used linear built-in twist to stabilize the rolling moment. In this case also,we see how poor such a solution would be as compared to the case of a built-in dihedral.

The effectiveness of the linear twist decreases with the cosine of the skew angle; thus, the amount of twist required at 45^{o} to trim the aircraft would introduce a strong positive rolling moment when the wing is unskewed.

Since a sideslip perturbation affects the total lift distribution, the contribution due to twist in a positive sideslip situation is an increase in the undesired positive rolling and pitching moments. Since the equivalent twist due to dihedral varies with the sine of the skew angle, the previous unfavorable situation now becomes a favorable one; in fact, a decrease in sweep will introduce a variation in the equivalent twist which results in a decrease in the forward wing lift and an increase in the aft wing lift, which is a stabilizing trend. The yawing moment due to the variation in the longitudinal force, ΔX , is positive for our negative sideslip simulation (Fig. 5.25a), and this is a favor-

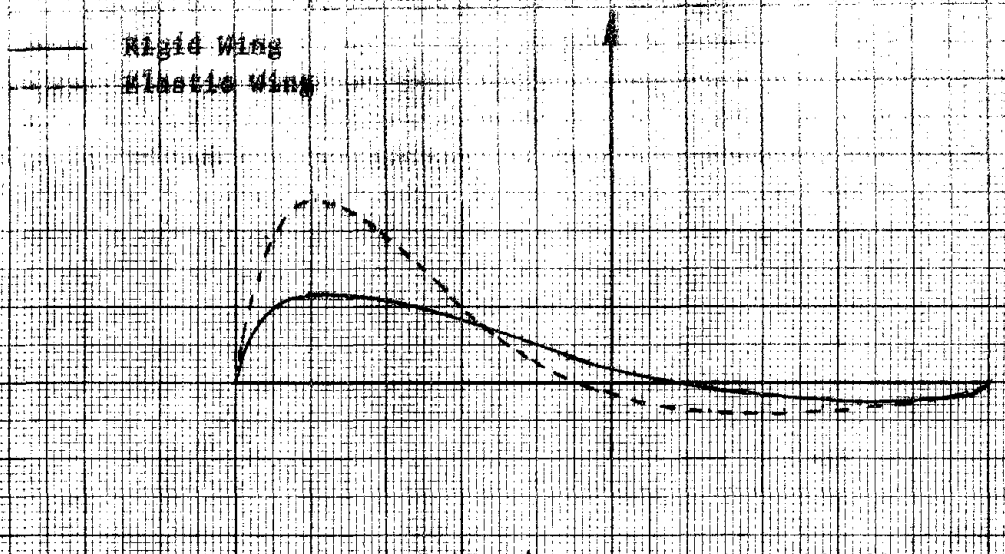

FIGURE 5.25a ΔX for Negative Sideslip

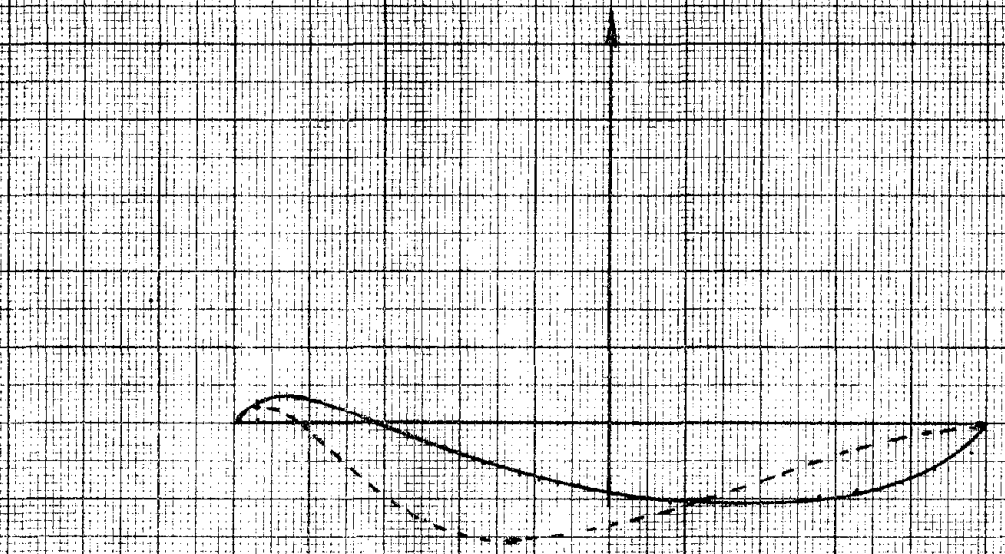

FIGURE 5.25b ΔY for Negative Sideslip.

able result.

From the shape of the side force (fig. 5.25b) we can observe that the contributions of flat and rigid wings to the yawing moment can differ even in sign. In fact, for the negative sideslip case, the rigid wing shows a decrease in side force whose resultant force is applied to some point on the aft (right) wing. The rigid wing, instead, shows the resultant side force acting on the forward (left) wing. Therefore, the rigid wing, in sideslip, experiences a side force that produces a destabilizing yawing moment (positive for the negative sideslip case shown in Figure 5.25b), whereas the elastic wing shows a tendency to produce a favorable yawing moment.

The effect of the wing rotation on the ailerons geometry has already been discussed in section 3.1.3.

Table 5-Ia shows the ailerons dimensions for the unswept case, and Table 5-Ib shows the corresponding ones assumed in the computer simulation for the 45° skew angle; the quantities used in this Table are defined in Figure 3.6.

Three aileron deflections are considered:

1) left aileron deflected 5 degrees

2) right aileron deflected 5 degrees

3) both ailerons deflected; left 5 degrees, right - 5 degrees.

The elastic wing case considered so far assumed the elastic axis (E.A.) to coincide with the wing quarter-chord line. In addition to this elastic case and to the rigid one, we also considered, for the ailerons only, the case when the E.A. is at a distance from the quarter

	YCNTOL = 93.63 ft	CNTCOL = 2.2 ft
Left Aileron		
	YCNTIL = 73.93 ft	CNTCIL = 3.66 ft
	YCNTOR = 93.63 ft	CNTCOR = 2.2 ft
Right Aileron		
	YCNTIR = 73.93 ft	CNTCTR = 3.66 ft

a) Ailerons Nominal Dimensions at $\Lambda = 0$

	Wing Station (non dimen.)		Distance from A/C Centerline [ft]	
	Outboard	Inboard	Outboard	Inboard
Left Aileron	.937	.837	64.45	55.31
Right Aileron	.862	.662	66.03	51.75

b) Computer Approximation at $\Lambda = 45^{\circ}$

TABLE 5-I Ailerons Dimensions

chord. The latter represents the real situation, but, since at 45^{o} skew angle the bending contribution to the wing twist is by far more important than the contribution due to torsion, the differences between the two elastic cases are small, at least as far as our analysis is concerned. We shall see how the same is true for the ailerons also.

Figures 5.26 through 5.28 show the total lift distribution corresponding to the three aileron deflections considered, for both the rigid and elastic wing cases, having the E.A. coinciding with the quarter-chord line.

The aileron effectiveness for these three cases is shown in Figures 5.29a, b, and c.

Once more, we can observe the peculiar behavior of the oblique wing. In fact, the forward aileron, affected by a stronger downwash, is less effective than the aft one, which is instead influenced by a strong upwash. The variations in horizontal force, ΔX, are shown in Figures 5.30a, b, and c.

Because of the lack of points in the areas of interest, the shape of the curves looks unusual; nevertheless it is interesting to notice the ΔX variation introduced by the aft (right) aileron.

The positive right aileron deflection produces an adverse yaw moment much smaller than the corresponding one produced by the left aileron (fig. 5.29 and 5.30). We have already noticed how the favorable upwash field decreases the drag on the aft wing; in case of right aileron deflection the induced drag rise is not only lower than the corresponding one for the forward aileron, but the increment in lift, because of the

FIGURE 5.26 Total Lift for only Left Aileron Deflected.

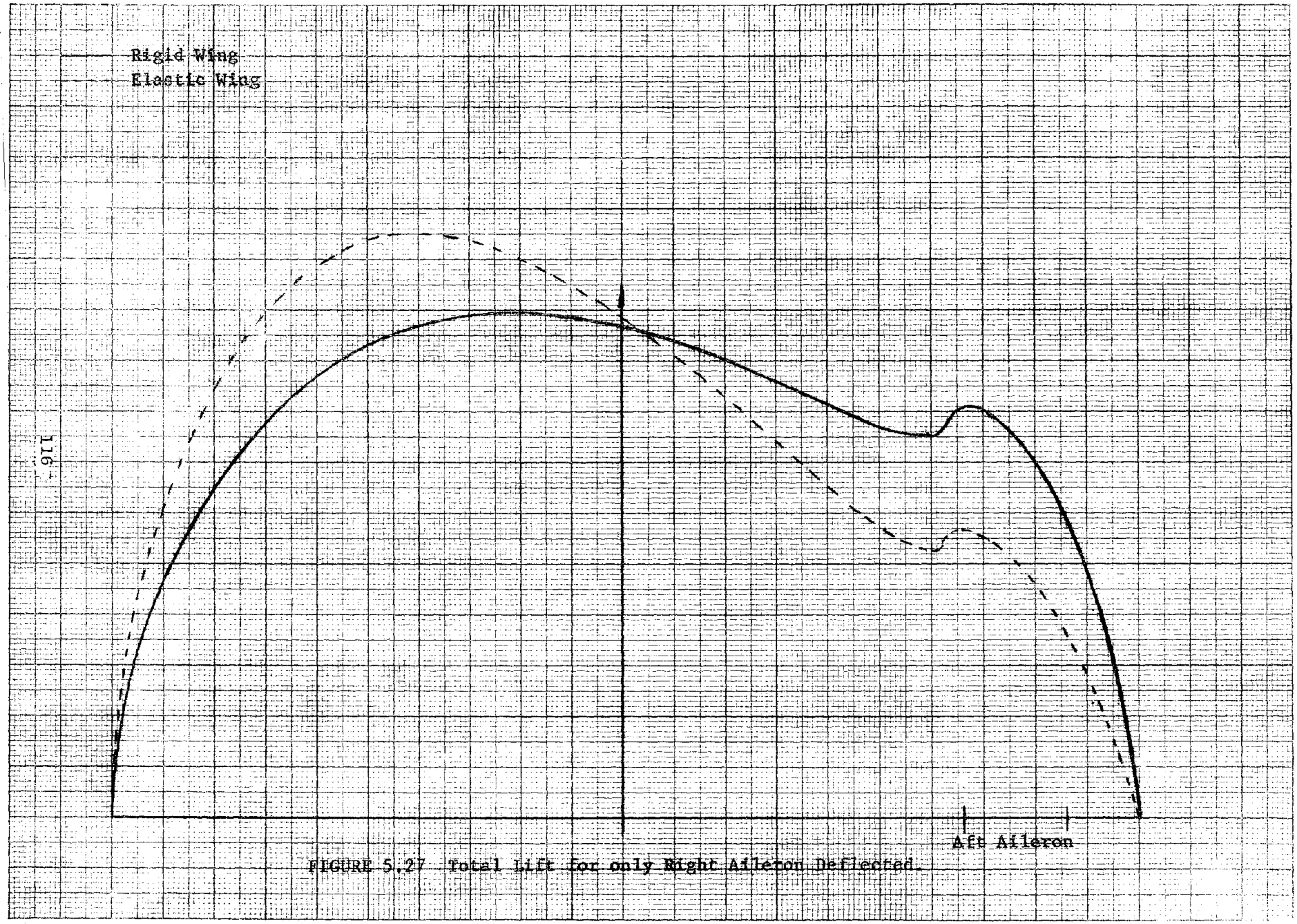

FIGURE 5.27 Total Lift for only Right Aileron Deflected.

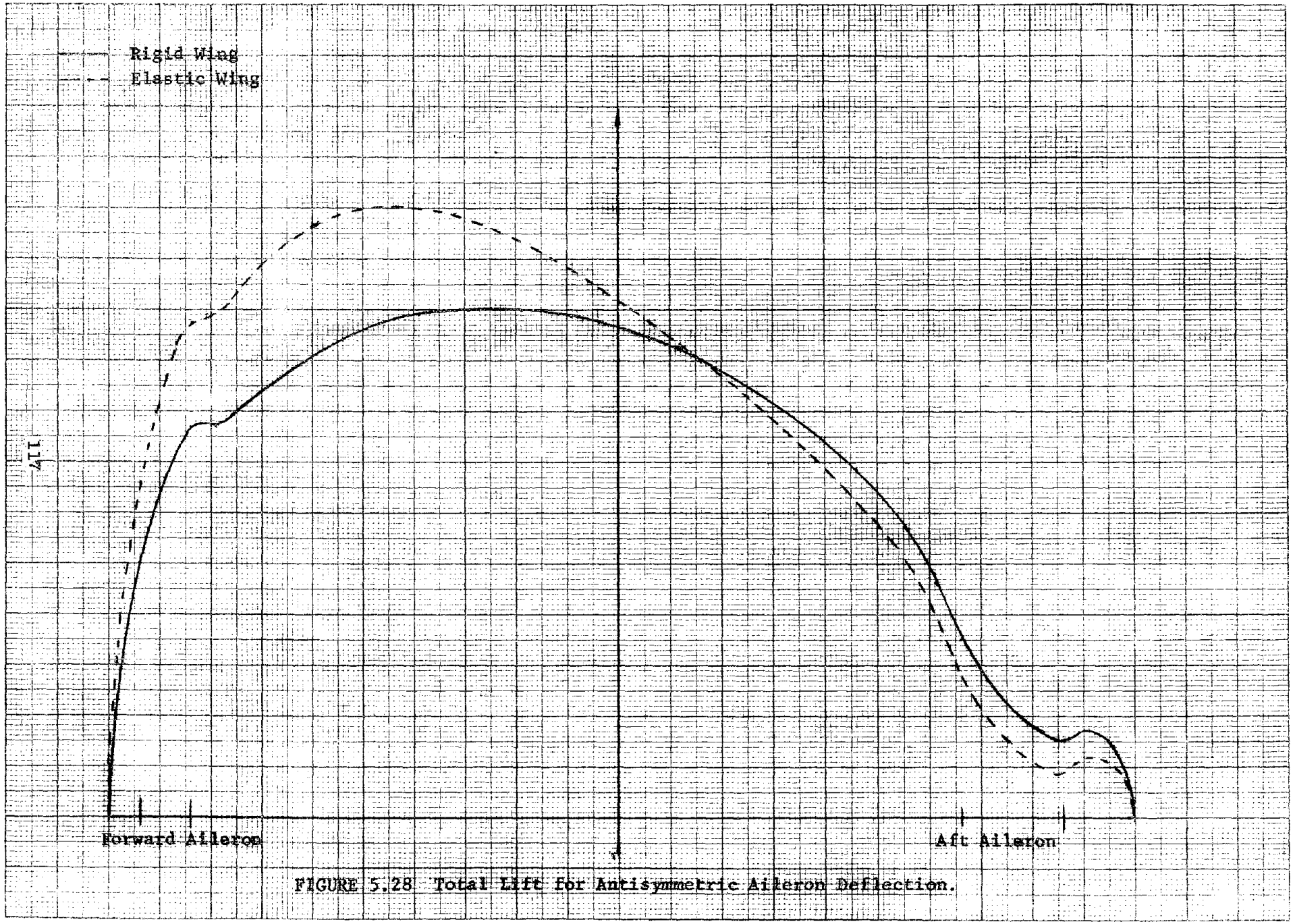

FIGURE 5.28 Total Lift for Antisymmetric Aileron Deflection.

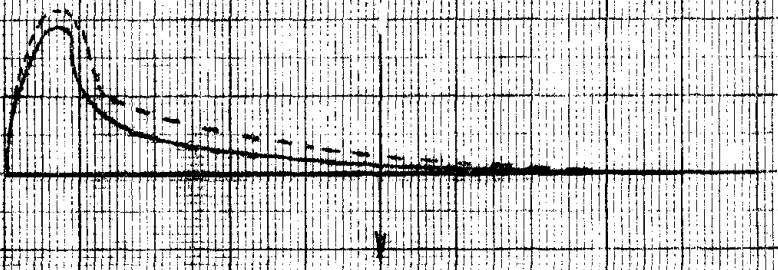

FIGURE 5.29a ΔZ for Left Aileron Deflection only.

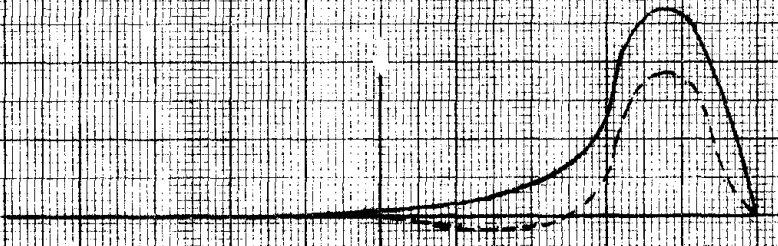

FIGURE 5.29b ΔZ for Right Aileron Deflection Only.

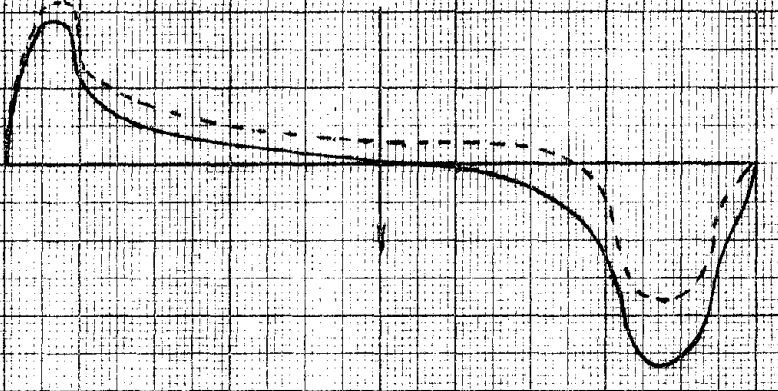

FIGURE 5.29c ΔZ for Antisymmetric Deflection.

——— Rigid Wing

– – – – Elastic Wing

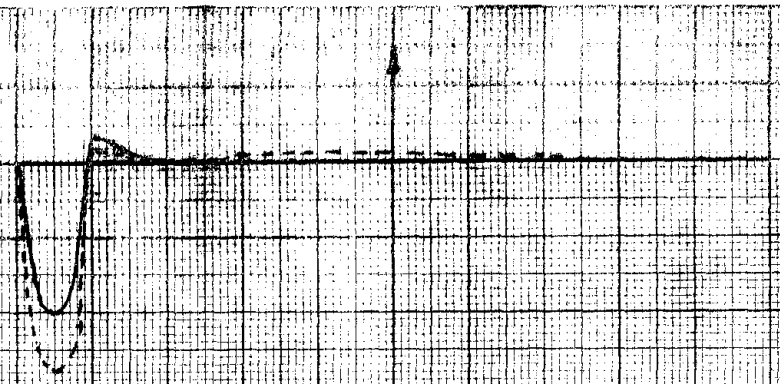

FIGURE 5.30a ΔX for Left Aileron Deflection only.

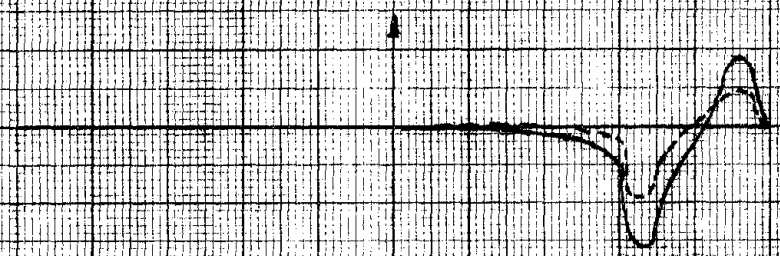

FIGURE 5.30b ΔX for Right Aileron Deflection only.

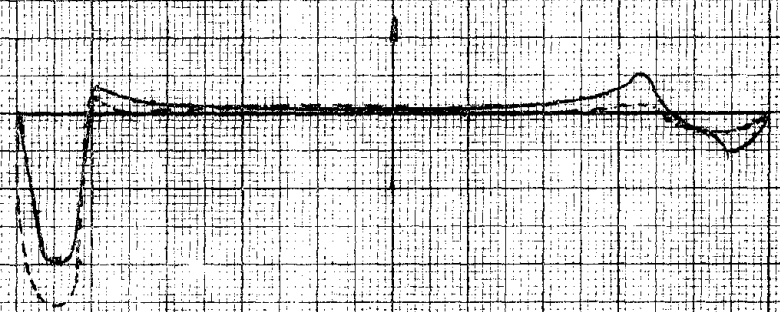

FIGURE 5.30c ΔX for Antisymmetric Deflection.

——— Rigid Wing
– – – – Elastic Wing

upwash, results in a thrust force outboard of the aft aileron.

The same effect can be noticed in the case of antisymmetric deflection (Fig. 5.30c).

The negative deflection in the right (aft) aileron produces a decrease in drag, or equivalent thrust, followed by a drag increase on the outboard part of the wing. This behavior suggests the possibility of using the aft aileron only for control during the cruise condition; but this solution implies, first, the experimental confirmation of the analytic results and, second, that there are no adverse aeroelastic effects related to that solution.

Figures 5.31 through 5.34 are referred to the elastic wing case having the E.A. passing through the wing pivot (50% root chord) and parallel to the quarter-chord line. Very little difference can be noticed between these results and the corresponding ones for the other elastic wing case considered.

In fact, the twist contribution due to bending is much larger than the contribution due to torque.

5.3 Stability Derivatives and their Influence on the Natural Modes.

At this point, the logic flow of our analysis would require the discussion of the numerical results of the stability derivatives. We shall postpone it to the next section and carry on, instead, a qualitative analysis of the influence of the stability derivatives on the natural mode of an oblique wing aircraft.

FIGURE 5.31 Total Lift for only Left Aileron Deflected
(C.A. not Coinciding with Quarter-Chord)

FIGURE 5.32 Total Lift for only Right Aileron Deflected
(E.A. not Coinciding with Quarter-Chord)

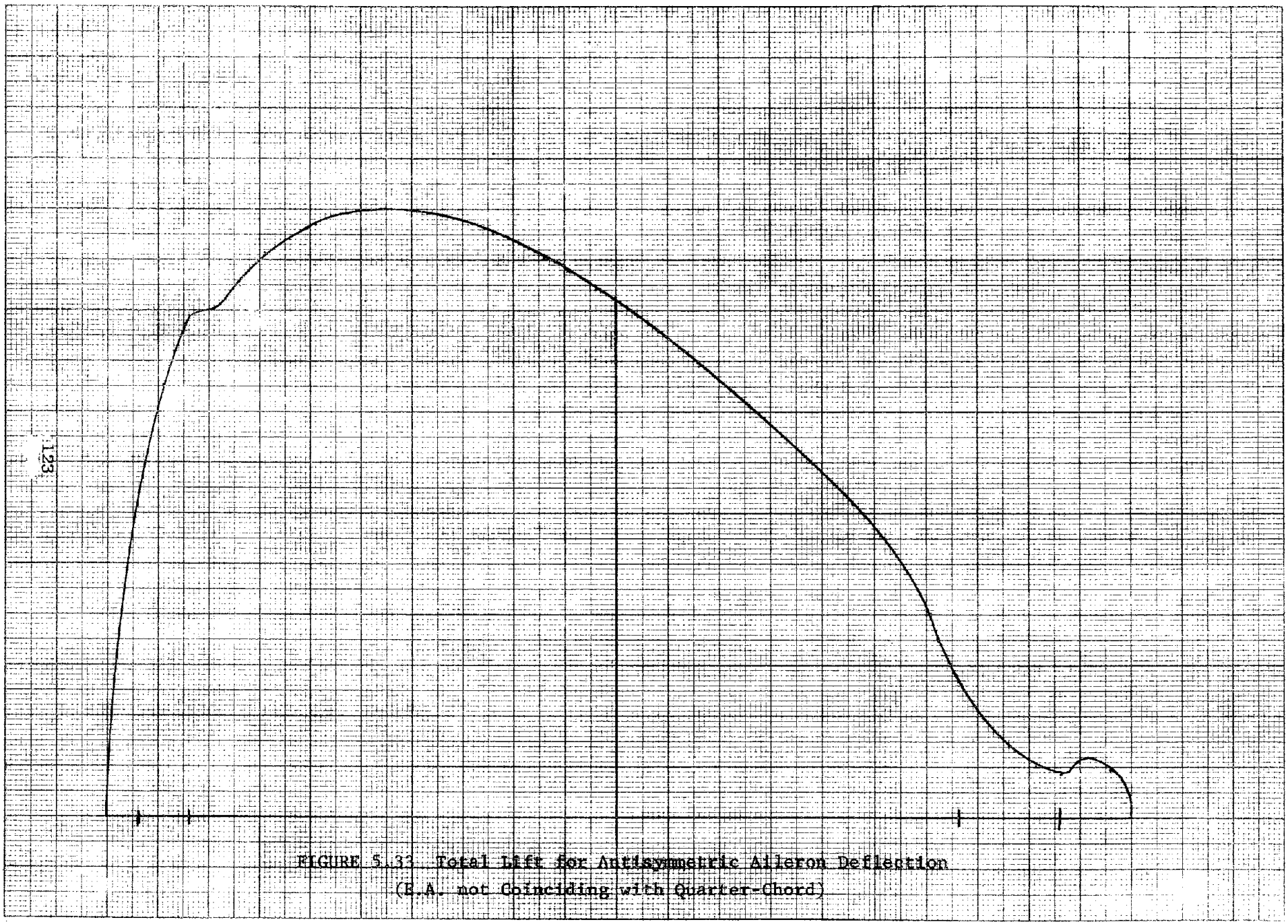

FIGURE 5.33 Total Lift for Antisymmetric Aileron Deflection
(E.A. not Coinciding with Quarter-Chord)

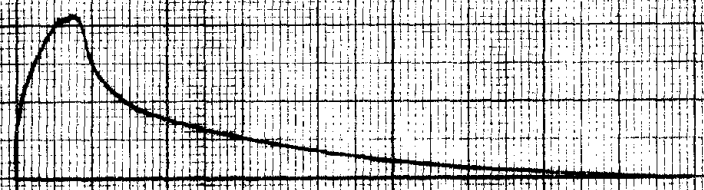

a) Left Aileron only

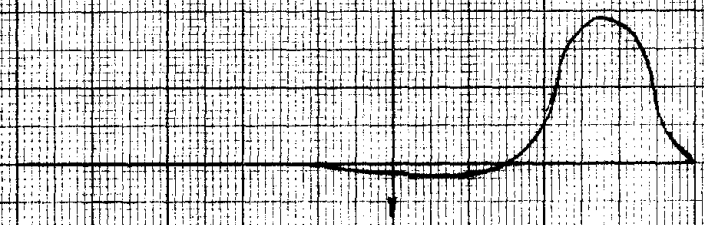

b) Right Aileron only

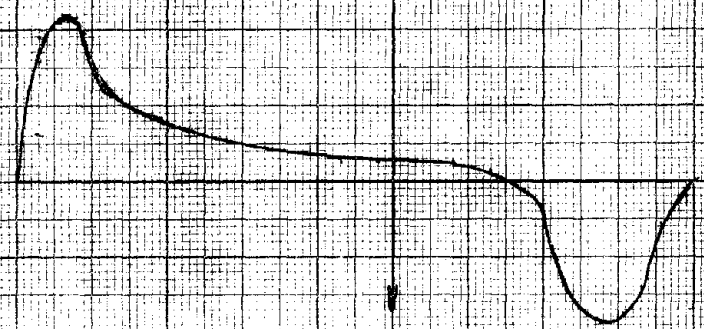

c) Antisymmetric Deflection

FIGURE 5.34 ΔZ for Aileron Deflection

In Chapter III, the new stability derivatives due to the skewed wing were introduced without any attempt to define their importance to the dynamic stability and natural modes of the aircraft. This analysis had been carried out only on the basis of understanding the behavior of an oblique wing aircraft and its differences from a symmetric aircraft. We shall now discuss the result of a numerical investigation to determine the influence of the new stability derivatives, as well as of the usual ones, on the dynamic stability of an oblique wing aircraft.

The set of six linear differential equations dervied in Chapter IV was numerically solved using an available computer program (GSA), which was originally developed by Lockheed Missiles and Space Company. The program solves a set of linear differential equations using the Laplace transform method and gives root locus, bode or time domain plots for the system. The characteristic polynomial is of the 8th order.

The influence on the roots of the characteristic equation is now analyzed for each nonzero derivative by means of a root locus. In this way, it is possible to find the derivatives having influence on the natural modes. This study has been carried out for the new as well as the conventional derivatives, by varying one derivative at a time, starting from zero to a value double that of the corresponding one reported in Table 5-III, column 1.

It is obvious that this is actually not possible in a realistic analysis, since the parameters affecting one derivative may affect other derivatives also; the range itself does not reflect a real case except for some of the derivatives depending on the skew angle. The purpose of

this analysis is only to localize those derivatives whose contribution to the root location is negligible and to compare them with each other.

For the sake of clarity, we have labeled the roots according to the classical definitions though, in the case of a skewed wing, they may lose part of their meaning. Table 5-II reports the results of this investigation and shows the influence on each natural mode. They were evaluated according to the percent change in the natural modes while the value of the derivative ranged from zero to the maximum value assumed. The symbols used are:

——	:	less than 5 %
*	:	5 to 20 %
**	:	20 to 50 %
***	:	50 to 80 %
****	:	over 80 %

5.4 Stability Derivatives.

In section 5.2 we have analyzed the spanwise lift distribution of the aerodynamic forces as computed with our numerical models. The stability derivatives are the direct consequences of those spanwise distributions.

To date, neither program computes the stability derivatives with respect to rate of change of $\dot{\alpha}$. These derivatives take into account the time required for the effect of downwash produced by the wing to reach the horizontal tail. For symmetric aircraft, the methods described in

References 27 and 28 are usually used.

The effect of downwash is to reduce the angle of attack of the stabilizer. Because the wing is at a skew angle, the distance from the wing to a conventional stabilizer varies from tip to tip and complicates the computation of such derivatives.

Since the analysis done in section 5.3 showed that the influence of these derivatives on the dynamic of the aircraft is negligible and because of lack of time, we decided not to further investigate the analytic and numerical evaluation of such derivatives.

We recall that the nondimensionalizing quantities used in our analysis [Appendix A] are: cruise speed, wing span, and mean aerodynamic chord, both for the unskewed configuration.

The results obtained, together with the Boeing ones, are shown in Table 5-III. Tables 5-IV through 5-IX are the computer printouts of the first six cases of table 5-III. The symbols in these printouts are explained in Appendix E.

In addition to the stability derivatives, the wing contributions are reported separately.

Whenever a stability derivative differs from its corresponding wing contribution, this is because of the tail contribution.

We shall now make a few remarks concerning the most influential derivatives (Table 5-II) as computed with lifting line theory.

The comparison between rigid and flexible wing, in terms of stability derivatives, can be done by comparing columns 3 and 4 in Table 5-III.

TABLE 5-II - INFLUENCE OF THE STABILITY DERIVATIVES ON THE NATURAL MODES.

	Phugoid		Spiral	Short Period		Dutch Roll		Rolling
	Damp.	ω_n	Mode	Damp.	ω_n	Damp.	ω_n	Mode
C_{xu}	****	--	--	--	--	--	--	--
$C_{x\alpha}$	**	--	--	--	--	--	--	--
C_{zu}	****	****	--	--	--	--	--	--
$C_{y\alpha}$	--	--	--	--	--	--	--	--
$C_{z\alpha}$	*	**	--	*	***	*	--	**
$C_{\ell\alpha}$	****	*	****	****	****	**	--	****
$C_{m\alpha}$	****	**	****	*	*	*	--	****
$C_{n\alpha}$	--	--	*	--	--	**	--	*
$C_{x\beta}$	--	--	--	--	--	--	--	--
$C_{y\beta}$	--	--	--	--	--	****	--	--
$C_{z\beta}$	--	--	--	--	--	--	--	--
$C_{\ell\beta}$	****	--	****	--	--	****	*	****
$C_{m\beta}$	--	--	--	--	--	--	--	--
$C_{n\beta}$	****	*	****	--	--	****	****	****
C_{xp}	--	--	--	--	--	--	--	--
C_{yp}	--	--	--	--	--	--	--	--
C_{zp}	--	--	--	--	--	--	--	--
$C_{\ell p}$	****		****	****	****	**	--	****
C_{mp}	**	--	****	**	***	*	--	****
C_{np}	--	--	*	--	--	*	--	*
C_{xq_t}	--	--	--	--	--	--	--	--
C_{yq_t}	--	--	--	--	--	--	--	--
C_{zq_t}	--	--	--	--	--	--	--	--

	Phugoid		Spiral	Short Period		Dutch Roll		Rolling
	Damp.	ω_n	Mode	Damp.	ω_n	Damp.	ω_n	Mode
$C_{\ell q}$	**	*	--	*	--	*	--	**
C_{mq}	****	**	--	--	**	*	--	****
C_{nq}	--	--	--	--	--	--	--	--
C_{yr}	--	--	--	--	--	--	--	--
$C_{\ell r}$	****	--	****	--	--	*	--	**
C_{mr}	**	--	****	--	--	--	--	*
C_{nr}	**	--	****	--	--	****	--	****
$C_{z\dot{\alpha}}$	--	--	--	--	--	--	--	--
$C_{m\dot{\alpha}}$	--	--	--	--	--	--	--	*

Influence of the Stability Derivatives on the Natural Modes

TABLE 5-III - COMPARISON BETWEEN STABILITY DERIVATIVES FOR $\Lambda = 45^{o}$

	1	2	3	4	5	6	7
C_{x_α}	.108	.108	.123	.133	.131	N.A.	N.A.
C_{y_α}	.378	.283	.563	.568	.537	--	--
C_{z_α}	-4.24	-4.24	-4.24	-4.11	-4.11	-4.24	-4.53
C_{ℓ_α}	-.203	-.164	-.17	-.0127	-.0133	-.297	-.0573
C_{m_α}	-1.55	-1.10	-1.16	.297	.292	-1.63*	.281*
C_{n_α}	-.0359	-.00235	-.0913	-.0647	-.0673	.0084	.0075
C_{x_β}	-.00657	-.00657	-.00857	-.00929	-.00895	--	--
C_{y_β}	-.282	-.282	-.283	-.283	-.283	-.252	-.252
C_{z_β}	-.459	-.459	-.525	-.546	-.535	-0.228	-0.258
C_{ℓ_β}	-.0239	-.0237	-.0172	-.0146	-.0881	.0705	-.0493
C_{m_β}	.00223	.004	.195	.510	.282	-.0378	.108
C_{n_β}	.131	.131	.125	.125	.131	.035	.034
$C^{**}_{z_{\dot\alpha}}$	-1.03	-1.03	-1.03	-1.03	-1.03	-1.03	-1.03
$C^{**}_{m_{\dot\alpha}}$	-4.78	-4.78	-4.78	-4.78	-4.78	-4.78	-4.78
C_{y_p}	.0105	-.0279	-.06	-.0937	-.109	-.044	-.044
C_{z_p}	-.406	-.328	-.0685	.299	.298	0	.61
C_{ℓ_p}	-.251	-.278	-.212	-.193	-.193	-.4	-.444
C_{m_p}	-2.23	-2.50	-1.94	-1.85	-1.84	-2.66	-3.12
C_{n_p}	-.0153	.0064	.0146	.0184	.0175	.0085	.0119

cont'd

C_{y_q}	.0202	.059	-.0305	-.378	-.55	--	--
C_{z_q}	-4.23	-3.17	-6.73	-3.08	-3.09	-2.02	1.58
C_{ℓ_q}	-2.23	-2.50	-2.14	-1.84	-1.84	-2.66	-2.79
C_{m_q}	-30.1	-32.8	-28.6	-26.7	-26.6	-27.1	-28.7
C_{n_q}	-.354	-.163	-.133	-.0908	-.0831	-.163	-.159
C_{y_r}	.260	.263	.258	.261	.26	.229	.229
C_{z_r}	--	--	--	--	--	--	-.13
C_{ℓ_r}	.0525	.0549	.0544	.0541	.055	.0885	.095
C_{m_r}	.266	.244	.292	.298	.296	.379	.436
C_{n_r}	-.129	-.13	-.13	-.131	-.130	-.1650	-.1654

* No Stability Augmentation (SAS) included.

** These data were taken from Boeing study [Ref. 5] since our program does not have the capability, to date, of computing these derivatives.

The eight columns represent:

1) Strip Theory: spanwise flat and total lift distributions as from Reference 5 (Fig. 5.35). Sideslip evaluated according to empirical method described in section 2.5.
2) Strip Theory: spanwise flat and total lift distributions as computed by lifting line theory (Fig. 5.2). Sideslip evaluated as for case 1 .
3) Lifting line theory, rigid wing.
4) Lifting line theory, elastic wing (E.A. coinciding with quarter-chord axis.
5) Same as No. 4, but no built-in twist.
6) Boeing results rigid wing.
7) Boeing results elastic wing.

```
THE FOLLOWING ARE THE WING CONTRIBUTIONS TO STABILITY DERIVATIVES(STABILITY AXES)

CLPW = 0.748E-05   CMBW = 0.223E-02   CLAW =-0.203E 00   CMAW =-0.148E 01   CNAW =-0.359E-01   CYAW = 0.378E 00
CLRW =-0.247E 00   CMQW =-0.223E 01   CNPW =-0.393E-01   CLQW =-0.223E 01   CMQW =-0.205E 02   CNQW =-0.354E 00
CZAW =-0.222E 01   CLRW = 0.287E-01   CMRW = 0.266E 00   CNPW = 0.141E-02   CZPW =-0.406E 00   CYQW = 0.377E 00
CYRW = 0.532E-01   CYPW =-0.279E-02


                                        STABILITY DERIVATIVES(STABILITY AXES)

 CXU =-0.443E-04                         CZU =-0.553E-03
 CXA = 0.108E 00    CYA = 0.378E 00      CZA =-0.424E 01    CLA =-0.203E 00    CMA =-0.155E 01    CNA =-0.359E-01
 CXB =-0.657E-02    CYB =-0.282E 00      CZB =-0.459E 00    CLB =-0.239E-01    CMB = 0.223E-02    CNB = 0.131E 00
CXAD = 0.0         CYAD = 0.0           CZAD =-0.103E 01   CLAD = 0.0         CMAD =-0.478E 01   CNAD = 0.0
CXBD = 0.0         CYBD = 0.0           CZBD = 0.0         CLBD = 0.0         CMBD = 0.0         CNBD = 0.0
 CXP = 0.0          CYP = 0.105E-01      CZP =-0.406E 00    CLP =-0.251E 00    CMP =-0.223E 01    CNP =-0.155E-01
 CXQ = 0.0          CYQ = 0.202E-01      CZQ =-0.423E 01    CLQ =-0.223E 01    CMQ =-0.301E 02    CNQ =-0.354E 00
 CXR = 0.0          CYR = 0.266E 00      CZR = 0.0          CLR = 0.525E-01    CMR = 0.266E 00    CNR =-0.129E 00

                                        AERODYNAMIC CENTER BUILDUP

ACWB                  =  0.250MAC(@ZERO SWEEP)
 ACT                  =  0.122MAC(@ZERO SWEEP)
ACFS                  =  0.349MAC(@ZERO SWEEP)
 SAS                  =  0.0   MAC(@ZERO SWEEP)
-------------------------------------------------
XAC(NET)              =  0.721MAC(@ZERO SWEEP)

FOR A CENTER OF GRAVITY @ 0.355MAC(@ZERO SWEEP) THE STATIC MARGIN IS   0.366MAC(@ZERO SWEEP)

                                        CONTROL DERIVATIVES

ELEVATOR DEFLECTION DE =  0.0  DEGREE(S)
CZDE =-0.188E-02   CMDE =-0.890E-02

RUDDER DEFLECTION DR =  0.0  DEGREE(S)
CYDR = 0.197E-02   CLDR = 0.178E-03   CNDR = 0.215E-05

AILERONS DEFLECTIONS DA-LEFT =  0.0  DEGREE(S)  DA-RIGHT =  0.0  DEGREE(S)
CYDA = 0.0         CZDA = 0.0         CLDA = 0.0         CMDA = 0.0         CNDA = 0.0
```

TABLE 5-IV Computer Printout for Case 1 of Table 5-III.

```
THE FOLLOWING ARE THE WING CONTRIBUTIONS TO STABILITY DERIVATIVES(STABILITY AXES)

CL8W = 0.218E-03   CMBW = 0.399E-02   CLAW =-0.164E 00   CMAW =-0.103E 01   CNAW =-0.235E-02   CYAW = 0.283E 00
CLPW =-0.273E 00   CMPW =-0.259E 01   CNPW =-0.174E-01   CLQW =-0.250E 01   CMQW =-0.233E 02   CNQW =-0.163E 00
CZQW =-0.116E 01   CLRW = 0.312E-01   CMRW = 0.294E 00   CNRW = 0.998E-03   CZPW =-0.328E 00   CYQW = 0.589E-01
CYPW = 0.199E-01   CYRW = 0.106E-03

                                        STABILITY DERIVATIVES(STABILITY AXES)

 CXU =-0.433E-04                         CZU =-0.553E-03
 CXA = 0.108E 00    CYA = 0.283E 00      CZA =-0.424E 01    CLA =-0.164E 00    CMA =-0.110E 01    CNA =-0.235E-02
 CXB =-0.657E-02    CYB =-0.282E 00      CZB =-0.459E 00    CLB =-0.237E-01    CMB = 0.399E-02    CNB = 0.131E 00
CXAD = 0.000E 00   CYAD = 0.000E 00     CZAD =-0.103E 01   CLAD = 0.000E 00   CMAD =-0.478E 01   CNAD = 0.000E 00
CXBD = 0.000E 00   CYBD = 0.000E 00     CZBD = 0.000E 00   CLBD = 0.000E 00   CMBD = 0.000E 00   CNBD = 0.000E 00
 CXP = 0.000E 00    CYP =-0.279E-01      CZP =-0.328E 00    CLP =-0.278E 00    CMP =-0.250E 01    CNP = 0.639E-02
 CXQ = 0.000E 00    CYQ = 0.202E-01      CZQ =-0.317E 01    CLQ =-0.250E 01    CMQ =-0.328E 02    CNQ =-0.163E 00
 CXR = 0.000E 00    CYR = 0.263E 00      CZR = 0.000E 00    CLR = 0.549E-01    CMR = 0.294E 00    CNR =-0.130E 00

                                        AERODYNAMIC CENTER BUILDUP

ACWB                 =  0.250MAC(@ZERO SWEEP)
 ACT                 =  0.122MAC(@ZERO SWEEP)
ACPS                 =  0.242MAC(@ZERO SWEEP)
 SAS                 =  0.000MAC(@ZERO SWEEP)
-------------------------------------------------
XAC(NET)             =  0.614MAC(@ZERO SWEEP)

FOR A CENTER OF GRAVITY @ 0.355MAC(@ZERO SWEEP) THE STATIC MARGIN IS   0.259MAC(@ZERO SWEEP)

                                        CONTROL DERIVATIVES

ELEVATOR DEFLECTION DE =  0.00 DEGREE(S)
CZDE =-0.188E-02   CMDE =-0.890E-02

RUDDER DEFLECTION DR =  0.00 DEGREE(S)
CYDR = 0.197E-02   CLDR = 0.178E-03   CNDR =-0.000E 00

AILERONS DEFLECTIONS DA-LEFT =  0.00 DEGREE(S)  DA-RIGHT =  0.00 DEGREE(S)
CYDA = 0.000E 00   CZDA = 0.000E 00   CLDA = 0.000E 00   CMDA = 0.000E 00   CNDA = 0.000E 00
```

TABLE 5-V Computer Printout for Case 2 of Table 5-III.

TABLE 5-VI Computer Printout for Case 3 of Table 5-III.

THE FOLLOWING ARE THE WING CONTRIBUTIONS TO STABILITY DERIVATIVES(STABILITY AXES)

RIGID WING ANALISYS

CLBW = 0.630E-02	CMBW = 0.195E 00	CLAW =-0.170E 00	CMAW =-0.109E 01	CNAW =-0.913E-01	CYAW = 0.563E 00
CLPW =-0.208E 00	CMPW =-0.194E 01	CNPW =-0.878E-02	CLQW =-0.214E 01	CMQW =-0.191E 02	CNQW =-0.133E 00
CZQW =-0.471E 01	CLRW = 0.310E-01	CMRW = 0.292E 00	CNPW = 0.858E-03	CZPW =-0.685E-01	CYQW =-0.305E-01
CYPW =-0.129E-01	CYRW =-0.505E-02	CZBW =-0.600E 00	CNBW =-0.673E-02		

STABILITY DERIVATIVES(STABILITY AXES)

CXU =-0.467E-04		CZU =-0.632E-03			
CXA = 0.123E 00	CYA = 0.563E 00	CZA =-0.424E 01	CLA =-0.170E 00	CMA =-0.116E 01	CNA =-0.913E-01
CXB =-0.859E-02	CYB =-0.283E 00	CZB =-0.525E 00	CLB =-0.172E-01	CMB = 0.195E 00	CNB = 0.125E 00
CXAD = 0.0	CYAD = 0.0	CZAD =-0.103E 01	CLAD = 0.0	CMAD =-0.478E 01	CNAD = 0.0
CXBD = 0.0	CYBD = 0.0	CZBD = 0.0	CLBD = 0.0	CMBD = 0.0	CNBD = 0.0
CXP = 0.0	CYP =-0.599E-01	CZP =-0.685E-01	CLP =-0.212E 00	CMP =-0.194E 01	CNP = 0.146E-01
CXQ = 0.0	CYQ =-0.305E-01	CZQ =-0.673E 01	CLQ =-0.214E 01	CMQ =-0.286E 02	CNQ =-0.133E 00
CXR = 0.0	CYR = 0.258E 00	CZR = 0.0	CLR = 0.544E-01	CMR = 0.292E 00	CNR =-0.130E 00

AERODYNAMIC CENTER BUILDUP

ACWB	=	0.250MAC(@ZERO SWEEP)
ACT	=	0.122MAC(@ZERO SWEEP)
ACPS	=	0.256MAC(@ZERO SWEEP)
SAS	=	0.0 MAC(@ZERO SWEEP)
XAC(NET)	=	0.627MAC(@ZERO SWEEP)

FOR A CENTER OF GRAVITY @ 0.355MAC(@ZERO SWEEP) THE STATIC MARGIN IS 0.272MAC(@ZERO SWEEP)

CONTROL DERIVATIVES

ELEVATOR DEFLECTION DE = 0.0 DEGREE(S)
CZDE =-0.213E 00 CMDE =-0.101E 01

RUDDER DEFLECTION DR = 0.0 DEGREE(S)
CYDR = 0.113E 00 CLDR = 0.101E-01 CNDR =-0.563E-01

AILERONS DEFLECTIONS DA-LEFT = 0.0 DEGREE(S) DA-RIGHT = 0.0 DEGREE(S)

AILERONS GEOMETRY W.R.T. WING CENTERLINE (NON-DIM. STAT)

	LEFT WING OUTBOARD	LEFT WING INBOARD	RIGHT WING OUTBOARD	RIGHT WING INBOARD
DESIGN CONDITIONS	-0.927	-0.732	0.927	0.732
COMPUTER APPROXIMATION	-0.937	-0.837	0.862	0.662

LEFT WING AILERON DEFLECTED ONLY
CYDA = 0.253E-02 CZDA =-0.128E 00 CLDA = 0.242E-01 CMDA = 0.257E 00 CNDA =-0.372E-02

RIGHT WING AILERON DEFLECTED ONLY
CYDA = 0.564E-02 CZDA =-0.202E 00 CLDA =-0.521E-01 CMDA =-0.445E 00 CNDA =-0.420E-03

ANTISYMMETRIC AILERON DEFLECTION
CYDA =-0.898E-02 CZDA = 0.745E-01 CLDA = 0.763E-01 CMDA = 0.702E 00 CNDA =-0.457E-03

```
THE FOLLOWING ARE THE WING CONTRIBUTIONS TO STABILITY DERIVATIVES(STABILITY AXES)

   ELASTIC WING ANALISYS

CLBW = 0.381E-01   CMPW = 0.510E 00   CLAW =-0.127E-01   CMAW = 0.382E 00   CNAW =-0.647E-01   CYAW = 0.568E 00
CLPW =-0.169E 00   CMPW =-0.185E 01   CNPW =-0.502E-02   CLQW =-0.184E 01   CMQW =-0.171E 02   CNQW =-0.908E-01
CZQW =-0.107E 01   CLPW = 0.307E-01   CMRW = 0.298E 00   CNRW = 0.156E-03   CZPW = 0.299E 00   CYQW =-0.378E 00
CYPW =-0.467E-01   CYAW =-0.203E-02   CZBW =-0.664E 00CNBW =-0.585E-02


                                   STABILITY DERIVATIVES(STABILITY AXES)

 CXU =-0.476E-04                                  CZU =-0.658E-03
 CXA = 0.133E 00    CYA = 0.568E 00               CZA =-0.411E 01    CLA =-0.127E-01    CMA = 0.297E 00    CNA =-0.647E-01
 CXB =-0.929E-02    CYB =-0.283E 00               CZB =-0.546E 00    CLB = 0.146E-01    CMB = 0.510E 00    CNB = 0.125E 00
CXAD = 0.0         CYAD = 0.0                     CZAC =-0.103E 01   CLAD = 0.0         CMAD =-0.478E 01   CNAD = 0.0
CXBD = 0.0         CYBD = 0.0                     CZBC = 0.0         CLBD = 0.0         CMBD = 0.0         CNBD = 0.0
 CXP = 0.0          CYP =-0.937E-01               CZP = 0.299E 00    CLP =-0.193E 00    CMP =-0.185E 01    CNP = 0.184E-01
 CXQ = 0.0          CYQ =-0.378E 00               CZC =-0.308E 01    CLQ =-0.184E 01    CMQ =-0.267E 02    CNQ =-0.908E-01
 CXR = 0.0          CYR = 0.261E 00               CZR = 0.0          CLR = 0.541E-01    CMR = 0.298E 00    CNR =-0.131E 00

                                   AERODYNAMIC CENTER BUILDUP

ACWB                  =  0.250MAC(@ZERO SWEEP)
 ACT                  =  0.126MAC(@ZERO SWEEP)
ACPS                  = -0.093MAC(@ZERO SWEEP)
 SAS                  =  0.0  MAC(@ZERO SWEEP)
-------------------------------------------
XAC(NET)              =  0.283MAC(@ZERO SWEEP)

FOR A CENTER OF GRAVITY @ 0.355MAC(@ZERO SWEEP) THE STATIC MARGIN IS  -0.072MAC(@ZERO SWEEP)


                                   CONTROL DERIVATIVES

ELEVATOR DEFLECTION DE =  0.0  DEGREE(S)
CZDE =-0.213E 00   CMDE =-0.101E 01

RUDDER DEFLECTION DR =  0.0  DEGREE(S)
CYDR = 0.113E 00   CLDR = 0.101E-01   CNDR =-0.563E-01

AILERONS DEFLECTIONS DA-LEFT =  0.0  DEGREE(S)  DA-RIGHT =  0.0  DEGREE(S)

AILERONS GEOMETRY W.R.T. WING CENTERLINE (NON-DIM. STAT)

                          LEFT  WING                RIGHT  WING
                       OUTBOARD    INBOARD       OUTBOARD    INBOARD
DESIGN CONDITIONS        -0.927     -0.732          0.927      0.732
COMPUTER APPROXIMATION   -0.937     -0.837          0.862      0.662

LEFT WING AILERON DEFLECTED ONLY
CYDA = 0.103E-01   CZDA =-0.177E 00   CLDA = 0.312E-01   CMDA = 0.334E 00   CNDA =-0.443E-02

RIGHT WING AILERON DEFLECTED ONLY
CYDA =-0.150E-02   CZDA =-0.888E-01   CLDA =-0.279E-01   CMDA =-0.243E 00   CNDA = 0.520E-03

ANTISYMMETRIC AILERON DEFLECTION
CYDA = 0.741E-02   CZDA =-0.887E-01   CLDA = 0.591E-01   CMDA = 0.577E 00   CNDA =-0.300E-02
```

TABLE 5-VII Computer Printout for Case 4 of Table 5-III.

THE FOLLOWING ARE THE WING CONTRIBUTIONS TO STABILITY DERIVATIVES(STABILITY AXES)

ELASTIC WING ANALISYS

CLBW = 0.147E-01	CMBW = 0.292E 00	CLAW =-0.133E-01	CMAW = 0.376E 00	CNAW =-0.673E-01	CYAW = 0.537E 00
CLPW =-0.138E 00	CMPW =-0.184E 01	CNPW =-0.593E-02	CLQW =-0.184E 01	CMQW =-0.171E 02	CNQW =-0.831E-01
CZQW =-0.138E 01	CLRW = 0.316E-01	CMRW = 0.296E 00	CNRW = 0.858E-03	CZPW = 0.298E 00	CYQW =-0.550E 00
CYPW =-0.625E-01	CYRW =-0.228E-02	CZBW =-0.631E 00	CNBW =-0.337E-02		

STABILITY DERIVATIVES(STABILITY AXES)

CXU =-0.472E-04		CZU =-0.645E-03			
CXA = 0.131E 00	CYA = 0.537E 00	CZA =-0.411E 01	CLA =-0.133E-01	CMA = 0.292E 00	CNA =-0.673E-01
CXB =-0.895E-02	CYB =-0.283E 00	CZB =-0.535E 00	CLB =-0.882E-02	CMB = 0.282E 00	CNB = 0.128E 00
CXAD = 0.0	CYAD = 0.0	CZAD =-0.103E 01	CLAD = 0.0	CMAD =-0.478E 01	CNAD = 0.0
CXBD = 0.0	CYBD = 0.0	CZBD = 0.0	CLBD = 0.0	CMBD = 0.0	CNBD = 0.0
CXP = 0.0	CYP =-0.109E 00	CZP = 0.298E 00	CLP =-0.193E 00	CMP =-0.184E 01	CNP = 0.175E-01
CXQ = 0.0	CYQ =-0.550E 00	CZQ =-0.309E 01	CLQ =-0.184E 01	CMQ =-0.266E 02	CNQ =-0.831E-01
CXR = 0.0	CYR = 0.260E 00	CZR = 0.0	CLR = 0.550E-01	CMR = 0.296E 00	CNR =-0.130E 00

AERODYNAMIC CENTER BUILDUP

ACWB	=	0.250MAC(@ZERO SWEEP)
ACT	=	0.126MAC(@ZERO SWEEP)
ACPS	=	-0.092MAC(@ZERO SWEEP)
SAS	=	0.0 MAC(@ZERO SWEEP)
XAC(NET)	=	0.284MAC(@ZERO SWEEP)

FOR A CENTER OF GRAVITY @ 0.355MAC(@ZERO SWEEP) THE STATIC MARGIN IS -0.071MAC(@ZERO SWEEP)

CONTROL DERIVATIVES

ELEVATOR DEFLECTION DE = 0.0 DEGREE(S)
CZDE =-0.213E 00 CMDE =-0.101E 01

RUDDER DEFLECTION DR = 0.0 DEGREE(S)
CYDR = 0.113E 00 CLDR = 0.101E-01 CNDR =-0.563E-01

AILERONS DEFLECTIONS DA-LEFT = 0.0 DEGREE(S) DA-RIGHT = 0.0 DEGREE(S)

AILERONS GEOMETRY W.R.T. WING CENTERLINE (NON-DIM. STA)

	LEFT WING		RIGHT WING	
	OUTBOARD	INBOARD	OUTBOARD	INBOARD
DESIGN CONDITIONS	-0.927	-0.732	0.927	0.732
COMPUTER APPROXIMATION	-0.937	-0.837	0.862	0.662

LEFT WING AILERON DEFLECTED ONLY
CYDA = 0.110E-01 CZDA =-0.177E 00 CLDA = 0.312E-01 CMDA = 0.334E 00 CNDA =-0.303E-02

RIGHT WING AILERON DEFLECTED ONLY
CYDA =-0.574E-02 CZDA =-0.888E-01 CLDA =-0.279E-01 CMDA =-0.243E 00 CNDA = 0.211E-02

ANTISYMMETRIC AILERON DEFLECTION
CYDA = 0.123E-01 CZDA =-0.887E-01 CLDA = 0.591E-01 CMDA = 0.577E 00 CNDA =-0.319E-02

TABLE 5-VIII Computer Printout for Case 5 of Table 5-III

The elastic wing, unlike the rigid one, shows a positive $C_{m\alpha}$ or pitch-up moment.

There are no major discrepancies between our results and Boeing's except in the $C_{n\beta}$ derivative. Since the major contribution to the latter is from the fin, the difference may result from our assumption $\frac{\alpha\delta}{\alpha\beta} = 0$.

It is useful to consider stability derivatives as functions of skew angle before discussing dynamic response.

The effect of skew is seen in the accompanying graphs (Figures 5.35 through 5.41) on a configuration that was stabilized by moving the C.G. .15 M.A.C. further forward.

The behavior of these derivatives is explainable in terms of two important changes in the lift distribution resulting from an angle of attack perturbation.

The first of these is the predominance of lift on the trailing wing. The second is the effective reduction of the lift forces arising from roll and pitch rates or changes in pitch attitude, that is, $C_{L\alpha}$ is reduced.

The program approximates $C_{L\alpha}$ as the calculated lift divided by dynamic pressure, wing area, and cruise angle of attack. From simple two dimensional sweep theory, the lift on a wing at constant angle of attack and free stream velocity varies as the cube of the cosine of the sweep angle. The effective dynamic pressure is reduced by a factor $\text{Cos}^2\Lambda$ and the effective section angle of attack by a further factor of $\text{Cos}\Lambda$. The lift distrubition calculated by the program

closely matches this $Cos^3\Lambda$ variation. $C_{L\alpha}$ is proportional to C_L and hence behaves as $Cos^3\Lambda$ as well.

It is not possible to easily follow the details of a change of skew angle through the lifting line analysis to verify the $Cos^3\Lambda$ dependence which results.

The trailing vortices move closer to the downwash control points, and bound vortex segments decrease in length in proportion to $Cos\Lambda$, which accounts for a factor $Cos^2\Lambda$. The change in the geometry relating the vortex segments to the control points is complex however and gives rise to three dimensional effects such as the lop-sided lift distribution, which are totally unaccounted for in two dimensional simple sweep theory.

In addition to decreasing $C_{L\alpha}$, the closer lateral proximity of the skewed wing to the body reduces the roll induced velocities. However the extension of the skewed wing fore and aft of the C.G. causes increased pitch induced velocities.

In pitch, roll, and yaw manouvers the lift perturbation distribution is unsymmetrical with respect to the center line so that consideration must be given to the changing moment arms in interpreting the behavior of the derivatives.

The moment arms are decreased for rolling moment derivatives, increased for pitching moment derivatives and relatively unchanged for yawing moment derivatives.

These observations lead to the following understandings of the effect of skew on individual derivatives:

(1) C_L, $C_{L\alpha}$ experience a decrease as explained earlier. A $Cos^3\Lambda$ dependence applies only to small variations about

an equilibrium position. The airplane C_L would be maintained at a constant cruise velocity by increasing cruise angle of attack as $\cos^{-3}\Lambda$.

(2) $C_{m\alpha}$: The tendency of lift to shift to the rear wing leads to a rearwand shift of the neutral point as shown in the graph of vehicle aerodynamic center, or an increase in the static margin. However the decrease in $C_{L\alpha}$ dominates, and $C_{m\alpha} = C_{L\alpha}$ x static margin is reduced.

(3) $C_{x\alpha}$: displays slight increase until skew reaches 20° decreasing thereafter. From Appendix B, $C_{x\alpha} = C_L(1-2kC_{L\alpha})\ C_L$ and $C_{L\alpha}$ are both decreasing which results in the calculated reversal. ("Reversal" will be used to mean a reversal in the sign of a curve's slope, and "reversal in sign" a zero crossing of the curve). The second term in the parenthesis is the contribution of induced drag, while the first results from the rotation in the perturbed body frame of a lift vector fixed in stability reference axes.

(4) $C_{y\alpha}$: increases with the appearance of a sideways rotation of the lift vector and a sideways component of induced drag. The reversal is caused by the dramatic decrease of C_L and $C_{L\alpha}$ at high skew angles.

(5) $C_{z\alpha} = -C_{L\alpha}$

(6) $C_{\ell\alpha}$, where ℓ is rolling moment, increases with the shift of lift to the trailing wing, but eventually reverses with decreasing $C_{L\alpha}$ and moment arm

(7) $C_{\eta\alpha}$ is the result of X_α, the X force due to an α perturbation, acting through a moment arm proportional to $\cos\Lambda$ and Y_α through

an arm proportional to Sin Λ : initially side force generated yawing moment predominates and $C_{n\alpha}$ increases. Decline sets in as the longitudinal force generated moment becomes increasingly smaller and $C_{y\alpha}$ itself begins to decline. Again the reduction of C_L and $C_{L\alpha}$ with skew has an important role.

(8) C_{yp} : Monotonicly increases for the same reasons as $C_{y\alpha}$. The increase is less dramatic because of the decreasing distance of the wing tip from the centerline, and reduced roll induced angles of attack. The non-zero value at zero skew is due to the rudder.

(9) C_{zp} : Normally zero for symmetric aircraft which have an antisymmetric roll generated lift distribution, the C_{zp} curve has two startling reversals and a reversal in sign. The derivative is very sensitive to slight departures of the lift distribution from antisymmetry. In the range 0^o to 10^o skew, lift decreases more on the leading wing in a roll than it increases on the trailing wing. After 10^o the trend is reversed until the lift increment on the right trailing wing dominates as in figure 5-18 for $\Lambda = 45^o$.

The final reversal reflects decreasing lift curve slope and effective roll induced angles of attack.

(10) $C_{\ell p}$: decreases monotonicly with declining roll induced velocities, effective section angle of attack, and lift curve slope, causing a reduction in roll damping

(11) C_{m_p}: increases with skew because of an antisymmetric roll distribution acting through an increasing moment arm. Declining roll induced effective angles of attack and lift curve slope cause a reversal.

(12) $C_{\eta p}$: Decreasing X- force yawing moment arms are offset by increasing Y- force arms. The longitudinal position of the center of gravity will influence the shape. Figures 5-19 (a) and (b) show distortion of the expected antisymmetric X and Y force distribution. Since the incremental lift distribution in roll shown in figure 5-18 for $\Lambda = 45^{\circ}$ is almost normal, the distortion is related to an abnormal downwash distribution, figure 5.13 a). The departure from an antisymmetric force distribution decreases $C_{\eta p}$ from 0° to 30°.

(13) C_{yq}: Figures 5-22 (a) and (b), showing pitch generated X and Y- force distributions, are similar to those for roll generated horizontal force distributions. In figure 5-21 the corresponding lift increment is noticeable greater on the trailing wing. Skewing the wing has a less detractive effect on pitching stability derivatives because induced velocities and aerodynamic twist increase. The detractive effects of diminishing effective angle of attack, and dynamic pressure remain however. The horizontal force distributions are symmetric at 0° skew but become less so as portions of the leading wing extend in front of the center of gravity. The distortion mentioned earlier opposes this tendency.

(14) C_{zq}: declines steadily with an increasingly antisymmetric lift distribution (Figure 5-21)

(15) $C_{\ell q}$: increases for the same reasons that C_{zq} decreases, until the familiar high skew angle deterioration takes place.

(16) C_{mq}: is initially non-zero for a center of gravity not on the quarter chord. The introduction of antisymmetry in the incremental pitching lift distribution, and increased induced velocities, and pitching moment arms increase C_{mq} rapidly at first.

(17) C_{hq}: The rapid increase after $\Lambda = 15^{o}$, and the tapering off above $\Lambda = 30^{o}$ correspond to the varying antisymmetry in C_{yq}. The initial decrease may be because the wing quarter chord lies behind the center of gravity at $\Lambda = 0^{o}$, so that when side force components of induced drag first appear their contribution to yawing moment is positive. As the skew angle increases, and the forward wing extends ahead of the center of gravity, its contribution to yawing moment becomes negative. The non-zero initial value of C_{nq} could not be explained, but may result from an unsymmetrical downwash distribution at zero sweep.

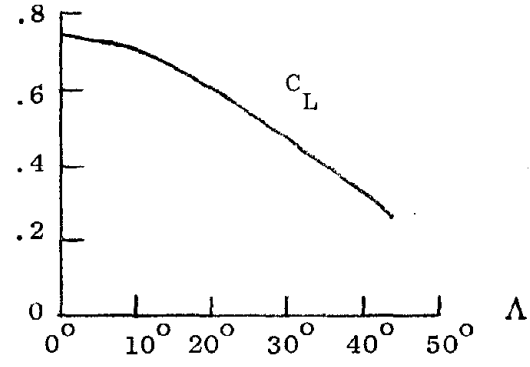

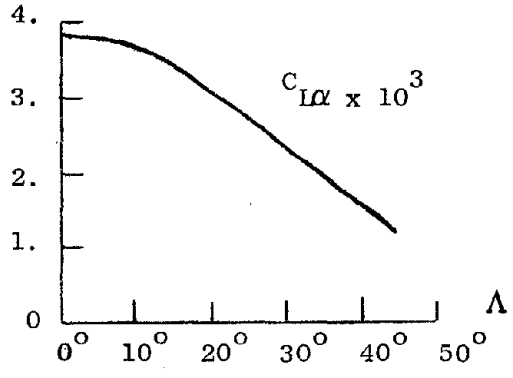

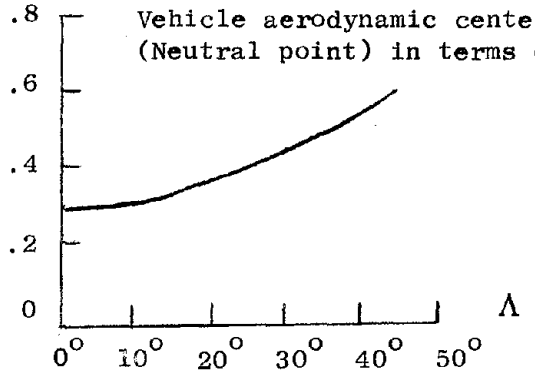

Figure 5.35 - Lift coefficient, lift curve slope, and aerodynamic center versus skew angle

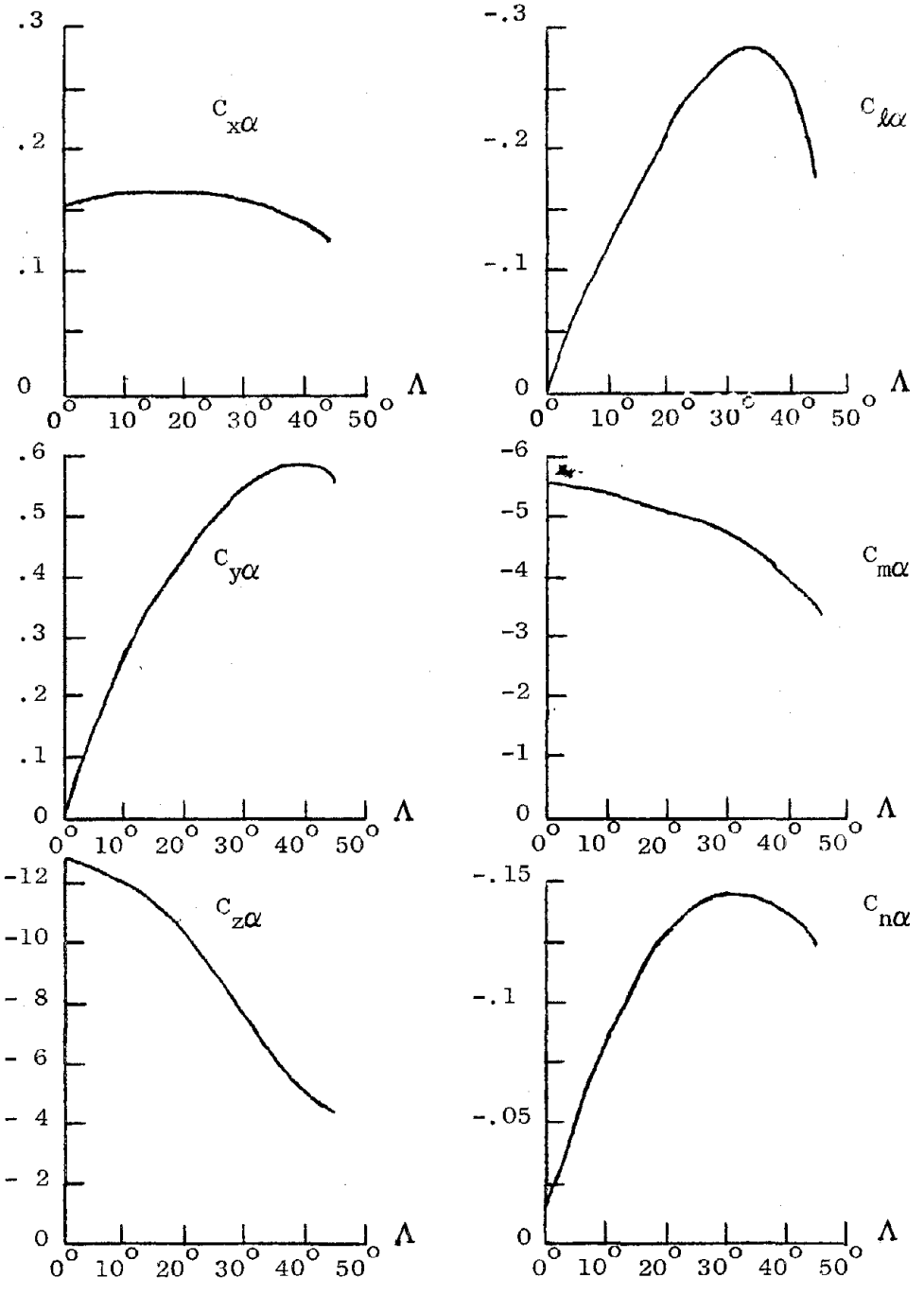

Figure 5.36 - α stability derivatives versus skew angle

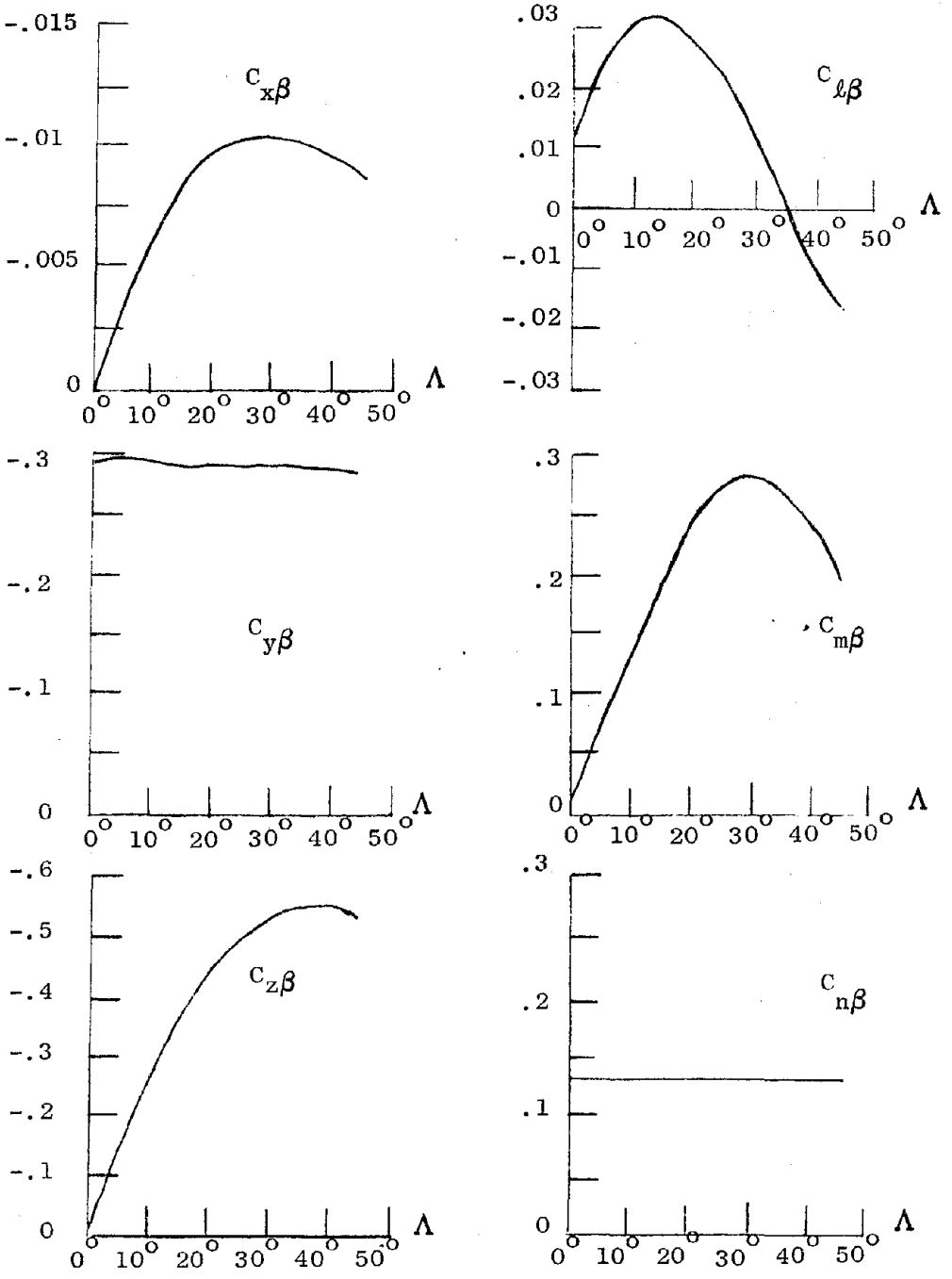

Figure 5.37 - β stability derivatives versus skew angle

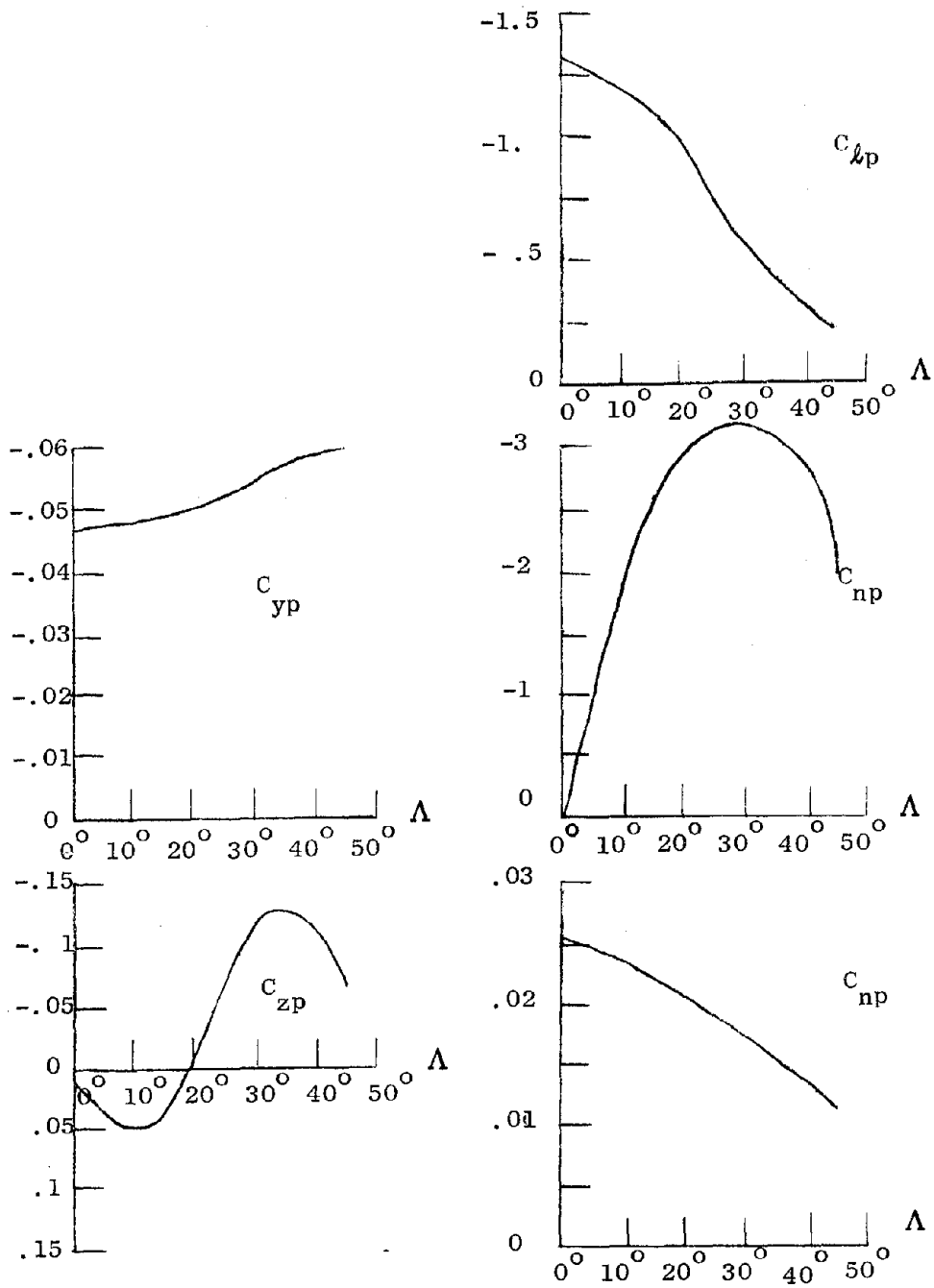

Figure 5.38 - p stability derivatives versus skew angle

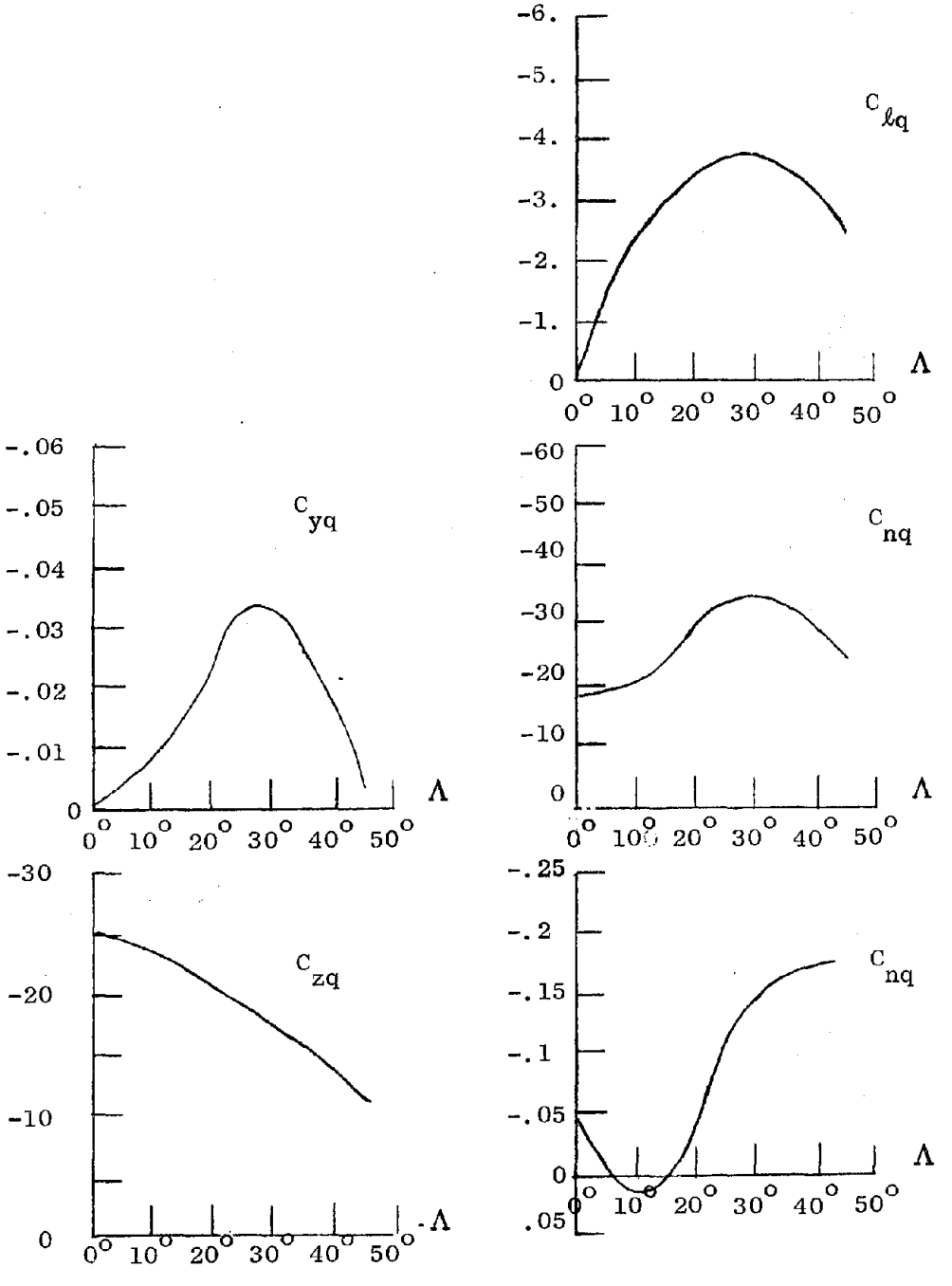

Figure 5.39 - q stability derivatives versus skew angle

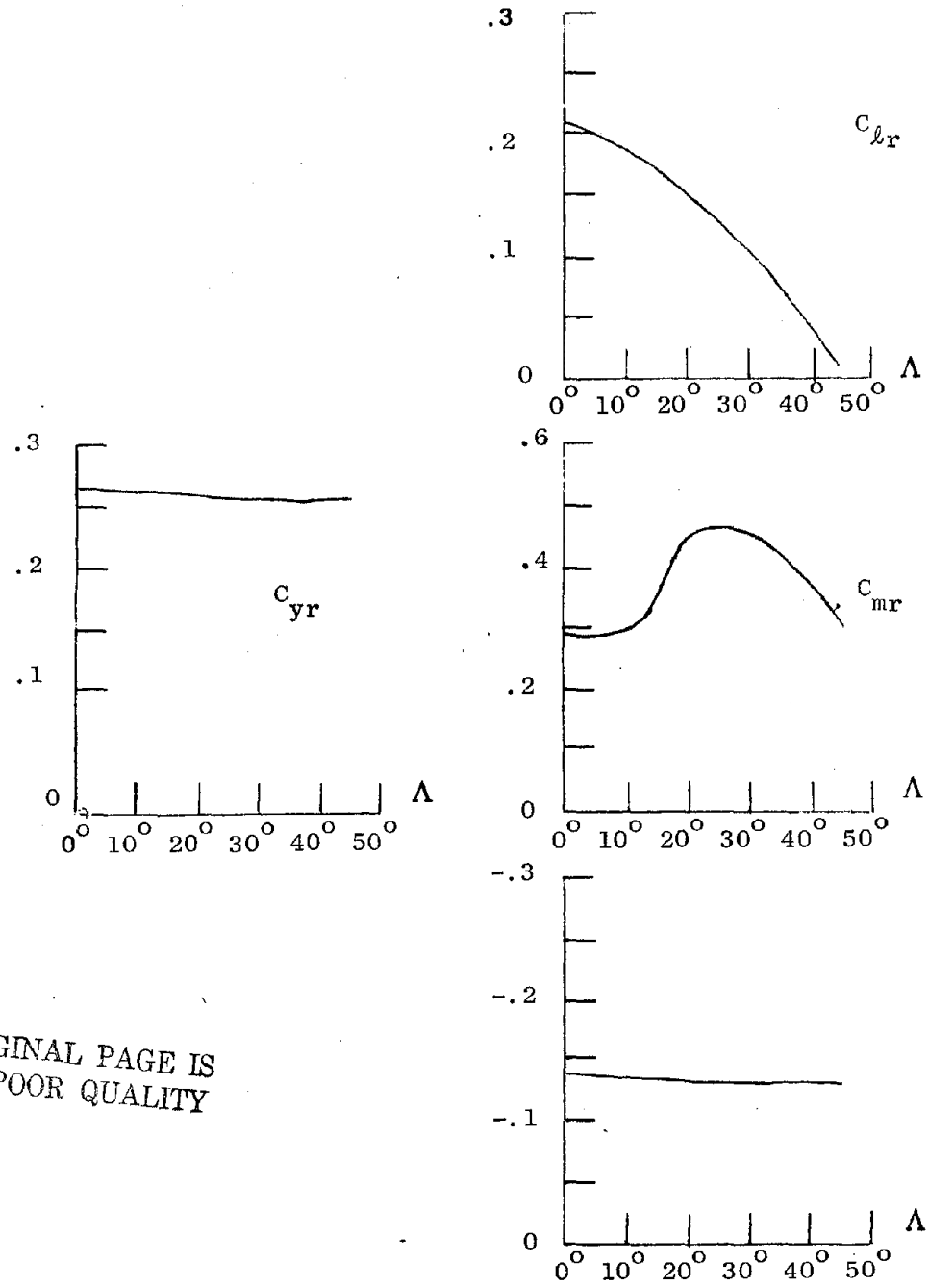

Figure 5.40 - r stability derivatives versus skew angle

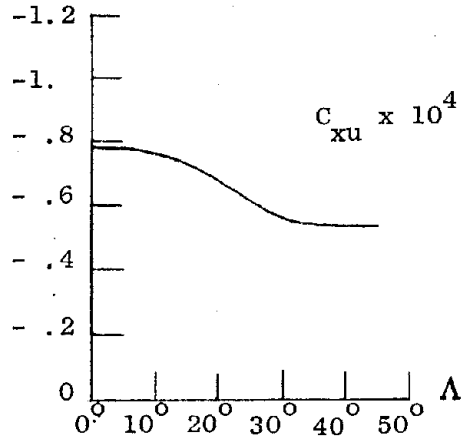

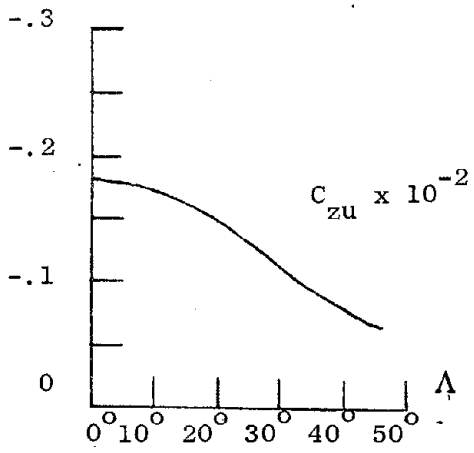

Figure 5.41 - u stability derivatives

versus skew angle

5.5 Dynamic Results

5.5.1 Natural Modes

In 5.1, Model description, it was noted that a C.G. location of 355 M.A.C. resulted in longitudinal instability. In case 3 of Table 5-III the instability is not apparent from $C_{m\alpha}$ which is less than zero, however the roots illustrate the unstable short period mode discussed in 5.1:

	Damping	Wn	Real Root	Imag. Root
Phugoid	.1265	.063	-.00797	$\pm$ .0652
Dutch Roll	.1001	1.058	-.1059	$\pm$ 1.053
"Rolling-Short-Period"	.8007	2.120	-.1713	$\pm$ 1.25
Spiral Mode			.0166	
Unstable "Short Period"			.1542	

Table 5-X records similar roots for case 1 and case 5. These configurations are therefore longitudinally unstable as well. The standard short period and rolling convergence modes are recovered for both cases when 40% SAS is introduced (equivalent to moving the C. G. forward .4 M.A.C.) The added static margin decreased $C_{m\alpha}$ to -2.85 and -1.35 for cases 3 and 5 respectively.

Since the numerical integration is sensitive to the number of wing stations, to obtain good results a large number of stations should be considered.

For example, the stability derivatives for cases 3 and 5 (40% SAS) are shown in Tables 5-XI and 5-XII and the corresponding natural modes in Table 5-X for 36 wing stations, compared to 40 for previous cases.

The roots of the dynamic equations were computed at $\Lambda = 0^{\circ}$, 15°, 30°, and 45° for the configuration having a C.G. at -.15 M.A.C., and the accompanying root loci plotted. (Figures 5.42 through 5.46)

These reveal the variation of dynamic behavior corresponding to the stability derivative versus skew angle curves plotted earlier.

The effect of skew is to cause minor variation in the natural frequencies of all but the rolling convergence mode, which experiences a large reduction in roll damping. This is traceable to the diminishing of $C_{\ell p}$ and further to declining $C_{L\alpha}$, moment arms, and induced velocities.

The mode shapes corresponding to the new roots at $\Lambda = 45^{\circ}$ are shown in the form of Argand diagrams. (Figures 5.47 through 5.50) Although the characteristic roots have changed only moderately the dynamic modes no longer resemble the familiar ones of a symmetric airplane.

The diagrams show the phase and magnitude relation of the six state variables describing the dynamic state. When the magnitude of a state variable is insignificant its relative phase angle is still shown by a line. State variables for non-oscillatory modes have only 0° or 180° phase relations between them. The rolling convergence mode is one of these. The Argad diagram for $\Lambda = 45^{\circ}$ shows the diminished roll rate r resulting from the reduction in roll damping.

In summary, the most dramatic change in dynamic characteristics appears to be the reduction in the roll mode damping. No other large changes in root locations due to sweep were encountered

for this configuration. The changes in mode shapes due to the longitudinal/lateral coupling are generally small with the exception of the short period; which takes on a substantial amount of rolling along with the normal θ and α .

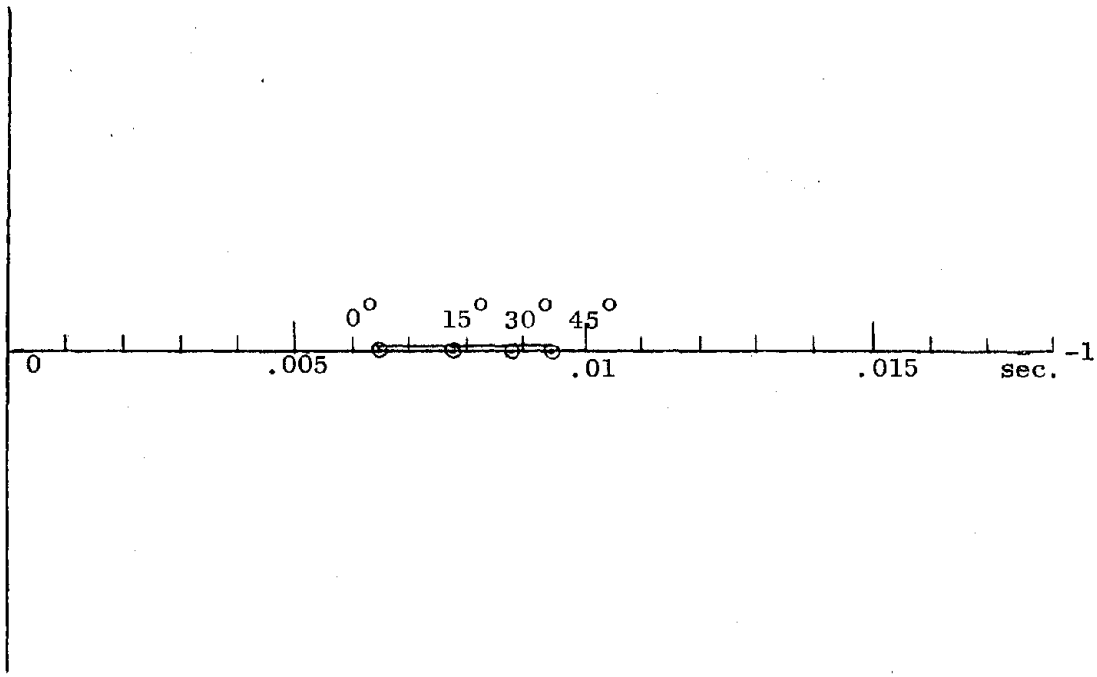

Figure 5.42 - Root locus versus skew angle for spiral mode.

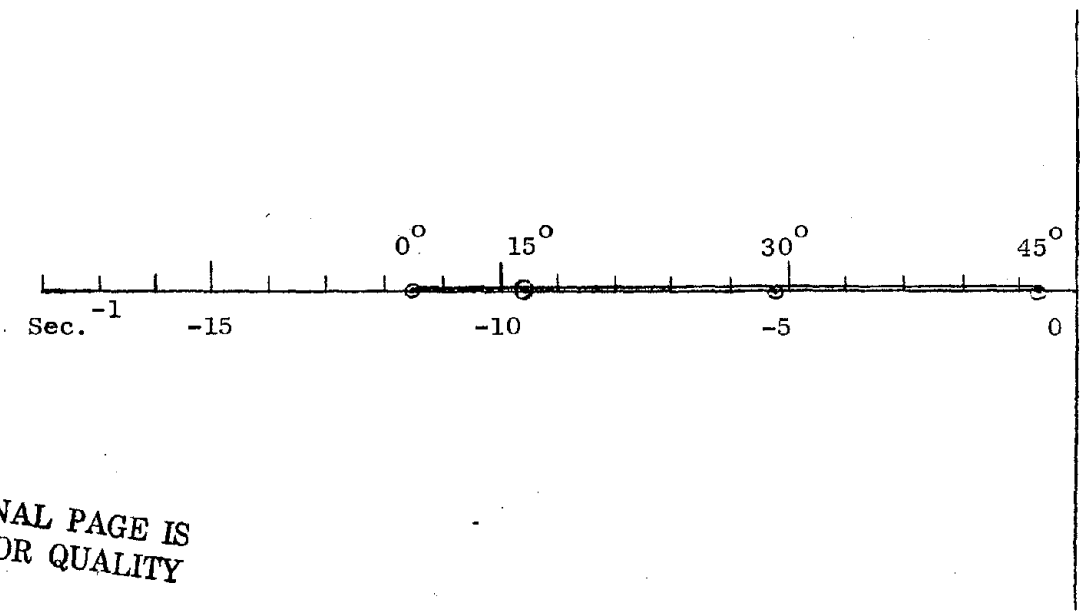

Figure 5.43 - Root locus versus skew angle for rolling convergence

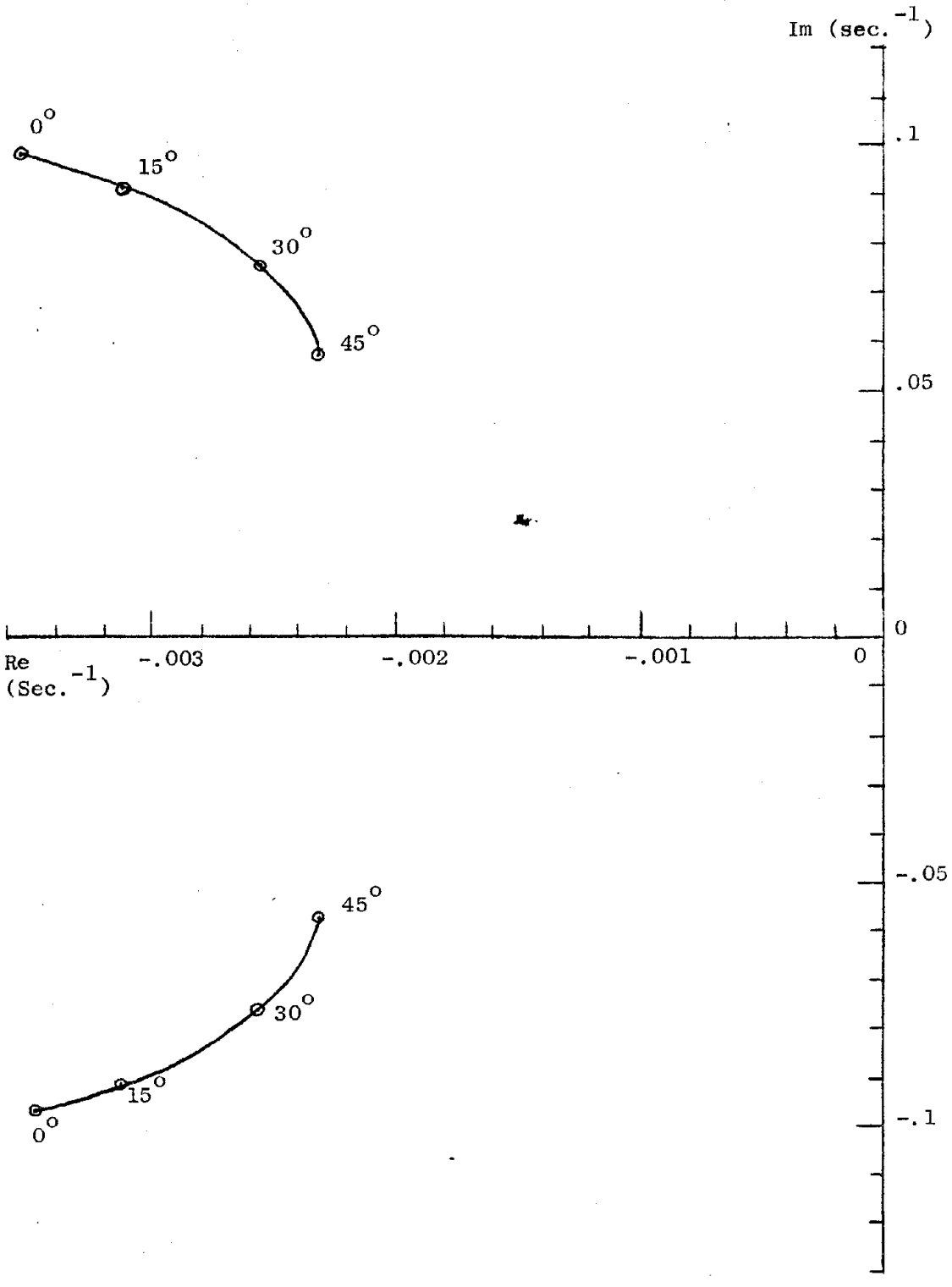

Figure 5.44 - Root locus versus skew angle for phugoid mode

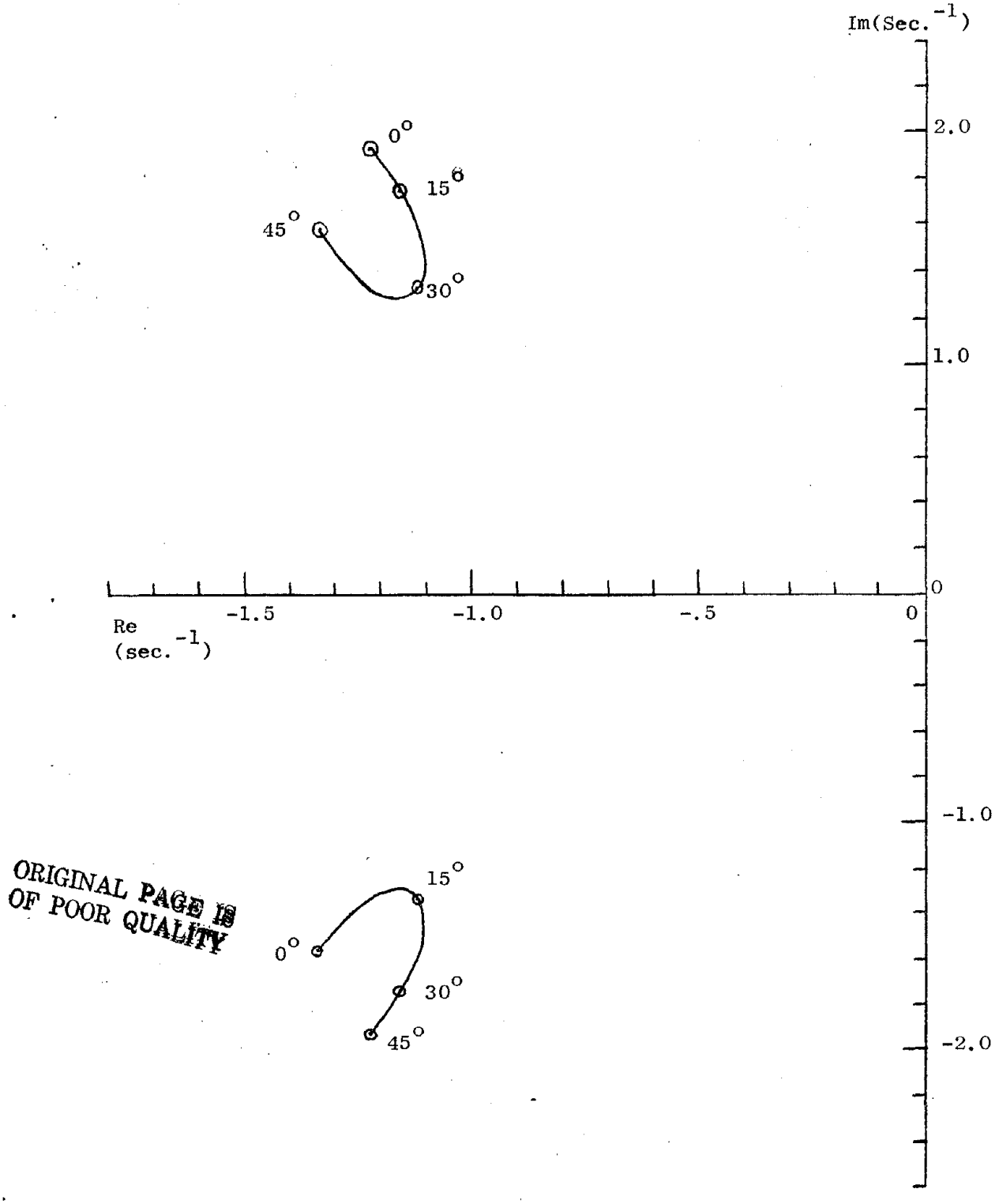

Figure 5.45 - Root locus versus skew angle for short period mode.

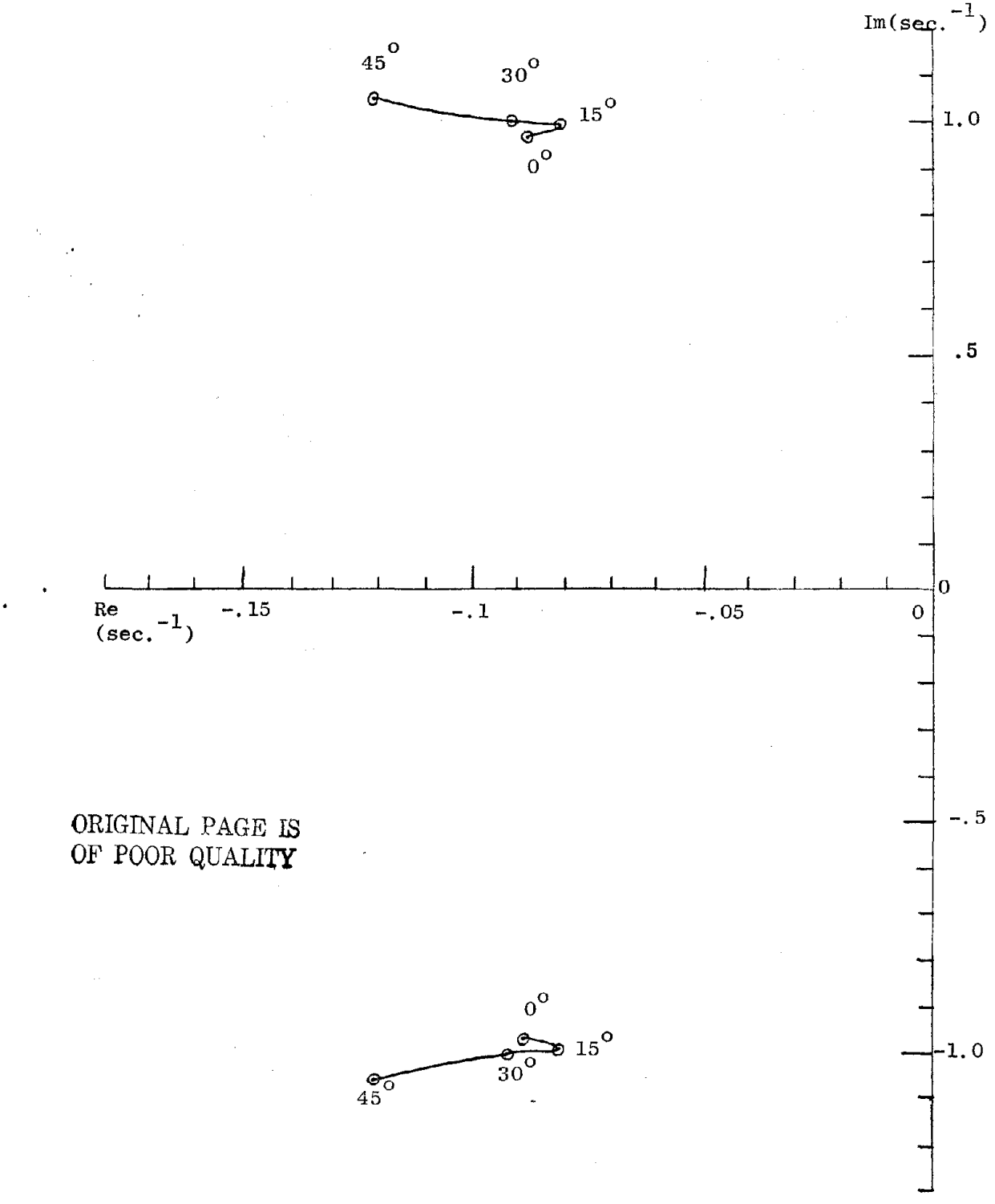

Figure 5.46 - Root locus versus skew angle for lateral oscillation or Dutch roll

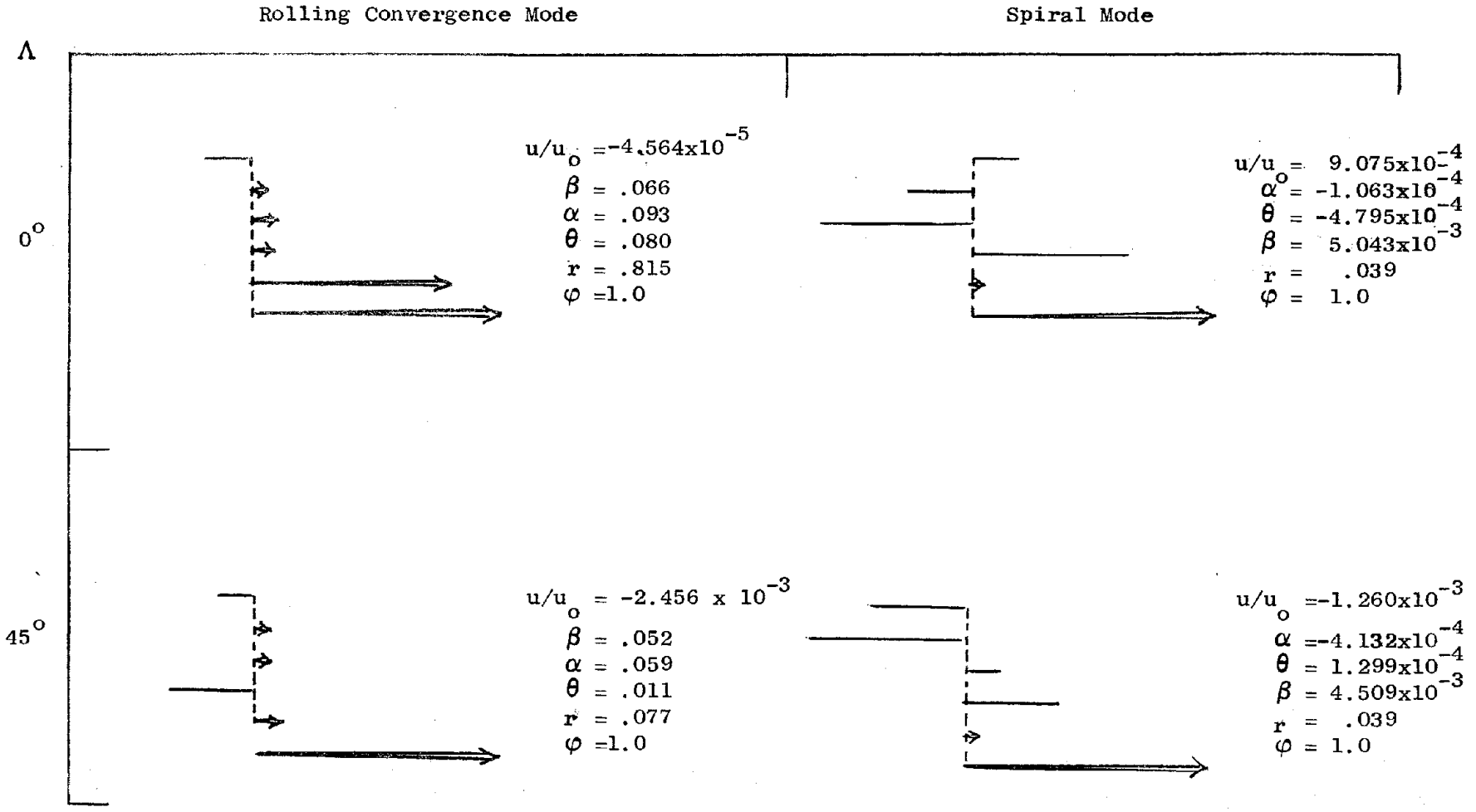

Figure 5.47 - Effect of skew on rolling convergence and spiral mode shapes

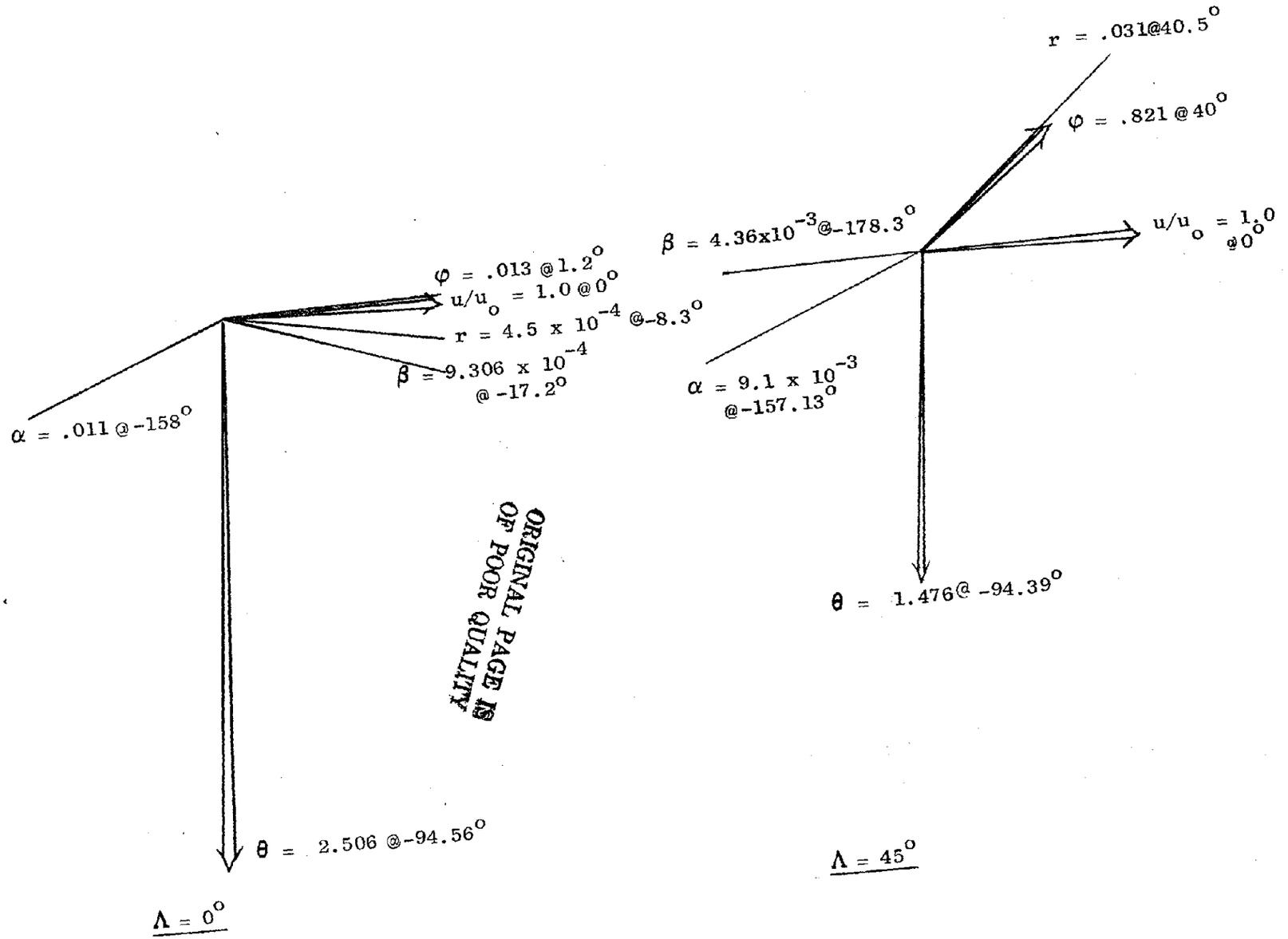

Figure 5.48 - Effect of skew on the phugoid mode shape

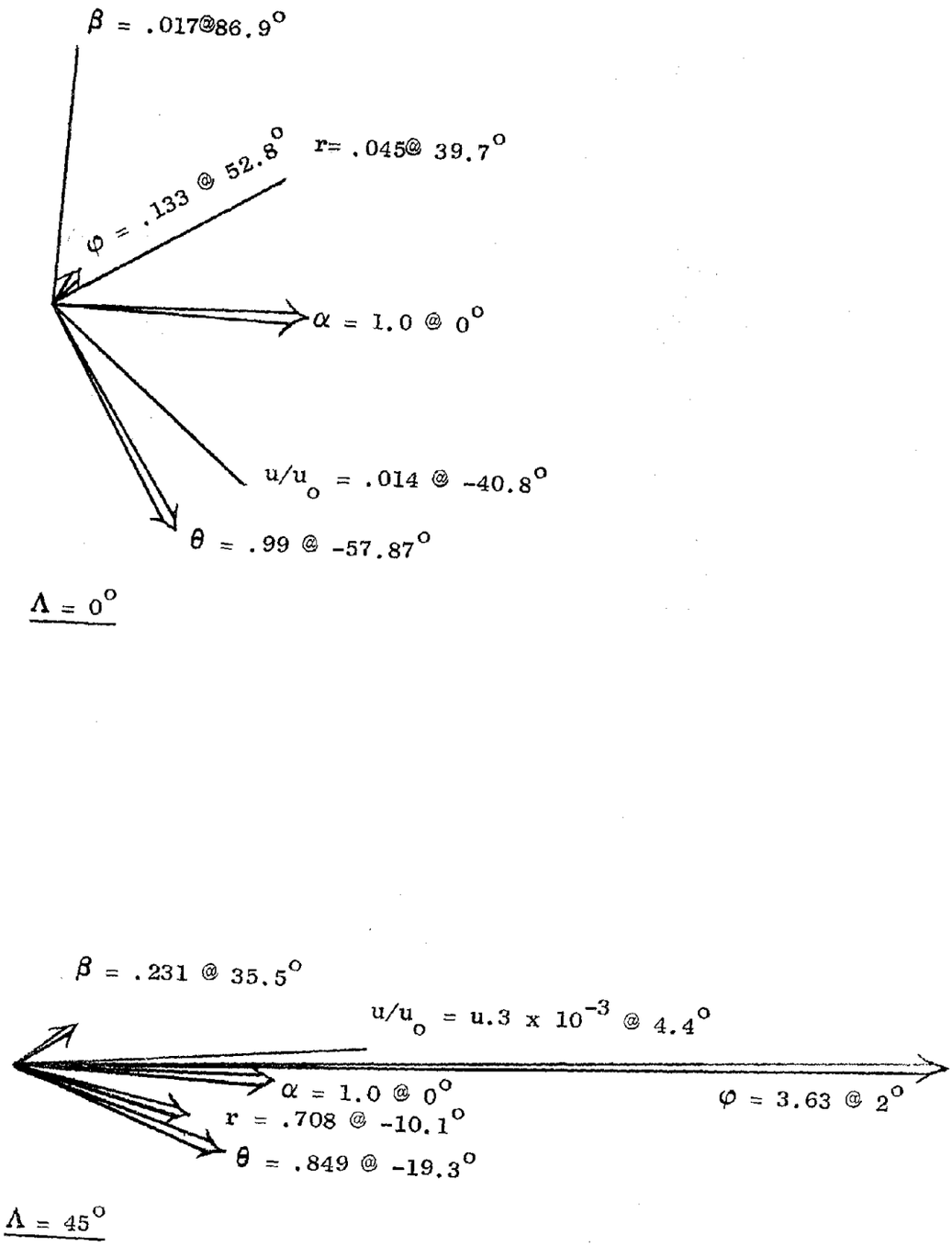

Figure 5.49 - Effect of skew on short period mode shape.

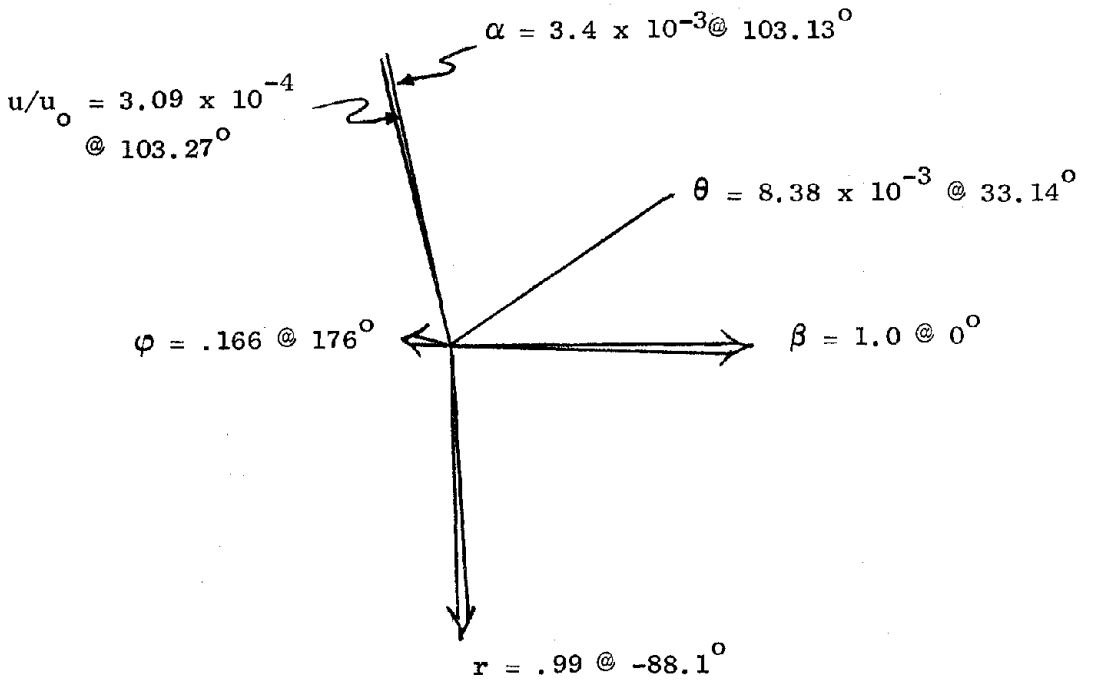

$\Lambda = 0^{o}$

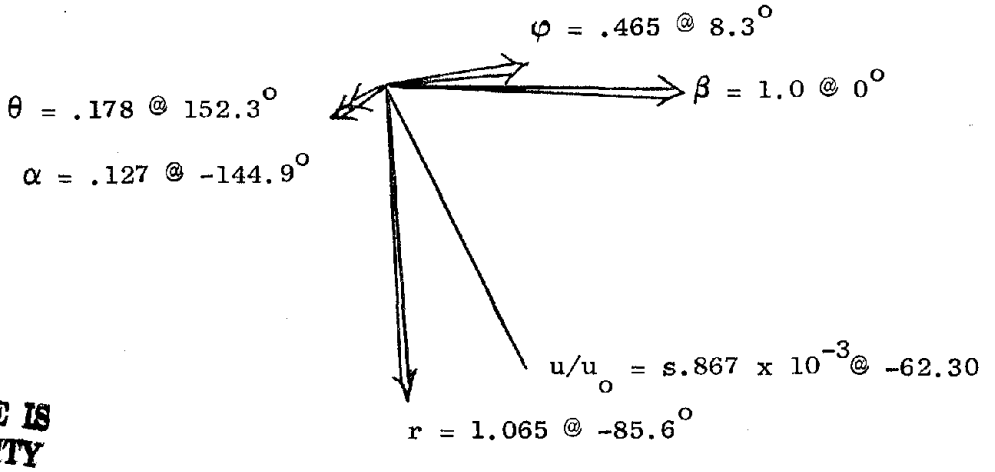

$\Lambda = 45^{o}$

Figure 5.50 - Effect of skew on lateral oscillation on Dutch roll

5.5.2 Transient Response

The transient responses have been computed for two cases:

(1) Rigid wing, 40% SAS added.

(2) Flexible wing, no twist, 40% SAS added

Figure 5.51 compares with α and β responses to an aileron impulse for the 40% SAS rigid wing case and shows the cross coupling between the lateral and longitudinal modes.

Figure 5.52 compares the α and β responses to an elevator impulse for the elastic wing with 40% SAS. Note that the β response is larger than the α response after the initial peak in the first second and will no doubt have some effect on a pilot's evaluation of the handling qualities. This same result was found for the rigid wing with 40% SAS.

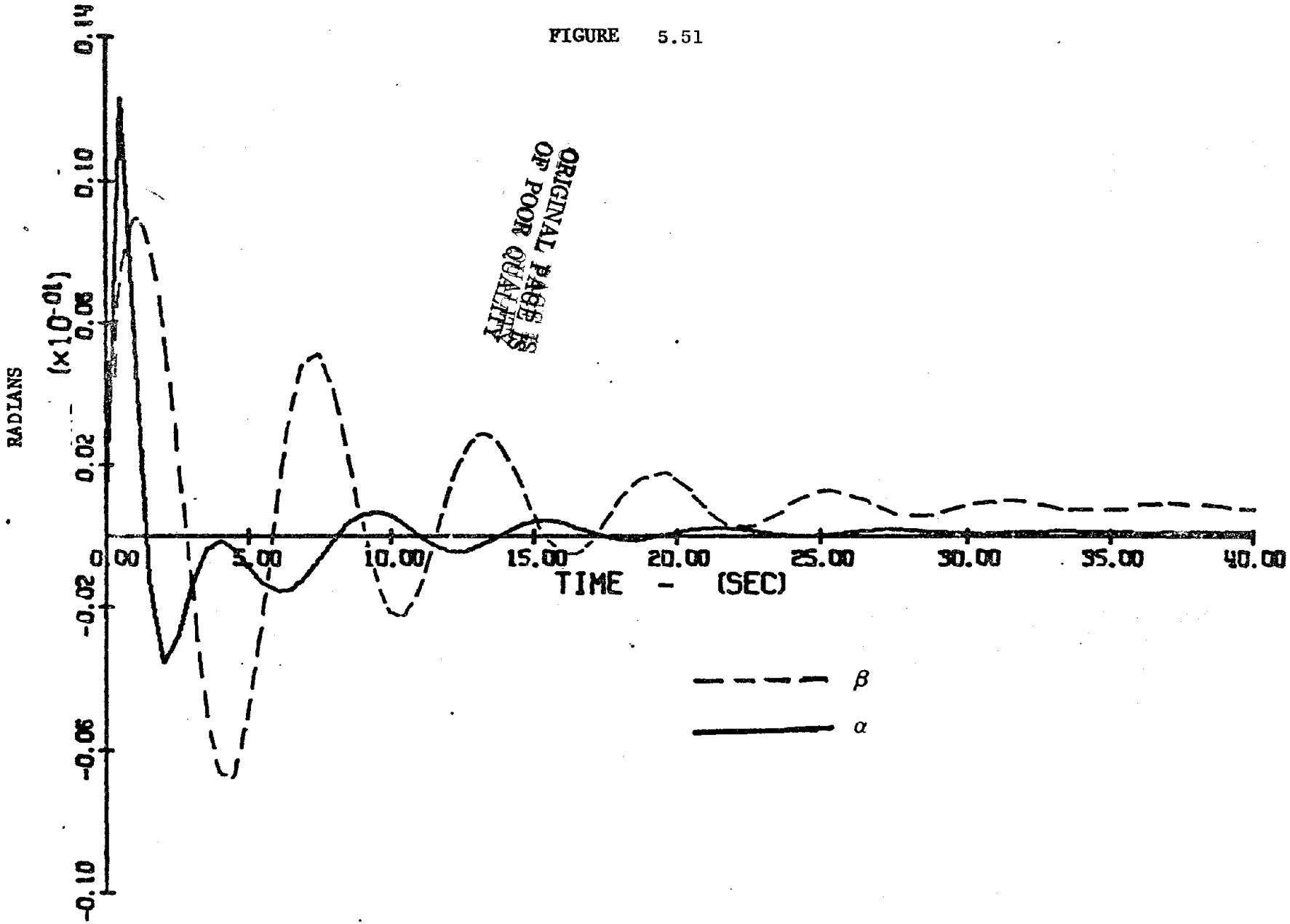

FIGURE 5.51

ORIGINAL PAGE IS
OF POOR QUALITY

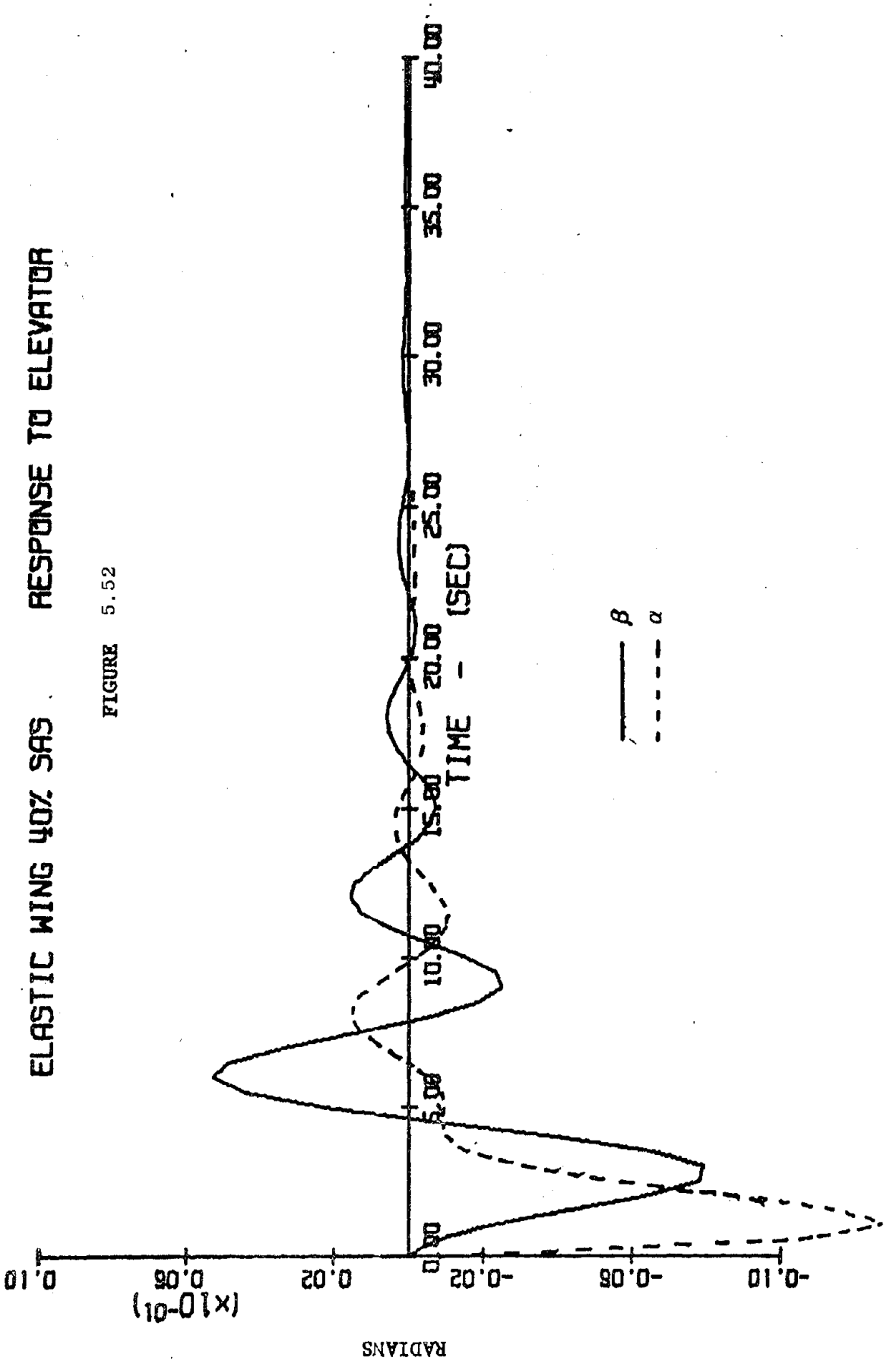

FIGURE 5.52

5.6 Summary

The model used and the aerodynamic result obtained with both strip and linear theory were discussed in detail and compared. The strip theory approach, though very simple, showed results not always satisfactory; in addition, its limitation to rigid wing case only turned out to be too restrictive, since the elastic wing behavior strongly differs from the rigid one.

The effect of stability derivative changes on the natural modes was tabulated. The derivatives of a longitudinally stable configuration were graphed for skew angles from 0^{o} to 45^{o}, and discussed in light of the geometric and aerodynamic effects of skew.

Substitution of these in the eighth order dynamic system gave the characteristic root loci as functions of skew angle.

Calculation of the mode shapes revealed significant changes in dynamics, although the natural frequencies had not changed greatly, (apart from the rolling convergence mode).

Transient responses to elevator and aileron deflections were presented.

VI CONCLUSIONS

The analysis and computer program for the adaptation of the lifting line aerodynamic theory to the oblique wing have been described.

The existence of a side force component, due both to induced drag and to the tilting of the lift force when the wing is skewed, has been shown. Stability derivatives were obtained for an aircraft used in a Boeing study with the oblique wing placed at 0^{o}, 15^{o}, 30^{o}, and 45^{o}. The derivatives were generated using the lifting line theory and a simple strip theory (for sweep = 45^{o}). The two results are compared with each other and with the Boeing results and show reasonable agreement in most cases

The stability derivatives computed using the lifting line theory were used in a linearized dynamic model of the aircraft to determine the effect of sweep on dynamic behavior. No instabilities or large changes occurred in the root locations for sweep angles varying from 0^{o} to 45^{o} with the exception of roll convergence. The damping of the rolling mode was reduced by more than an order of magnitude due in most part to a similar decrease in $C_{\ell p}$.

A dramatic increase in the characteristic roll angle, in comparison to other state variables, was prominent in the rolling convergence, and the three oscillatory modes at $\Lambda = 45^{o}$. The rolling motion in the Dutch roll is exaggerated with increasing skew, and surprisingly both the phugoid and short period modes picked up significant rolling motion. In the latter mode rolling dominated by a factor of three.

APPENDIX A

A.1 Relations Between Dimensional and Nondimensional Derivatives (Stability Axes).

The geometric quantities b_0, wing span, and $\bar{c}$, mean aerodynamic chord, are referred to the wing in the unswept position.

$$x_u = 2 \frac{Sq}{U_0} Cx_u \qquad \left[\frac{lb \cdot sec}{ft}\right]$$

$$x_\alpha = qS\, Cx_\alpha \qquad [lb]$$

$$x_{\dot{\alpha}} = qS \frac{\bar{c}}{2U_0} Cx_{\dot{\alpha}} \qquad [lb \cdot sec]$$

$$x_\theta = - mg \cos\theta_0 \qquad [lb]$$

$$x_\beta = qSCx_\beta \qquad [lb]$$

$$x_{\dot{\beta}} = qS \frac{b}{2U_0} Cx_{\dot{\beta}} \qquad [lb \cdot sec]$$

$$x_p = qS \frac{b}{2U_0} Cx_p \qquad [lb \cdot sec]$$

$$x_q = qS \frac{\bar{c}}{2U_0} Cx_q \qquad [lb \cdot sec]$$

$$x_r = qS \frac{b}{2U_0} Cx_r \qquad [lb \cdot sec]$$

The same relationship can be obtained for y and z.

$$L_{\alpha} = qSbC_{\ell\alpha} \quad ; \quad M_{\alpha} = qS\bar{c}Cm_{\alpha} \qquad [lb \cdot ft]$$

$$L_{\dot{\alpha}} = qSb\frac{\bar{c}}{2U_0}C_{\ell\dot{\alpha}} \; ; \quad M_{\dot{\alpha}} = qS\bar{c}\frac{\bar{c}}{2U_0}Cm_{\dot{\alpha}} \qquad [lb \cdot ft \cdot sec]$$

$$L_{\beta} = qSbC_{\ell\beta} \quad ; \quad M_{\beta} = qS\bar{c}Cm_{\beta} \qquad [lb \cdot ft]$$

$$L_{\dot{\beta}} = qSb\frac{b}{2U_0}C_{\ell\dot{\beta}} \; ; \quad M_{\dot{\beta}} = qS\bar{c}\frac{b}{2U_0}Cm_{\dot{\beta}} \qquad [lb \cdot ft \cdot sec]$$

$$L_{p} = qSb\frac{b}{2U_0}C_{\ell p} \; ; \quad M_{p} = qS\bar{c}\frac{b}{2U_0}Cm_{p} \qquad [lb \cdot ft \cdot sec]$$

$$L_{q} = qSb\frac{\bar{c}}{2U_0}C_{\ell q} \; ; \quad M_{q} = qS\bar{c}\frac{\bar{c}}{2U_0}Cm_{q} \qquad [lb \cdot ft \cdot sec]$$

$$L_{r} = qSb\frac{b}{2U_0}C_{\ell r} \; ; \quad M_{r} = qS\bar{c}\frac{b}{2U_0}Cm_{r} \qquad [lb \cdot ft \cdot sec]$$

The relationships for the yawing moment are the same as for the rolling moment.

APPENDIX B

Since only the wing contribution to stability derivatives is a new element in the stability analysis, we shall limit ourselves to deriving only wing derivatives and provide a list of the ones which can be computed in a classical way and can be found in the literature [Ref. 15, 21 and 22]. The normalizing quantities b_0 , $\bar{c}$ are referred to the $\Lambda = 0$ condition.

B.1 "u" Derivatives [Ref. 22].

C_{x_u}

$$C_{x_u} = \frac{1}{qS}\frac{\partial F_x}{\partial u} = \left[-2C_D + M_a\left(\frac{1}{qS}\frac{\partial T_h}{\partial M_a} - \frac{\partial C_D}{\partial M_a}\right)\right] \qquad (B\text{-}1)$$

C_{z_u}

$$C_{z_u} = \frac{1}{qS}\frac{\partial F_z}{\partial u} = -\left(2\,C_L + M_a\frac{\partial C_L}{\partial M_a}\right) \qquad (B\text{-}2)$$

B.2 "β" Derivatives.

Figure B-1 shows the case of the aircraft experiencing a sideslip velocity v .

The effect of introducing a β corresponds to a $-\Delta\Lambda$ for the wing. The fuselage also is affected, but we neglect its contribution since it is too complicated to evaluate it.

Neglecting the induced drag due to the fin, we consider only the component of the lift due to the fin in the x_s direction.

$$F_x = - D \cos\beta + L_{Fin} \sin(\beta - \delta)$$

$$C_{x_\beta} = \frac{1}{S} \frac{\partial}{\partial\beta} F_x = \left[- \frac{\partial C_D}{\partial\beta} \cos\beta + C_D \sin\beta + \frac{S_F}{S} C_{L_{\alpha_{Fin}}} (\beta - \delta) \sin(\beta - \delta) \right.$$

$$\left. + C_{L_{Fin}} \cos(\beta - \delta) \left(1 - \frac{\partial\delta}{\partial\beta}\right) \right]_{\beta=0}$$

Since when $\beta=0$ also $\delta=0$

$$C_{x_\beta} = - \frac{\partial C_D}{\partial\beta} + C^*_{L_{Fin}} \left(1 - \frac{\partial\delta}{\partial\beta}\right) \simeq \frac{\partial C_D}{\partial\beta}$$

$$\frac{\partial C_D}{\partial\beta} \simeq - \frac{\partial C_D}{\partial\Lambda} \simeq - \frac{\partial C_{D_i}}{\partial\Lambda}$$

$$\frac{\partial C_{D_i}}{\partial\Lambda} = \frac{2C_L}{\pi AR} \frac{\partial C_L}{\partial\Lambda} + C_L^2 \frac{\partial}{\partial\Lambda} \frac{1}{\pi AR} \qquad \text{(B-3)}$$

since

$$AR = \frac{b_0 \cos\Lambda}{S} \qquad \text{(B-4)}$$

and assuming

$$(C_L)_\Lambda = (C_L)_{\Lambda_0} \frac{\cos^2\Lambda}{\cos\Lambda_0^2} \qquad \text{(B-5)}$$

we obtain

$$\left(\frac{\partial C_L}{\partial\Lambda}\right)_{\Lambda=\Lambda_0} = - \frac{4C_L^2}{\pi AR} \tan\Lambda_0 \qquad \text{(B-6)}$$

---

* $C_{L_F} = 0$ assuming the trimmed condition does not require any rudder.

$$\left(\frac{\partial}{\partial\Lambda}\frac{1}{\pi AR}\right)_{\Lambda=\Lambda_0} = \frac{2}{AR}\tan\Lambda_0 \qquad \text{(B-7)}$$

and after substituting into (B-3), the final expression becomes

$$C_{x_\beta} \simeq -\frac{\partial C_D}{\partial\beta} - \frac{\partial C_D}{\partial\Lambda} = -\frac{2C_L^2}{\pi AR}\tan\Lambda_0 \qquad \text{(B-8)}$$

or, in terms of the induced drag coefficient

$$C_{x_\beta} \simeq -2C_{D_i}\tan\Lambda_0$$

C_{y_β}

In a similar way we can compute C_{y_β}. The side force coefficient for a sideslip is

$$C_y = -C_c\cos\beta - C_D\sin\beta \qquad \text{(B-9)}$$

where C_c derives from fuselage and tail contribution

$$C_{y_\beta} = -\left[-C_c\sin\beta + \frac{\partial C_c}{\partial\beta} + C_D\cos\beta + \frac{\partial C_D}{\partial\beta}\right]_{\beta=0}$$
$$= -\frac{\partial C_c}{\partial\beta} + C_{D_0} \qquad \text{(B-10)}$$

The main constribution fo C_c usually comes from the body and the vertical tail, for the oblique wing case the side force generated by the wing also should be included in C_c, but it turns out that such contribution is of second order and therefore negligible.

The tail contribution is a conventional one and it is given by

Figure B-1 - Side-slip of an Oblique Wing Aircraft.

$$\left(\frac{\partial C_c}{\partial \beta}\right)_{Fin} = C_{L_{\alpha\ Fin}}\left(1 - \frac{\partial \delta}{\partial \beta}\right) \qquad \text{(B-11)}$$

similarly to the C_{x_β} derivatives, no attempt is here made to evaluate the fuselage contribution.

C_{z_β}

$$C_{z_\beta} = \frac{\partial C_L}{\partial \beta} - \frac{\partial C_L}{\partial \Lambda} = -\ 2\ C_L\ \tan\Lambda_0 \qquad \text{(B-12)}$$

C_{ℓ_β}

For simplicity, we shall neglect the influence of fuselage on C_{ℓ_β}.

Wing Contribution

$$\left(\frac{\partial C_\ell}{\partial \beta}\right)_w \simeq -\frac{\partial C_\ell}{\partial \Lambda} \simeq -\frac{\Delta C_\ell}{\Delta \Lambda} \qquad \text{(B-13)}$$

The magnitude of this term is strongly dependent on the FWLD, therefore no approximation is possible which would give a meaningful result. Assuming a zero rolling moment for the cruise condition, it is possible to evaluate $\left(C_{\ell_\beta}\right)_w$ by computing the wing rolling moment at the perturbed sweep angle and dividing it by the increment in sweep.

Tails (Fin) Contribution [Ref. 21]

$$\left(\frac{\partial C_\ell}{\partial \beta}\right)_F = \frac{\partial}{\partial \beta}\left[-\ C_{L_{\alpha_F}}\ (\beta - \delta)\ \cos\ (\beta - \delta)\ \frac{S_F}{S}\ \frac{\ell_{ZF}}{b}\right]_{\beta=0} \qquad \text{(B-14)}$$

$$\left(\frac{\partial C_\ell}{\partial \beta}\right)_F = - C_{L_{\alpha_F}} \left(1 - \frac{\partial \delta}{\partial \beta} \frac{S_F}{S}\right) \frac{\ell_{ZF}}{b} \tag{B-15}$$

The same approach used in computing $\left(C_{L_\beta}\right)_w$ is necessary when evaluating the wing contribution to $\left(C_{m_\beta}\right)_w$ and $\left(C_{n_\beta}\right)_w$

C_{m_β}

The tail contribution is negligible, therefore

$$C_{m_\beta} = \left(C_{m_\beta}\right)_w \tag{B-16}$$

C_{n_β}

The fin contribution is given by [Ref. 21]

$$\left(C_{n_\beta}\right)_{Fin} = V_v \left(C_{L_\alpha}\right)_{Fin} \left(1 - \frac{\partial \delta}{\partial \beta}\right) \tag{B-17}$$

where

$$V_v = \frac{S_{Fin} \ell_{Fin}}{S_w b_0} \tag{B-18}$$

vertical tail volume.

The sidewash factor $\frac{\partial \delta}{\partial \beta}$, generally speaking is difficult to estimate with engineering precision. Suitable wind-tunnel tests are required for this purpose. The contribution from the fuselage arises through its behavior as a lifting body when yawed. Associated with the side force that develops is a vortex wake which induces a lateral-flow-field at the tail. The contribution from the wing is associated with the asymmetric structure of the flow that develops when the airplane is yawed. This

phenomenon is especially pronounced with low-aspect-ratio swept wings. When such tests are not available, References 27 and 28 can be used for empirical values.

B.3 "α" Derivatives.

C_{x_α}

$$C_{x_\alpha} = \frac{1}{qS}\frac{\partial F_x}{\partial \alpha} = C_L - \frac{\partial C_D}{\partial \alpha} = C_L\left(1 - 2k\ C_{L_\alpha}\right) \tag{B-19}$$

where

$$k \triangleq \frac{\partial C_D}{\partial C_L^2}$$

C_{y_α}

For a rigid wing, $\frac{\partial \gamma}{\partial \alpha} = \tan\Lambda$, therefore integrating (3.28) over the span and normalizing the result

$$C_{y_\alpha} = \frac{1}{qS}\frac{\partial F_y}{\partial \alpha} = \frac{1}{qS}\int_{-b/2}^{b/2}\left(L_\alpha \gamma_0 + L_0 \tan\Lambda - 2k\ L_0\ C_{L_\alpha}\right)\tan\Lambda\ dy \tag{B-20}$$

we obtain

$$C_{y_\alpha} = \left[C_{L_\alpha}\nu_0 + C_L\left(1 - 2k\ C_{L_\alpha}\right)\ \tan\Lambda\right] \tag{B-21}$$

C_{z_α}

In stability axes

$$C_{z_\alpha} = -\ C_{L_\alpha} \tag{B-22}$$

C_{m_α}

The presence of an unsymmetric lift distribution due to the angle of attack introduces a new wing contribution to C_{m_α}.

Let us first evaluate this contribution before considering all the other ones which are common to symmetric aircraft. We shall refer to Figures 3.5 and B-2 for the symbols used. To be consistent with the conventional notations we shall consider this contribution as a part of $C_{m_0} = C_{m_0}(\Lambda)$ referred to the M.A.C. at zero sweep (y_{MAC}).

The wing moment about y_{MAC} is given by

$$(M)_{w_\Lambda} = - q \int_{-b/2}^{b/2} Z \, y_{MAC} \, dy \qquad \text{(B-23)}$$

where $(M)_{w_\Lambda}$ is the wing pitching moment due to the effects of skew.
Let us now consider the general problem.

Moments about C.G.

a) Wing contribution

$$M = M_0 + (M)_{w_\Lambda} + (L \cos\alpha_0 + D \sin\alpha)(h - h_{wh})\,\bar{c} \qquad \text{(B-24)}$$

b) Tail contribution

$$M_t = - \ell_t \, L_t \qquad \text{(B-25)}$$

c) Total moment

$$M_T = M_0 + (M)_{w_\Lambda} + (L \cos\alpha_0 + D \sin\alpha)(h - h_{wb})\bar{c} - \ell_t \, L_t$$

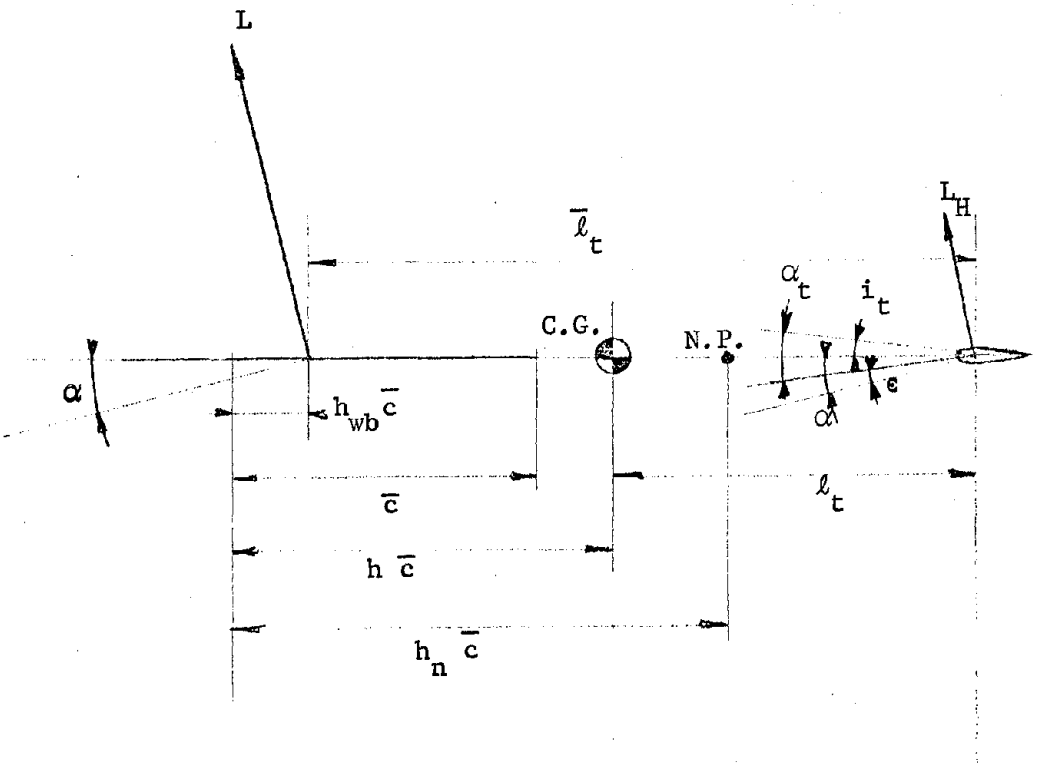

Figure B-2 Moment about the C.G. in the Plane of Symmetry.

N.P. = Neutral Point

$\bar{c}$ = M.A.C. at $\Lambda = 0$

α_0 = Angle of attack (wing-body)

ϵ = Effective wing downwash at tail

i_t = H-tail trim angle

$\alpha_t = \alpha_0 - (\epsilon - i_t)$ = H-tail angle of attack.

$$= M_0 + (M)_{w_\Lambda} + L \left[\cos\alpha_0 + \frac{D}{L}\sin\alpha\right](h - h_{wb})\bar{c} - \ell_t L_t$$

$$\simeq M_0 + (M)_{w_\Lambda} + L\,(h - h_{wb})\bar{c} - \ell_t\, L_t \tag{B-26}$$

having assumed

$$\cos\alpha_0 + \frac{D}{L}\sin\alpha_0 \simeq 1 + \frac{D}{L}\,\alpha_0 \simeq 1$$

$$C_{m_T} = \frac{1}{qS\bar{c}}\; M_T \tag{B-27}$$

$$C_{m_T} = C_{m_0} + (C_m)_{w_\Lambda} + C_L\,(h - h_{wb}) - C_{L_t}\,\frac{S_F \ell_t}{S\bar{c}} \tag{B-28}$$

$$= C_{m_0} + (C_m)_{w_\Lambda} + C_L\,(h - h_{wb}) - V_H\, C_{L_t}$$

where

$$V_H \triangleq \frac{S_F \ell_t}{S\bar{c}} \tag{B-29}$$

$$C_{L_t} = C_{L_{\alpha_t}}\,(\alpha_0 + i_t - \varepsilon) \tag{B-30}$$

$$C_{m_t} \triangleq - V_H\, C_{L_t} \tag{B-31}$$

$$C_{m_\alpha} = \frac{\partial}{\partial\alpha} C_{m_T} = \cancel{\frac{\partial}{\partial\alpha} C_{m_0}}^{\,0} + \frac{\partial}{\partial\alpha}(C_m)_{w_\Lambda} + C_{L_\alpha}\,(h - h_{wb})$$

$$- C_{L_{\alpha_t}}\left[1 - \frac{\partial\varepsilon}{\partial\alpha}\right] V_H \tag{B-32}$$

Neutral Point (C.G. location about which $C_{m_\alpha} = 0$)

$$C_{m_\alpha} = \frac{\partial}{\partial\alpha}(C_m)_{w_\Lambda} + C_{L_\alpha}(h - h_{wb}) - V_H C_{L_{\alpha_t}}\left[1 - \frac{\partial\epsilon}{\partial\alpha}\right] = 0$$

$$h = \bar{h} \triangleq h_{wb} - \frac{1}{C_{L_\alpha}}\left[\frac{\partial}{\partial\alpha}(C_m)_{w_\Lambda} - V_H C_{L_{\alpha_t}}\left(1 - \frac{\partial\epsilon}{\partial\alpha}\right)\right] \qquad \text{(B-33)}$$

or

$$h_{wb} = \bar{h} + \frac{1}{C_{L_\alpha}}\left[\frac{\partial}{\partial\alpha}(C_m)_{w_\Lambda} - V_H C_{L_{\alpha_t}}\left(1 - \frac{\partial\epsilon}{\partial\alpha}\right)\right] \qquad \text{(B-34)}$$

and by substituting (B-34) into (B-32)

$$C_{m_\alpha} = \frac{\partial}{\partial\alpha}(C_m)_{w_\Lambda} + C_{L_\alpha}(h - \bar{h}) - \left[\frac{\partial}{\partial\alpha}(C_m)_{w_\Lambda} - V_H C_{L_{\alpha_t}}\left(1 - \frac{\partial\epsilon}{\partial\alpha}\right)\right] - V_H C_{L_{\alpha_t}}\left(1 - \frac{\partial\epsilon}{\partial\alpha}\right) \qquad \text{(B-35)}$$

$$C_{m_\alpha} = C_{L_\alpha}(h - \bar{h}) \qquad \text{(B-36)}$$

$$h - \bar{h} \triangleq \text{Static Margin} \qquad \text{(B-37)}$$

Aerodynamic Center Build-up.

$$\bar{X}_{AC} = h_{wb}\bar{c} \qquad \text{(B-38)}$$

where

$$h_{wb} \equiv .25$$

$$\bar{X}_{AC_{Tails}} = V_H \frac{C_{L_{\alpha_t}}}{C_{L_\alpha}}\left(1 - \frac{\partial\epsilon}{\partial\alpha}\right)\bar{c} \qquad \text{(B-39)}$$

$$\bar{X}_{AC_{\text{Pivot and Sweep}}} = -\frac{1}{C_{L_\alpha}} \frac{\partial}{\partial \alpha} (C_m)_{w_\Lambda} \bar{c} \tag{B-40}$$

C_{n_α}

This is one of the new derivatives and only the wing contributes to it. It is formed of two terms: one due to the lift and one due to the side force.

$$C_{n_\alpha} = \frac{1}{Sb_0} \int_{-b/2}^{b/2} (X \bar{x} + Y \bar{y})\, dy \tag{B-41}$$

The knowledge of the spanwise distribution of X and Y is needed in order to evaluate C_{n_α}.

B.4 "p" Derivatives.

The local angle of attack varies linearly according to

$$\alpha_p = \frac{p}{U_0} \bar{x} \tag{B-42}$$

C_{z_p}

For the symmetric wing case this derivative is zero since the increase in lift on one side of the wing is balanced by an equal decrease on the other side.

This is no longer true for the oblique wing, therefore

$$C_{z_p} = \frac{2U_0}{Sb_0} \int_{-b/2}^{b/2} \frac{\partial Z}{\partial p}\, dy \tag{B-43}$$

The evaluation of $\frac{\partial Z}{\partial p}$ can be done according to the method outlined in section 3.2.2. However, such an approach will require the evaluation of $\frac{\partial \ell}{\partial \alpha}$ that will take into account the behavior of the oblique wing.

To remind us of this detail, we shall add the subscript p to the derivatives that must be evaluated in that way.

Since

$$\frac{\partial}{\partial p} = \frac{\partial}{\partial \alpha} \frac{\partial \alpha_p}{\partial p}$$

and

$$\frac{\partial \alpha_p}{\partial p} = \frac{\bar{x}}{U_0}$$

$$\frac{\partial Z}{\partial p} = \left(\frac{\partial Z}{\partial \alpha}\right)\frac{\bar{x}}{U_0} = \left[\left(\frac{\partial \ell}{\partial \alpha}\right)_p + \bar{d}_0\right]\frac{\bar{x}}{U_0} \qquad \text{(B-44)}$$

Therefore

$$C_{z_p} = \frac{-2}{Sb_0} \int_{-b/2}^{b/2} \left[\left(\frac{\partial \ell}{\partial \alpha}\right)_p + \bar{d}_0\right] \bar{x}\, dy \qquad \text{(B-44)}$$

C_{y_p}

Wing Contribution.

Similarly to $\left(C_{z_p}\right)_w$, $\left(C_{y_p}\right)_w$ would be zero if the change in lift was antisymmetric.

$$C_{y_p} = \frac{2U_0}{b_0 S} \int_{-b/2}^{b/2} \frac{\partial y}{\partial p}\, dy = \frac{2U_0}{b_0 S} \int_{-b/2}^{b/2} \frac{\partial}{\partial p} (\ell\, \gamma - \bar{d} \tan\Lambda)\, dy \qquad \text{(B-46)}$$

We notice that $\frac{\partial \gamma}{\partial p} = 0$ for a rigid wing, but it would be different from zero for a flexible one.

Fin Contribution [Ref. 21].

$$\left(C_{y_p}\right)_{Fin} = -\frac{2U_0}{b_0 S} C_{L_{\alpha_{Fin}}} \left[\frac{\ell_{F_z}}{U_0} - \frac{\partial \delta}{\partial p}\frac{b}{2U_0}\right] \ell_{FZ} \cdot S_F$$

$$= -\frac{S_F}{S} C_{L_{\alpha_{Fin}}} \left(\frac{2\ell_{FZ}}{b_0} - \frac{\partial \delta}{\partial p}\right) \tag{B-47}$$

Therefore, for a rigid wing

$$C_{y_p} = \frac{2}{b_0 S} \int_{-b/2}^{b/2} \left[\left(\frac{\partial \ell}{\partial \alpha}\right)_p \gamma_0 - \left(\frac{\partial \bar{d}}{\partial \alpha}\right)_p \tan\Lambda\right] dy - \frac{S_F}{S} C_{L_{\alpha_{Fin}}} \left(\frac{2\ell_{FZ}}{b_0} - \frac{\partial \delta}{\partial p}\right) \tag{B-48}$$

For the flexible wing, the term $\frac{\partial \gamma}{\partial \alpha}$ is no longer zero, therefore the term $\ell_0 \frac{\partial \gamma}{\partial \alpha}$ should be included in the integration representing the wing contribution.

$\underline{C_{\ell_p}}$

Wing Contribution

$$\left(C_{\ell_p}\right)_w = \frac{2U_0}{b_0^2 S} \int_{-b/2}^{b/2} \frac{\partial Z}{\partial p} \bar{x}\, dy = \frac{-2}{b_0^2 S} \int_{-b/2}^{b/2} \left[\left(\frac{\partial \ell}{\partial \alpha}\right)_p + \bar{d}_0\right] \bar{x}^2\, dy \tag{B-49}$$

Fin Contribution

$$\left(C_{\ell_p}\right)_{Fin} = \left(C_{y_p}\right)_{Fin} \frac{\ell_{FZ}}{b_0} \tag{B-50}$$

Therefore

$$C_{\ell_p} = \frac{-2}{b_0^2 S} \int_{-b/2}^{b/2} \left(\frac{\partial \ell}{\partial \alpha}\right)_p + \bar{d}_0 \quad \bar{x}^2 \quad dy + \left(C_{y_p}\right)_{Fin} \frac{\ell_{FZ}}{b_0} \tag{B-51}$$

C_{m_p}

No tail contribution to this new derivative

$$C_{m_p} = \left(C_{m_p}\right)_w = \frac{-2U_0}{b_0 \bar{c} S} \int_{-b/2}^{b/2} \frac{\partial Z}{\partial p} \bar{y} \, dy = \frac{2}{b_0 \bar{c} S} \int_{-b/2}^{b/2} \left[\left(\frac{\partial \ell}{\partial \alpha}\right)_p + \bar{d}_0\right] \bar{x} \, \bar{y} \, dy \tag{B-52}$$

C_{n_p}

Wing Contribution

The side force is the new element in the wing contribution to C_{n_p}

$$\left(C_{n_p}\right)_w = \frac{2U_0}{b_0^2 S} \int_{-b/2}^{b/2} \left[\frac{\partial X}{\partial p} \bar{x} + \frac{\partial Y}{\partial p} \bar{y}\right] dy \tag{B-53}$$

where

$$\left(\frac{\partial X}{\partial p}\right) = \left[\frac{\partial}{\partial \alpha} (\ell \alpha - \bar{d})\right] \frac{\partial \alpha_p}{\partial p} = \left[\ell_0 - \left(\frac{\partial \bar{d}}{\partial \alpha}\right)_p\right] \bar{x} \tag{B-54}$$

Tail Contribution [Ref. 21].

$$\left(C_{n_p}\right)_{Fin} = V_v \left[\frac{2\ell_{FZ}}{b_0} - \frac{\partial\delta}{\partial p}\right] C_{L_{\alpha_{Fin}}} \tag{B-55}$$

Therefore, by adding the two contributions, for a rigid wing we obtain

$$C_{n_p} = \frac{2}{b_0^2 S} \int_{-b/2}^{b/2} \left\{ \left[\ell_0 - \left(\frac{\partial \bar{d}}{\partial \alpha}\right)_p \right] \bar{x} + \left[\left(\frac{\partial \ell}{\partial \alpha}\right)_p \gamma_0 - \left(\frac{\partial \bar{d}}{\partial \alpha}\right)_p \tan\Lambda \right] \bar{y} \right\} dy + V_v \left[\frac{2\ell_{FZ}}{b_0} - \frac{\partial\delta}{\partial p}\right] C_{L_{\alpha_{Fin}}} \tag{B-56}$$

The flexible wing would have the extra term

$$\ell_0 \frac{\partial \gamma}{\partial \alpha} \bar{y}$$

B.5 "q" Derivatives.

The q derivatives are derived in the same way as for the p ones.

All the comments made in the previous group of derivatives can be extended to this one and therefore they will not be repeated.

The local angle of attack now varies linearly according to

$$\alpha_q = \frac{q}{U_0} \bar{y}$$

C_{y_q}

Wing contribution only

$$C_{y_q} = \left(C_{y_q}\right)_w = \frac{2U_0}{\bar{c}S} \int_{-b/2}^{b/2} \frac{\partial y}{\partial q}\, dy = \frac{2U_0}{\bar{c}S} \int_{-b/2}^{b/2} \left(\frac{\partial y}{\partial \alpha}\right)_q \frac{\partial \alpha_q}{\partial q}\, dy$$

$$= \frac{2}{\bar{c}S} \int_{-b/2}^{b/2} \left(\frac{\partial y}{\partial \alpha}\right)_q \bar{y}\, dy = \frac{2}{\bar{c}S} \int_{-b/2}^{b/2} \left[\left(\frac{\partial \ell}{\partial \alpha}\right)_p \gamma_0 - \left(\frac{\partial \bar{d}}{\partial \alpha}\right)_q \tan\Lambda\right] \bar{y}\, dy \qquad \text{(B-57)}$$

For flexible wing the term $\ell_0 \frac{\partial y}{\partial \alpha} \bar{y}$ must be included in the integration.

C_{z_q}

Wing Contribution.

$$C_{z_q\,w} = \frac{2U_0}{\bar{c}S} \int_{-b/2}^{b/2} \frac{\partial Z}{\partial q}\, dy$$

$$= \frac{2}{\bar{c}S} \int_{-b/2}^{b/2} \left(\frac{\partial Z}{\partial \alpha}\right)_q \bar{y}\, dy = \frac{-2}{\bar{c}S} \int_{-b/2}^{b/2} \left[\left(\frac{\partial \ell}{\partial \alpha}\right)_q + \bar{d}0\right] \bar{y}\, dy \qquad \text{(B-58)}$$

Horizontal Tail Contribution [Ref. 21]

$$\left(C_{z_q}\right)_{H.Tail} = -\frac{S_t \ell_t}{S\bar{c}}\, C_{L_{\alpha_{HT}}} = -2\, V_H\, C_{L_{\alpha_{HT}}} \qquad \text{(B-59)}$$

and

$$C_{z_q} = -\frac{2}{\bar{c}S} \int_{-b/2}^{b/2} \left[\left(\frac{\partial \ell}{\partial \alpha}\right)_q + \bar{d}_0\right] \bar{y}\, dy - 2\, V_H\, C_{L_{\alpha_{HT}}} \qquad \text{(B-60)}$$

C_{ℓ_q}

Wing contribution only

$$C_{\ell_q} = \left(C_{\ell_q}\right)_w = \frac{2U_0}{b_0 \bar{c} S} \int_{-b/2}^{b/2} \frac{\partial Z}{\partial q} \bar{x}\, dy$$

$$= \frac{-2}{b_0 \bar{c} S} \int_{-b/2}^{b/2} \left[\left(\frac{\partial \ell}{\partial \alpha}\right)_q + \bar{d}_0\right] \bar{x}\, \bar{y}\, dy \qquad \text{(B-61)}$$

C_{m_q}

Wing Contribution

$$\left(C_{m_q}\right)_w = \frac{2U_0}{\bar{c}^2 S} \frac{\partial Z}{\partial q} \bar{y}\, dy$$

$$= \frac{-2}{\bar{c}^2 S} \int_{-b/2}^{b/2} \left[\left(\frac{\partial \ell}{\partial \alpha}\right)_q + d_0\right] \bar{y}^2\, dy \qquad \text{(b-62)}$$

Tail Contribution [Ref. 21]

$$\left(C_{m_q}\right)_T = - V_H\, C_{L_{\alpha_{HT}}} \frac{\ell_t}{\bar{c}} \qquad \text{(B-63)}$$

Therefore

$$C_{m_q} = \frac{-2}{\bar{c}^2 S} \int_{-b/2}^{b/2} \left[\left(\frac{\partial \ell}{\partial \alpha}\right)_q + \bar{d}_0\right] \bar{y}^2\, dy - V_H\, C_{L_{\alpha_{HT}}} \frac{\ell_t}{\bar{c}}$$

C_{n_q}

Wing Contribution only

$$C_{n_q} = \left(C_{n_q}\right)_w = \frac{2U_0}{b_0 \bar{c} S} \int_{-b/2}^{b/2} \frac{\partial}{\partial q} (X \bar{x} + Y \bar{y}) \, dy$$

$$= \frac{2}{b_0 \bar{c} S} \int_{-b/2}^{b/2} \left\{ \left[\ell_0 - \left(\frac{\partial \bar{d}}{\partial \alpha}\right)_q \right] \bar{x} + \left[\left(\frac{\partial \ell}{\partial \alpha}\right)_q \gamma_0 - \left(\frac{\partial \bar{d}}{\partial \alpha}\right)_q \tan\Lambda \right] \bar{y} \right\} \bar{y} \, dy \tag{B-64}$$

B.6 "r" Derivatives.

Except for the new C_{m_r} derivative, due to the wing aerodynamic coupling, and for the wing side force contribution to yaw moments, all the other derivatices are standard.

The method used in evaluating r derivatives in section 3.2.4 will be applied here without any further explanation.

Assuming the steady state flight condition to be straight levelled flight

$$C_{z_r} = C_{y_{r\,w}} = C_{x_r} = 0$$

C_{y_r}

Fin Contribution only [Ref. 21]

$$C_{y_r} = \frac{S_F}{S} C_{L_{\alpha_{Fin}}} \left[\frac{2 \ell_{FH}}{b_0} + \frac{\partial \delta}{\partial r} \right] \tag{B-65}$$

C_{ℓ_r}

Wing Contribution

$$\left(C_{\ell_r}\right)_w = \frac{-2U_0}{qb_0^2 S} \int_{-b/2}^{b/2} \ell_0 \, \bar{x} \, \frac{\partial q(y)}{\partial r} \, dy = \frac{-4}{b_0^2 S} \int_{-b/2}^{b/2} \ell_0 \, \bar{x}^2 \, dy \tag{B-66}$$

Tail Contribution [Ref. 21]

$$\left(C_{\ell_r}\right)_{Fin} = C_{y_r} \frac{\ell_{FZ}}{b_0} \tag{B-67}$$

Therefore

$$C_{y_r} = \frac{-d}{b_0 S} \int_{-b/2}^{b/2} \ell_0 \, \bar{x}^2 \, dy + C_{y_r} \frac{\ell_{FZ}}{b_0} \tag{B-68}$$

C_{m_r}

Wing Contribution only

$$C_{m_r} = \left(C_{m_r}\right)_w = \frac{-2U_0}{q \, b_0 \, \bar{c} S} \int_{-b/2}^{b/2} \ell_0 \, \bar{y} \, \frac{\partial q(y)}{\partial r} \, dy = \frac{-4}{b_0 \, \bar{c} S} \int_{-b/2}^{b/2} \ell_0 \, \bar{y} \, \bar{x} \, dy \tag{B-69}$$

C_{n_r}

Wing Contribution (including side force)

$$\left(C_{n_r}\right)_w = \frac{2U_0}{q \, b_0^2 S} \int_{-b/2}^{b/2} \left[\bar{d}_0 \, \bar{x} + (\ell_0 \gamma_0 - \bar{d} \tan\Lambda) \, \bar{y} \right] \frac{\partial q(y)}{\partial r} \, dy$$

$$= \frac{4}{b_0^2 S} \int_{-b/2}^{b/2} \left| \bar{d}_0 \ (\bar{x} - \tan\Lambda \bar{y}) + \ell_0 \gamma_0 \ \bar{y}) \right| \bar{x} \ dy \qquad \text{(B-70)}$$

Tail Contribution [Ref. 21]

$$\left(C_{n_r}\right)_{Fin} = - \left(C_{y_r}\right)_{Fin} \frac{\ell_{FH}}{b_0} \qquad \text{(B-71)}$$

$$C_{n_r} = \frac{4}{b_0^2 S} \int_{-b/2}^{b/2} \left[\bar{d} \ (\bar{x} - \tan\Lambda \bar{y}) + \ell_0 \gamma_0 \ \bar{y} \right] \bar{x} \ dy - \left(C_{y_r}\right)_{Fin} \frac{\ell_{FH}}{b_0} \qquad \text{(B-72)}$$

APPENDIX C

C.1 Similarity Transformation between Inertia Matrices.

The conversion of an Inertia Matrix from body into stability axes occurs according to a similarity transformation [Ref. 26].

$$[I_s] = [T_{s/b}]\,(I_b]\,[T_{s/b}]^T \tag{C-1}$$

where

$[I_s]$ = Inertia Matrix in stability axes

$[I_b]$ = Inertia Matrix in body axes

$[T_{s/b}]$ = Rotation (or direction cosine) matrix from body to stability axes

$[\ ]^T$ = Transposed matrix

The stability axes are obtained by rotating the body axes about the y_b axes by an angle α, therefore $y_b \equiv y_s$.

The rotation matrix $[T_{s/b}]$ is given by

$$[T_{s/b}] = \begin{bmatrix} \cos\alpha & 0 & \sin\alpha \\ 0 & 1 & 0 \\ -\sin\alpha & 0 & \cos\alpha \end{bmatrix} \tag{C-2}$$

and

$$[T_{s/b}]^T = \begin{bmatrix} \cos\alpha & 0 & -\sin\alpha \\ 0 & 1 & 0 \\ \sin\alpha & 0 & \cos\alpha \end{bmatrix} \tag{C-3}$$

In a symmetrical aircraft both the I_{xy} and I_{yz} components of the inertia matrix are zero. When the wing is skewed, the I_{xy} component is no longer zero, therefore for an oblique wing aircraft the inertia matrix, in body axes, looks like

$$[I_b] = \begin{bmatrix} I_{xx} & I_{xy} & I_{xz} \\ I_{xy} & I_{yy} & 0 \\ I_{xz} & 0 & I_{yy} \end{bmatrix}_0 \qquad \text{(C-4)}$$

If we know transform $[I_b]$ according to the similarity transformation (C-1), we shall obtain the inertia matrix expressed in terms of the stability axes, $[I_s]$.

After some algebra we obtain

$$[I_s] = \begin{bmatrix} I'_{xx} & I'_{xy} & I'_{xz} \\ I'_{xy} & I'_{yy} & I'_{yz} \\ I'_{xz} & I'_{yz} & I'_{zz} \end{bmatrix}$$

where

$$I'_{xx} = I_{xx} \cos^2\alpha + I_{xz} \sin 2\alpha + I_{zz} \sin^2\alpha$$

$$I'_{yy} = I_{yy}$$

$$I'_{zz} = I_{xx} \sin^2\alpha - I_{xz} \sin 2\alpha + I_{zz} \cos^2\alpha$$

$$I'_{xy} = I_{xy} \cos\alpha$$

$$I'_{xz} = I_{xz} \cos 2\alpha + \frac{1}{2} (I_{zz} - I_{xx}) \sin 2\alpha$$

$$I'_{yz} = - I_{xy} \sin\alpha$$

APPENDIX D

D.1 Downwash Matrix $[S_1]$.

The lift or circulation distribution can be visualized as resulting from a system of horseshoe vortices, each of which is of constant strength (Fig. D-1).

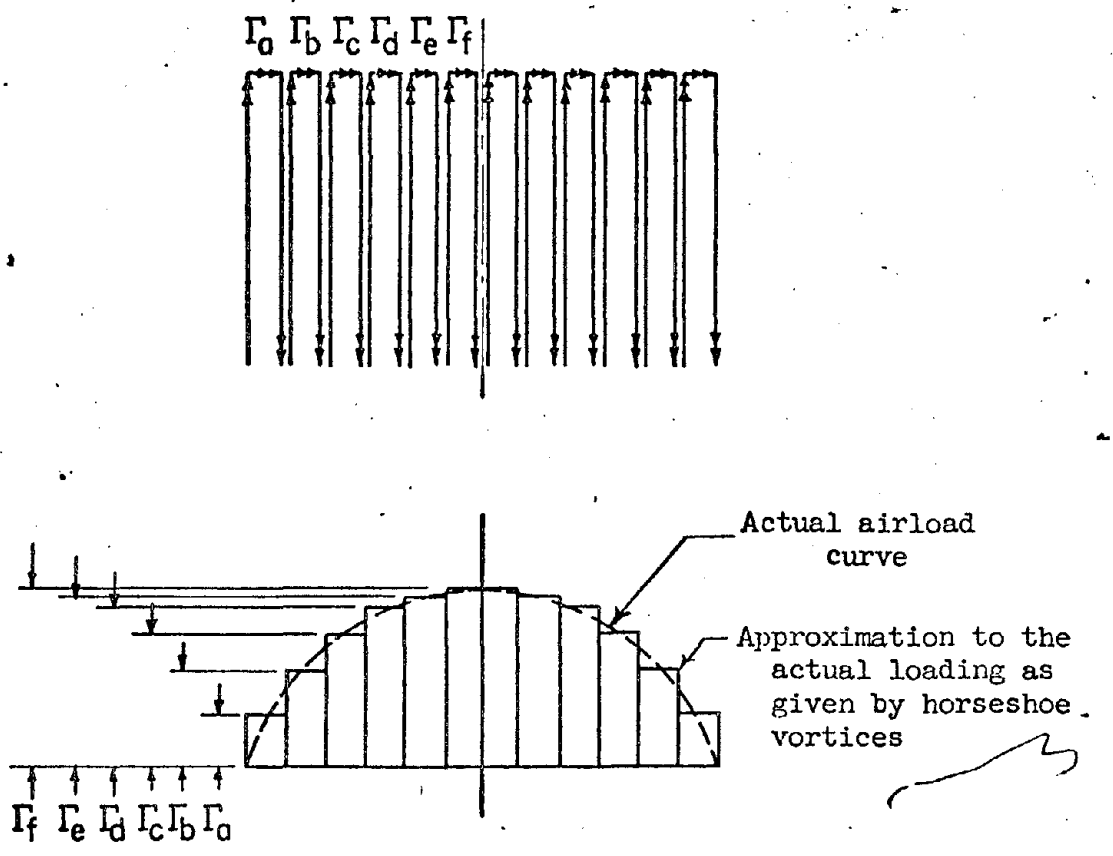

Figure D-1 [Ref. 14].
Horseshoe Vortex System

The net strength of the trailing vortex at any point on the span of the wing is numerically equal to the rate of change of strength of the bound vortex in the spanwise direction. Little loss in accuracy with respect to the spanwise airload distribution will be entailed if:

a) The total strength of the chordwise system of bound vortices is concentrated in one bound vortex located at the local spanwise quarter-chord point.

b) The downwash angle at each vortex station across the span of the wing, at the local streamwise three-quarter-chord point ($\stackrel{\Delta}{=}$ downwash control point D) is equal to the geometric angle of attack for airfoil having a 2-D lift curve slope equal to 2π . When the section 2-D lift slope is different from 2π , equation D-1 must be used

$$\left(\frac{W}{V}\right)_{3C/4} = \frac{m_0}{2\pi}\,\alpha_f \qquad \text{(D-1)}$$

The downwash angle at any one downwash control point is the sum of the incremental downwash angles due to the horseshoes in the system of horseshoes which represent the wing and its lift distribution.

Assuming the geometry of the wing platform, the angle of attack and section 2-D lift curve slope variation are given across the span, the unknowns are the values of the running lift at each point on the span. The strength of each bound vortex represents the average airload over its own portion of the wing span.

The method for determining the downwash matrix for an oblique wing is now illustrated.

In Fig. D-2 a system of horseshoe vortices and the associated downwash control points are shown.

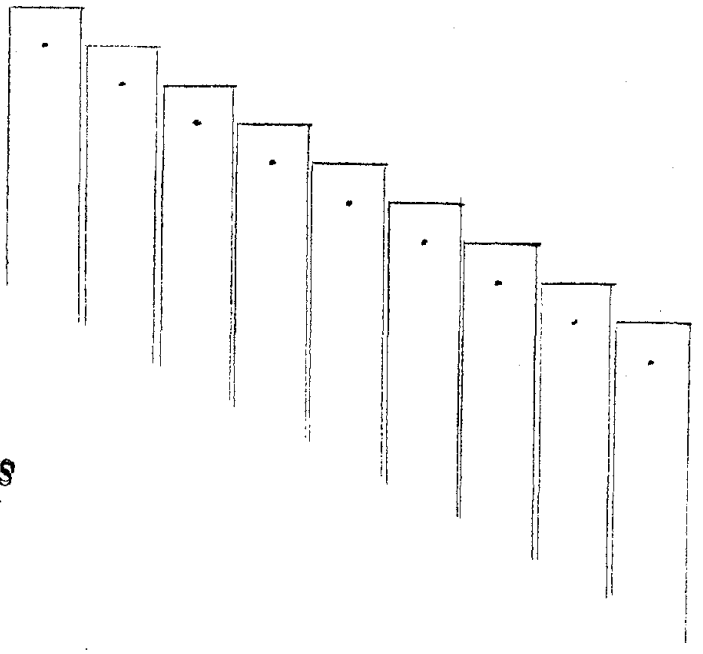

Figure D-2

At the η_i station the section lift curve slope will be m_i and the angle of attack of the section zero lift line is α_{fi} .

Since a linear relationship exists between the strength Γ_j of a particular horseshoe vortex j and the downwash velocity W_{ij} at the point i

$$W_{ij} = K_{ij} \Gamma_j \tag{D-2}$$

where K is a constant, and the downwash at i due to the entire vortex system is

$$W_i = \sum_j W_{ij} = \sum_j K_{ij} \Gamma_j \tag{D-3}$$

From equation (D-1), which expresses the relationship which must exist between the downwash angle $\frac{W}{V}$ at each control point, the wing angle of attack and the section lift curve slope M_0 for the wing station at the control point, the following series of equations result

$$\frac{W_1}{V} = \frac{m_1}{2\pi}\alpha_1 \quad ; \qquad \frac{W_2}{W} = \frac{m_1}{2\pi}\alpha_2 \quad ; \ \ldots$$

and in general

$$\frac{W_i}{V} = \frac{m_i}{2\pi}\alpha_i \tag{D-4}$$

and substituting (D-3) into (D-4)

$$\frac{W_i}{V} = \frac{1}{V}\sum_j K_{ij}\,\Gamma_j \tag{D-5}$$

The relation between the running load 1 and the circulation at the i^{th} station is

$$1_i = \rho V \Gamma_i \tag{D-6}$$

Equation (D-5) can therefore be rewritten in terms of the running load 1

$$\frac{W_i}{V} = \frac{1}{V}\sum_j K_{ij}\,\Gamma_j = \frac{1}{\rho V^2}\sum_j K_{ij}\,1_j \tag{D-7}$$

Substituting (D-7) into (D-4) results in

$$\frac{1}{\rho V^2}\sum_j K_{ij}\,1_j = \frac{m_i}{2\pi}\alpha_i \tag{D-8}$$

or

$$\sum_j K_{ij}\,1_j = \frac{q m_i}{\pi}\alpha_i \tag{D-9}$$

And in matrix form

$$[K] \{\ell\} = \left[\frac{qm_0}{\pi}\right] \{\alpha_f\} \tag{D-10}$$

where $\left[\frac{qm_0}{\pi}\right]$ is a diagonal matrix.

Defining a new matrix

$$[S_1] \triangleq 4\pi [K] \tag{D-11}$$

Equation (D-10) can be rewritten as

$$[S_1] \{\ell\} = [4qm_0] \{\alpha_f\} \tag{D-12}$$

The elements of the $[S_1]$ matrix are to be influence coefficients relating the incremental downwash angle at each control point to the intensity of the running lift over each increment of the semispan of the wing.

D.2 Evaluation of K_{ij} Elements.

The velocity induced by a vortex of strength Γ at a point P can be written as [Ref. 24]

$$W_P = \frac{\Gamma (\cos\alpha - \cos\beta)}{4\pi R} \qquad \text{(D-13)}$$

where α and β are the angles between the direction of the vortex segment and lines joining the ends of the segment to the point as shown in Figure D-3.

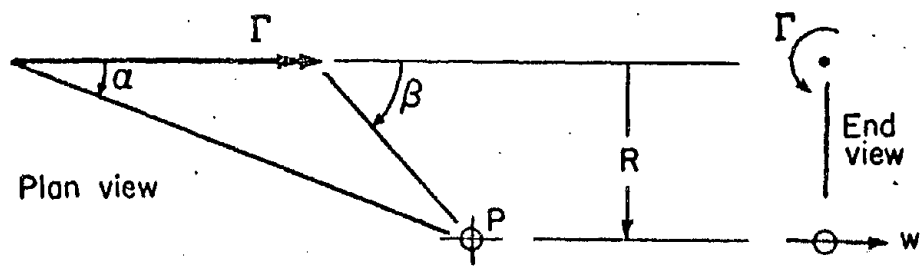

Figure D.3 - Finite Segment of a Straight Vortex Filament [Ref. 14].

A plan view of the geometry of a typical horseshoe vortex is given in Figure D-4.

In order to evaluate the incremental downwash velocity induced by a single horseshoe vortex it is convenient to consider the following three cases:

1) Control point to the left of the horseshoe vortex.

2) Control point within the horseshoe vortex.

3) Control point to the right of horseshoe vortex.

Fig. D-4 shows the quantity that will be used in the derivation; by the subscript i we shall indicate quantities relative to the control point D_i, whereas by j we shall refer to the horseshoe reference point V_j.

The origin of the axis system is at root quarter chord point. Whenever the locus of the quarter chord point does not lie on a straight line, it is assumed to be given by an equation $f(y)$ w.r.t. a straight line passing through the root quarter chord point and aligned with the wing span (unswept case)

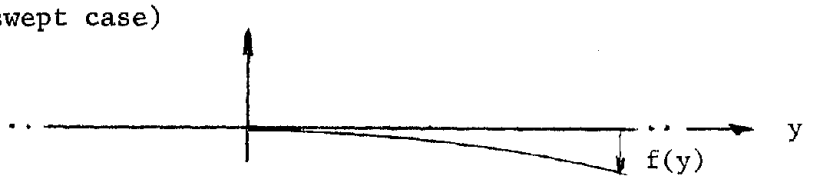

X_j , Y_j coordinates of horseshoe reference point V_j

$X_i - \frac{C_i}{2}$, Y_i coordinates of control point D_i

C_i chord length at station i

$$X_i = - y_i \tan \Lambda + f(y_i) \tan \Lambda$$

1) Control point to the right of the horseshoe vortex (Fig. D-4a) defining

$$\Delta X_{ij} = X_j - X_i$$

$$R_{ij} = \Delta X_{ij} + Ci/2$$

$$\Delta Y_{ij} = Y_i - Y_j$$

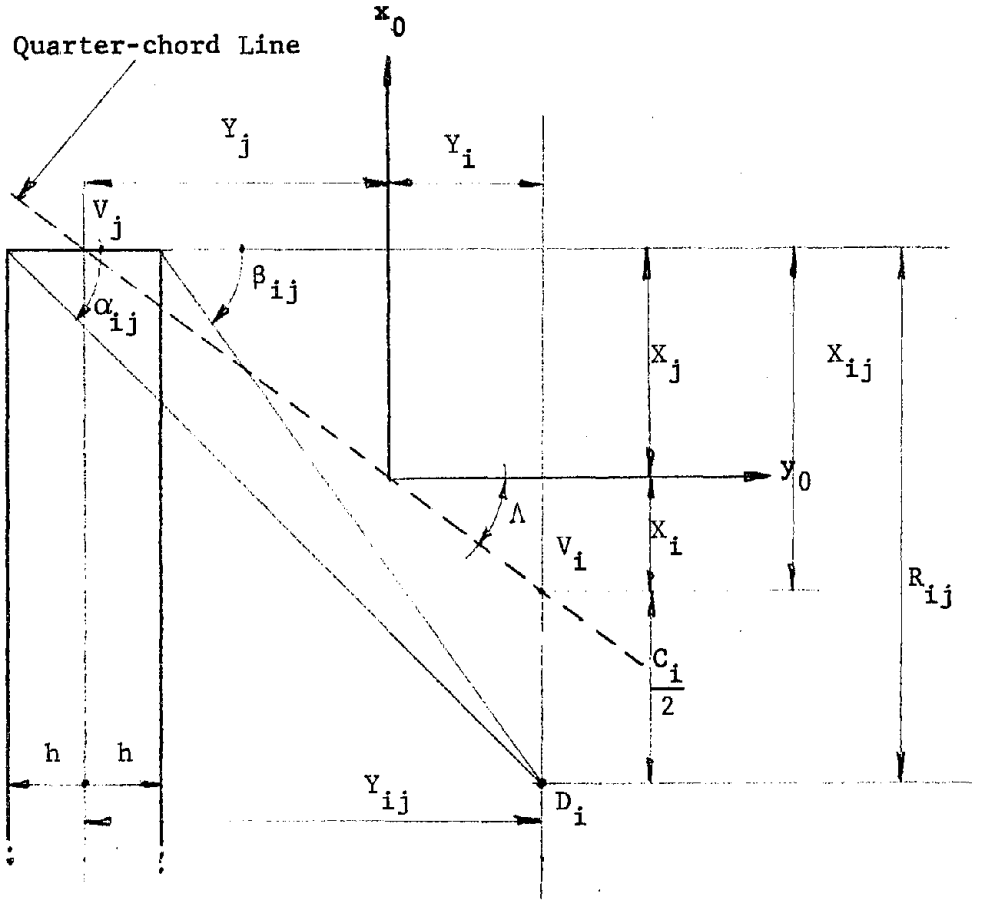

Fig. D-4a Control Point to the Right of Horseshoe Vortex.

For the left trailing vortex

$$\alpha = 0^{\circ}$$

$$\beta = \alpha_{ij} + 90^{\circ}$$

and equation (D-13) becomes

$$(W_{ij})_L = \Gamma_j \frac{[1 - \cos(\alpha_{ij} + 90^{\circ})]}{4\pi(\Delta Y_{ij} + h)} = \frac{1 + \sin \alpha_{ij}}{4\pi(\Delta Y_{ij} + h)} \Gamma_j \qquad \text{(D-14)}$$

$$\sin \alpha_{ij} = \frac{R_{ij}}{\sqrt{(\Delta Y_{ij} + h)^2 + R_{ij}^2}} \qquad \text{(D-15)}$$

For the right trailing vortex

$$\alpha = 90^{\circ} - \beta_{ij}$$

$$\beta = 180^{\circ}$$

$$(W_{ij})_R = -\Gamma_j \frac{[\cos(90 - \beta_{ij}) - \cos 180^{\circ}]}{4\pi(\Delta Y_{ij} - h)} = -\left[\frac{\sin \beta_{ij} + 1}{4\pi(\Delta Y_{ij} - h)}\right] \Gamma_j \qquad \text{(D-16)}$$

The minus sign derives from having assumed positive downwash velocities.

$$\sin \beta_{ij} = \frac{R_{ij}}{\sqrt{(\Delta Y_{ij} - h)^2 + R_{ij}^2}} \qquad \text{(D-17)}$$

For the bound vortex

$$\alpha = \alpha_{ij}$$

$$\beta = B_{ij}$$

$$W_{ij} = \Gamma_j \frac{(\cos \alpha_{ij} - \cos \beta_{ij})}{4\pi R_{ij}} \qquad \text{(D-18)}$$

$$\cos \alpha_{ij} = \frac{\Delta Y_{ij} + h}{\sqrt{(\Delta Y_{ij} + h)^2 + R_{ij}^2}} \tag{D-19}$$

$$\cos \beta_{ij} = \frac{\Delta Y_{ij} - h}{\sqrt{(\Delta Y_{ij} - h)^2 + R_{ij}^2}} \tag{D-20}$$

The total downwash velocity at the control point D_i is therefore given by

$$W_{ij} = (W_{ij})_L + (W_{ij})_R + (W_{ij})_B$$

$$W_{ij} = \frac{\Gamma_j}{4\pi}\left[\frac{1+\sin \alpha_{ij}}{\Delta Y_{ij} + h} - \frac{1+\sin \beta_{ij}}{\Delta Y_{ij} - h} + \frac{\cos \alpha_{ij} - \cos \beta_{ij}}{R_{ij}}\right] \tag{D-21}$$

and

$$K_{ij} \triangleq \frac{W_{ij}}{\Gamma_j} = \frac{1}{4\pi}\left[\frac{1+\sin \alpha_{ij}}{\Delta Y_{ij} + h} - \frac{1+\sin \beta_{ij}}{\Delta Y_{ij} - h} + \frac{\cos \alpha_{ij} - \cos \beta_{ij}}{R_{ij}}\right] \tag{D-22}$$

2) Control point within the horseshoe vortex (Fig. D-4b).

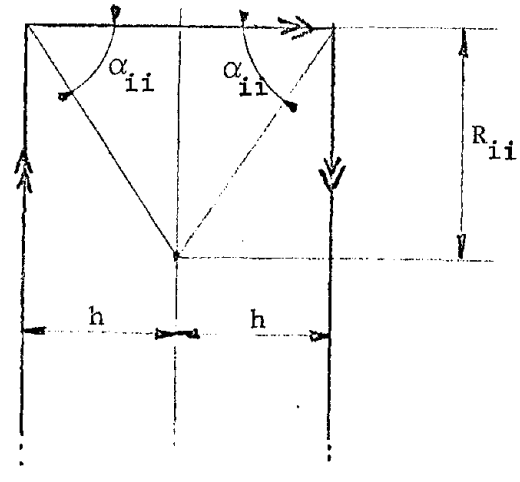

Figure D-4b.

Since

$$i \equiv j$$

$$\Delta X_{ij} = \Delta Y_{ii} = 0$$

$$R_{ii} = C_i/2$$

Both trailing vortices will induce the same downwash velocity

$$\alpha = 0$$

$$\beta = \alpha_{ii} + 90^{o}$$

$$(W_{ii})_L = (W_{ii})_R = \frac{\Gamma_i}{4\pi h} (1+\sin \alpha_{ii}) \qquad \text{(D-23)}$$

$$\sin \alpha_{ii} = \frac{R_{ii}}{\sqrt{h^2 + R_{ii}^2}} = \frac{C_i/2}{\sqrt{h^2 + (Ci/2)^2}} \qquad \text{(D-24)}$$

For the bound vortex

$$\alpha = \alpha_{ii}$$

$$\beta = 180^{o} + \alpha_{ii}$$

$$(W_{ii})_B = \frac{\Gamma_i}{4\pi R_{ii}} \left(\cos \alpha_{ii} + \cos \alpha_{ii}\right) \qquad \text{(D-25)}$$

$$\cos \alpha_{ii} = \frac{h}{\sqrt{h^2 + \frac{1}{4} C_i^2}} \qquad \text{(D-26)}$$

Therefore

$$W_{ii} = \frac{\Gamma_i}{4\pi} \left[\frac{2}{h} (1+\sin \alpha_{ii}) + \frac{4}{C_i} \cos \alpha_{ii}\right] \qquad \text{(D-27)}$$

3) Control point to the left of horseshoe vortex (Fig. D-4c), defining

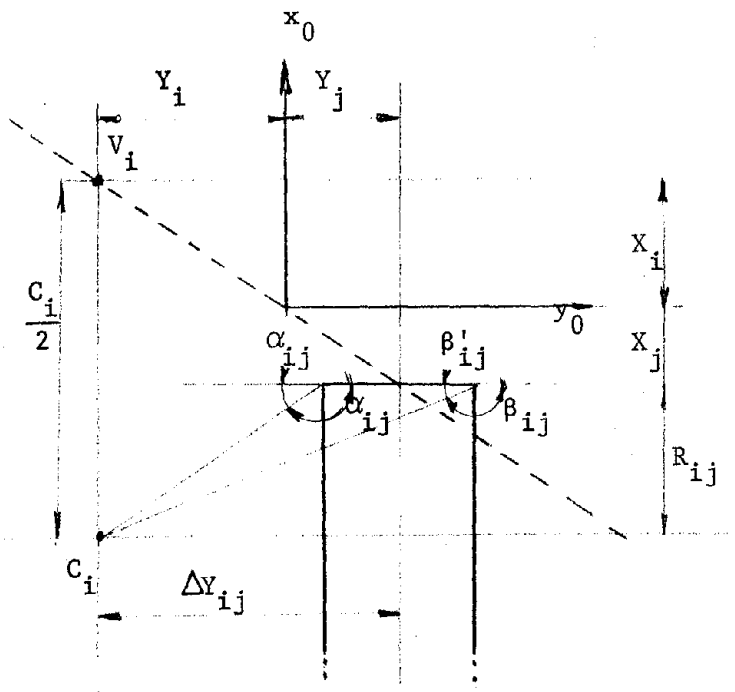

Figure D-4c

$$\alpha'_{ij} \triangleq 180^\circ - \alpha_{ij}$$

$$\beta'_{ij} \triangleq 180^\circ - \beta_{ij}$$

$$\Delta X_{ij} = X_j - X_i$$

$$R_{ij} = \Delta X_{ij} + \frac{C_i}{2}$$

$$\Delta Y_{ij} = Y_j - Y_i$$

For the left trailing vortex

$$\alpha = 0$$

$$\beta = 90^\circ + \alpha'_{ij}$$

$$(W_{ij})_L = -\frac{\Gamma_j}{4\pi}\left[\frac{1-\cos(90^\circ+\alpha'_{ij})}{\Delta Y_{ij}-h}\right] = -\frac{\Gamma_j}{4\pi}\frac{(1+\sin\alpha'_{ij})}{(\Delta Y_{ij}-h)} \qquad \text{(D-28)}$$

$$\sin\alpha'_{ij} = \frac{R_{ij}}{\sqrt{(\Delta Y_{ij}-h)^2 + R_{ij}^2}} \qquad \text{(D-29)}$$

For the bound vortex

$$\alpha = \alpha_{ij} = 180^\circ - \alpha'_{ij}$$

$$\beta = \beta_{ij} = 180^\circ - \beta'_{ij}$$

$$(W_{ij})_B = \frac{\Gamma_j}{4\pi R_{ij}}(\cos\alpha_{ij} - \cos\beta_{ij}) \qquad \text{(D-30)}$$

$$\cos\alpha_{ij} = \cos(180^\circ - \alpha'_{ij})$$

Therefore

$$\cos\alpha_{ij} = -\cos\alpha'_{ij} = -\frac{\Delta Y_{ij}-h}{\sqrt{(\Delta Y_{ij}-h)^2 + R_{ij}^2}} \qquad \text{(D-31)}$$

Similarly

$$\cos\beta_{ij} = -\cos\beta'_{ij} = -\frac{\Delta Y_{ij}+h}{\sqrt{(\Delta Y_{ij}+h)^2 + R_{ij}^2}} \qquad \text{(D-32)}$$

For the right trailing vortex

$$\alpha = 90^\circ - \beta'_{ij}$$

$$\beta = 180^\circ$$

$$(W_{ij})_R = \frac{\Gamma_j}{4\pi} \frac{[\cos(90^o - \beta'_{ij}) - \cos\ 180^o]}{(\Delta Y_{ij} + h)} = \frac{\Gamma_j}{4\pi} \frac{(\sin \beta'_{ij} + 1)}{(\Delta Y_{ij} + h)} \qquad \text{(D-33)}$$

$$\sin \beta'_{ij} = \frac{R_{ij}}{\sqrt{(\Delta Y_{ij} + h)^2 + R_{ij}^2}}$$

Therefore

$$W_{ij} = \frac{\Gamma_j}{4\pi} \left[- \frac{1 + \sin \alpha'_{ij})}{(\Delta Y_{ij} - h)} + \frac{1 + \sin \beta'_{ij}}{\Delta Y_{ij} + h} + \frac{\cos \alpha_{ij} - \cos \beta_{ij}}{R_{ij}} \right] \qquad \text{(D-34)}$$

It is now possible to derive the matrix K of equation (D-10) since each element will be given by

$$K_{ij} = \frac{W_{ij}}{\Gamma_j} \quad .$$

D.3 Structures Fundamentals.

As done in the previous section, the continuously varying spanwise airload distribution will be replaced by a series of constant intensity running loads.

The assumption of the section aerodynamic center acting at the quarter chord becomes weak when considering the bending and torsion due to the airload distribution whereas it is quite good when computing spanwise lift distribution. This inconvenience, due to the lack of predicting chord-wise lift distribution, can be reduced by introducing a correction factor f which will allow the section aerodynamic center to be placed in any desired place along the chord. Such a correction factor is here assumed to be known.

Because of reasons which will appear more evident in this section, the horseshoe vortices must be chosen in a way such that the aircraft centerline will coincide with one trailing vortex.

Let us consider the geometry of the structural skeleton of the wing as shown in Figure D-5 and define

$M_{x_1}, M_{x_2}, \ldots, M_{x_i}$ Rolling moment due to total lift of all the vortices outboard of this point (positive when raises left wing tip).

$M_{y_1}, M_{y_2}, \ldots, M_{y_i}$ Pitching moment due to total lift of all the vortices outboard of this point (positive when nose up).

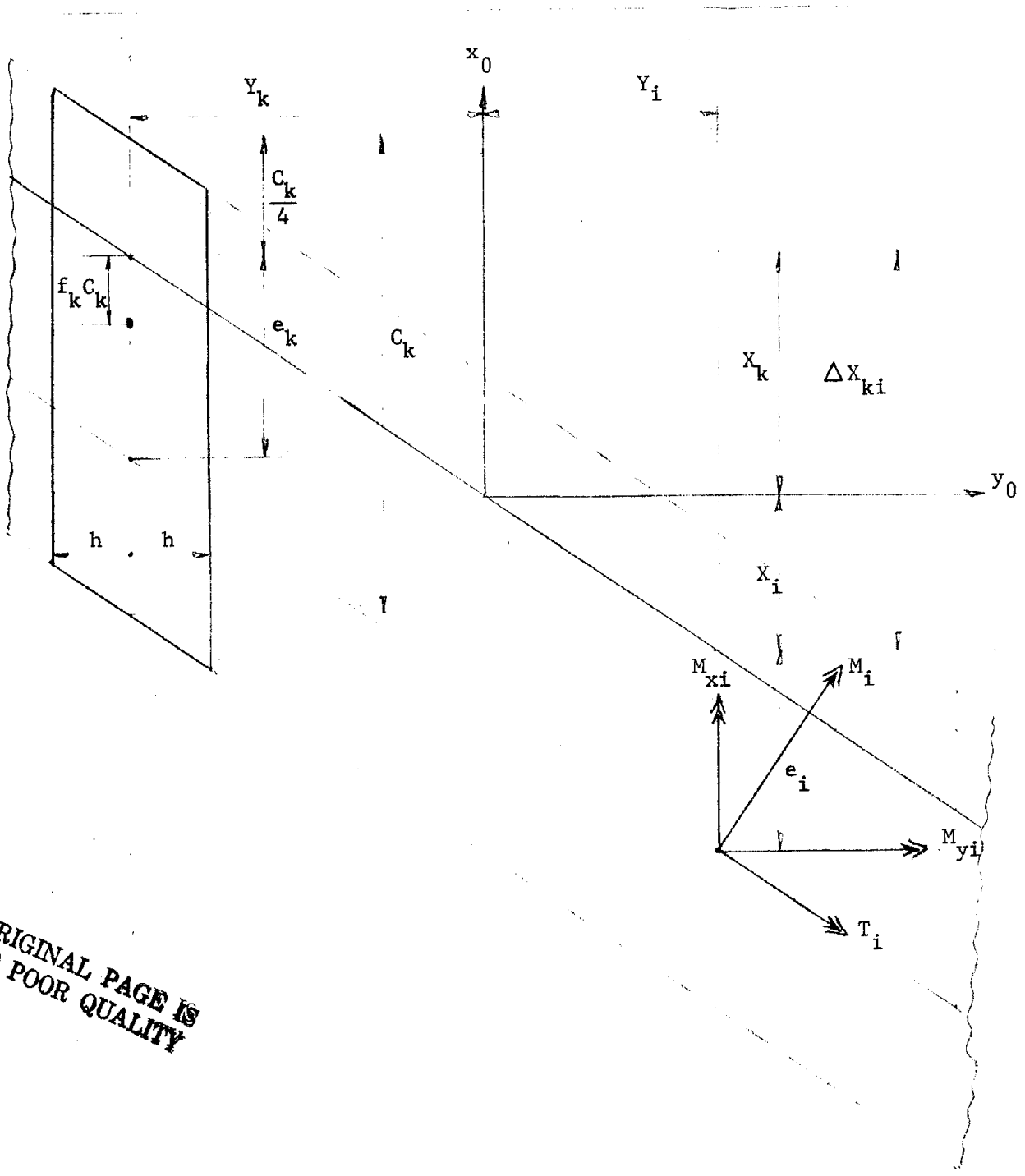

Figure D-5 - Structural Skeleton of the Wing.

$M_1 , M_2 , \ldots , M_i$ Beam bending moment at elastic axis point about axis perpendicular to local elastic axis (positive when it compresses wing upper surface).

$T_1 , T_2 , \ldots , T_i$ Torsional moment around elastic axis (positive when leading edge up).

$L_1 , L_2 , \ldots , L_i$ Total lift acting on the wing section having span $2h$, numbered from the left wing tip

$$L_i = 2h\ell_i$$

ℓ_i being the intensity of the running lift at station i.

$e_1 , e_2 , \ldots , e_i$ Streamwise distance from horseshoe reference point at a wing station to the corresponding point on the elastic axis (positive when elastic axis point is to rear of horseshoe reference point).

$f_1 , f_2 , \ldots , f_i$ Section aerodynamic center correction factor; (f positive when aircraft is to rear of quarter chord point).

The general form for the bending moment is

$$M_i = M_{x_i} \cos \Lambda + M_{y_i} \sin \Lambda \qquad \text{(D-35)}$$

and for the torsional moment

$$T_i = M_{y_i} \cos \Lambda - M_{x_i} \sin \Lambda \qquad \text{(D-36)}$$

At station 1, on the center line of the horseshoe vortex nearest to

the left wing tip (Fig. D-6) the following equations apply:

$$M_{x_1} = \frac{L_1}{2}\frac{h_1}{2} = L_1\frac{h_1}{4}$$

$$M_{y_1} = \frac{L_1}{2}\left(e_1 - f_1 C_1 + \frac{h \tan\Lambda}{2}\right)$$

and substituting into equations (D-35) and (D-36)

$$M_1 = \frac{L_1}{2}\left[\frac{h_1 \cos\Lambda}{2} + (e_1 - f_1 C_1 + \frac{h}{2}\tan\Lambda)\sin\Lambda\right] \qquad \text{(D-37)}$$

$$T_1 = \frac{L_1}{2}\left[(e_1 - f_1 C_1 + \frac{h}{2}\tan\Lambda)\cos\Lambda - \frac{h_1}{2}\sin\Lambda\right] \qquad \text{(D-38)}$$

At station 2

$$M_{x_2} = L_1(h_1 + h) + \frac{L_2 h}{4} \qquad \text{(D-39)}$$

$$M_{y_2} = L_1(\Delta X_{12} - f_1 C_1 + e_2) + L_2(e_2 - f_2 C_2 + \frac{h}{2}\tan\Lambda) \qquad \text{(D-40)}$$

and in general, for the left wing (forward), for $i > 1$

$$\left(M_{x_i}\right)_L = \sum_{k=1}^{i-1} 2 h L_k (i - k) + L_i \frac{h}{4} \qquad \text{(D-41)}$$

$$\left(M_{y_i}\right)_L = \sum_{k=1}^{i-1} L_k(\Delta X_{ki} + e_i - f_k C_k) + \frac{L_i}{2}\left(e_i - f_i C_i + \frac{h}{2}\tan\Lambda\right) \qquad \text{(D-42)}$$

where

$$\Delta X_{ki} = X_k - X_i$$

herefore, for $i > 1$, the bending moment and torsion for the left wing are given by:

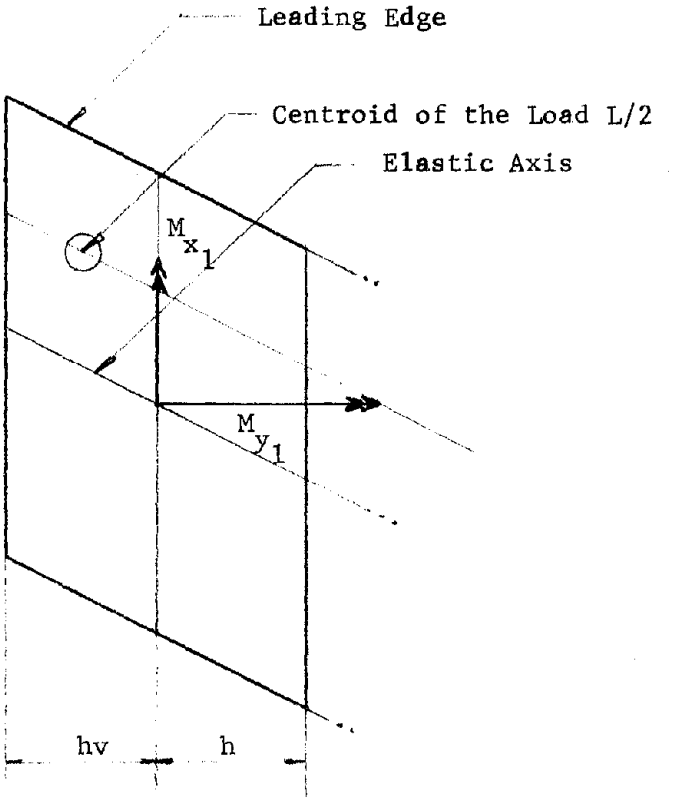

Figure D-6 - Plan View of Left Wing Tip Section.

$$(M_i)_L = \left[\sum_{k=1}^{i-1} 2\,h\,L_k(1-k) + L_i\,\frac{h}{4}\right]\cos\Lambda$$

$$+\left[\sum_{k=1}^{i-1} L_k(\Delta X_{ki} + e_i - f_k\,C_k) + \frac{L_i}{2}\,(e_i - f_i\,C_i + \frac{h}{2}\tan\Lambda)\quad \sin\Lambda\right] \tag{D-43}$$

$$(T_i)_L = \left[\sum_{k=1}^{i-1} L_k(\Delta X_{ki} + e_i - f_k\,C_k) + \frac{L_i}{2}\,(e_i - f_i\,C_i + \frac{h}{2}\tan\Lambda)\right]\cos\Lambda$$

$$-\left[\sum_{k=1}^{i-1} 2\,h\,L_k\,(i-k) + L_i\,\frac{h}{4}\right]\sin\Lambda \tag{D-44}$$

For $i = 1$ expressions (D-37) and (D-38) should be used.

For the right wing, assuming n to be the farthest right station

$$M_{x_n} = \frac{L_n}{2}\,\frac{h_n}{2} \tag{D-45}$$

$$M_{y_n} = \frac{L_n}{2}\,(e_n - f_n\,C_n - \frac{h_n}{2}\tan\Lambda) \tag{D-46}$$

$$(M_n)_R = -\,L_n\,\frac{h_n}{4}\cos\Lambda + \frac{L_n}{2}\,(e_n - f_n\,C_n - \frac{h_n}{2}\tan\Lambda)\sin\Lambda \tag{D-47}$$

$$(T_n)_R = \frac{L_n}{2}\left[(e_n - f_n\,C_n - \frac{h_n}{2}\tan\Lambda)\,\cos\Lambda + \frac{h_n}{2}\sin\Lambda\right] \tag{D-48}$$

and in general, for the right wing, for $k < n$

$$\left(M_{x_i}\right)_R = \sum_{k=n}^{i+1} 2\,h\,L_k\,(i-k) - L_i\,\frac{h}{4} \tag{D-49}$$

$$\left(M_{y_i}\right)_R = \sum_{k=n}^{i+1} L_k(\Delta X_{ki} + e_i - f_k\,C_k) + \frac{L_i}{2}\,(e_i - f_i\,C_i - \frac{h}{2}\tan\Lambda) \tag{D-50}$$

where

$$\Delta X_{ki} = X_k - X_i$$

Therefore the bending moment and torsion, for the right wing and for $k < n$, are given by

$$(M_i)_R = \left[\sum_{k=n}^{i+1} 2\,h\,L_k(i-k) - L_i\,\frac{h}{4}\right]\cos\Lambda + \left[\sum_{k=n}^{i+1} L_k(\Delta X_{ki} + e_i - f_k\,C_k) + \frac{L_i}{2}\,(e_i - f_i\,C_i - \frac{h}{2}\tan\Lambda)\right]\sin\Lambda \tag{D-51}$$

$$(T_i)_R = \left[\sum_{k=n}^{i+1} L_k(\Delta X_{ki} + e_i - f_k\,C_k) + \frac{L_i}{2}\,(e_i - f_i\,C_i - \frac{h}{2}\tan\Lambda)\right]\cos\Lambda - \left[\sum_{k=n}^{i+1} 2\,h\,L_k(i-k) - L_i\,\frac{h}{4}\right]\sin\Lambda \tag{D-52}$$

At the root station of the elastic axis the bending moments of the right and left wing cancel each other in a trimmed flight condition. The presence of an unsymmetric airload would introduce a non-zero aerodynamic moment at the root station.

In Figure D-7, such a case is shown.

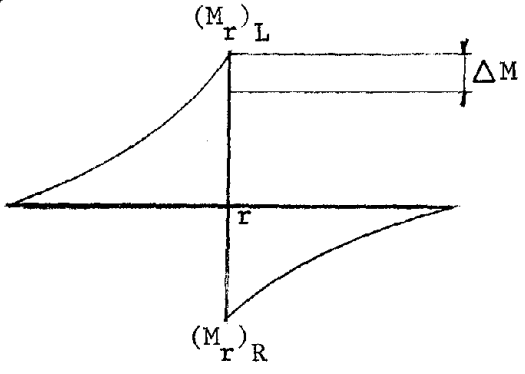

Figure D-7

where

$\Delta M = (M_r)_R + (M_r)_L$

$(M_r)_R$ = Root bending moment due to right wing airload

$(M_r)_L$ = Root bending moment due to left wing airload

r = Root station

In such a case the following considerations can be made:

a) Instantaneously the wing is assumed clamped at the centerline, allowing for the discontinuity in the bending moment. The structural rotation angle across the span, due to bending, can be computed as shown in the next pages by simply substituting, for the semi-wing considered, the corresponding root bending moment.

b) The ΔM produces an angular acceleration which can be decomposed w.r.t. the roll and pitch axes.

This acceleration introduces angular velocities about the roll and pitch axes which results in an apparent or aerodynamic twist. This new twist contribution modifies the spanwise airload distribution and, consequently, the root ΔM. A change in ΔM changes the angular acceleration and so on.

Because of this discontinuity at the root it is convenient not to consider the root station.

In case such a point were included in order to take into account the two different values of the bending moment it would be necessary to

write two separate matrices: one for the left and one for the right wing. In addition, when computing the streamwise twist due to wing flexibility, this discontinuity in the root moment comes up again.

By using a system of vortices such that the aircraft centerline coincides with one trailing vortex, the root double-valued point will not be computed. In doing so nothing is lost in accuracy but there is a gain in simplicity for the matrix analysis.

In matrix form, equations D-37, D-38, D-43, D-44, D-45, D-46, D-51, and D-52 can be opportunely combined and become

$$\{M\} = \left[\cos\Lambda \; [r] + \sin\Lambda [u] \right] \{L\} \tag{D-53}$$

$$\{T\} = \left[- \sin\Lambda [r] + \cos\Lambda [u] \right] \{L\} \tag{D-54}$$

where

$$\{M\} = \begin{Bmatrix} M_1 \\ \vdots \\ M_L \\ M_R \\ \vdots \\ M_n \end{Bmatrix} ; \quad \{T\} = \begin{Bmatrix} T_1 \\ \vdots \\ T_L \\ T_R \\ \vdots \\ T_n \end{Bmatrix} ; \quad L = 2h \{\ell\} = 2h \begin{Bmatrix} \ell_1 \\ \vdots \\ \ell_L \\ \ell_R \\ \vdots \\ \ell_n \end{Bmatrix}$$

M_L , T_L , ℓ_L are the values at the last station to the left of the aircraft centerline (Fig. D-8).

M_R , T_R , ℓ_R are the values at the first station to the right of the aircraft centerline (Fig. D-8).

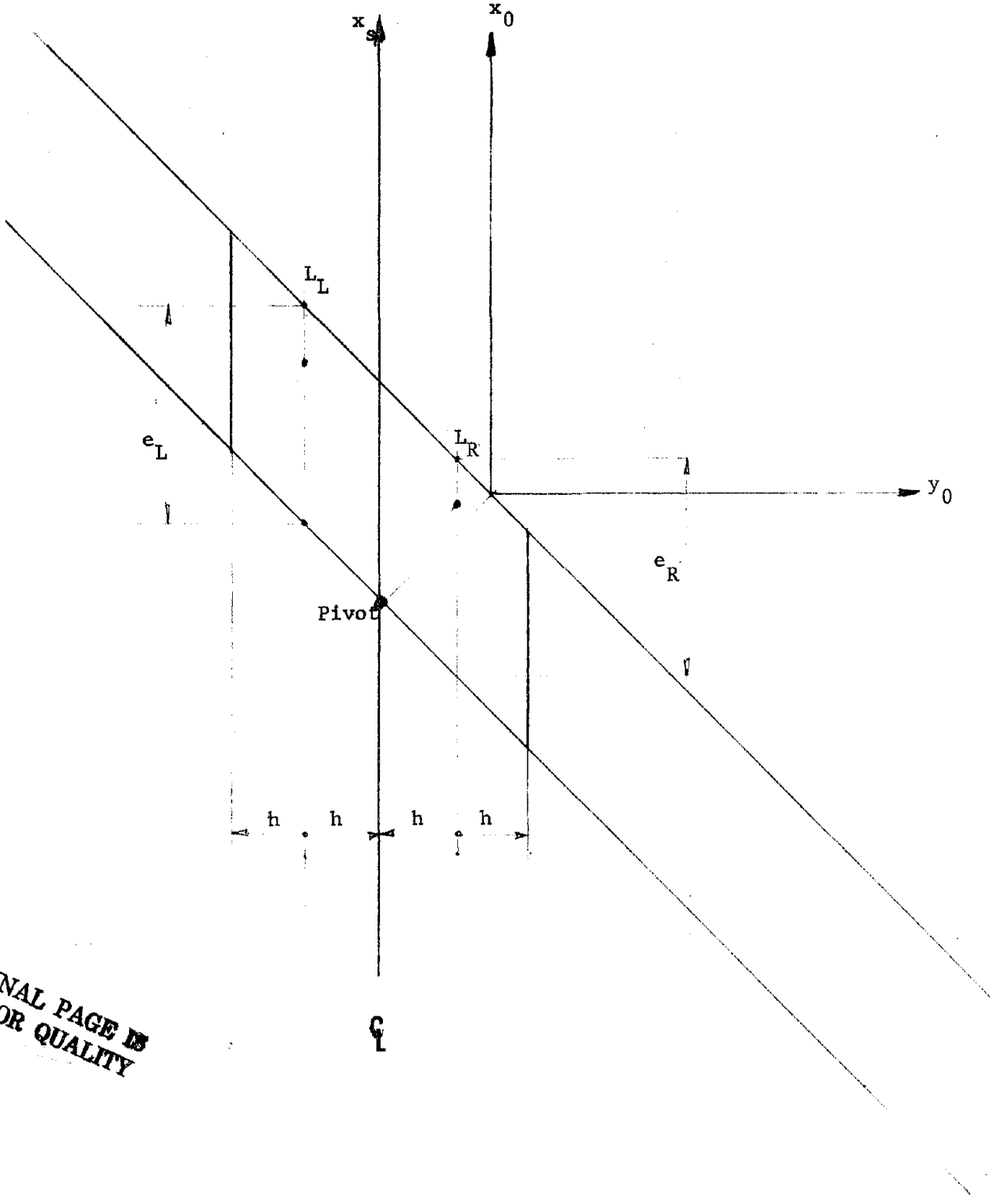

Figure D-8 - Plan View of Aircraft Centerline.

$$[r] = \left[\begin{array}{c|c} \begin{matrix} \frac{h_1}{4} & & & \\ 2h & \frac{h}{4} & & \mathbf{0} \\ \cdots & \cdots & \cdots & \\ (i-1)\,2h & (i-2)\,2h & \frac{h}{4} & \\ \cdots & \cdots & \cdots & \\ (R-1)\,2h & (R-2)\,2h & & \end{matrix} & \begin{matrix} & & \\ & & \\ & \mathbf{0} & \\ & & \\ & & \\ \frac{h}{4} & & \end{matrix} \\ \hline \mathbf{0} & \begin{matrix} -\frac{h}{4} & -2h & \cdots & (L-n)2h \\ \cdots & \cdots & \cdots & \\ -\frac{h}{4} & -2h & \cdots & (j-n)2h \\ \cdots & \cdots & \cdots & \\ -\frac{h}{4} & -2h & & \\ & & & -\frac{h_n}{4} \end{matrix} \end{array}\right] \qquad \text{(D-55)}$$

and

$$[u] = \left[\begin{array}{c|c} [A] & [0] \\ \hline [0] & [B] \end{array}\right] \tag{D-56}$$

where [A] and [B] are reported in Tables D-I and D-II.

The moment at the aircraft centerline can be computed as follows

$$\left(M_{x_r}\right)_L = M_{x_L} + L_L \frac{h}{4} \tag{D-57}$$

$$\left(M_{y_r}\right)_L = M_{y_L} + L_L(e_r - f_L C_L + \frac{h}{2} \tan \Lambda) \tag{D-58}$$

$$\left(M_{x_r}\right)_R = M_{x_R} - L_R \frac{h}{4} \tag{D-59}$$

$$\left(M_{y_r}\right)_R = M_{y_R} + \frac{L_R}{2} (e_r - f_R C_R - \frac{h}{2} \tan \Lambda) \tag{D-60}$$

where

$\left(M_{x_r}\right)_L$ = Rolling moment at the aircraft centerline elastic axis due to left wing airload distribution.

$\left(M_{y_r}\right)_L$ = Pitching moment at the aircraft centerline elastic axis due to left wing airload distribution.

Similarly $\left(M_{x_r}\right)_R$ and $\left(M_{y_r}\right)$ indicate the corresponding moment due to the right wing contribution.

The total rolling and pitching moments acting on the airplane are:

for the rolling moment $\overline{\mathcal{L}}$

$$\Delta\overline{\mathcal{L}} = M_{x_L} + M_{x_R} + \frac{h}{4} (L_L - L_R) \tag{D-61}$$

$$[A] = \begin{bmatrix} \frac{1}{2}(e_1 - f_1C_1 + \frac{h_1}{2}\tan\Lambda) & & & \\ (\Delta X_{12} + e_2 - f_1C_1) & \frac{1}{2}(e_2 - f_2C_2 + \frac{h}{2}\tan\Lambda) & & \mathbf{0} \\ \cdots & \cdots & \cdots & \\ (\Delta X_{1i} + e_i - f_1C_1) & (\Delta X_{2i} + e_i - f_2C_2) \cdots & \frac{1}{2}(e_i - f_iC_i + \frac{h}{2}\tan\Lambda) & \\ \cdots & \cdots & \cdots & \\ (\Delta X_{1L} + e_L - f_1C_1) & (\Delta X_{2L} + e_L - f_2C_2) \cdots & \cdots & \frac{1}{2}(e_L - f_LC_L + \frac{h}{2}\tan\Lambda) \end{bmatrix}$$

TABLE D-I

$$[B] = \begin{bmatrix} \frac{1}{2}(e_R - f_R C_R - \frac{h}{2}\tan\Lambda) & \cdots & (\Delta X_{nR} + e_R - f_n C_n) \\ & \cdots & \\ & \frac{1}{2}(e_{(n-1)} - f_{(n-1)} C_{(n-1)} - \frac{h}{2}\tan\Lambda) & (\Delta X_{(n-1)R} + e_{(n-1)} - f_n C_n) \\ & & \frac{1}{2}(e_n - f_n C_n - \frac{h_n}{2}\tan\Lambda) \\ \mathbf{0} & & \end{bmatrix}$$

TABLE D-II

for the pitching moment M

$$\Delta M = M_{y_L} + M_{y_R} + \frac{1}{2} e_r (L_L + L_R) + \frac{h}{4} (L_L - L_R) \tan \Lambda - L_L f_L C_L - L_R f_R C_R \tag{D-62}$$

The streamwise angle of attack contribution due to wing flexibility can then be obtained from

$$\alpha_{s_i} = \int_k^i \frac{M}{EI} \, ds \, \sin \Lambda + \int_k^i \frac{T}{GJ} \, ds \, \cos \Lambda \tag{D-63}$$

where

α_{s_i} = Streamwise angle of attack contribution at station i due to values of bending and torsional moments acting inboard and at station i .

k = R Station when i on the right wing

k = L Station when i on the left wing

EI Effective beam bending stiffness around elastic axis

GJ Effective torsional stiffness around elastic axis.

Since $dS = \frac{2h}{\cos\Lambda}$ for this study, the integrals in equation (D-62) for station 1 can be written as

$$\int_L^1 \frac{M}{EI} \, ds \cong \left[\frac{M_1}{E_1 I_1} \frac{h}{\cos\Lambda} + \frac{M_2}{E_2 I_2} \frac{2h}{\cos\Lambda} + \ldots + \frac{M_{(L-1)}}{E_{(L-1)} I_{(L-1)}} \frac{2h}{\cos\Lambda} + \frac{M_L}{E_L I_L} \frac{2h}{\cos\Lambda} \right]$$

$$= \frac{2h}{\cos\Lambda} \left[\frac{M_1}{2 E_1 I_1} + \sum_{i=2}^{L} \frac{M_i}{E_i I_i} \right]$$

$$\int_L^1 \frac{T}{GJ}\, ds \simeq \frac{2h}{\cos\Lambda}\left[\frac{T_1}{2\ G_1 J_1} + \sum_{i=2}^{L} \frac{T_i}{G_i J_i}\right]$$

And similarly it is possible to obtain the expressions for the corresponding values at each station.

In matrix form:

$$\{\alpha_S\} = \frac{2h}{\cos\Lambda}\left[\sin\Lambda\ [EI]\ \{M\} + \cos\Lambda [GJ]\ \{T\}\right] \qquad \text{(D-64)}$$

where

$$[EI] = \left[\begin{array}{c:c} [C] & [0] \\ \hdashline [0] & [D] \end{array}\right] \qquad \text{(D-65)}$$

where [C] and [D] are reported in table D-III.

The matrix [GJ] is similar to [EI] and can be ontained from equation (D-65) by simply replacing EI with GJ .

Substituting equations (D-53) and (D-54) into equation (D-64)

$$\{\alpha_S\} = \frac{2h}{\cos\Lambda}\left[\sin\Lambda\ [EI]\ (\cos\Lambda\ [r] + \sin\Lambda\ [u])\right.$$
$$\left. + \cos\Lambda [GJ]\ (\sin\Lambda [r] - \cos\Lambda [u])\right]\{L\} \qquad \text{(D-66)}$$

which can be written as

$$\{\alpha_S\} = 4h^2\left[\sin\Lambda([EI]+[GJ])[r] + \left(\frac{\sin^2\Lambda}{\cos\Lambda}\ [EI] - \cos\Lambda [GJ]\right)[u]\right]\{\ell\} \qquad \text{(D-67)}$$

It is now possible to define the elasticity matrix $[S_2]$.

$$[C] = \begin{bmatrix} \frac{1}{2} & \frac{1}{E_1 I_1} & \frac{1}{E_2 I_2} & \cdots & \cdots & \cdots & \frac{1}{E_L I_L} \\ & & \frac{1}{2} & \frac{1}{E_2 I_2} & \cdots & \cdots & \frac{1}{E_L I_L} \\ & & & & \cdots & \cdots & \\ & & & & & \frac{1}{2} \frac{1}{E_{(L-1)} I_{(L-1)}} & \frac{1}{E_L I_L} \\ & & & \mathbf{0} & & & \frac{1}{2} \frac{1}{E_L I_L} \end{bmatrix}$$

$$[D] = \begin{bmatrix} \frac{1}{2} \frac{1}{E_R I_R} & & & \\ & & \mathbf{0} & \\ \frac{1}{E_R I_R} & \frac{1}{2E_{(R+1)} I_{(R+1)}} & & \\ \cdots & \cdots & & \\ \frac{1}{E_R I_R} & \frac{1}{E_{(R+1)} I_{(R+1)}} & \cdots \cdots & \frac{1}{2E_i I_i} \\ \cdots & \cdots & & \\ \frac{1}{E_R I_R} & \frac{1}{E_{(R+1)} I_{(R+1)}} & \cdots \cdots & \frac{1}{2E_n I_n} \end{bmatrix}$$

TABLE D-III

$$[S_2] \triangleq 4h^2 \left[\sin\Lambda \left([EI]+[GJ]\right) [r] + \left(\frac{\sin^2\Lambda}{\cos\Lambda} [EI] - \cos\Lambda [GJ] \right) [u] \right] \quad \text{(D-68)}$$

Then

$$\{\alpha_s\} = [S_2] \{\ell\} \quad \text{(D-69)}$$

The $S2_{ij}$ element of the $[S_2]$ matrix represents the angle of attack change in radians at station i due to the structural deflection of the wing caused by a unit loading at station J.

D.4 Wing Twist.

The twist in a flexible wing can have several contributions or twists which can be divided into two classes: I) those which would be present even if the wing were rigid, and II) those due to inertia effects, thrusts or drag, and section pitching movements on the flexible wing.

$$\{\alpha_g\} = \{\alpha_{g_I}\} + \{\alpha_g\} \qquad \text{(D-70)}$$

Class I: Aerodynamic Twists $\{\alpha_{g_I}\}$

a) Built-in geometric twist due to camber or construction (including eventual dihedral contribution) or both.

b) Interference twist (not considered in this study).

c) Twist due to control surfaces deflection (flap, aileron, spoilers).

d) Apparent twist due to airplane rolling and/or pitching velocities (the angles of attack due to pitching velocities should be measured at 3C/4).

Class II: Structural Twist due to Wing Deflections caused by Aerodynamic Loading which are independent of Wing Lift Distribution $\{\alpha_{g_{II}}\}$

a) Vertical acceleration upon dry wing and internal fuel dead weights.

b) Effects of airplane rolling and/or pitching acceleration upon dry wing dead weight, wing internal fuel dead weight.

c) Section pitching moment with control surfaces in neutral position (C_{m0} of the airfoil).

d) Incremental section pitching moment due to control surfaces deflection.

The type of twist due to the effects of wing deflections arising from loads which are independent of wing angle of attack, such as those listed under Class II, may be computed with the aid of equation (D-63)

$$\left\{\alpha_{g_{II}}\right\} = \frac{2h}{\cos\Lambda}\left[\sin\Lambda\,[EI]\,\{M\} + \cos\Lambda\,[GJ]\,\{T\}\right] \qquad \text{(D-71)}$$

where M and T are the wing bending moments and torsion along the wing elastic axis due to the loadings of Class II. For cases a) and b) the knowledge of mass for each section of span 2h and the position of the corresponding C.M. w.r.t. the elastic axis must be known.

No attempt is made here to compute the section pitching moment with control surfaces in neutral position.

D.4.1 Twist due to Control Surface Deflection.

The effect of a control surface deflection is of introducing an aerodynamic as well as a structural twist.

The aerodynamic twist can be computed from the following expression for the lift produced by control deflection [Ref. 25].

$$\{C_\ell\}_\delta = 2\left[(\pi - \theta_0 + \sin\theta_0)\right]\{\delta\} \qquad \text{(D-72)}$$

where

$$\theta_0 = \sin^{-1}\left[2\sqrt{\xi(1-\xi)}\right]$$

$$\theta_0 = \cos^{-1}(2\xi - 1)$$

$$\xi = \frac{C_f}{c}$$

C_f = control surface chord

$\{\delta\}$ control surface deflection in radians

Equation (D-71) applies for a 2-D lift curve slope of 2π. For a 2-D lift curve slope of m_0, this equation can be written as

$$\{C_\ell\}_\delta = \left[m_0\right]\left[\left(1 - \frac{\theta_0}{\pi} + \frac{\sin\theta_0}{\pi}\right)\right]\{\delta\} \qquad \text{(D-73)}$$

Substituting the value for θ_0 results in

$$\{C_\ell\}_\delta = \left[m_0\right]\left[\left(1 - \frac{1}{\pi}\cos^{-1}(2\xi - 1) + \frac{1}{\pi}2\sqrt{\xi(1-\xi)}\right)\right]\{\delta\} \qquad \text{(D-74)}$$

And dividing both sides by $\left[m_0\right]$

$$\{\alpha_{g_I}\} = \left[\left(1 - \frac{1}{\pi}\cos^{-1}(2\xi - 1) + \frac{1}{\pi}2\sqrt{\xi(1-\xi)}\right)\right]\{\delta\} \qquad \text{(D-75)}$$

Structural twist derives from the section pitching movement due to control deflection. Once the spanwise bending moments and torsion distributions are known, equation (D-71) can be used to compute the section structural twist where M and T are replaced by the corresponding ones due to controls, M_c and T_c.

In Figure D-9 the symbols used are shown.

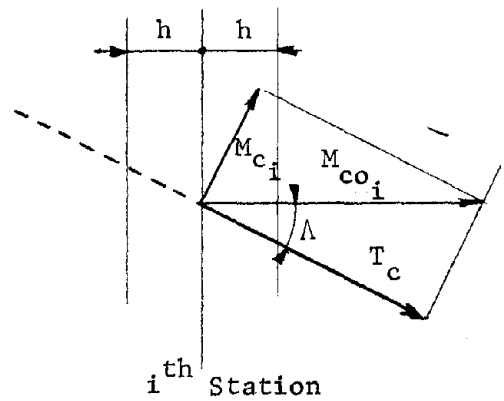

Figure D-9 - Structural Moments due to Control.

M_{c0_i} Station pitching moment due to controls

$$M_{c0_i} = q\ 2h\ C^2\ C_{m_{0i}}$$

C Local chord length

$C_{m_{0i}}$ Local pitching moment coefficient

$$M_{c_i} = M_{c0_i} \sin\Lambda$$

$$T_{c_i} = M_{c0_i} \cos\Lambda$$

The station pitching moments can be computed similarly to what was done in equations (D- 42) for the left wing, and (D-50) for the right wing.

For stations 1 and n

$$M_{c0_1} = q\ h\ C_1^2\ C_{m_{01}} \qquad \text{(D-76)}$$

$$M_{c0_n} = q\ h\ C_1^2\ C_{m_{0n}} \qquad \text{(D-77)}$$

For stations 2 and n - 1

$$M_{c0_2} = q\ 2h \left[C_1^2\ C_{m_{01}} + \frac{1}{2}\ C_1^2\ C_{m_{01}} \right] \tag{D-78}$$

$$M_{c0_{(n-1)}} = q\ 2h \left[\frac{1}{2}\ C^2_{(n-1)}\ C_{m_{0(n-1)}} + C_n^2\ C_{m_{0n}} \right] \tag{D-79}$$

... and so forth.

And in general, for the left wing

$$\left(M_{c0_i}\right)_L = q\ 2h \left[\sum_{k=1}^{i-1} C_k^2\ C_{m_{0k}} + \frac{1}{2}\ C_i^2\ C_{m_{0i}} \right] \tag{D-70}$$

for the right wing

$$\left(M_{c0_i}\right)_R = q\ 2h \left[\sum_{k=n}^{i+1} C_k^2\ C_{m_{0k}} + \frac{1}{2}\ C_i^2\ C_{m_{0i}} \right] \tag{D-81}$$

Equations (D-80) and (D-81) are derived for the general case where the control surface can be extended from tip to tip.

In matrix form, (D-80) and (D-81) become

$$\{M_{c0}\} = 2h\ q\ [D\ I\ 1] \left[C^2\right] \{C_{m0}\} \tag{D-82}$$

where

$$[DI1] = \left[\begin{array}{cccccc:cccccc}
1/2 & & & & & & & & & & & \\
1 & 1/2 & & & & & & & & & & \\
1 & 1 & 1/2 & & & & & & & & & \\
\cdot & \cdot & \cdot & \cdot & \cdot & \cdot & & & & & & \\
1 & 1 & 1 & \cdot & \cdot & 1/2 & & & & & & \\
\hdashline
 & & & & & & 1/2 & 1 & 1 & \cdot & \cdot & 1 \\
 & & & & & & & 1/2 & 1 & \cdot & \cdot & 1 \\
 & & & & & & & & \cdot & \cdot & \cdot & \cdot \\
 & & & & & & & & & & 1/2 & 1 \\
 & & & & & & & & & & & 1/2
\end{array}\right] \tag{D-83}$$

If wind tunnel data are not available, theoretical expressions for C_{m0} in terms of the deflection δ may be used.

From reference [25]

$$\{C_{m0}\}_\delta = -\frac{1}{2}\left[(\sin\theta_0 - \frac{1}{2}\sin 2\theta_0)\right]\{\delta\} \tag{D-84}$$

Substituting $\sin\theta_0$ and $\sin 2\theta_0 = 2\sin\theta_0\cos\theta_0$ results in

$$\begin{aligned}\{C_{m0}\}_\delta &= -\frac{1}{2}\left[2\sqrt{\xi(1-\xi)} - 2\sqrt{\xi(1-\xi)(2\xi-1)}\right]\{\delta\} \\ &= -2\left[\sqrt{\xi(1-\xi)^3}\right]\{\delta\}\end{aligned} \tag{D-85}$$

Therefore, the structural bending moment and torsion are

$$\{M_c\} = -4\,q\,h\,\sin\Lambda\,[D\,I\,1]\left[\sqrt{\xi(1-\xi)^3}\right]\left[C^2\right]\{\delta\} \tag{D-86}$$

$$\{T_c\} = -4\,q\,h\,\cos\Lambda\,[D\,I\,1]\left[\sqrt{\xi(1-\xi)^3}\right]\left[C^2\right]\{\delta\} \tag{D-87}$$

and the structural twist is

$$\begin{aligned}\{\alpha_{g_{II}}\} &= \frac{2h}{\cos\Lambda}\left[\sin\Lambda\,[EI]\{M_c\} + \cos\Lambda\,[GJ]\{T_c\}\right] \\ &= -8\,q\,h^2\left[\frac{\sin^2\Lambda}{\cos\Lambda}\,[EI] + \cos\Lambda\,[GJ]\right][D\,I\,1]\left[\sqrt{\xi(1-\xi)^3}\right]\left[C^2\right]\{\delta\}\end{aligned} \tag{D-88}$$

The total twist due to control deflection is

$$\{\alpha_g\} = \{\alpha_{g_I}\} + \{\alpha_{g_{II}}\}$$

$$= \left[\left[\left(1 - \frac{\cos^{-1}(2\xi - 1)}{\pi} + \frac{2\sqrt{\xi(1-\xi)}}{\pi}\right)\right] - 8\,q\,h^2\left[\frac{\sin^2\Lambda}{\cos\Lambda}[EI] + \cos\Lambda\,[GJ]\right][DI1]\left[\sqrt{\xi(1-\xi)^3}\right]\left[C^2\right]\right]\{\delta\} \qquad \text{(D-89)}$$

Equation (D-89) can be applied to both aileron and/or flap systems with no requirements for symmetry or antisymmetry in their displacement since, once $\{\xi\}$ is specified, the deflection vector $\{\delta\}$ can assume any configuration.

D.4.2 Apparent Twist due to Rolling and Pitching Velocities.

When the wing is at a skew angle, the apparent twist is computed similarly for both the rolling and pitching case, the only difference being in the way the station arms are computed.

A plan view of the geometry of the quantity used in computing the apparent twist is given in Figure D-10.

Consequently, the apparent twist is given by:

1) for rate of roll p

$$\left(\alpha_p\right)_i = \frac{p}{V}\,\bar{x}_i$$

2) for rate of pitch q

$$\left(\alpha_q\right)_i = -\frac{q}{V}\left(\bar{y}_{3/4}\right)_i$$

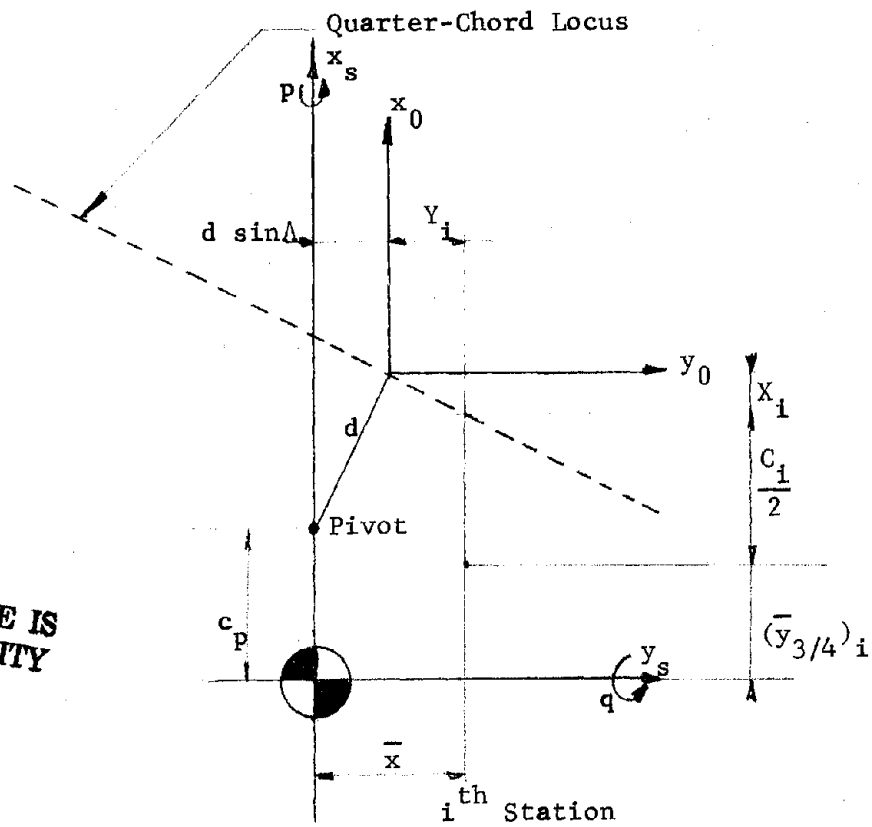

$$X_i = - Y_i \tan\Lambda + f(y_i) \cos\Lambda$$

$$\bar{y}_i = c_p + d \cos\Lambda + X_i$$

$$(\bar{y}_{3/4})_i = \bar{y}_i - \frac{C_i}{2}$$

$$\bar{x} = d \sin\Lambda + Y_i$$

Figure D-10 - Planview of the Geometric Parameters Used in Computing the Apparent Twist due to Angular Velocities.

and in matrix form

$$\left\{\alpha_{g_I}\right\} = \frac{1}{V}\left[p\left\{\bar{x}\right\} - q\left\{\bar{y}_{3/4}\right\}\right]$$

D.5 Unsymmetrical Flight Conditions.

Because of the oblique wing, whenever an unsymmetric spanwise lift distribution occurs, the aircraft will experience accelerations about its rolling as well as pitching axis.

A number of unsymmetrical flight conditions are usually investigated in structural design; for the purpose of this study, such investigation will be restricted to those which arise through the use of control surfaces on the wing, such as ailerons.

The load distribution on an elastic wing associated with control deflections may be thought of as the summation of distributions from the following specific loadings.

1) Symmetrical loading with controls in meutral position.
2) Incremental loading due to controls deflection.
3) Incremental loading associated with constant rolling and/or pitching velocity with controls in neutral position.
4) Incremental loading caused by rolling and/or pitching angular acceleration. This loading results from the structural twist described under "Structural Twist" (class II b).

In a steady roll and/or pitch condition, the span load distribution for the elastic wing is given by the first three loadings enumerated. For this condition the $\left\{\alpha_g\right\}$ values vary linearly and antisymmetrically

across the span from $-(p+q\tan\Lambda)\frac{b}{2V}$ at the left (forward) tip, and $(p+q\tan\Lambda)\frac{b}{2V}$ at the other.

The wing being at a skew angle, any unsymmetry in the spanwise lift distribution produces both pitching and rolling moments and, therefore, it introduces angular accelerations about the corresponding axes. Such a condition occurs when deflecting the desired wing control surface, unless some corrective action is taken in compensating the pitching moment by mean of the horizontal tail.

We shall now investigate this case which implies non-zero $\dot{p}$ and/or $\dot{q}$ and divide it into three parts: initiation, steady state, and termination of the motion. The second part, the steady roll and/or pitch condition, has already been discussed. The first and third ones differ only for the initial condition: no angular velocities for the initiation and a steady angular velocity for the termination. Therefore the analysis is the same for both cases.

Let us therefore consider the initiation of the motion due to an instantaneous deflection of the ailerons.

There will be contributions to the unsymmetric loading from all of the four loadings enumerated above. The first three ones having already been discussed, so only the loading due to the angular accelerations needs to be analyzed. The result of the angular accelerations is a new contribution to the structural twist due to inertia bending and torsional moments. The resulting twist distribution will superimpose an unsymmetric lift distribution on the already existing spanwise lift distribution. Because of the linear theory assumption this structural twist contribution

is independent from the other ones and, therefore, can be analyzed separately.

Figure D-11 shows the geometry of the wing section center of mass. The acceleration acting on the i^{th} center of mass is

$$a_i = \bar{x}_i \dot{p} + \overline{ym}_i \dot{q} \tag{D-90}$$

and the corresponding loading

$$F_i = m_i(\bar{x}_i \dot{p} + \overline{ym}_i \dot{q}) \tag{D-91}$$

Similarly to what done in "Structures Fundamentals" it is now possible to determine the pitching and rolling moments distributions and therefore the bending moment and torsion distributions.

For the left wing

$$M_{x_1} = \frac{h}{2}\frac{F_1}{2} = -\frac{h}{2}\frac{m_1}{2}(\bar{x}_1 \dot{p} + \overline{ym}_1 \dot{q}) \tag{D-92}$$

$$M_{y_1} = -\frac{m_1}{2}(\bar{x}_1 \dot{p} + \overline{ym}_1 \dot{q})(xm_1 + \frac{h}{2}\tan\Lambda) \tag{D-93}$$

and in general (for $1 < i \leq L$ where $L \triangleq$ last station to the left of aircraft centerline)

$$M_{x_i} = \sum_{k=1}^{i-1} 2h\, m_k(k-i)(\bar{x}_k \dot{p} + \overline{ym}_k \dot{q}) - \frac{h}{4} m_i(\bar{x}_i \dot{p} + \overline{ym}_i \dot{q}) \tag{D-94}$$

$$M_{y_i} = \sum_{K=1}^{i-1} -m_i[\Delta x_{ki} - (e_k - xm_k) + e_i](\bar{x}_k \dot{p} + \overline{ym}_k \dot{q}) - \frac{m_i}{2}(xm_i + \frac{h}{2}\tan\Lambda)(\bar{x}_i \dot{p} + \overline{ym}_k \dot{q}) \tag{D-95}$$

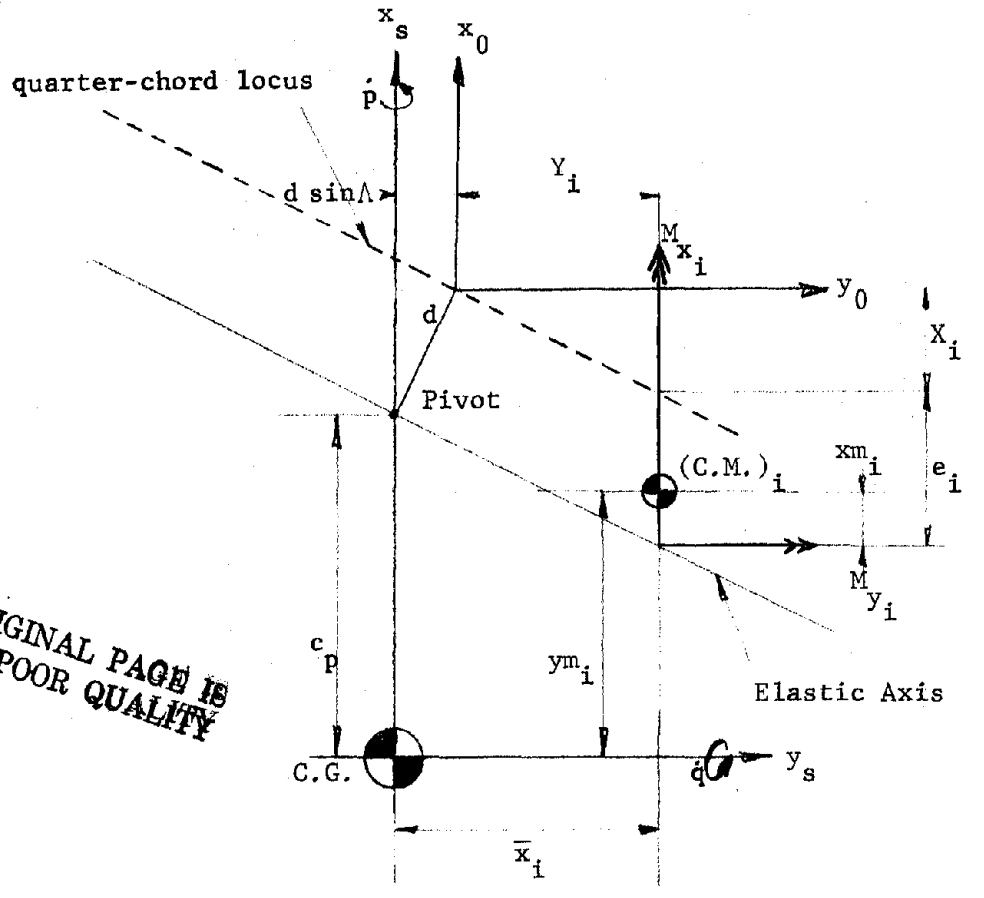

$(C.M.)_i$ = Center of Mass of i^{th} wing section

xm_i = distance of $(C.M.)_i$ from elastic axis

$\overline{ym}_i = c_p + d\ \cos\Lambda + X_i - (e_i - xm_i)$

$X_i = - Y_i\ \tan\Lambda + f(y_i)$

Figure D-11 - Wing Section Center of Mass.

For the right wing

$$M_{x_n} = \frac{h}{2}\frac{m}{2}\left(\bar{x}_n \dot{p} + \overline{ym}_n \dot{q}\right) \tag{D-96}$$

$$M_{y_n} = -\frac{m_n}{2}\left(xm_n - \frac{h}{2}\tan\Lambda\right)\left(\bar{x}_n \dot{p} + \overline{ym}_k \dot{q}\right) \tag{D-97}$$

and in general for $(n > i \geq R)$ where $R \triangleq$ first station to the right of aircraft centerline

$$M_{x_i} = \sum_{k=n}^{i+1} 2h\, m_k(k-1)\left(\bar{x}_k \dot{p} + \overline{ym}_k \dot{q}\right) + \frac{h}{4} m_i\left(\bar{x}_i \dot{p} + \overline{ym}_i \dot{q}\right) \tag{D-98}$$

$$M_{y_i} = \sum_{k=n}^{i+1} -m_k\left(\Delta X_{ki} - (e_k - e_i) + xm_i\right)\left(\bar{x}_k \dot{p} + \overline{ym}_k \dot{q}\right) - \frac{m_i}{2}\left(xm_i - \frac{h}{2}\tan\Lambda\right)\left(\bar{x}_i \dot{p} + \overline{ym}_i \dot{q}\right) \tag{D-99}$$

and in matrix form

$$\begin{aligned} \{M_x\} &= \{A\,1\}\dot{p} + \{A\,2\}\dot{q} \\ \{M_y\} &= \{B\,1\}\dot{p} + \{B\,2\}\dot{q} \end{aligned} \tag{D-100}$$

where

$$\begin{aligned} \{A\,1\} &= h[A][m_i]\{\bar{x}\} \\ \{A\,2\} &= h[A][m_i]\{\overline{ym}\} \\ \{B\,1\} &= [B][m_i]\{\bar{x}\} \\ \{B\,2\} &= [B][m_i]\{\overline{ym}\} \end{aligned}$$

$[m_i]$ = mass matrix (diagonal).

$$[B] = \left[\begin{array}{c|c} [E] & [0] \\ \hline [0] & [F] \end{array}\right] \tag{D-101}$$

where [E] and [F] are reported in Table D-IV.

$$[A] = \left[\begin{array}{cccc|ccccc} -\frac{1}{4} & & & & & & & & \\ -2 & -\frac{1}{4} & & & & & & & \\ 2(1-i) & 2(2-i) & -\frac{1}{4} & & & & & & \\ 2(1-L) & 2(2-L) & -2 & -\frac{1}{4} & & & & & \\ \hline & & & & \frac{1}{4} & 2 & \cdots & 2(n-R) & \\ & & & & & & & \frac{1}{4} & 2 \\ & & & & & & & & \frac{1}{4} \end{array}\right] \qquad (D\text{-}102)$$

$$[E] = \begin{bmatrix} -\frac{1}{2}\left(Xm_1 + \frac{h}{2}\tan\Lambda\right) & & & \\ -\left[\Delta X_{12} - (e_1 - e_2) + xm_1\right] & -\frac{1}{2}\left(Xm_2 + \frac{h}{2}\tan\Lambda\right) & & \\ \cdots & \cdots & \cdots & \\ -\left[\Delta X_{1i} - (e_1 - e_i) + Xm_1\right] & -\left[\Delta X_{2i} - (e_2 - e_i) + xm_2\right] & \cdots & -\frac{1}{2}\left(Xm_i + \frac{h}{2}\tan\Lambda\right) \\ \cdots & \cdots & \cdots & \\ -\left[\Delta X_{1L} - (e_1 - e_L) + Xm_1\right] & \cdots & \cdots & -\frac{1}{2}\left(Xm_L + \frac{h}{2}\tan\Lambda\right) \end{bmatrix}$$

$$[F] = \begin{bmatrix} -\frac{1}{2}\left(Xm_R - \frac{h}{2}\tan\Lambda\right) & \cdots & \cdots & -\left[\Delta X_{nR} - (e_n - e_R) + Xm'_R\right] \\ \cdots & \cdots & \cdots & \cdots \\ 0 & & & -\frac{1}{2}\left(Xm_n - \frac{h}{2}\tan\Lambda\right) \end{bmatrix}$$

TABLE D - IV

Since

$$\{M_b\} = \{M_x\} \cos\Lambda + \{M_y\} \sin\Lambda$$

$$\{T\} = \{M_y\} \cos\Lambda - \{M_x\} \sin\Lambda$$

it is now possible to compute $\{\alpha_{g_{II}}\}_{\dot{p}}$ and $\{\alpha_{g_{II}}\}_{\dot{q}}$ from equation (D-71).

The solution of the following equation will give the lift distribution arising from the twist contribution due to $\dot{p}$ and $\dot{q}$

$$\left[[S_1] - [S_2]\right] \{\ell\} = \{\alpha_{g_{II}}\}_{\dot{p}} + \{\alpha_{g_{II}}\}_{\dot{q}} \qquad \text{(D-103)}$$

It is now possible to compute the aerodynamic pitching and rolling moment due to $\dot{p}$ and $\dot{q}$ by integrating over the entire span the lift force times the corresponding moment arm.

$$\begin{aligned} M_{x_j} &= h \lfloor 1\ 2\ 2\ \ldots\ 2\ 1 \rfloor \ [\bar{x}] \ \{\ell\}_j \\ M_{y_j} &= h \lfloor 1\ 2\ 2\ \ldots\ 1 \rfloor \ [\bar{y}] \ \{\ell\}_j \end{aligned} \qquad \text{(D-104)}$$

where $j = \dot{p}\ ,\ \dot{q}$.

By assuming now that $\dot{p}$ and $\dot{q}$ are small quantities, it is possible to linearize even the $\dot{p}$ and $\dot{q}$ contributions to aerodynamic pitching and rolling moments

$$\begin{aligned} M_x = L &= \frac{\partial M_x}{\partial \dot{p}} \dot{p} + \frac{\partial M_x}{\partial \dot{q}} \dot{q} \\ M_y = M &= \frac{\partial M_y}{\partial \dot{p}} \dot{p} + \frac{\partial M_y}{\partial \dot{q}} \dot{q} \end{aligned} \qquad \text{(D-105)}$$

where

$$\frac{\partial M_x}{\partial j} \simeq \frac{M_{x_j}}{j}$$

$$\frac{\partial M_y}{\partial j} \simeq \frac{M_{y_j}}{j}$$

and

$$j = \dot{p} \ , \ \dot{q}$$

REFERENCES

1. Jones, R. T.
   "New Design Goals and a New Shape for the SST"
   Astronautics & Aeronautics, Vol. 10, No. 12, December 1972
   pp. 66-70

2. Campbell, J. P., and H. M. Drake
   "Investigation of Stability and Control Characteristics of an Airplane Model with Skewed Wing in the Langley Free-Flight Tunnel"
   TN 1208, 1945, NACA

3. Jones, R. T.
   "Reduction of Wave Drag by Antisymmetric Arrangement of Wings and Bodies"
   AIAA J., Vol. 10, No. 2, Feb. 1972, pp. 171-176

4. Jones, R. T., and J. W. Nisbet
   "Transonic Transport Wings - Oblique or Swept?"
   Astronautics and Aeronautics, Vol. 12, No. 1, January 1974
   pp. 40-47

5. Kulfan, R. M., and J. W. Nisbet
   "Study of the Single-Body Yawed Wing Aircraft Concept"
   Boeing Commercial Airplane Company, Seattle, Wash., February 1974, NASA CR 137483 (N-74-27485 Microfiche)

6. Pope, A.
   Basic Wing and Airfoil Theory
   McGraw Hill Book Co., Inc., 1951.

7. Milne-Thomson, L.M., C.B.E.
   Theoretical Aerodynamics
   Dover Publications, Inc., New York, 1973

8. Jones, R. T., and D. Cohen
   High Speed Wing Theory
   Princeton University Press, Princeton, New Jersey, 1960

9. Multhopp, H.
   "Method for Calculating the Lift Distribution of Wings (Subsonic Lifting-Surface Theory)"
   R & M 2884, January 1950, Aeronautical Research Council

10. Garner, H. C.
    "Some Remarks on Vortex Drag and its Spanwise Distribution in Incompressible Flow"
    J. of the Royal Aeronautical Society, July 1968, pp. 623-625

11. Robinson, A. and J. A. Laurmann
Wing Theory
University Press, Cambridge, England, 1956

12. Pope, A. and W. R. Haney, Jr.
"Spanwise Lift Distribution for Sweptback Wings"
J. A. S., August 1949

13. Abbott, I . H. and A. E. von Doenhoff
Theory of Wing Sections
Dover Publications, Inc., New York, 1959

14. Gray, W. L. and K. M. Schenk
"A Method for Calculating the Subsonic Steady-State Loading on an Airplane with a Wing of Arbitrary Plan Form and Stiffness"
NACA TN 3030, December 1953

15. Ashley, H.
Engineering Analysis of Flight Vehicles
Addison-Wesley Publishing Co., Inc., Reading, Mass., 1974

16. Kalman, T. P., J. P. Giesing and W. P. Rodden
"Spanwise Distribution of Induced Drag in Subsonic Flow by the Vortex Lattice Method"
J. of Aircraft, Vol. 7, No. 6, Nov.-Dec. 1970, pp. 574-576

17. von Mises, R.
Theory of Flight
Dover Publications, Inc., New York, 1945

18. Flatt, J.
"Evaluation of Methods for Determining Spanwise Lift Distributions"
Army Air Force Tech. Report 4952, 1943

19. Schrenk, O.
"A Simple Approximation Method for Obtaining the Spanwise Lift Distribution"
TM 948, 1940

20. Carmichael, R. L., C. R. Castellano and C. F. Chen
"The Use of Finite Element Methods for Predicting the Aerodynamics of Wing-Body Combinations"
Analytic Methods in Aircraft Aerodynamics, NASA SP 228, 1969, pp. 37-51

21. Etkin, B.
Dynamics of Atmospheric Flight
John Wiley & Sons, Inc., New York, 1972

22. Blakelock, J. H.
Automatic Control of Aircraft and Missiles
John Wiley & Sons, Inc., New York, 1965

23. Bisplinghoff, R. L. and H. Ashley
Principles of Aeroelasticity
John Wiley & Sons, Inc., New York, 1962

24. Karamcheti, K.
Principles of Ideal Fluid Aerodynamics
John Wiley & Sons, Inc., New York, 1966

25. Cahill, Jones R.
"Summary of Section Data on Trailing-Edge High-Lift Devices"
NACA Rep. 938, 1949. (Supersedes NACA RM L8D09)

26. Greenwood, D. T.
Principles of Dynamics
Prentice-Hall, Inc., Englewood Cliffs, New Jersey, 1965

27. Roskam, J. and Dusto, A.
"A Method for Predicting Longitudinal Stability Derivatives of Rigid and Elastic Airplanes"
J. of Aircraft, Vol. 6, No. 6, 1969

28. USAF Stability and Control Dactom.
Air Force Flight Dynamics Laboratory, Wright Patterson Air Force Base

29. Witsmeer, Arthur J.
"Preliminary Design Studies of Attitude-Control Systems for the Stanford Relativity Satellite"
Center for Systems Research, Stanford University SUDAAR 337, January, 1968.